

Open Research Online

The Open University's repository of research publications and other research outputs

The petrogenesis of the Penmaenmawr intrusion, North Wales

Thesis

How to cite:

Durham, John (2004). The petrogenesis of the Penmaenmawr intrusion, North Wales. MPhil thesis The Open University.

For guidance on citations see [FAQs](#).

© 2004 John Durham

Version: Version of Record

Copyright and Moral Rights for the articles on this site are retained by the individual authors and/or other copyright owners. For more information on Open Research Online's data [policy](#) on reuse of materials please consult the policies page.

oro.open.ac.uk

The Petrogenesis of the Penmaenmawr Intrusion, North Wales

A thesis submitted for the degree of Master of Philosophy

by

John Durham

Department of Earth Sciences
The Open University

August 2004

ProQuest Number:27532732

All rights reserved

INFORMATION TO ALL USERS

The quality of this reproduction is dependent upon the quality of the copy submitted.

In the unlikely event that the author did not send a complete manuscript and there are missing pages, these will be noted. Also, if material had to be removed, a note will indicate the deletion.



ProQuest 27532732

Published by ProQuest LLC (2019). Copyright of the Dissertation is held by the Author.

All rights reserved.

This work is protected against unauthorized copying under Title 17, United States Code
Microform Edition © ProQuest LLC.

ProQuest LLC.
789 East Eisenhower Parkway
P.O. Box 1346
Ann Arbor, MI 48106 – 1346

Abstract

The Penmaenmawr Intrusion forms a prominent hill on the north Wales coast and consists of a very fine- to medium-grained microdiorite. Previous studies have considered the Penmaenmawr Intrusion to be related to the extrusive rocks of the Llewelyn Volcanic Group, that were erupting in early Caradoc times in a back arc basin associated with subduction due to the closure of the Iapetus Ocean to the northwest.

The objective of this study was to examine the mineralogical and geochemical variations within the intrusion in order to investigate its petrogenesis. Seventy samples were collected for petrological examination and geochemical analysis and the results were used to model possible magmatic processes.

This study proposes that the Penmaenmawr Intrusion was the result of two emplacements of magma from an underlying, already fractionated and layered, magma chamber. Initial injections of magma took place along the southern boundary and in the east of the present intrusion resulting in the very fine-grained rocks at the margins of the intrusion. The second, larger emplacement, with a slightly more basic composition forms the main body of the intrusion. Local mixing between the two batches of magma took place along their common boundary blurring their junctions and some localised mixing also took place during the transport and emplacement of the second batch of magma, which served to obscure the evidence for the original compositional layering of the underlying magma chamber.

Following emplacement, the Penmaenmawr Intrusion was variably altered forming a range of secondary minerals. This study proposes that the alteration is mainly due to the ingress of hydrothermal fluids along faults and shear planes during two alteration episodes. The first associated with emplacement where hot fluids, originating from the cooling magma, caused changes to the original minerals and the second associated with sub-greenschist facies metamorphism during the Acadian regional metamorphic event of early to mid Devonian times.

Acknowledgements

I would like to acknowledge the assistance of many people who have helped me to carry out and complete this project.

I would like to acknowledge the contribution of the late Richard Thorpe who originally initiated this study and inspired me to start on what was to become a longer project than was originally intended.

I would like to thank my supervisors Peter Webb of the Open University and Richard Bevins of the National Museum of Wales for their perseverance and encouragement. Without their tolerance and support this project would not have been completed. I would also like to extend my gratitude to all the staff in the Earth Sciences Department at the Open University who have assisted in the preparation and analysis of numerous samples, in particular John Watson and Andy Tindle.

I would also like to thank the management and staff of ARC (Northern) for permission to visit and collect samples from the Penmaenmawr Quarry and in particular the Regional Geologist Helen Mayfield who provided me with plans and other useful data.

I owe a special debt to my daughter, Emma Durham, who spent a long time putting the figures and diagrams together for this thesis, and I would like to thank my family generally for their tolerance and I promise that I will now get on with the garden.

TABLE OF CONTENTS

CHAPTER 1. INTRODUCTION

- 1.1. Background
- 1.2. Previous work on the Penmaenmawr Intrusion
- 1.3. Aims and objectives of the current study

CHAPTER 2. REGIONAL GEOLOGICAL AND TECTONIC SETTING

- 2.1 Introduction
- 2.2. Age of the Penmaenmawr Intrusion
- 2.3. Tectonic setting of north Wales in the Ordovician times
- 2.4 The Welsh basin
- 2.5 Sedimentation in the Welsh Basin
- 2.6. Volcanism in the Welsh Basin

CHAPTER 3. LOCAL AND FIELD GEOLOGY OF THE PENMAENMAWR INTRUSION

- 3.1. Introduction
- 3.2. General geology of the area around the Penmaenmawr Intrusion
- 3.3. Field description of the Penmaenmawr Intrusion
- 3.4. Penmaenmawr Lithologies
- 3.5. Veins, segregations and inclusions
- 3.6. Structures
- 3.7. Sampling methodology

CHAPTER 4. THE PETROGRAPHY OF THE PENMAENMAWR INTRUSION

- 4.1 Introduction
- 4.2 Rocks from the Western Quarries
- 4.3. Rocks from the Central Quarries
- 4.4. Rocks from the Graig Lwyd Quarries and adjacent to the southern boundary
- 4.5 Veins, segregations and inclusions
- 4.6 Petrographic classification
 - 4.6.1. Group 1 rocks
 - 4.6.2. Group 2 rocks
 - 4.6.3. Group 3 rocks
 - 4.6.4. Group 4 rocks
- 4.7. Summary of the main rock types
- 4.8. Alteration indices
 - 4.8.1. Application of alteration indices to the Penmaenmawr Intrusion

CHAPTER 5. MINERAL CHEMISTRY OF THE PENMAENMAWR INTRUSION

- 5.1 Introduction
- 5.2. Plagioclase feldspar
- 5.3. Alkali feldspar
- 5.4. Orthopyroxene

- 5.5. Clinopyroxene
- 5.6. Amphibole
- 5.7. Iron and titanium minerals
- 5.8. Biotite
- 5.9. Chlorite
- 5.10. Apatite
- 5.11 Mineral chemistry - Summary

CHAPTER 6. THE MAGNETIC SUSCEPTIBILITY OF THE PENMAENMAWR INTRUSION

- 6.1. Introduction
- 6.2. Application of magnetic susceptibility to the Penmaenmawr Intrusion
- 6.3. Variations in magnetic susceptibility
- 6.4. Magnetic susceptibility and the petrographic groups
- 6.5. Magnetic susceptibility – interpretation and discussion

CHAPTER 7. THE WHOLE ROCK GEOCHEMISTRY OF THE PENMAENMAWR INTRUSION

- 7.1. Introduction
- 7.2. Geochemical classification of the rocks from the Penmaenmawr Intrusion
- 7.3. Main geochemical variation and spatial distribution
 - 7.3.1. Main geochemical variations with height
 - 7.3.2. Geochemical variations across the intrusion
- 7.4. Element mobility
 - 7.4.1. Zr content plots
 - 7.4.2. Element Mobilisation, Summary

CHAPTER 8. DISCUSSION AND POSSIBLE ORIGINS OF THE ALTERATION OBSERVED IN THE PENMAENMAWR INTRUSION

- 8.1. Introduction
- 8.2. Regional metamorphism
- 8.3. Hydrothermal fluids
- 8.4. Alteration - summary

CHAPTER 9. MAGMA CHAMBER PROCESSES THAT PRODUCE VARIATIONS IN GEOCHEMISTRY

- 9.1. Introduction
- 9.2. Fractional crystallisation
- 9.3. Magma mixing
- 9.4. Assimilation
- 9.5. Complex magma chambers
- 9.6. Applicability of magma chamber processes to the Penmaenmawr Intrusion

CHAPTER 10. WHOLE ROCK GEOCHEMICAL VARIATION PATTERNS

- 10.1. Introduction
- 10.2. Description of the variation patterns
- 10.3. Interpretation of the variation patterns
- 10.4. Variation diagrams and fractional crystallisation
 - 10.4.1. Summary of variation diagrams according to the fractional crystallisation model
- 10.5. Variation diagrams and magma mixing
- 10.6. Variations in compatible and incompatible trace element contents
 - 10.6.1. Variation in compatible and incompatible trace element contents for the Penmaenmawr Intrusion
 - 10.6.2. Interpretation of the variations in compatible and incompatible trace element contents
- 10.7. Mineral fractionation vector diagrams for the Penmaenmawr Intrusion
 - 10.7.1. Calculation of mineral vectors
 - 10.7.2. Description of the vector diagrams
 - 10.7.3. Interpretation of the vector diagrams

CHAPTER 11. FRACTIONAL CRYSTALLISATION MODELLING

- 11.1. Introduction
- 11.2. Major element modelling - theoretical considerations
- 11.3. Major element modelling - constraints and assumptions
- 11.4. Trace element modelling – theoretical considerations, constraints and assumptions
- 11.5. Modelling the less evolved rocks (Group 3)
 - 11.5.1. Major element modelling for the less evolved rocks (Group 3)
 - 11.5.2. Trace element modelling for the less evolved rocks (Group 3)
 - 11.5.3. Less evolved rocks (Group 3) – summary
- 11.6. Modelling the intermediate rocks (Group 2)
 - 11.6.1. Major element modelling for the intermediate rocks (Group 2)
 - 11.6.2. Trace element modelling for the intermediate rocks (Group 2)
 - 11.6.3. Intermediate rocks (Group 2) - summary
- 11.7. Modelling the more evolved rocks (Group 1)
 - 11.7.1. Major element modelling for the more evolved rocks (Group 1)
 - 11.7.2. Trace element modelling for the more evolved rocks (Group 1)
 - 11.7.3. More evolved rocks (Group 1) rocks - summary
- 11.8. Fractional crystallisation modelling - summary

CHAPTER 12. MAGMA MIXING (HYBRIDISATION) MODELLING

- 12.1. Introduction
- 12.2. Magma mixing modelling - theoretical considerations
- 12.3. Whole intrusion magma mixing modelling
- 12.4. Group 3 rocks magma mixing modelling
 - 12.4.1. Group 3 rocks magma mixing modelling - results and interpretation
- 12.5. Group 2 rocks magma mixing modelling
- 12.6. Group 1 rocks magma mixing modelling
- 12.7. Group 4 rocks magma mixing modelling

- 12.7.1. Group 4 rocks magma mixing modelling - results and interpretation
- 12.8. Magma mixing modelling - summary

CHAPTER 13. SEGREGATIONS AND INCLUSIONS

- 13.1. Introduction
- 13.2. Variation diagrams
- 13.3. Variation diagrams - description
- 13.4. Variation diagrams- interpretation

CHAPTER 14. DISCUSSION OF THE MAGMATIC PETROGENESIS OF THE PENMANMAWR INTRUSION

- 14.1. Introduction
- 14.2. Fractional crystallisation
- 14.3. Other possible mechanisms
 - 14.3.1. Mixing (including assimilation and/or periodic influx of fresh magma)
 - 14.3.2. Emplacement in several separate batches
 - 14.3.3. Emplacement of an essentially single pulse of magma from a deeper level magma chamber with a vertical compositional gradient
- 14.4. Evidence for magma emplacement processes from segregations
- 14.5. The preferred model for the magmatic petrogenesis of the Penmaenmawr Intrusion

CHAPTER 15. CONCLUSION

- 15.1. Introduction
- 15.2. Mineralogical differences within the Penmaenmawr Intrusion
- 15.3. Alteration
- 15.4. Whole rock geochemical variation within the Penmaenmawr Intrusion
- 15.5. The petrogenesis of the Penmaenmawr Intrusion
- 15.6. Future Work

APPENDICES

REFERENCES

LIST OF FIGURES

- Figure 1.1. A sketch map showing the location of the Penmaenmawr Intrusion and the plugs at Garreg Fawr and Dinas on the north Wales coast.
- Figure 1.2a. (Upper photograph). The Penmaenmawr Intrusion looking east from Llanfairfechan.
- Figure 1.2b. (Lower photograph). General view from the Western Quarries of the Penmaenmawr Intrusion looking west.
- Figure 2.1. Simplified geological sketch map showing the distribution of the Llewelyn Volcanic Group and associated intrusions including the Penmaenmawr Intrusion. (From Ball & Merriman, 1989).
- Figure 2.2. The location of the continents Gondwana, including southern Britain, Laurentia and Baltica in Arenig times. (From Fortey & Cocks, 1982).
- Figure 2.3. Simplified geological map of Wales showing the Welsh Basin between the Menai Straits Fault System and the Church Stretton and Pontesford-Linley Fault System. (From Kokelaar *et al.*, 1984).
- Figure 3.1. Geological sketch map showing the Penmaenmawr Intrusion and the immediate surrounding area. Based on the British Geological Survey, sheet 106, Bangor.
- Figure 3.2. (Upper photograph). An irregular segregation from the Central Quarries of the Penmaenmawr Intrusion.
- Figure 3.3. (Lower photograph). A series of inclusions in a hand specimen from the Central Quarries of the Penmaenmawr Intrusion.
- Figure 3.4a. (Upper photograph). Vertical fault or joint planes approximately 650 mm wide, filled with pale-grey material from the Central Quarries of the Penmaenmawr Intrusion.
- Figure 3.4b. (Lower photograph). Vertical fault or joint planes approximately 800 mm wide, filled with pale-grey material from the Central Quarries of the Penmaenmawr Intrusion.
- Figure 3.5. An outline plan of the Penmaenmawr Intrusion showing the shear zones and zones A, B and C identified by S Penn Associates (1991). Also shown are the main quarry faces and the location of samples, which are discussed in Section 3.7.
- Figure 3.6. An outline plan of the Penmaenmawr Intrusion showing the quarry faces and the locations of the samples utilised in this study with their identification numbers.

- Figure 4.1. Outline plan of the Penmaenmawr Intrusion showing the location of samples utilised in this study and the areas covered by the 4 petrographic groups.
- Figure 4.2. Outline plot of the Penmaenmawr Intrusion showing the alteration index (1-5) for fine- to medium grained samples.
- Figure 4.3. Contour diagram for the alteration index using Surfer for Windows, surface-mapping system.
- Figure 5.1. Ternary Ab-An-Or diagram showing the compositions of Plagioclase and Alkali Feldspar for the Penmaenmawr samples from Groups 1-4.
- Figure 5.2. Ca_2SiO_6 (Wo) – $\text{Mg}_2\text{Si}_2\text{O}_6$ (En) – $\text{Fe}_2\text{Si}_2\text{O}_6$ (Fs) diagram showing the composition of the clinopyroxenes and orthopyroxenes from the Penmaenmawr Intrusion.
- Figure 5.3. Plot of the Ca + Na content of Penmaenmawr amphiboles, showing the separation into calcic amphiboles and Fe-Mg-Mn amphiboles.
- Figure 5.4. Plot of $\text{Mg}/(\text{Mg} + \text{Fe})$ against Silica (Si) for Penmaenmawr calcic amphiboles.
- Figure 5.5. Plot of $\text{Mg}/(\text{Mg} + \text{Fe})$ against silica (Si) for Penmaenmawr Fe-Mg-Mn amphiboles.
- Figure 5.6. Plots of (a) K_2O and (b) TiO_2 concentrations of Penmaenmawr amphiboles, divided according to their groups.
- Figure 5.7. Fe versus Si concentration diagram for the Penmaenmawr samples from Groups 1 to 4. Plot after Hey (1954).
- Figure 6.1. Magnetic susceptibility values for samples from Groups 1-4 from the Penmaenmawr Intrusion, in ascending magnetic susceptibility value order.
- Figure 6.2. Plot of magnetic susceptibility values of the samples from Groups 1-4 from the Penmaenmawr intrusion, with respect to the location of the samples.
- Figure 6.3. Contour plot for the magnetic susceptibility values from the Penmaenmawr Intrusion using Surfer for Windows, surface-mapping system.
- Figure 6.4. Magnetic susceptibility values for the Penmaenmawr samples from Groups 1-4, divided according to their groups.
- Figure 6.5. Magnetic susceptibility values for the Penmaenmawr samples from Group 3 against silica content (SiO_2) (wt%).

- Figure 7.1. Total alkalis ($\text{Na}_2\text{O}+\text{K}_2\text{O}$) (wt%) versus silica (SiO_2) (wt%), TAS diagram for plutonic rocks (from Cox *et al.*, 1979, adapted by Wilson, 1989), showing the Penmaenmawr samples from Groups 1-4.
- Figure 7.2. Total alkalis ($\text{Na}_2\text{O}+\text{K}_2\text{O}$) (wt%) versus silica (SiO_2) (wt%) (from Le Maitre *et al.*, 1987), for Penmaenmawr samples from Groups 1-4.
- Figure 7.3. Log-log plot of Zr/TiO_2 versus Nb/Y (from Winchester and Floyd 1987), for the Penmaenmawr samples from Groups 1-4.
- Figure 7.4. Plot of height above sea-level against silica (SiO_2) (wt%) for the Penmaenmawr samples from Groups 1-4.
- Figure 7.5. Plot of silica (SiO_2) (wt%) values of the Penmaenmawr samples from Groups 1-4, with respect to the location of the samples.
- Figure 7.6. Plot of Zr (ppm) values of the Penmaenmawr samples from Groups 1-4, with respect to the location of the samples.
- Figure 7.7. Plot of Y (ppm) values of the Penmaenmawr samples from Groups 1-4, with respect to the location of the samples.
- Figure 7.8. Contour plots of (a) SiO_2 , (b) Zr and (c) Y contents across the Penmaenmawr Intrusion using the Surfer for Windows surface mapping program.
- Figure 7.9. Plots of selected major elements (wt%) against Zr (ppm), for the Penmaenmawr samples from groups 1-4.
- Figure 7.10. Plots of selected trace elements (ppm) against Zr (ppm), for the Penmaenmawr samples from groups 1-4.
- Figure 10.1. Plots of selected major elements (wt%) against silica (SiO_2) (wt%), for the Penmaenmawr samples from Groups 1-4.
- Figure 10.2. Plots of selected trace elements (ppm) against Silica (SiO_2) (wt%), for the Penmaenmawr samples from Groups 1-4.
- Figure 10.3. Plots showing the contents of compatible against incompatible elements (ppm) for the Penmaenmawr samples from Groups 1-4.
- Figure 10.4. Log-log plots of compatible against incompatible elements for the Penmaenmawr samples from Groups 1-4.
- Figure 10.5. Vector diagrams for the Penmaenmawr rocks from all 4 groups. Incompatible trace elements against incompatible trace elements,
- Figure 10.6. Vector diagrams for the Penmaenmawr rocks from all 4 Groups. Compatible trace elements against incompatible trace elements,

- Figure 11.1. Plots of (a) MgO against SiO₂ and (b) Zr against SiO₂ for the Penmaenmawr samples used for fractional crystallization modelling.
- Figure 11.2. Diagrams illustrating the alternative fractional crystallisation models for the Penmaenmawr Intrusion.
- Figure 12.1. Plots of (a) MgO against SiO₂ and (b) Zr against SiO₂ for the 14 Penmaenmawr Intrusion samples selected for whole intrusion magma mixing models.
- Figure 12.2. Plots of magma mixing for the whole intrusion using Penmaenmawr samples JD2912 and JD2938 as end members.
- Figure 12.3. Magma mixing plots for Group 3 Penmaenmawr samples, using the end members JD2938 and JD2923.
- Figure 12.4. Magma mixing plots for Group 3 Penmaenmawr samples, using (a) the end members JD2936 and JD2946, with the samples from the western area of the intrusion (JD2945, JD2962, JD2955, JD2941, JD2943, and JD2939), and (b) the end members JD2923 and JD2948, with the samples JD2911, JD2922, JD2925 and JD2951.
- Figure 12.5. Magma mixing plot for Group 2 Penmaenmawr samples JD2945, JD2955, JD2941, and JD2943, using samples JD2908 and JD2924A as the end members.
- Figure 12.6. Magma mixing plot for Group 1 Penmaenmawr samples JD2903, JD2913, JD2917, JD2933, JD2964, JD2967 and JD2969, using samples JD2905 and JD2912 as the end members.
- Figure 12.7. Magma mixing plots for Group 4, Penmaenmawr samples JD2927, JD2930, JD2931, and JD2932, using (a) JD2928 and JD2929 as the end members, and (b) JD2913 (Group 1) and JD2953 (Group 3) as end members.
- Figure 13.1. Plots of selected major elements (wt%) against Silica (SiO₂) (wt%), for the Penmaenmawr samples from Groups 1-4, and the segregation, the inclusion and the source rock, containing the inclusion.
- Figure 13.2. Plots of selected trace elements (ppm) against Silica (SiO₂) (wt%), for the Penmaenmawr samples from Groups 1-4 and the segregation, the inclusion and the source rock, containing the inclusion.
- Figure 14.1. The preferred model for the magmatic petrogenesis of the Penmaenmawr Intrusion.

LIST OF TABLES

- Table 2.1. Ordovician Stratigraphic Table (from Fortey *et al.*, 2000).
- Table 4.1. The principal characteristics of the four main petrographic groups from the Penmaenmawr Intrusion.
- Table 4.2. Alteration indices based on the character of plagioclase feldspar.
- Table 5.1. Typical Ca, Mg and Fe (as atomic %) values for clinopyroxene from the different groups from the Penmaenmawr Intrusion.
- Table 6.1. Magnetic susceptibility values for samples from the Penmaenmawr Intrusion.
- Table 7.1. SiO₂ contents of the 4 Groups from the Penmaenmawr Intrusion.
- Table 7.2. Zr contents of the 4 Groups from the Penmaenmawr Intrusion.
- Table 7.3. Y contents of the 4 Groups from the Penmaenmawr Intrusion.
- Table 10.1. Mineral/Melt partition coefficients for andesitic liquids. The biotite mineral/melt partition coefficients are for dacitic and rhyolitic liquids (from Rollinson, 1993).
- Table 11.1. Major element compositions of Penmaenmawr samples used for fractional crystallisation modelling, normalised to 100% after the removal of the LOI (loss on ignition).
- Table 11.2. The mineral compositions used for major element modelling based on the average mineral chemistry determined by electron probe analysis from Group 3 rocks.
- Table 11.3. A summary of the results of major element modelling for five Group 3 daughter samples using JD2938 (SiO₂ content 56.8%) as the parent magma.
- Table 11.4. A summary of the results of major element modelling for four Group 3 daughter samples using JD2925 (SiO₂ content 59.70%) as the parent magma.
- Table 11.5. Results of trace element modelling using sample JD2938 as the parent magma and five samples as daughter magmas.
- Table 11.6. Results of trace element modelling using sample JD2925 as the parent magma and sample JD2923 as the daughter magma.
- Table 11.7. A summary of the results of major element modelling for Group 2 samples using JD2906 (SiO₂ content 61.82%) as the parent magma.

Table 11.8. Results of trace element modelling using sample JD2906 as the parent magma and samples JD2924A and JD2919 as daughter magmas.

Table 11.9. A summary of the results of major element modelling for Group 1 samples using JD2903 (SiO₂ content 63.01%) as the parent magma.

Table 11.10. Results of trace element modelling using sample JD2903 as the parent magma and samples JD2947 and JD2958 as daughter magmas.

LIST OF APPENDICES

- Appendix 1. A summary of the mineralogy of the samples from the Penmaenmawr Intrusion.
- Appendix 2. Description and photomicrographs of representative samples from the Penmaenmawr Intrusion.
- Sample JD2936. from the Western Quarries (Group 3).
Sample JD2951 from the northern Central Quarries (Group 3).
Sample JD2918. from the main Central Quarries (Group 2).
Samples JD2934 and JD2912 from the Graig Lwyd Quarries (Group 1).
Sample JD2932 from the small quarries north-west of the Graig Lwyd Quarries (Group 4).
Sample JD2926, a segregation from the Central Quarries.
- Appendix 3. Electron microprobe operating details and standards.
- Appendix 4. Mineral chemistry.
- Plagioclase feldspar
Alkali feldspar
Orthopyroxene
Clinopyroxene
Amphibole
Biotite
Chlorite
Fe-Ti Oxides
Apatite
- Appendix 5. The Open University standard procedures, technical and instrumental specification and precision for X-ray fluorescence (XRF) analysis for whole rock major and trace element compositions.
- Appendix 6. The major and trace element composition of all samples from the Penmaenmawr Intrusion.
- Appendix 7. The results of major element fractional crystallisation modelling based on sample JD2938 as the assumed parental magma (assumed parent), and progressively more evolved samples as the daughter magmas.
- Appendix 8. The detailed results of the major element fractional crystallisation modelling based on sample JD2925 as the assumed parental magma and selected more evolved Group 3 samples as the daughter magmas.

- Appendix 9 Estimates of the composition of a cumulate, based on the sum of the compositions and proportions of the minerals being removed during the proposed fractional crystallisation of sample JD2925.
- Appendix 10 The detailed results of major element fractional crystallisation modelling based on samples JD2908 and JD2906 as the assumed parental magmas and selected more evolved Group 2 samples as the daughter magmas.
- Appendix 11 The detailed results of major element fractional crystallisation modelling based on sample JD2914 and JD2903 as the assumed parental magmas and progressively more evolved samples from Group 1 as the daughter magmas.
- Appendix 12 Location of Samples (5 figure grid references and altitude)

CHAPTER 1. INTRODUCTION

1.1. Background

The Penmaenmawr Intrusion forms a prominent hill rising from sea level to a height slightly in excess of 400 metres above the small town of Penmaenmawr on the north coast of Wales. A sketch map, showing the location and outline of the Penmaenmawr Intrusion is presented at Figure 1.1 and photographs showing the Penmaenmawr Intrusion rising above sea level are presented in Figure 1.2. The highest point, Clip yr Orsedd, is 429m above sea level on the southern boundary of the intrusion. The intrusion is oval in plan view, approximately 2.5km long and approximately 1km wide, with its long axis in an east-west orientation (see Figure 1.1b). Two smaller plug-like intrusions occur to the south of the main intrusion, at Garreg Fawr and Dinas. The Penmaenmawr Intrusion has intruded slates and shales of early Ordovician age (Arenig to early Caradoc) and the intrusion is considered to be related to the Ordovician (Caradoc) volcanic activity of Snowdonia, North Wales (Howells *et al.*, 1991). The Penmaenmawr Intrusion has been classified as a pyroxene-quartz-microdiorite (British Geological Survey, 1985).

The Penmaenmawr Intrusion has a long history of exploitation, and rock from the intrusion is currently being extracted by ARC (Northern) Limited for hard rock aggregate. The recent upgrading of the A55 road along the north Wales coast has benefited from this extraction and has involved building a tunnel through the intrusion. The intrusion was exploited as far back as Neolithic times, when the tough, uniform, very fine-grained rocks from the Graig Lwyd area, in the east of the intrusion, were used to produce stone axes. The Graig Lwyd axes are now classified archaeologically as Group VII axes and the factories in the Penmaenmawr area are considered to be some of the most important in Wales (Clough & Cummins, 1988).

The current area being worked is the centre of the intrusion, but the intrusion contains a number of disused quarry faces that are the remains of previous quarrying operations. This history of exploitation, and the abundant quarry faces, has allowed samples to be collected for examination and analysis from a

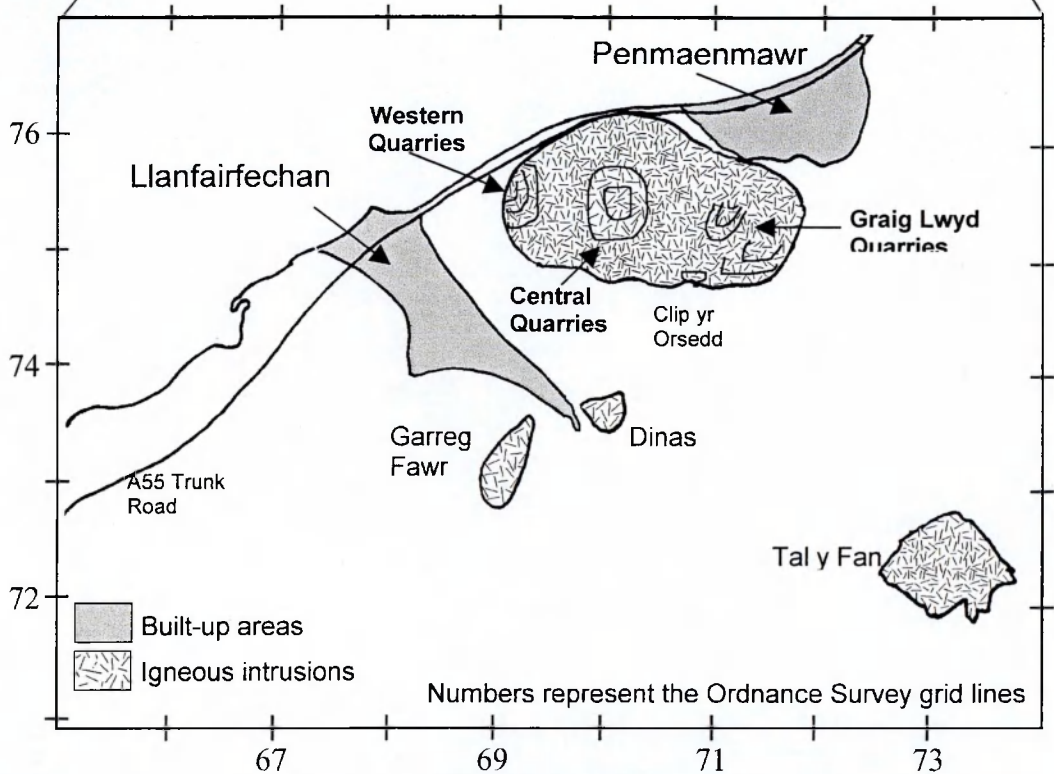
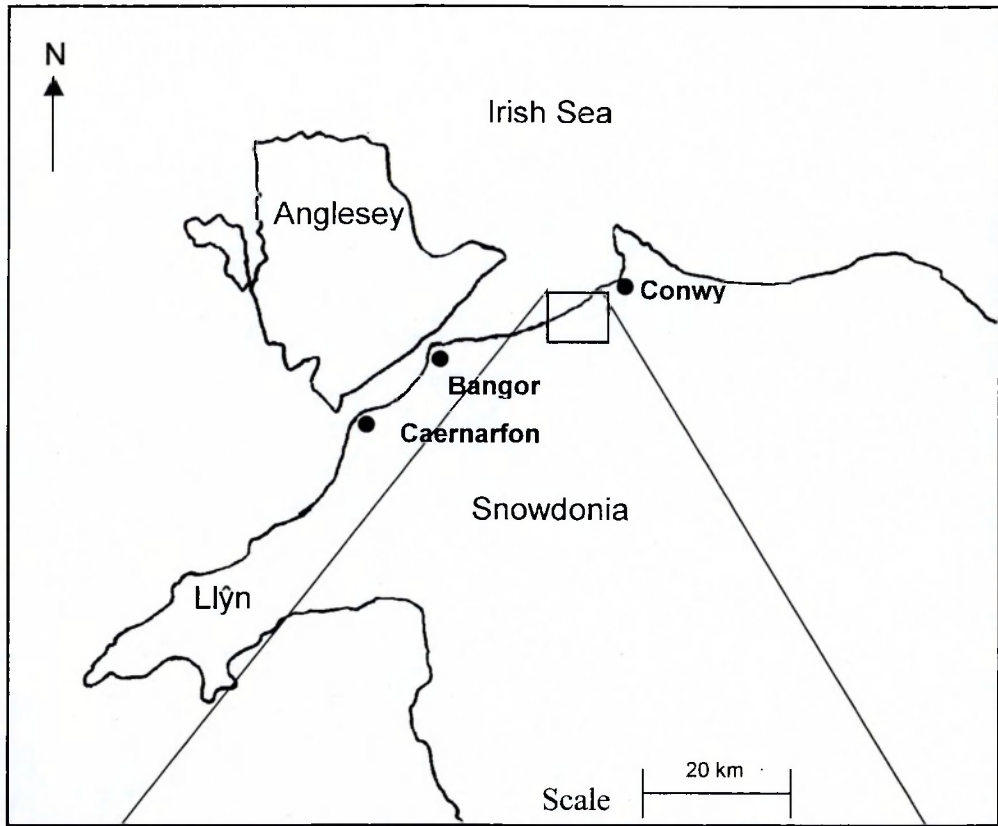


Figure 1.1. A sketch map showing the location of the Penmaenmawr Intrusion and the plugs at Garreg Fawr and Dinas on the north Wales coast.



Figure 1.2a. (Upper photograph). The Penmaenmawr Intrusion looking east from Llanfairfechan.

Figure 1.2b. (Lower photograph). General view from the Western Quarries of the Penmaenmawr Intrusion looking west.

large number of locations within the intrusion. However, large areas of the intrusion remain unexposed, covered by superficial deposits and more recently by overburden due to landscaping activities by ARC (Northern) Limited.

1.2. Previous work on the Penmaenmawr Intrusion

Early studies of the Penmaenmawr Intrusion were carried out by Sargent (1915,1924,1925), who separated the intrusion into three parts, based on grain size and mineralogy, which he termed; the main Penmaenmawr area, consisting of the main mass of the intrusion; the eastern shoulder of Graig Lwyd; and the marginal rock type along the southern boundary of the intrusion. Sargent (1915,1924) described the mineralogy of the intrusion and observed differences in mineralogy with height above sea level, concluding that it was linked to magmatic differentiation during the cooling of the intrusion. Sargent (1924) suggested that the differentiation was caused by early-formed crystals being separated from the residual liquid by a 'straining-off' process due to the lower specific gravity of the residual liquid.

Sargent (1925) also examined acid segregations, white or pale-grey, irregular streaks, patches and veins present within the intrusion and suggested that they were generated by volatiles in the later stages of cooling which carried silica- and water-rich residual magma to areas of decreased pressure.

Ball and Merriman (1989) carried out a petrological and geochemical survey of the Llewelyn Volcanic Group and related high-level intrusions, including the Penmaenmawr Intrusion as part of a multidisciplinary investigation of Caradoc volcanism in Snowdonia (Howells *et al.*, 1991). Ball and Merriman (1989) considered the Penmaenmawr Intrusion to be comagmatic with the extrusive rocks of the Llewelyn Volcanic Group and suggested that the various igneous rocks of this Group were generated by the high-level storage and fractionation of magma prior to eruption and that the Penmaenmawr Intrusion represents a high-level, sub-volcanic, magma chamber. They showed that the Llewelyn Volcanic Group consists of a high Zr and a low Zr series of intermediate to acid magmas, the Penmaenmawr Intrusion belonging to the high Zr series. They suggested that this separation into high Zr and low Zr magma could be due

either to two separate parental magmas or to a single parent magma evolving a low Zr and a high Zr magma by varying degrees of fractionation.

Tremlett (1997) investigated the pattern of geochemical variation within the Penmaenmawr Intrusion and suggested that the variation was due to "pulsational emplacement of sheets of magma from a body of magma at depth undergoing crystallization differentiation." He also presented evidence to suggest that the Penmaenmawr Intrusion was derived from a parental magma of intermediate composition.

1.3. Aims and objectives of the current study

The aims and objectives of this study were: -

1. To investigate the petrogenesis of the Penmaenmawr intrusion, using field and petrographic observations and mineralogical and geochemical data,
2. To develop a model for magma evolution and emplacement for the Penmaenmawr Intrusion.
3. To assess the role of post-emplacement alteration on the intrusion.
4. To compare the findings of this study with earlier studies involving the Ordovician (Caradoc) igneous activity in Snowdonia.
5. To provide a source for discussion and assessment of the petrogenesis of other intermediate igneous intrusions in both North Wales and further afield.

CHAPTER 2. REGIONAL GEOLOGICAL AND TECTONIC SETTING

2.1. Introduction

In Chapter 1, it was reported that the Penmaenmawr Intrusion was intruded into slates and shales of early Ordovician age and the intrusion is considered to be related to the later (Caradoc) Ordovician volcanic rocks of north Wales. This Chapter reviews the stratigraphy of the north Wales area in order to establish a possible timing for the intrusive activity. This chapter also reviews the tectonic setting of the region in Ordovician times, with particular reference to north Wales, in order to establish the tectonic environment that led to the magmatic activity that produced the Penmaenmawr Intrusion. Finally this chapter reviews Ordovician sedimentation and volcanism within the Welsh Basin in order to demonstrate the relationship between the Penmaenmawr Intrusion and the associated volcanic rocks in the area.

2.2. Age of the Penmaenmawr Intrusion

The Penmaenmawr Intrusion was emplaced into blue-black slaty shales of the Nant Ffrancon Formation of Arenig to the early Caradoc age (British Geological Survey, 1985). This indicates that the intrusion is post early Caradoc in age. All contacts are steep to vertical and the shales show little evidence of contact metamorphism. Ball and Merriman (1989) suggested that the poorly developed thermal aureoles indicated intrusion temperatures of about 300°C at most.

Roberts (1979) reported that the cleavage in the country rocks deflects around the intrusion and suggested that the intrusion predates the folding and the development of cleavage of the rocks. Merriman & Roberts (1985), in a study of white mica crystallinity, concluded that the intrusion was emplaced prior to the phase of the Caledonian Orogeny during which the deformation occurred.

Ball & Merriman (1989) used the spatial association and geochemical characteristics of the intrusion to suggest that it was comagmatic with the extrusive rocks of the Llewelyn Volcanic Group (see Figure 2.1). This

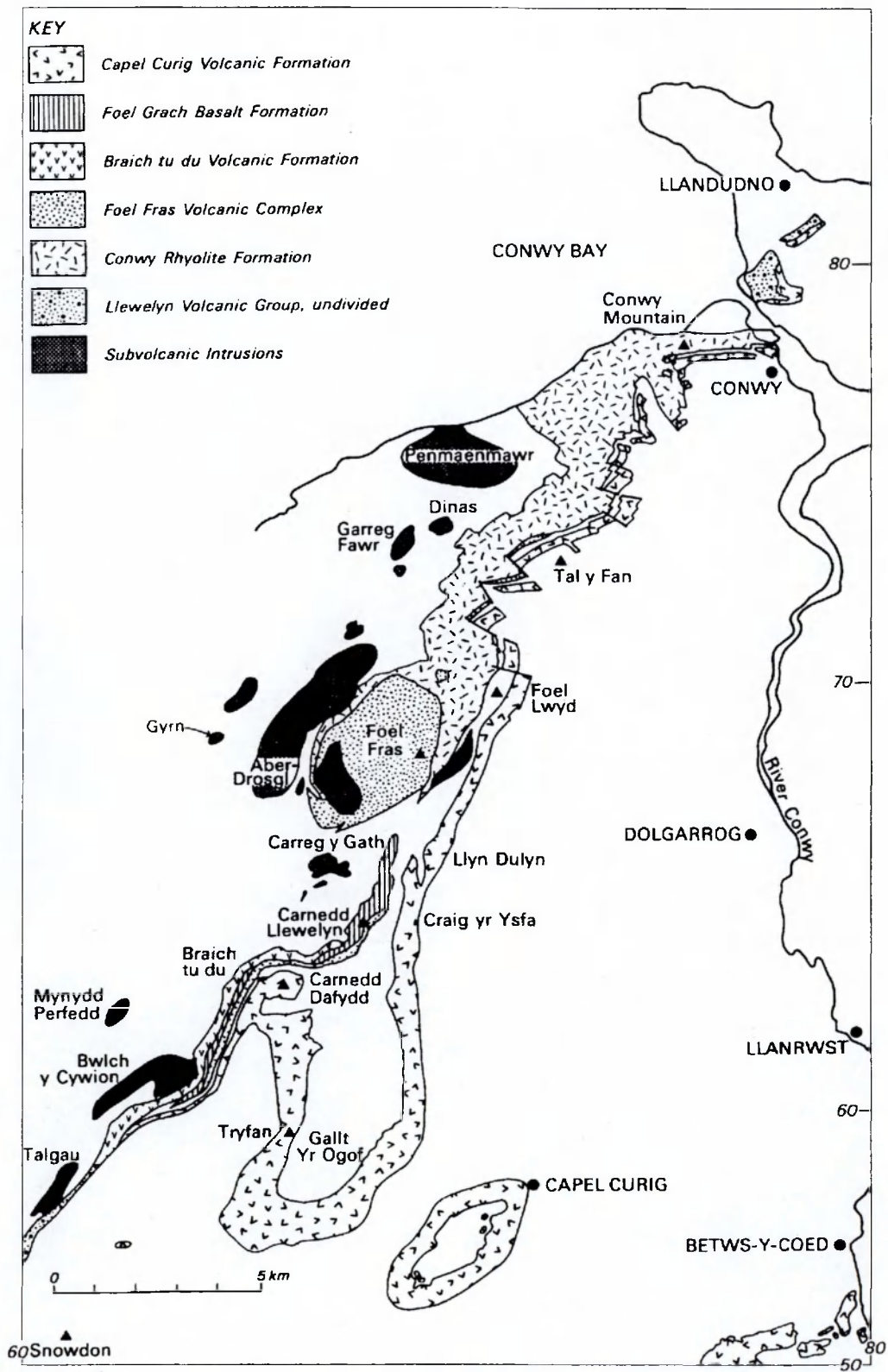


Figure 2.1. Simplified geological sketch map showing the distribution of the Llewelyn Volcanic Group and associated intrusions including the Penmaenmawr Intrusion. (From Ball & Merriman, 1989).

relationship was subsequently accepted by Howells *et al.* (1991). The Llewelyn Volcanic Group represents the first eruptive cycle of Caradoc volcanic activity in north Wales and post dates the deposition of the Nant Ffrancon Formation (Howells *et al.*, 1991). Graptolites belonging to the *D. multidentis* zone and a Soudleyan shelly fauna have been reported in the uppermost strata of the Nant Ffrancon Formation, while poorly preserved brachiopods indicative of a Soudleyan age have been found in sedimentary rocks within the Llewelyn Volcanic Formation (Howells *et al.*, 1991). The Llewelyn Volcanic Group is overlain by siliciclastic rocks of the Cwm Eigiau Formation, which contain fossils whose ages straddle the boundary between the Soudleyan and Longvillian sub-stages (Howells *et al.*, 1991 and references within). It is thought likely, therefore, that the first eruptive cycle of Caradoc volcanism in north Wales took place entirely within the Soudleyan sub-stage.

Table 2.1. Ordovician Stratigraphic Table (from Fortey *et al.*, 2000).

Divisions of the Ordovician		Stages of the Caradoc		Sub-stages of the Burrellian
Ashgill	/	Streffordian	/	Longvillian
Caradoc		Cheneyan		Soudleyan
Llanvirn		Burrellian		Harnagian
Arenig		Aurelucian		
Tremadoc				

The top of the Soudleyan sub-stage has been dated as falling between 457–448 Ma (Fortey *et al.*, 2000) although an Rb-Sr whole rock isochron from the Penmaenmawr Intrusion has given an age of 386 ± 24 Ma (Evans, 1991). However other intrusions from Snowdonia and Llŷn thought to be contemporaneous with Penmaenmawr have given Ordovician dates; for example a microdiorite intrusion from the Foel Fras Volcanic Complex, also considered to be part of the Llewelyn Volcanic Group (Ball & Merriman, 1989), has provided a date of 456 ± 52 Ma (Evans, 1991).

Evans *et al.* (1995) cite an age of 453 ± 2.2 Ma based on U-Pb techniques on zircons from the Garn Fadryn sub-volcanic intrusion on Llŷn. They suggested that

this date represented the first reliable emplacement age for an intrusion in the Caradoc volcanic province of north Wales, and argued that earlier ages, including that for the Penmaenmawr Intrusion, based on Rb-Sr isochrons were the result of re-setting. It was concluded by Evans (1989 and 1990) that most of the Ordovician volcanic and intrusive rocks of north Wales have had their Rb-Sr systematics reset during low grade metamorphism. Some rocks, however, show preservation of their primary mineralogy and give reliable intrusive ages.

The Penmaenmawr Intrusion is therefore considered to be comagmatic with the Llewelyn Volcanic Group and to have been emplaced into shales in Soudleyan sub-stage times just prior to the period 457 - 448Ma.

2.3. Tectonic setting of north Wales in Ordovician times

In early Ordovician times, southern Britain and southern parts of Ireland were separated from northern Britain and northern parts of Ireland by the Iapetus Ocean. Southern Britain, including Wales, at this time was situated on the northern margin of a continent called Gondwana, and northern Britain was situated on the southern margin of a continent called Laurentia (Cocks & Fortey, 1982; Pickering *et al.*, 1988).

Cocks and Fortey (1982), using faunal and sedimentary evidence, placed Gondwana at high southern latitudes in Arenig times, and Laurentia at equatorial to low southern latitudes. They also placed a third continent, called 'Baltica', at mid southern latitudes to the east of Gondwana. The Iapetus Ocean therefore separated Laurentia from both Gondwana and Baltica, which in turn were separated by Tornquist's Sea, an eastern limb of the Iapetus Ocean (Cocks & Fortey, 1982; Fortey & Cocks, 1988) (Figure 2.2).

During later Ordovician times, southern Britain formed a microcontinent known as Avalonia, which appears to have separated from Gondwana and to have migrated across the Iapetus Ocean. Baltica also drifted north while Laurentia to a much lesser extent drifted south (Cocks & Fortey, 1982; Pickering *et al.*, 1988). The latitudes suggested by the faunal and sedimentary evidence are generally

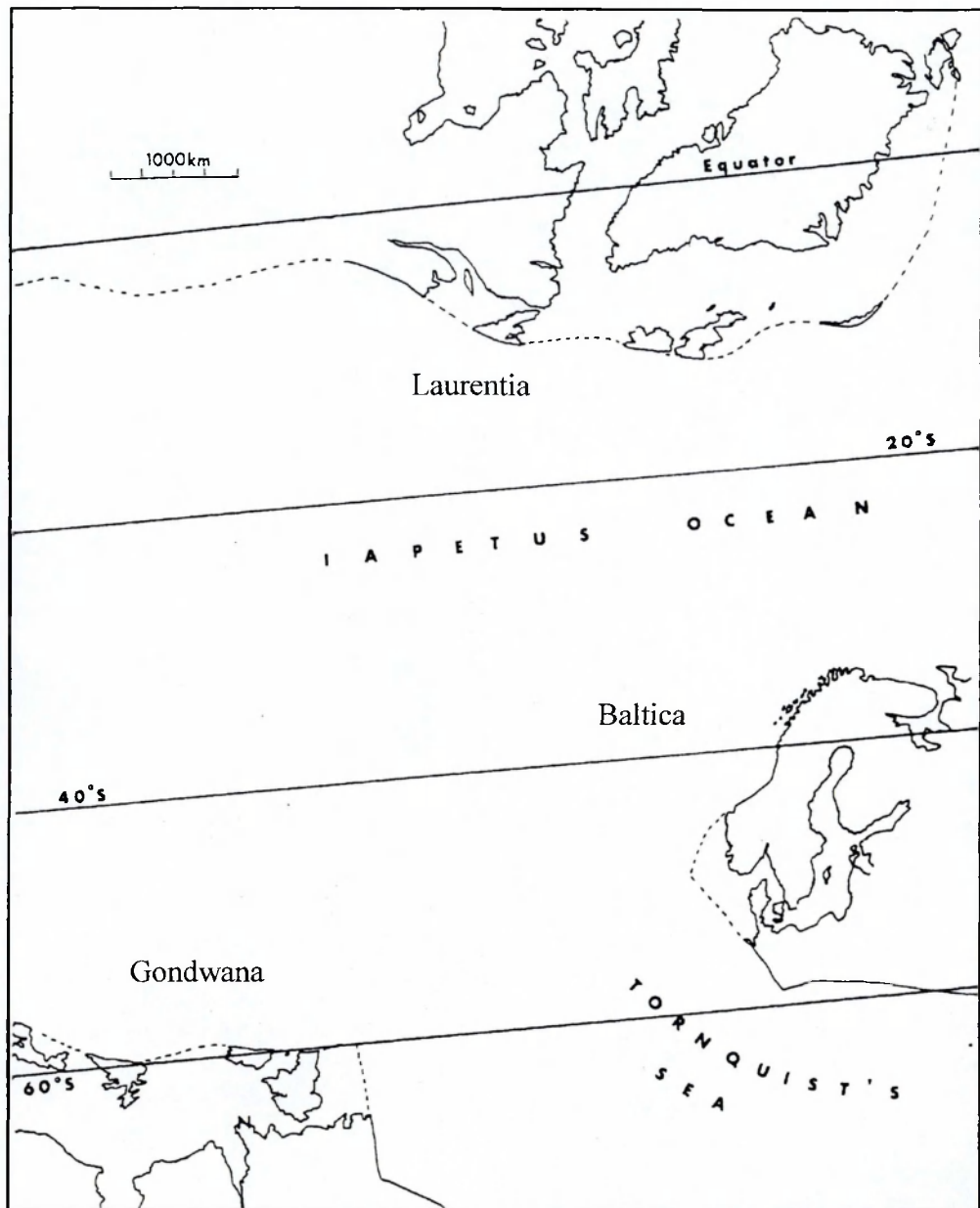


Figure 2.2. The location of the continents Gondwana, including southern Britain, Laurentia and Baltica in Arenig times. (From Fortey & Cocks, 1982).

supported by palaeomagnetic studies (Scotese & McKerrow, 1990). These movements resulted in a three plate collision between the continents of Laurentia and Baltica and the microcontinent of Avalonia in what is known as the Caledonian Orogeny (Soper & Hutton, 1984; Pickering *et al.*, 1988). This collision is variably thought to have occurred in late Ordovician (Pickering *et al.*, 1988), Silurian (Soper & Woodcock, 1990) or early Devonian times (Soper & Hutton, 1984; McKerrow, 1988).

Most models suggest that Avalonia collided first with Baltica, closing the Tornquist's Sea, and that Baltica and Avalonia then collided with Laurentia. However, Soper *et al.* (1992) suggested that Baltica and Laurentia collided obliquely, with major sinistral strike slip movement in mid-Silurian times, and that the western part of Avalonia (Newfoundland) docked sinistrally with Laurentia, while the eastern part of Avalonia (southern Britain) rotated towards the Scottish corner of Laurentia into a re-entrant between Laurentia and Baltica.

Across Britain the site of closure is marked by the Iapetus Suture, which lies roughly between the Southern Uplands and northern England. The suture runs in a line approximately from the Solway Firth to the Shannon Estuary, the Solway - Navan - Silvermines line (Soper & Hutton, 1984). It cannot be defined exactly as it is located in a region where Silurian turbidites were being deposited during final closure and it is further obscured by post-Silurian cover (Soper & Hutton, 1984).

The closure of the Iapetus Ocean is thought to have been due to the subduction of oceanic lithosphere at both margins (Fitton *et al.*, 1982). The Ordovician and Silurian sedimentary and volcanic rocks of Wales were deposited in a basin on the northwest margin of Avalonia. The Caradoc volcanism in north Wales and the related intrusions, including the Penmaenmawr Intrusion, are therefore considered to be related to a destructive plate boundary where an oceanic plate was being consumed by subduction under a continental plate.

2.4. The Welsh Basin

In early Palaeozoic times, southern Britain was the site of a northwest facing continental margin to the Iapetus Ocean. This margin has been divided into two parts, an southeastern, inboard platform, including the Midland Platform of Shropshire, the Malverns and the East Midlands of England, and a northwestward, outboard zone consisting of a series of structural basins, including the Welsh and the Lake District - Leinster basins (Anderson & Cameron, 1979; Schwab *et al.*, 1988; Woodward and Strachan, 2000).

The area now occupied by Wales was a marine basin in which both shallow and deep water sediments were deposited and volcanism occurred at various centres at different times across the basin (Kokelaar *et al.*, 1984). The basin comprised an area of approximately 200 x 100 km and was flanked to the northwest by the Irish Sea Horst and to the southeast by the Midland Platform (Anderton *et al.*, 1979).

Sedimentation and volcanism in the basin were influenced by northeast-southwest trending faults, which also defined the northwest and southeast margins of the basin (Kokelaar *et al.*, 1984). In the northwest the Menai Straits Fault System separated the Welsh Basin from the Irish Sea Horst and in the southeast the Church Stretton - Carreg Cennon fault system separated the Welsh Basin from the Midland Platform (see Figure 2.3). Kokelaar (1988) also identified north-south trending faults and suggested that the Caradoc volcanism in central and northern Snowdonia resulted from an east-west extension of the north-south trending faults, which were subsequently rotated clockwise during later deformation.

The Welsh Basin was underlain by a Precambrian basement (Shackleton, 1954; Fitton *et al.*, 1982), which was formed in a late Precambrian orogenic episode at about 600Ma by the growth and accretion of sedimentary and igneous rocks from small ocean basins and volcanic arcs (Thorpe, 1979). The Precambrian basement has been estimated to be younger than about 900Ma (Thorpe *et al.*, 1984) and underlies a large part of central and southern England (Rast *et al.*, 1988). The remnants of this Precambrian basement are exposed on Anglesey and as scattered inliers along an arcuate, tectonically controlled zone through the Welsh

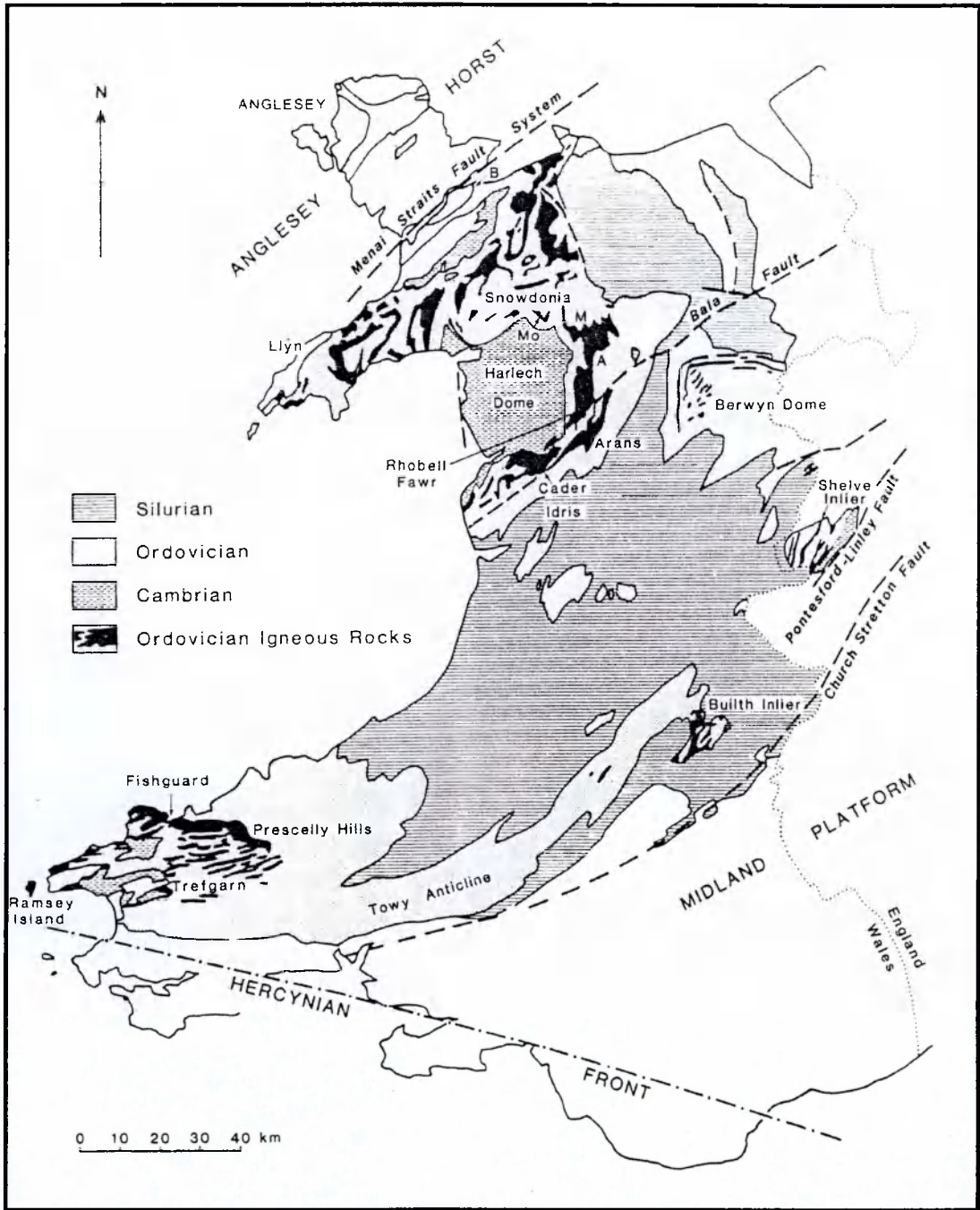


Figure 2.3. Simplified geological map of Wales showing the Welsh Basin between the Menai Straits Fault System and the Church Stretton and Pontesford-Linley Fault System. (From Kokelaar *et al.*, 1984).

Borderland into south Wales (Thorpe, 1979; Rast *et al.*, 1988; Gibbons & Harris, 1994). The Lake District-Leinster Basin was situated further to the northwest, beyond the Irish Sea Horst. The presence of Ordovician tholeiitic and calc-alkaline volcanic rocks in the Lake District has been taken to suggest that an island arc developed along the south-eastern margin of the Iapetus Ocean in this basin during Ordovician times (Fitton *et al.*, 1982). This places the Welsh Basin in a back-arc setting (Kokelaar *et al.*, 1984). Bevins *et al.* (1984), using petrological and geochemical criteria, supported this view and connected the beginning of extension and back arc conditions with a marine transgression in Arenig times.

The Caradoc volcanic rocks of north Wales, and thus the Penmaenmawr Intrusion, are therefore associated with a marginal basin, developed on immature continental crust in a back-arc setting where extension occurred although no oceanic lithosphere was formed.

2.5. Sedimentation in the Welsh Basin

During early Cambrian times, sedimentation in the Welsh Basin was mainly restricted to small fault-bound basins, which became progressively less complex with infilling and merging. Variations in lithologies however indicate that there was some local uplift related to intermittent reactivation of the basement fractures (Howells *et al.*, 1991). In late Tremadoc times a major episode of tectonism and volcanism terminated the Cambrian basinal sedimentation, and a widespread Arenig transgression took place that reflected a distinct change in tectonic conditions and heralded the development of the Ordovician marginal basin (Kokelaar *et al.*, 1984).

The Ordovician basin of Wales was predominantly the site of marine sedimentation, partly on shallow shelves and partly in deeper water with the demarcation of a shelf to slope transition. The general trend was from shallow water conditions in the Arenig times, with the deposition of sands, through transgression, to deepening water levels and the deposition of monotonous sequences of graptolite-bearing muds and silts in late Caradoc times (Howells *et al.*, 1983; Kokelaar *et al.*, 1984).

Topographic relief within the basin, due to contemporaneous movement along normal faults with northeast-southwest trends, produced marked facies variations (Kokelaar *et al.*, 1984). The fault system also greatly influenced the extensive volcanism that occurred in the Welsh Basin, which was essentially continuous from late Tremadoc times through to late Caradoc times (Allen, 1982).

By late Caradoc to early Ashgill times graptolitic muds were being deposited over much of the Welsh Basin area. Widespread subsidence occurred, and in the central parts of the Welsh Basin sedimentation was more or less continuous to the end of the Silurian. Volcanism was not renewed except in marginal areas far to the south of earlier activity (Allen, 1982). In the Silurian (Llandovery to Wenlock), sedimentation was dominated by the development of submarine fan complexes which gave way to a widespread shallow marine progradation during Ludlow times, finally infilling of the basin prior to Devonian molasse deposition (Howells *et al.*, 1991).

Compression and uplift occurred in early to mid Devonian times. The Lower Palaeozoic rocks of Wales were folded and metamorphosed during the Acadian phase of the Caledonian Orogeny (Soper *et al.*, 1987) and are usually characterised by upright folds and cleavage, together with low grade regional metamorphism (Coward & Siddons, 1979; Bevins & Rowbotham, 1983).

Caradoc volcanism and associated intrusions, in north Wales were therefore part of a continuous process that infilled a marine basin throughout Lower Palaeozoic times. The rocks, including the Penmaenmawr Intrusion, were then raised, folded and metamorphosed.

2.6. Volcanism in the Welsh Basin

Lower Palaeozoic times witnessed a period of intense volcanic activity around the southeastern margin of the Iapetus Ocean and there are extensive thicknesses of volcanic rocks among the Ordovician and Silurian strata in the Lake District, the Welsh Basin, and eastern and southeastern Ireland (Fitton *et al.*, 1982; Stillman, 2001).

In the Welsh Basin, volcanicity was both extensive in time and space and varied in character. The bulk of the activity took place in Ordovician times. The volcanic rocks have been divided into three distinct geochemical groups (Fitton *et al.*, 1982), which are summarised below.

The Rhobell Fawr Volcanic Group, which occurs to the south and east of the Harlech Dome, is of Tremadoc age and shows geochemical affinities with island arc tholeiitic suites (Kokelaar, 1979). Kokelaar *et al.* (1984) considered that the Rhobell Fawr Volcanic Group, together with the Trefgarn Volcanic Group in south Wales and the common occurrence of igneous rock clasts in the lowermost Arenig strata of north Wales, indicate that there was an extensive volcanic arc in the Welsh Basin in late Tremadoc times, marking the onset of the southeasterly subduction of Iapetus lithosphere.

The major group of Ordovician igneous rocks crops out in south, mid and north Wales and comprise a variety of basalts, chiefly tholeiitic but some with calc-alkaline affinities, and abundant rhyolites. The major period of Ordovician volcanism occurred from the Arenig to the Caradoc and includes the Llewelyn Volcanic Group. The rocks consist mainly of bimodal basalt-rhyolite suites and presence of tholeiitic basalts, with transitional ocean floor to arc-like compositions, is characteristic of basalts emplaced in back arc marginal basement environments (Kokelaar *et al.*, 1984; Saunders & Tarney, 1984).

The acid and basic rocks that comprise the bimodal basalt-rhyolite suites appear to be geochemically and probably petrogenetically distinct and although mixing of the two is known, it is not common (Howells *et al.*, 1991). The tholeiites were presumably mantle-derived while the acidic extrusives have variably been considered to be derived by partial fusion of the continental crust (Allen, 1982), or generated by fractional crystallisation of more basic magmas (Bevins *et al.*, 1994).

The youngest volcanic rocks in the Welsh Basin are the Skomer Volcanic Group in south Wales, which are thought to be of early Silurian age. They comprise a hawaiite-mugearite group and two groups of acid lavas/ignimbrites. They have dominantly within plate chemical characteristics but show some minor chemical

evidence for the influence of contemporaneous or earlier subduction. It has been suggested that they reflect a change from subduction related to within plate volcanism in Wales, after the termination of Caledonian subduction in this part of the orogenic belt (Thorpe *et al.*, 1989).

Bevins *et al.* (1984) suggested that the Welsh Basin represents a change in tectonic setting from an ensialic volcanic arc to a marginal basin. The Tremadoc volcanism is considered to reflect the onset of a period of major southerly subduction of the Iapetus Ocean and the development of a volcanic arc while the Arenig transgression is thought to represent the beginning of extension and back arc conditions in the Welsh Basin, with the focus of island arc volcanism becoming established to the north, in the Lake District-Leinster zone of the Caledonides.

Gibbons and Young (1999) suggested that the mid Caradoc volcanicity of North Wales, including the Llewelyn Volcanic Group, represented the climax of 38 Ma of arc magmatism and its sudden cessation records a change from oblique subduction to transcurrent movements along this part of the Iapetus Ocean.

The Llewelyn Volcanic Group, including the Penmaenmawr Intrusion, is therefore part of a volcanic evolution within the Welsh Basin, reflecting the progression of subduction of the Iapetus Ocean, from a volcanic arc through a back arc basin to within plate tectonic settings. The Llewelyn Volcanic Group, and hence the Penmaenmawr Intrusion, developed during the back arc basin stage of that evolution.

CHAPTER 3. LOCAL AND FIELD GEOLOGY OF THE PENMAENMAWR INTRUSION

3.1. Introduction

This chapter briefly describes the general geology of the area around the Penmaenmawr Intrusion, and includes a brief description of representative rock samples collected from the intrusion, as well as structures within the intrusion. It also outlines the sampling methodology used in this study and presents an outline plan showing the locations of the samples collected.

3.2. General geology of the area around the Penmaenmawr Intrusion

A simplified geological sketch map of the Penmaenmawr region is presented in Figure 3.1. It shows the oval outline of the Penmaenmawr Intrusion, the two smaller plug-like intrusions at Garreg Fawr and Dinas, and the surrounding strata. These intrusions have been emplaced into the Nant Ffrancon Formation, which is Ordovician (Arenig to early Caradoc) in age (British Geological Survey, 1985).

The Nant Ffrancon Formation consists of blue-black shales and mudstones which dip at between 38°-40° towards the southeast (Roberts, 1979; British Geological Survey, 1985). Towards the top of the formation there are thin outcrops of basic tuff, which are some of the earliest products of Caradoc volcanism in northern Snowdonia (Howells *et al.*, 1985). The Nant Ffrancon Formation is overlain to the southeast by the Conway Rhyolite Formation, which consists of rhyolite lavas and acidic ash-flow tuffs. This formation is considered to be one of the penecontemporaneous formations of the Llewelyn Volcanic Group, which represents the first stage of Caradoc volcanic activity in North Wales (Ball & Merriman, 1989), the so-called "first eruptive cycle" of Howells *et al.* (1991).

The Conway Rhyolite is overlain by the Capel Curig Volcanic Formation which is the most extensive formation of the Llewelyn Volcanic Group (Ball and Merriman, 1989). The Capel Curig Volcanic Formation consists of voluminous ash-flow tuffs and crops out extensively in northern and eastern Snowdonia (Howells *et al.*, 1991). Howells & Leveridge (1980) suggested that these outcrops of ash-flow

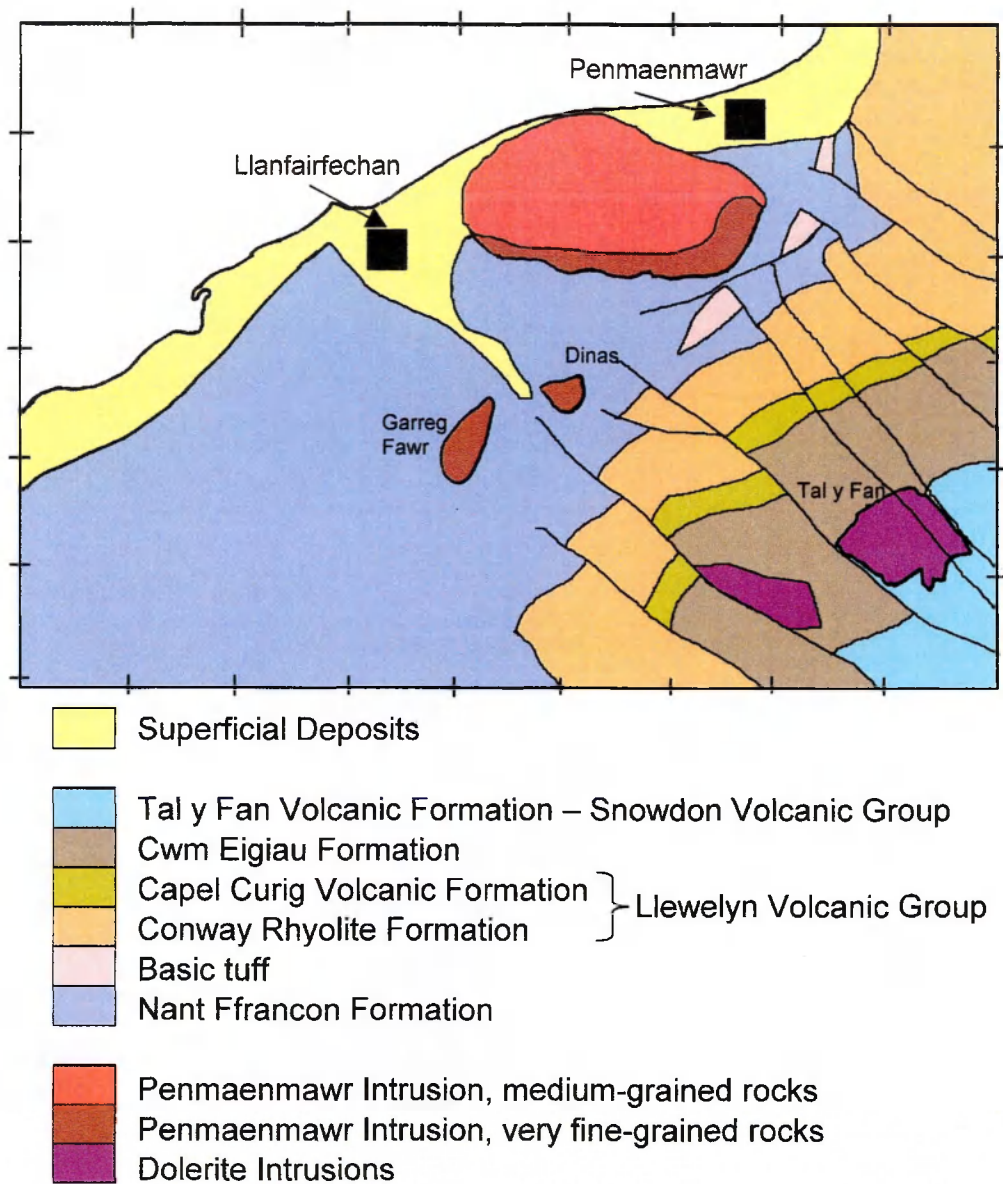


Figure 3.1. Geological sketch map showing the Penmaenmawr Intrusion and the simplified geology of the immediately surrounding area. Based on the British Geological Survey, sheet 106, Bangor.

tuffs in the northern part of Snowdonia were erupted from a volcanic centre to the north-east of the Penmaenmawr Intrusion, just off the present north Wales coast.

The Capel Curig Formation comprising of acidic ash-flow tuffs is taken to be the final phase of the Llewelyn Volcanic Group and is overlain by the Cwm Eigiau Formation, which consist predominately of siliciclastic sandstones (Howells *et al.*, 1991).

The Cwm Eigiau Formation is overlain by Tal y Fan Volcanic Formation, which is the local representative of the Snowdon Volcanic Group, the second major period of volcanic activity in north Wales, the so called second eruptive cycle of Howells *et al.* (1991). The Tal y Fan Volcanic Formation consists of basalts, hyaloclastite, basaltic breccias and basic tuffs, which are intercalated with thin mudstones (Howells *et al.*, 1985). This formation is intruded by thick dolerite sills, which are considered to be coeval with the volcanic sequence (Howells *et al.*, 1991).

3.3. Field description of the Penmaenmawr Intrusion

The Penmaenmawr Intrusion consists of fine- to medium-grained, grey coloured rocks, which are very fine-grained at the eastern part and along the southern boundary of the intrusion.

The smaller intrusions at Garreg Fawr and Dinas were not included in this project, but Ball & Merriman (1989), Howells *et al.* (1991), and Tremlett (1997) reported that they are similar to the very fine-grained rocks from the margin of the Penmaenmawr Intrusion and Howells *et al.* (1985) suggested that they are probably connected to it at depth.

Throughout the intrusion there are numerous thin, pale-green veins cutting the intrusion, ranging in size from 5 to 50 mm wide with sharp, straight contacts with the host rock of the intrusion. Within the central part of the intrusion there are a number of very pale, almost white, segregations. These segregations form irregularly-shaped veins and pods up to 30 cm wide.

The contact between the intrusion and the country rock is, in most cases, hidden being only visible at the southeast margin of the intrusion. Here the cleavage dips at about 70° towards the east. However due to the baking of the shales and the

very fine-grained texture of the intrusion it is difficult to determine the exact junction between the two with any certainty. Roberts (1979) reported that the intrusion appeared to be a vertical plug like mass and Tremlett (1997), based on the straight course of the southern edge suggested that the intrusion has faulted margins on both the southern and the northern boundaries.

3.4. Penmaenmawr Lithologies

Rocks from the Penmaenmawr Intrusion range from pale to dark grey in colour and most are fine- to medium-grained, with grain size ranging from 0.2 to 1 mm. Along the eastern margin of the intrusion, and extending along the southern boundary, very fine-grained rocks occur. These have a grain size of approximately 0.05mm, and break with a conchoidal fracture. Away from these margins, the grain size gradually becomes coarser and reaches an average grain size of between 0.1 - 0.2 mm at a distance of about 40 m in from the margin. These very fine-grained margins represent magma that has cooled quickly, probably in contact with cold country rocks. The fine- to medium-grained rocks away from the margins, represent magma that cooled more slowly, which suggests that it was insulated from the cold country rocks by the cooling marginal rocks.

The paler grey, medium-grained rocks from the central part of the intrusion can be seen to consist of white plagioclase feldspar and dark ferromagnesian crystals. The rocks from the western part of the intrusion are noticeably darker grey in colour than those from the central part of the intrusion due to the darker colour of the ferromagnesian minerals. The paler colour of the ferromagnesian minerals in the rocks from the central part of the intrusion suggests that the rocks have been altered and the original ferromagnesian minerals, such as pyroxenes, may have been replaced by paler minerals, such as chlorite. The rocks from the eastern and southern margins are dark grey and very fine-grained so that individual crystals are not visible in hand specimen. They contain sparse, small (0.5-2 mm) phenocrysts of white plagioclase feldspar and dark ferromagnesian minerals.

The intrusion has been extensively quarried over the years and rocks from most exposures lack surface weathering. However, away from the quarried areas, the exposed surfaces have an irregular weathered surface layer.

3.5. Veins, segregations and inclusions

The thin, pale-green veins are dominated by quartz and the sharp, straight contacts suggest that they formed after the magma had solidified. Associated with these veins, and generally more abundant within the very fine-grained rocks from the eastern quarries, are very thin veins of axinite, often seen as a sheet of small pink, platy crystals on joint surfaces.

The segregations (see Figure 3.2) from the central part of the intrusion contain coarse, 2 mm size, crystals of quartz and black green ferromagnesian minerals. The irregular boundaries between the segregations and the host rock of the intrusion suggest, however, that they did not form at the same time as the veins, and their irregular boundaries may indicate that the magma was not completely solidified when the segregations were formed.

Rounded, dark grey inclusions (see Figure 3.3), which range in diameter from 5 mm to 100 mm, also occur, and are commonly found in the central part of the intrusion. These inclusions can be seen more easily on freshly quarried rock faces and may only appear to be more abundant in those areas; however, they often occur in association with the pale segregations described above.

3.6. Structures

Throughout the central part of the Penmaenmawr Intrusion there are vertical fault zones, generally less than 1 m wide, filled with a pale-grey clay material (Figures 3.4a and 3.4b). These fault zones generally trend either northeast-southwest or northwest-southeast. A number of faults and shear zones have also been identified from geological and geophysical surveys and bore hole data (S Penn Associates, 1991, unpublished report). Seismic data, presented in this unpublished work, allowed division of the intrusion into 3 zones (presented in Figure 3.5), the boundaries of which are marked by two major tectonic shear zones. Zone A is in the western part of the intrusion and is topographically lower than Zone B, the part of the intrusion currently being worked. It consists of massive unaltered rock with widely spaced fractures and shears. Zone B lies in the central part of the intrusion and forms a wedge of rock narrowing to the south.

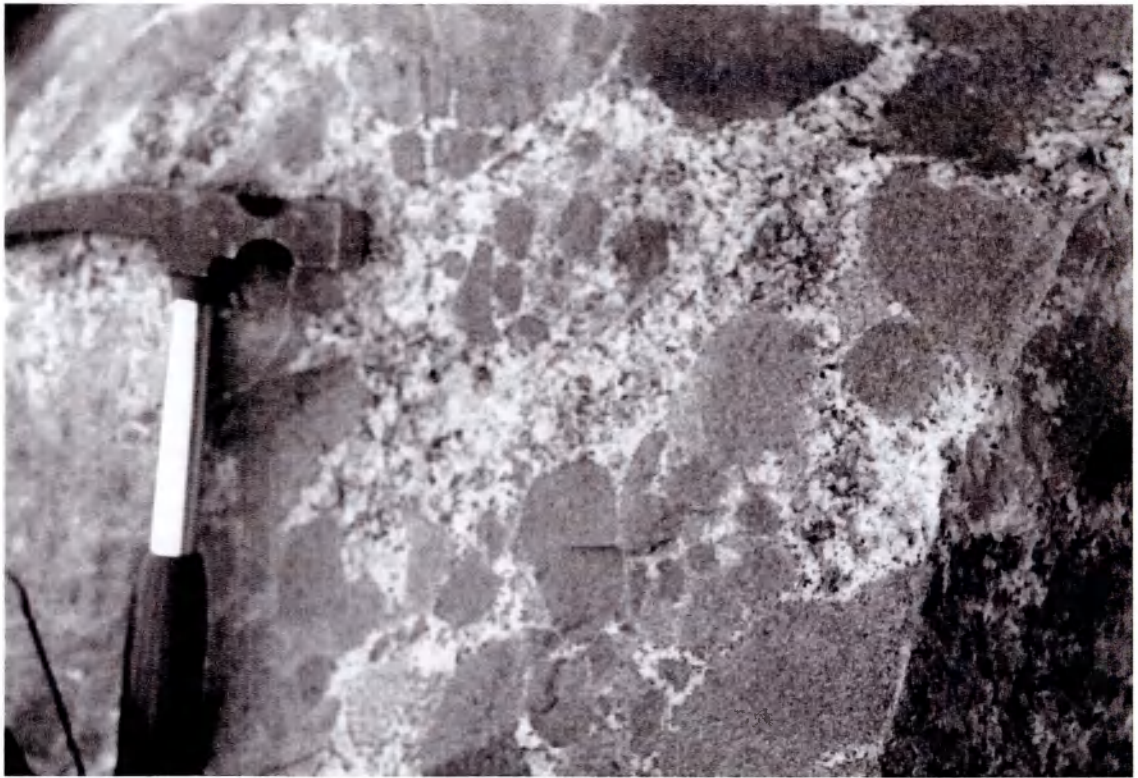


Figure 3.2. (Upper photograph). An irregular segregation from the Central Quarries of the Penmaenmawr Intrusion.

Figure 3.3. (Lower photograph). A series of inclusions in a hand specimen from the Central Quarries of the Penmaenmawr Intrusion.



Figure 3.4a. (Upper photograph). Vertical fault or joint planes approximately 650 mm wide, filled with pale-grey material from the Central Quarries of the Penmaenmawr Intrusion.

Figure 3.4b. (Lower photograph). Vertical fault or joint planes approximately 800 mm wide, filled with pale-grey material from the Central Quarries of the Penmaenmawr Intrusion.

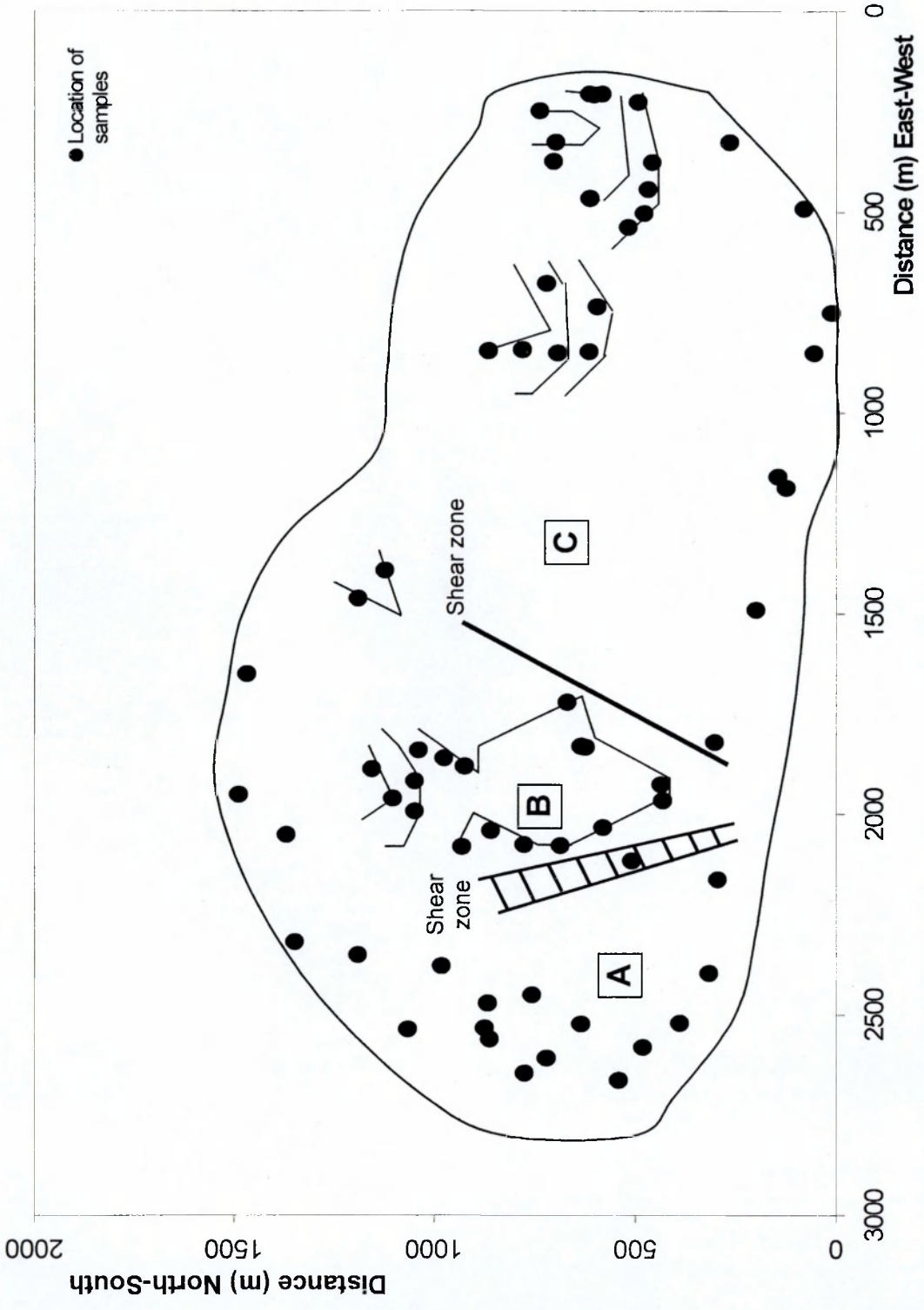


Figure 3.5. An outline plan of the Penmaenmawr Intrusion showing the shear zones and zones A, B and C identified by S. Penn Associates (1991). Also shown are the main quarry faces and the location of samples which are discussed in Section 3.7.

Zone C lies to the east of the current working quarry, and, like zone A, is topographically lower than Zone B. Between Zone A and Zone B there is a wide, north-northwest – south-southeast trending shear zone, up to 90 m wide, with shattered rock and closely-spaced fractures; between Zone C and Zone B there is a further shear zone, this time trending north-northeast – south-southwest.

These faults and shear planes suggest that there have been some considerable earth movements, which caused the intrusion to break and shear. These earth movements must have occurred after the intrusion had solidified and may be related to the regional deformation in north Wales, which is considered to have occurred in early to mid Devonian times (the Acadian phase of the Caledonian Orogeny).

3.7. Sampling methodology

During this investigation seventy samples were collected from the Penmaenmawr Intrusion, for mineralogical and geochemical examination. They were collected from as wide an area as possible in order to establish the range of both lateral and vertical variations in mineralogy and geochemistry within the intrusion. Most of the available rock exposure was linked to quarrying activities, and hence the majority of samples were collected from either disused or working quarry areas. Complete coverage of the intrusion, however, was not possible due to the lack of exposure, some of which is due to recent landscaping by quarry operators. Figure 3.6 presents an outline plan of the intrusion, showing the main quarry faces and locations of the samples collected.

The details of the samples collected were recorded in a pre-numbered log-book which began with number 2901. The samples were numbered consecutively and were prefixed with JD to allow for identification and traceability. Figure 3.6 presents an outline plan of the intrusion with the location of the samples identified by the last two digits of their identification number. Five figure map references and the heights above sea level for the samples are presented in Appendix 12. Samples will be added to the Rock Collection of the National Museums and Galleries of Wales.

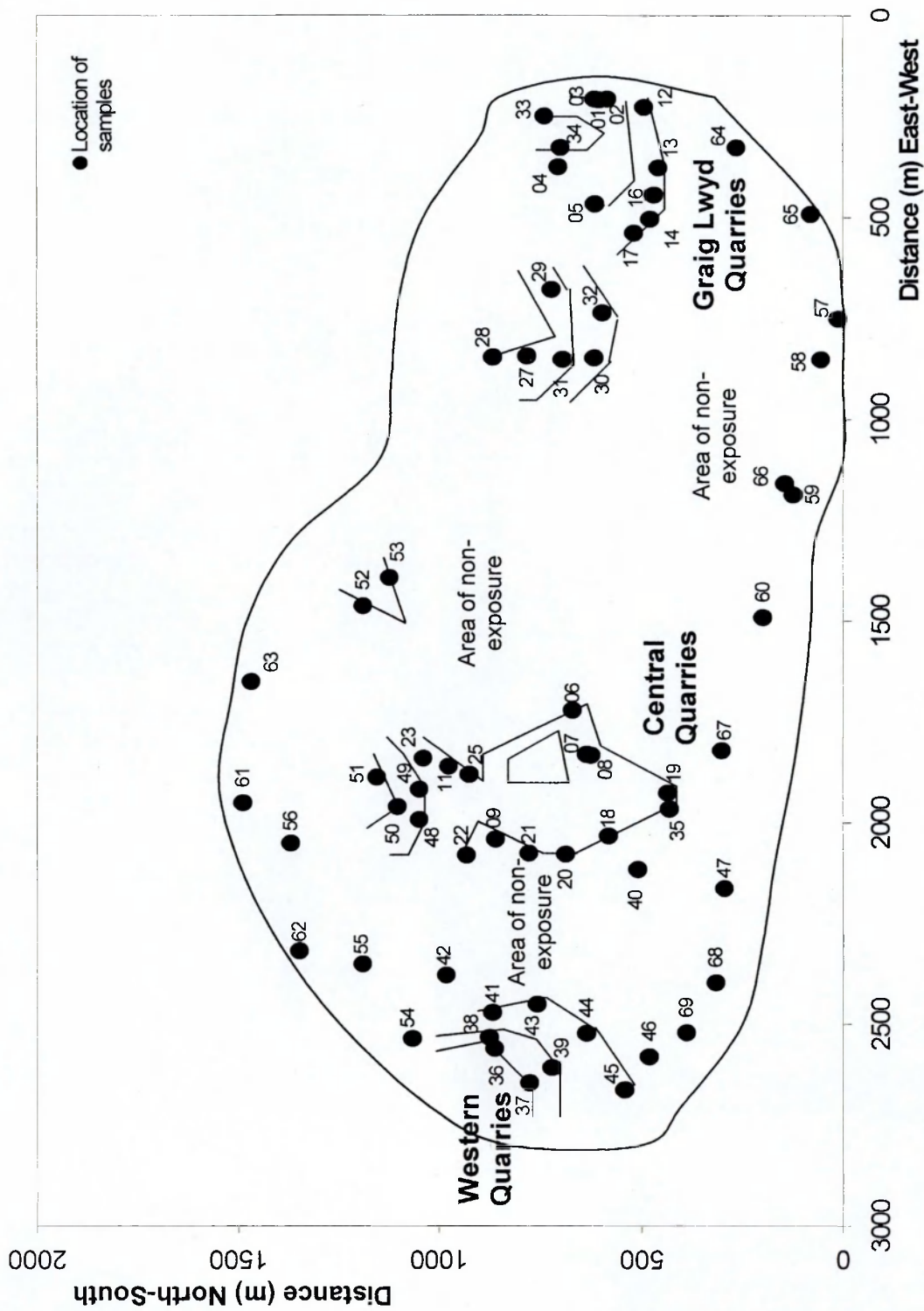


Figure 3.6. An outline plan of the Penmaenmawr Intrusion showing the quarry faces and the locations of the samples utilised in this study with their identification numbers.

CHAPTER 4. THE PETROGRAPHY OF THE PENMAENMAWR INTRUSION

4.1. Introduction

In Chapter 3 it was reported that seventy samples were collected from the Penmaenmawr Intrusion for mineralogical and geochemical examination. Petrographic thin sections were obtained for all 70 samples, which were examined using a Meija Labax, PTM 1A/05, petrological microscope. This chapter describes the main differences in mineralogy within the intrusion based on this examination, and uses the differences in texture and mineralogy to divide the intrusion into four distinct 'Groups'. A summary of the mineralogy of the samples is tabulated in Appendix 1 and representative photomicrographs are presented in Appendix 2.

The sections below are structured on the three areas associated with the main quarry exposures, the Western Quarries, the Central Quarries and the Graig Lwyd Quarries, as presented in Figure 3.6. Samples collected from areas adjacent to the southern Boundary have been included with the samples from the Graig Lwyd Quarries as they have similar petrographic textures.

4.2. Rocks from the Western Quarries

The rocks from the western part of the intrusion appear to be the least altered rocks of the intrusion. Principally, they contain plagioclase feldspar, orthopyroxene and clinopyroxene. Plagioclase feldspar occurs as subhedral rectangular laths, most of which are between 0.3 and 0.5 mm in length and 0.1 mm in width. Occasional larger crystals, 1-1.5 mm in length, occur and these often contain very small crystals of prehnite and/or pumpellyite in their cores. Orthopyroxene occurs in the unaltered rocks mainly as elongated rectangular crystals 0.1 – 0.5 mm in length and between 0.1 and 0.2 mm in width. These crystals have well-developed cleavage lines parallel to their long axes. In the more altered samples, orthopyroxene is partially replaced by a pale-green fibrous amphibole, particularly towards the ends of the long axes of the crystals, and in the most altered samples orthopyroxene has been completely replaced

by amphibole. Clinopyroxene occurs as stubby, often anhedral crystals, sometimes rectangular, between 0.2 and 0.3 mm in length, and between 0.1 and 0.2 mm in width. Larger clinopyroxene crystals tend to have a more irregular and embayed form.

A modal estimate for these samples is 60% plagioclase feldspar, 15% clinopyroxene and 25% orthopyroxene. Accessory minerals include quartz, which in most cases has a granophyric texture, and biotite, which occurs as small, 0.1-0.2 mm, anhedral plates with irregular and embayed crystal faces, and in many instances is partially replaced by chlorite. Additional accessory minerals include ilmenite and apatite. Samples collected towards the northern and the southern boundaries are richer in biotite, reaching an estimated 5% of the mode at these locations.

Photomicrographs and a description of a typical sample from the Western Quarries, JD2936, are presented in Appendix 2.

4.3. Rocks from the Central Quarries

The rocks become progressively altered towards the east of the intrusion and in rocks from the northern part of the Central Quarries orthopyroxene is completely replaced by green crystals of fibrous amphibole. Most small amphibole crystals are rectangular in shape and measure approximately 0.3 by 0.1 mm in size. Occasional elongate crystals of amphibole occur, up to 2 mm in length, which often show a change of orientation along their long axes, which could be the result of two crystals growing into each other. Plagioclase feldspar crystals are turbid when viewed in plane polarised light, while biotite is replaced by chlorite. In some samples alkali feldspar occurs as subhedral crystals with well-developed crystal faces, forming an estimated modal content of 5% of the rock. The well-developed crystal faces of the alkali feldspar crystals are in contrast to the irregular and embayed faces of the other minerals, suggesting that they are secondary after plagioclase feldspar.

Photomicrographs and a description of a typical sample from the northern Central Quarries, JD2951, are presented in Appendix 2.

In the main part of the Central Quarries the degree of alteration of the rocks is more intense. Orthopyroxene, amphibole and biotite have been replaced by pale-green, anhedral chlorite, which has an irregular outline. The shape of the chlorite crystals is variable, sometimes rectangular, representing a pseudomorph after fibrous amphibole, sometimes equant, but in most cases occurring as irregular areas of uncertain origin. Plagioclase feldspar is turbid when viewed in plane polarised light, and the multiple twinning is partially obscured when viewed in crossed polarised light. Some crystals of plagioclase feldspar are completely sericitised. Quartz occurs in greater abundance than in the rocks from the Western Quarries, forming anhedral, equant crystals in the range 0.2-0.5 mm in size and only occasionally showing granophyric texture. Prehnite and pumpellyite are more dominant in replacing plagioclase feldspar, and epidote is also present, often associated with clinopyroxene. In some samples epidote accounts for up to 2% of the mode of the rock. Alkali feldspar occurs in small amounts associated with plagioclase feldspar and often has turbid cores.

A modal estimate of the composition of these rocks is 40-50% plagioclase feldspar, 30-40% secondary chlorite, 10-20% clinopyroxene and 5-10% quartz. Additional minerals in minor amounts include ilmenite, pseudomorphed by titanite, and apatite. Small green to brown amphiboles occur in some samples, generally surrounded by and altering to chlorite.

Photomicrographs and a description of a typical sample from the main part of Central Quarries, JD2918, are presented in Appendix 2.

4.4. Rocks from the Graig Lwyd Quarries and adjacent to the southern boundary

Rocks from the Graig Lwyd Quarries, and from a band 50 m wide adjacent to the southern boundary of the intrusion, are very fine-grained, with average crystal sizes in the range 0.02-0.05 mm. In most samples phenocrysts account for less than 5% of the rock, but in samples from the western part of the southern boundary they can account for up to 10% of the rock.

The most frequently occurring phenocrysts are plagioclase feldspar, occurring as euhedral to subhedral rectangular crystals, 0.5-2 mm in length and 0.1-0.5

mm in width, which in most cases are filled with dark indeterminate secondary material. Clinopyroxene also occurs as phenocrysts, chiefly as small crystals grouped together to form larger glomerocrysts up to 0.5 mm in size. Orthopyroxene is present as a phenocryst phase in four samples only, and occurs as small, subhedral, rectangular crystals 0.3-0.5 mm in length. In most samples, however, it has been replaced by chlorite or, occasionally, amphibole. More rarely, quartz, biotite and ilmenite have been found as rare phenocryst phases. All of the phenocrysts are set in a groundmass of lath-like plagioclase feldspar, pyroxene, amphibole and ilmenite.

Photomicrographs and a description of two typical samples from the Graig Lwyd quarries, JD2934 and JD2912, are presented in Appendix 2.

Away from the margin of the intrusion the rocks become progressively coarser grained. At about 400 m from the margin, the rocks have an average grain size of between 0.1 and 0.25 mm and have an estimated modal composition of 45-55% plagioclase feldspar, 30-35% chlorite, 10-20% clinopyroxene and 5-10% quartz with graphic intergrowths. Accessory minerals include ilmenite and apatite. Epidote occurs as a secondary mineral in some samples. In two samples collected from the central part of the southern margin, biotite accounts for up to 5% of the mode of the rocks and amphibole occurs as brown to green anhedral crystals, which are not fibrous in form, unlike the amphiboles from elsewhere in the intrusion.

In a series of small quarries, to the north-west of the Graig Lwyd Quarries, the rocks tend to contain greater amounts of quartz than other samples from the intrusion and in these rocks both amphibole and chlorite are present; in some samples chlorite can be seen to be pseudomorphing fibrous amphibole. Samples from these quarries often contain small (5-10 mm), rounded inclusions composed of fine-grained, equigranular crystals mainly of clinopyroxene and plagioclase feldspar.

Photomicrographs and a description of a typical sample from the quarries to the north-west of the Graig Lwyd Quarries, JD2932, are presented in Appendix 2.

4.5. Veins, segregations and inclusions

The thin (5-50 mm), pale-green veins, which are present throughout the intrusion, consist essentially of quartz, occurring as small equigranular crystals up to 0.1 mm in size, intermixed with darker patches made up of aggregates of minute pumpellyite crystals. Rarer, large crystals of quartz up to 1 mm in size also occur and are typically surrounded by small, 0.05 mm sized crystals of pumpellyite and prehnite. Quartz also occurs as occasional 1 mm sized crystals showing a radiating granophyric texture.

The pale segregations which occur within the central part of the intrusion consist of large crystals, generally 2 mm in size, of granophyric quartz, where the alkali feldspar has been replaced by aggregates of pumpellyite crystals and chlorite, the latter occurring as large, irregular-shaped masses. Plagioclase feldspar occurs as infrequent, subhedral crystals, 2 mm across and square or rectangular in shape, in which there are patches altering to small crystals of prehnite and pumpellyite. Clinopyroxene is also infrequent and occurs as anhedral, rectangular crystals commonly with embayments to crystal faces. A modal estimate of the segregations is 70% granophyric quartz, 20% chlorite, 5% plagioclase feldspar and 5% clinopyroxene. Titanite is present as a secondary mineral.

Photomicrographs and a description of a segregation from the Central Quarries, JD2926, are presented in Appendix 2.

The small rounded inclusions, reported in Chapter 3, consist of small, equigranular crystals of plagioclase feldspar, clinopyroxene, and amphibole, the latter partially altered to chlorite. In some inclusions the crystals are 0.1 mm in size, while, in others they reach up to 0.2 mm in size. Proportions of the ferromagnesian minerals are greater in the inclusions than in the host rock, a modal estimate of their composition being 45% plagioclase feldspar, 30% clinopyroxene and 25% amphibole. Smaller inclusions, less than 5 mm in diameter, with a similar mineralogy also occur in samples collected towards the eastern part of the intrusion.

4.6. Petrographic classification

The differences in colour, texture and mineralogy of samples from the Penmaenmawr Intrusion have been used here to classify them into four 'Groups', which define four discrete petrological sectors within the intrusion, largely separated by areas of non-exposure. This section presents details of the characteristics that have been used to classify the samples. An outline plan of the intrusion showing the four petrological sectors is presented in Figure 4.1.

4.6.1. Group 1 rocks

Group 1 rocks consist of very fine-grained, 0.02-0.05 mm, dark-grey rocks that occur at the eastern margin of the intrusion and are well exposed in the Graig Lwyd Quarries. They also crop out along the southern boundary of the intrusion, forming the prominent high ground at Clip yr Orsedd (Figure 1.1), behind the main working quarry. This southern exposure, however, is not continuous and is separated into an eastern and a western part by an area where slightly coarser-grained rocks occur (see Figure 4.1). The rocks from the western part of the southern boundary are more porphyritic than the rocks from the eastern part (up to 10% modal phenocryst content in the former area, compared with less than 5% in the latter area).

The rocks of the Graig Lwyd quarries become gradually coarser grained to the west, towards the centre of the intrusion, and samples collected 400 m from the quarry margin contain crystals up to 0.25 mm in size. The boundaries between Group 1 and Group 2 rocks in the central part of the intrusion, and between the western area of Group 1 rocks and Group 3 rocks, are not exposed. Samples JD2934 and JD2912, presented in Appendix 2, are typical of rocks from Group 1.

The two smaller plug-like intrusions that occur away from the main intrusion, at Garreg Fawr and Dinas (Figure 1.1 and Figure 3.1), are also thought to belong to

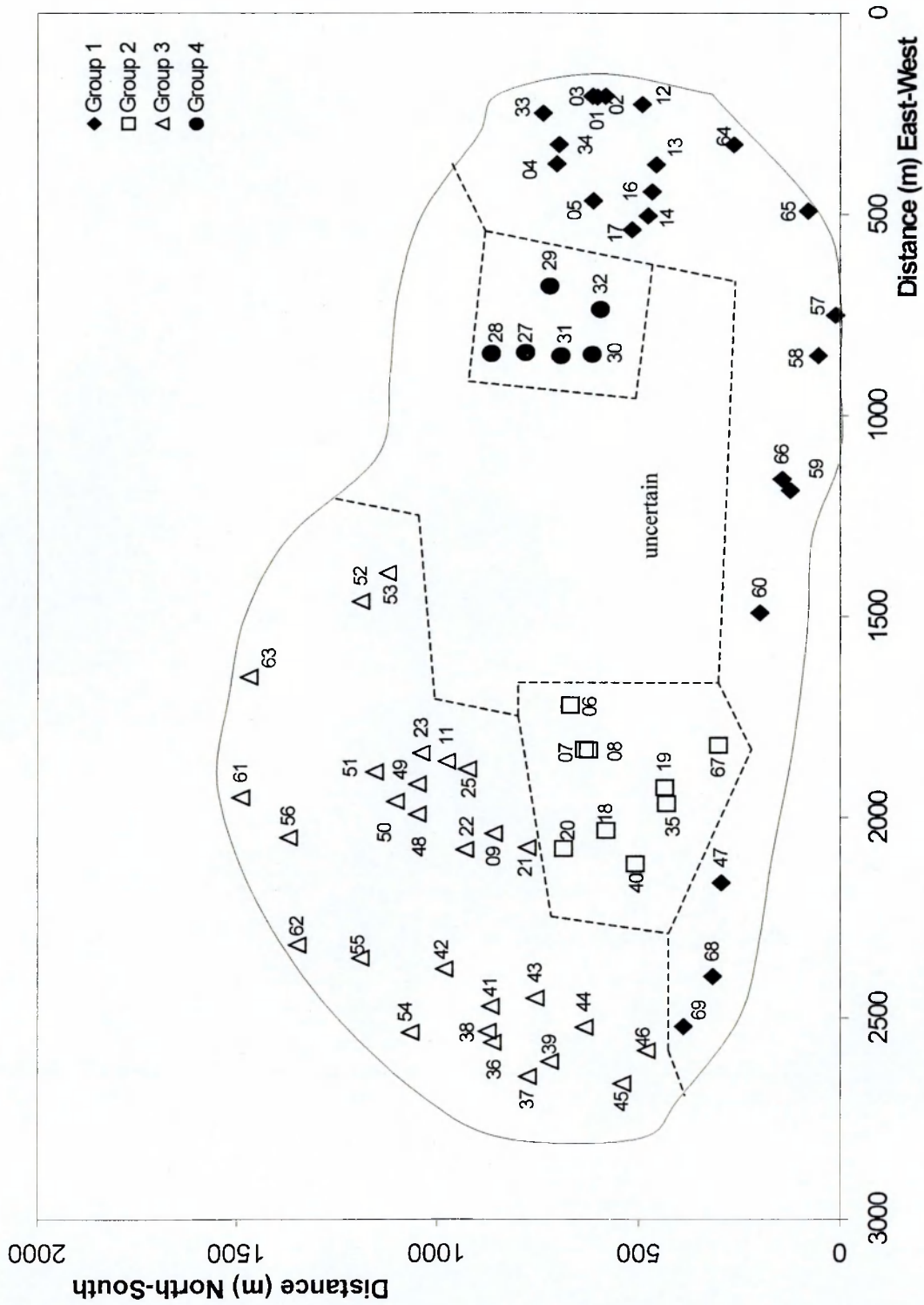


Figure 4.1. Outline plan of the Penmaenmawr Intrusion showing the location of samples utilised in this study and the areas covered by the 4 petrographic groups. The unmarked area in the centre of the intrusion is an area where there is no exposure.

Group 1. No samples from these bodies were collected during this study but their similarity, both petrographically and geochemically, to the fine-grained rocks found in the Graig Lwyd Quarries of the Penmaenmawr Intrusion, has been recognised and confirmed previously by Ball & Merriman (1989), Howells *et al.* (1991), and Tremlett (1997).

4.6.2. Group 2 rocks

This group comprises of rocks from the main Central Quarries, which, at the time of the fieldwork were being actively exploited. They are pale-grey in colour and are coarser grained than the rocks from Group 1, with crystals typically in the range of 0.2-0.5 mm. They are characterised by the presence of between 30 - 40% chlorite, which is pale-green in plane polarised light and occurs chiefly in irregularly shaped areas, but also, more rarely, forms rectangular crystals up to 0.5 mm in length, which appear to be pseudomorphs after fibrous amphibole.

Group 2 rocks are heavily altered and the plagioclase feldspars crystals are turbid when viewed in plane polarised light. They also tend to be heavily sericitised and often contain small crystals of pumpellyite and prehnite. Sample JD2918, presented in Appendix 2, is typical of Group 2 rocks.

The pale segregations and most of the rounded, dark-grey inclusions, described in Chapter 3 and Section 4.5. above, are found within the Group 2 rocks, and can be seen easily on freshly quarried surfaces.

4.6.3. Group 3 rocks

Group 3 rocks are dark-grey in colour and occur in the west and the north of the intrusion, including the Western Quarries and the northern Central Quarries. They are characterised by the presence of between 15-30% of orthopyroxene or, in most cases, green amphibole prisms replacing orthopyroxene. In a few cases orthopyroxene crystals are only partially altered to amphibole.

This group can be divided into two sub-groups, based on the degree of alteration (see Appendix 1). Samples from the Western Quarries are relatively unaltered and

plagioclase feldspars are clear when viewed in plane polarised light and show clear multiple twinning when viewed in crossed polarised light. The samples from the northern Central Quarries and northern part of the intrusion, however, are slightly more altered. The feldspars are turbid when viewed in plane polarised light and although sericitisation is present it does not totally mask the multiple twinning when viewed in crossed polarised light. Samples JD2936 and JD2951, presented in Appendix 2, are typical of Group 3 rocks.

4.6.4. Group 4 rocks

These rocks occur in a series of small quarries north-west of the Graig Lwyd Quarries. They are separated from the area of Group 2 rocks, to their west, by a large area of non-exposure. Samples from this group contain both chlorite and fibrous amphibole, and some samples show characteristics of Group 2 rocks while others show characteristics of Group 3 rocks. In some samples chlorite can be seen to be pseudomorphing the amphibole. They also generally contain greater amounts of quartz than other samples from the intrusion. Samples from this area often contain small (5-10 mm), rounded inclusions composed of fine-grained equigranular crystals mainly of clinopyroxene and plagioclase feldspar. Sample JD2932, presented in Appendix 2, is typical of Group 4 rocks.

4.7. Summary of the main rock types

The differences in texture and mineralogy seen in this section allow the Penmaenmawr Intrusion to be divided into four groups, the main characteristics of which are presented in Table 4.1.

The very-fine grained size of Group 1 rocks suggest that they were formed from a magma that cooled quickly. As the Group 1 rocks occur in eastern quarries and adjacent to the southern boundary, this rapid cooling is probably due to the magma coming into contact with cold country rocks. The rocks from the other Groups are coarser grained and thus cooled more slowly, perhaps because they were insulated from the cold country rocks by the Group 1 rocks. Alternatively, as

the rocks forming Groups 2 and 3 cover a larger area than the Group 1 rocks, they could have been derived from a larger body of magma that cooled more slowly than the magma that formed Group 1. The small intrusive bodies at Garreg Fawr and Dinas, which are similar petrographically to Group 1 rocks, suggest that there were a number of intrusions being injected from a lower magma chamber, each of which could have different cooling histories dependent on its size.

Table 4.1. Summary of the principal characteristics of the four main petrographic groups from the Penmaenmawr Intrusion.

Group	Colour	Texture	Distinctive Mineralogy	Location (see Figure 4.2)
Group 1	Very dark-grey	Very fine-grained		Eastern part and southern boundary of the intrusion
Group 2	Pale-grey	Fine- to medium-grained	> 25% chlorite	Central part of the intrusion
Group 3	Dark-grey	Fine- to medium-grained	> 15% orthopyroxene/ amphibole	Western and north-western part of the intrusion
Group 4	Pale- and dark-grey	Fine- to medium-grained	Some samples contain chlorite, others amphibole	North-east part of the intrusion

The major differences in the mineralogy, identified above, are in the abundance and range of secondary minerals present. Although these differences may reflect differences in primary mineralogy, they are predominantly due to varying degrees of alteration. The rocks of Group 3, which occur in the western part of the intrusion, appear relatively unaltered whereas the rocks of Group 2, in the central part of the intrusion, appear to be more extensively altered. The rocks of Group 4, in the northeast of the intrusion, although altered to a greater degree than Group 3 rocks, are not as extensively altered as those of Group 2. This suggests that the central part of the intrusion, occupied by Group 2 rocks, underwent more intense alteration than other areas of the intrusion.

4.8. Alteration indices

In order to determine the extent and variation of alteration within the Penmaenmawr Intrusion, a classification of alteration was developed based on the character of plagioclase feldspar in thin section. Plagioclase feldspar occurs in all samples collected from the intrusion and the extent of alteration of plagioclase feldspar can easily be observed by its appearance in thin section. This provides a means, albeit crude, to map the degree of alteration across the intrusion. Five degrees of alteration were identified, which subsequently allowed the extent of alteration to be mapped out. The alteration indices based on the appearance of plagioclase feldspar are defined in Table 4.2. These indices could not, however, be applied to the very fine-grained rocks from Group 1 as plagioclase feldspar phenocrysts tended to be filled with dark, indeterminate, secondary material and the groundmass crystals were too fine to determine.

4.8.1. Application of alteration indices to the Penmaenmawr Intrusion

The summary of the mineralogy presented in Appendix 1 includes the alteration index of each sample based on the criteria in Table 4.2. The variation in alteration across the intrusion is presented in Figure 4.2, which shows the sample locations and their corresponding alteration index.

Samples with an alteration index of 1 (no alteration) occur only in the Western Quarries and include the least altered samples from Group 3. The rocks are dark grey in hand specimen with plagioclase feldspars clear when viewed in plane polarised light and showing good multiple twinning in crossed polarised light. Orthopyroxene is present, generally as euhedral prismatic crystals with cleavage lines parallel to their long axes. Biotite is present in minor amounts and the iron-titanium minerals present are magnetite intergrown with ilmenite.

Samples with an alteration index of 1.5-2 occur to the north and east of the samples with an alteration index of 1. These samples include the more altered samples from Group 3 in the northern Central Quarries where orthopyroxene has been altered to amphibole. Biotite is present but is partially altered to dark-green chlorite.

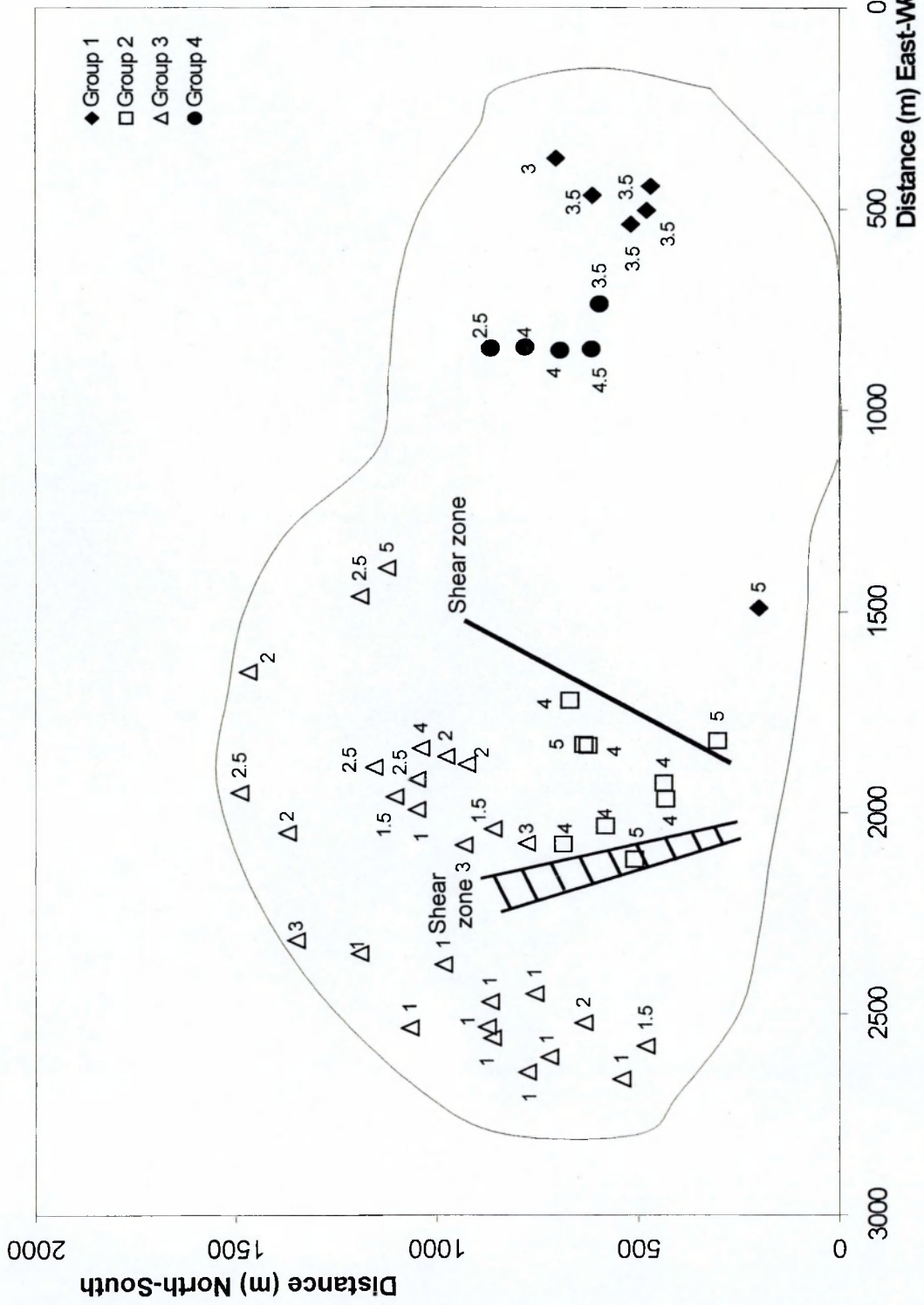


Figure 4.2. Outline plot of the Penmaenmawr Intrusion showing the alteration index (1-5) for fine- to medium-grained samples.

Alteration Index	Degree of alteration	Character of plagioclase feldspar
1	No alteration	Crystals are clear in ppl Multiple twinning clearly seen in xpl
2	Slight alteration	Crystals show a turbidity in ppl Multiple twinning clear in xpl
3	Medium alteration	Crystals turbid but original rectangular outlines clearly visible in ppl Multiple twinning is present but not clear in xpl
4	Significant alteration	Crystals turbid, original rectangular outlines not clear in ppl Multiple twinning can only just be determined in xpl
5	Extensive alteration	Crystals turbid, outlines not easily seen in ppl Multiple twinning not seen in xpl

Table 4.2. Alteration indices based on the character of plagioclase feldspar from the Penmaenmawr Intrusion.

(Key: ppl - plane polarised light, xpl - crossed polarised light)

Only a few samples have an alteration index of 2.5-3 and they occur in small patches mainly in the centre and north of the intrusion. They include samples from Group 3 and one sample from Group 4.

Samples with an alteration index of 4 include samples from Group 2 in the main Central Quarries, samples from Group 4 from the quarries to the north-west of the Graig Lwyd Quarries and some of the coarser-grained samples from Group 1 from the Graig Lwyd Quarries. In these samples chlorite has replaced both amphibole and biotite, plagioclase feldspars have the composition of albite, and secondary minerals such as pumpellyite, prehnite, epidote, and alkali feldspar occur. The opaque minerals have altered to titanite.

Samples with an alteration index of 5 occupy small areas in the Central Quarries; they include the most altered samples from Group 2 and one sample from Group 1. In these samples the plagioclase feldspars have been heavily sericitised.

In an attempt to map the variation in alteration across the intrusion, a contour diagram for the alteration index using Surfer for Windows, a surface-mapping system was prepared and is presented in Figure 4.3. This shows that the degree of alteration increases from the western and southern margins of the intrusion towards the centre where it reaches its maximum extent, then becomes slightly less intense toward the eastern margin. The area of maximum alteration occurs in the central area of the intrusion towards the southern boundary. However, there are some large areas within the intrusion where there is no alteration data so this diagram can only provide a general indication of the variation in alteration across the intrusion as a whole.

The alteration indices generally support the division of the intrusion into the Groups identified at Section 4.3 and confirm that the major petrographical differences within the intrusion are due in parts to varying degrees of alteration. This analysis also suggests that samples from Group 3 could be further divided into a less altered Sub-Group in the west of the intrusion and a more altered Sub-Group towards the centre and north of the intrusion. The alteration indices contour diagram shows that the most altered part of the intrusion is in the central area towards the southern boundary. In Chapter 3, this central area of the intrusion was identified as forming a wedge between two shear zones, one of which was up to 90 m wide with shattered rock and closely-spaced fractures (see Figure 3.5). The location of the most altered area of the intrusion contained within shear zones suggests that the alteration is due to the shear zones providing pathways for hydrothermal fluids to enter the intrusion, leading to extensive alteration.

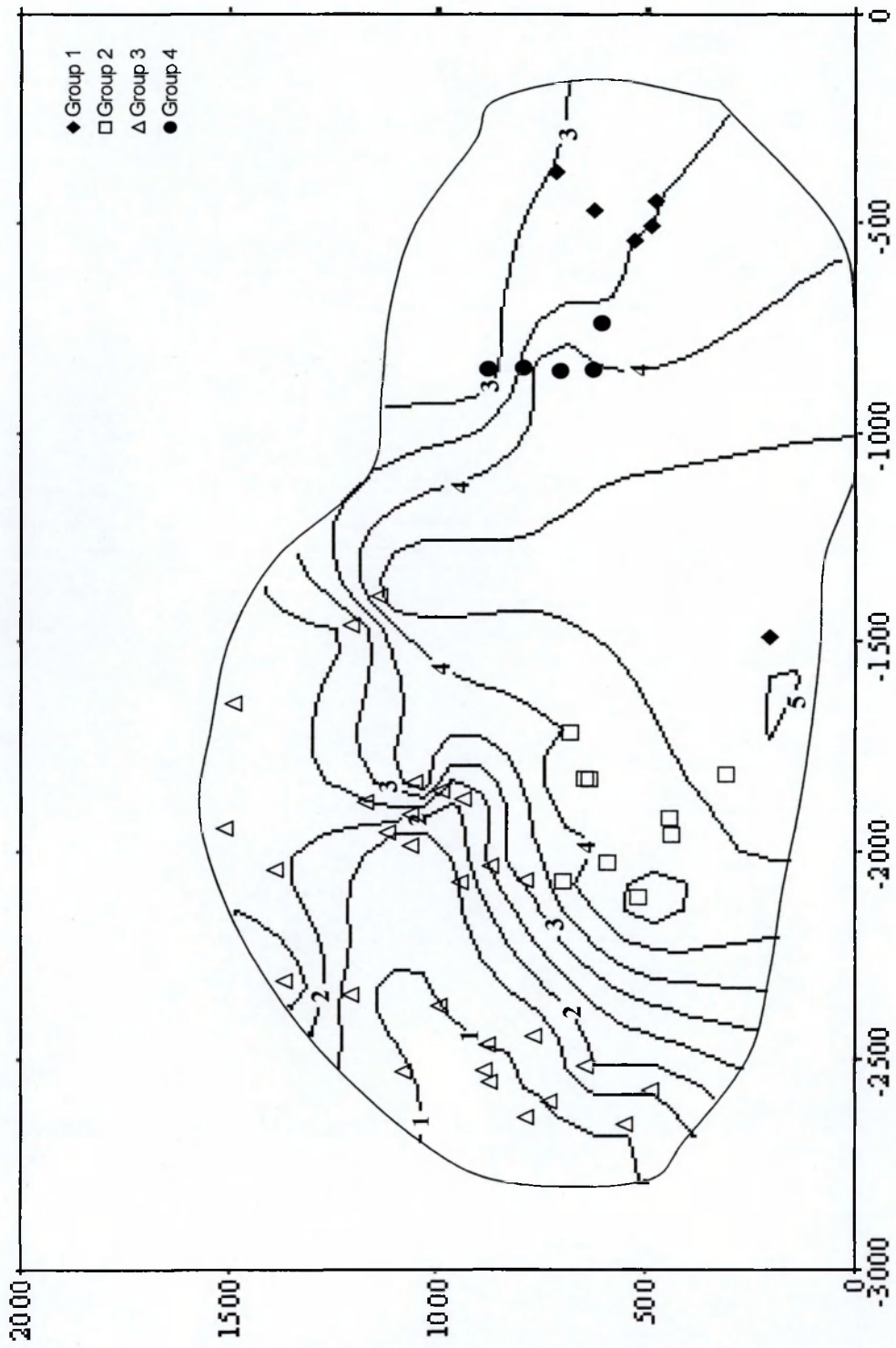


Figure 4.3. Contour diagram for the alteration index using Surfer for Windows, surface-mapping system.

CHAPTER 5. MINERAL CHEMISTRY OF THE PENMAENMAWR INTRUSION

5.1. Introduction

In Chapter 4, it was shown that the Penmaenmawr Intrusion could be divided into four petrographic groups based on texture and mineralogy. In particular the presence or absence of orthopyroxene, fibrous amphibole and chlorite could be used as key indicators. It was also suggested that these three minerals represent differing degrees of alteration, orthopyroxene altering to amphibole, then amphibole altering to chlorite. The differences in mineralogy, presented in Chapter 4, however, may also reflect differences in the primary mineralogy of the rocks due to magmatic, rather than alteration processes, and which may become more apparent by an examination of the chemistry of the minerals present.

This Chapter presents details of the mineral chemistry of the key minerals identified in Chapter 4, in order to identify any variations in mineral chemistry, which could assist in the determination of the processes responsible for variations present within the intrusion. The mineral chemistry data presented in this Chapter can also be used for whole rock geochemical modelling, in an attempt to establish the evolution of the intrusion.

Representative samples from the Penmaenmawr Intrusion were selected for mineral chemical analysis utilising an electron microprobe. Four samples were chosen from Group 1, three from Group 2, seven from Group 3, and three from Group 4. In addition, examples of a segregation and an inclusion were also selected. Most analyses were carried out using a Cameca SX100 electron microprobe operated from a SUN workstation running Solaris 2 and driven by proprietary software at the Open University but some analyses were carried out using a Cambridge Instruments Mark 9 electron microprobe, also at the Open University. The operating details for both machines were essentially the same and are presented in Appendix 3.

5.2. Plagioclase feldspar

In Chapter 4, it was shown that plagioclase feldspar occurs, in varying proportions, in all samples from the intrusion. Group 3 rocks tend to have higher modal concentrations, typically between 40% and 60%, than samples from the other groups, which have typical values of between 30% and 45%. Sixty-three plagioclase feldspar analyses were determined, ten from Group 1, five from Group 2, forty-one from Group 3, and seven from Group 4. Only a small number of analyses of plagioclase feldspar were obtained from Groups 1, 2 and 4 because of the high degree of alteration. The chemical analyses are presented in Appendix 4 and the compositions of plagioclase feldspars, plotted on an Ab (albite) – An (anorthite) – Or (orthoclase) ternary diagram are presented in Figure 5.1.

Plagioclase feldspars from Group 3 rocks tend to plot in a narrow area on the Ab-An-Or ternary diagram, generally in the labradorite field (Figure 5.1). Typical values are in the range Ab (35-52), An (50-60) and Or (1-2). Some crystals, particularly from the more altered samples, plot outside this range, falling in the andesine and oligoclase fields.

Plagioclase feldspars from Groups 2 and 1 tend to plot as a separate group, within the albite field, with typical values in the range Ab (95-98) and An (1-3). Crystals from two samples from Group 1 (JD2912 and JD2947) plot in the labradorite and andesine fields, with ranges of Ab (29-57) and An (40-70). Plagioclase feldspars from Group 4 have variable compositions, with crystals from the same sample plotting in the labradorite, andesine and oligoclase fields.

The least altered samples, from Group 3, have plagioclase compositions of labradorite, which is typical of primary plagioclase feldspars from intermediate igneous rocks. Theoretical considerations, based on the binary albite-anorthite phase diagrams, show that when plagioclase feldspar crystals are formed they are enriched in Ca with respect to the original liquid composition and that during fractional crystallization, residual liquids become enriched in Na (Hall, 1987). The compositions of plagioclase feldspar crystals from a series of rocks evolved by fractional crystallisation should therefore show an increase in Na₂O contents. The trend from labradorite to andesine shown by the plagioclase feldspars in

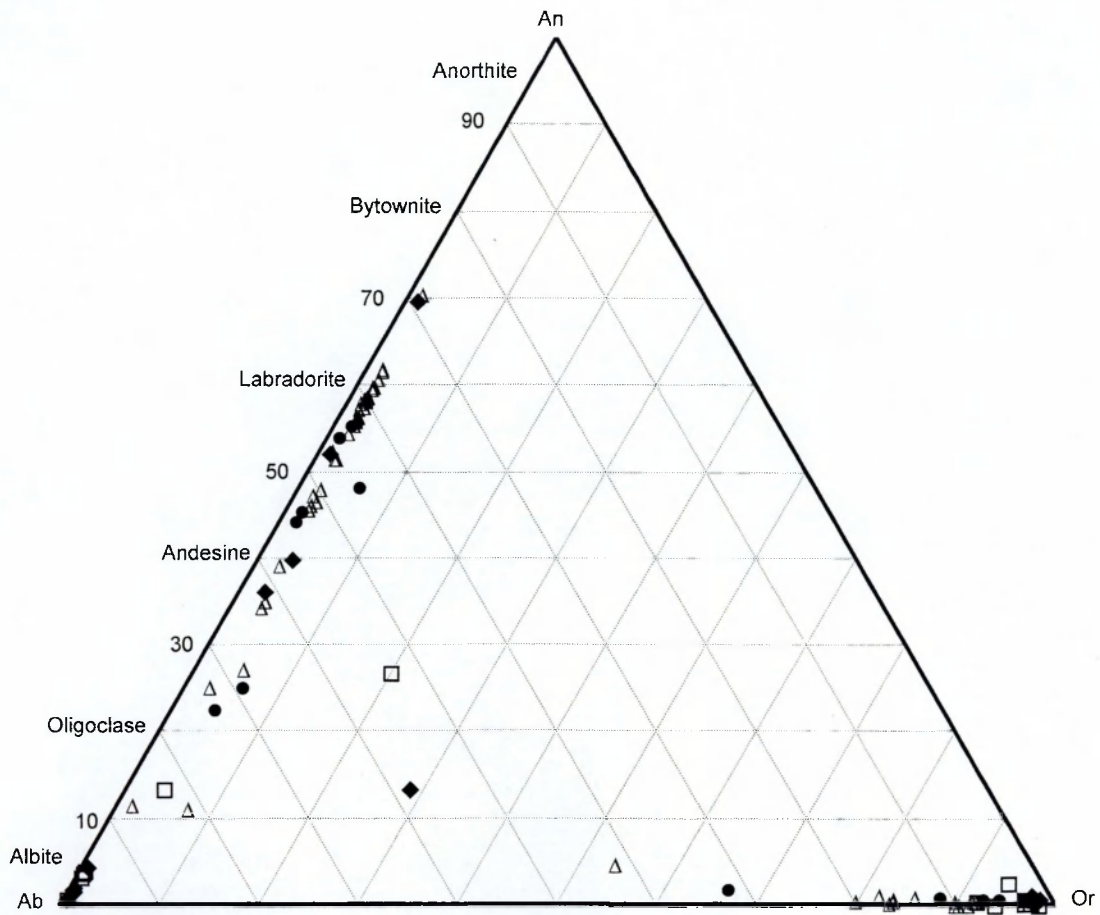


Figure 5.1. Ternary Ab-An-Or diagram showing the compositions of Plagioclase and Alkali Feldspar for the Penmaenmawr samples from Groups 1-4. (◆ = Group 1; □ = Group 2; Δ = Group 3; ● = Group 4.)

Group 3 rocks and the presence of andesine in some samples from Group 1 and Group 4 may therefore be the result of fractional crystallisation. However, although albite, found in rocks from Groups 2 and 1, could be formed by crystallisation in the later stages of a fractionation series, it is a common alteration product involving hydrothermal fluids and it was shown in Chapter 4 that the rocks from the Penmaenmawr Intrusion have been variably altered. The plagioclase feldspars from Groups 2 and 1 that plot in the albite field are undoubtedly the result of alteration.

5.3. Alkali feldspar

Alkali feldspar only occurs in the more altered rocks and in some of the samples from Group 2 its modal proportion has been estimated to reach up to 5%. It only rarely occurs in samples from Group 3 and only then in the most altered samples. Thirty-two alkali feldspar analyses were determined, four from Group 1, ten from Group 2, ten from Group 3, and eight from the Group 4. The chemical analyses are presented in Appendix 4. The compositions of the alkali feldspars are plotted on the Ab (albite) - An (anorthite) - Or (orthoclase) ternary diagram in Figure 5.1.

Alkali feldspars have compositions in the range Or (80-98), Ab (1-8), An (0.3-2); however, analyses from Group 3 tend to have lower orthoclase and higher albite compositions, typically Or (80-91) and Ab (6-7), than the samples from Groups 1, 2 and 4, which have typical values of Or (90-98) and Ab (1.7-8).

The absence of alkali feldspar in the least altered rocks, and the presence of well-developed crystal faces in contrast to plagioclase feldspar and other crystals in the more altered samples, suggest that alkali feldspar is of secondary origin after plagioclase feldspar. In Chapter 4 it was shown that alkali feldspar is beginning to breakdown in the most altered samples of Group 2, which suggests that they could be early-formed secondary minerals.

5.4. Orthopyroxene

In Chapter 4 it was noted that orthopyroxene is found in any abundance only in the fresher samples from Group 3, and in minor amounts in more altered rocks

from this Group. Orthopyroxene is clearly a primary mineral.

Twenty-four orthopyroxene analyses were determined, twenty-two of which were from the least altered samples from Group 3, with two from Group 1 samples. The chemical analyses are presented Appendix 4. Almost all orthopyroxene analyses from the intrusion plot in the enstatite field using the classification system of Morimoto (1988) (see Figure 5.2.), and show typical atomic percentages in the ranges of Mg 60–65%, Fe 30–36% and Ca 4–5%. Two analyses have Ca values of 8% and 9% and are considered to be products of partial alteration, as the content of Ca in orthopyroxenes is generally small due to the fact that Ca ions cannot be accommodated in the orthopyroxene structure and on cooling are exsolved. The maximum Ca content reported by Deer *et al.* (1992) is 3%.

5.5. Clinopyroxene

Clinopyroxenes have been found in all the samples collected in this study from the Penmaenmawr Intrusion and make up between 10–20 modal % of the rock. They occur as small (0.1 mm), brown crystals, usually embayed in the more altered samples. One hundred and three clinopyroxene analyses have been determined, seventeen from Group 1, twenty-five from Group 2, thirty-eight from Group 3, and twenty-three from Group 4. The chemical analyses are presented in Appendix 4. Most clinopyroxene analyses plot as a cluster, almost entirely in the augite field, following the classification of Morimoto (1988) (Figure 5.2.), although a few crystals from Groups 1 and 3 plot on the boundary with the diopside field, while one analysis from Group 1 actually plots within the diopside field and two samples from Group 4 plot in the hedenbergite field.

The chemical composition of all clinopyroxenes is fairly similar, apart from the two samples from Group 4, which are considered to be anomalous and due either to alteration or errors in the instrument operating process. However, although the clinopyroxenes plot as a cluster, the analyses show that there are slight differences between the Groups, as indicated by the ranges of atomic percentages of Ca, Mg, and Fe for the different Groups, presented in Table 5.2.

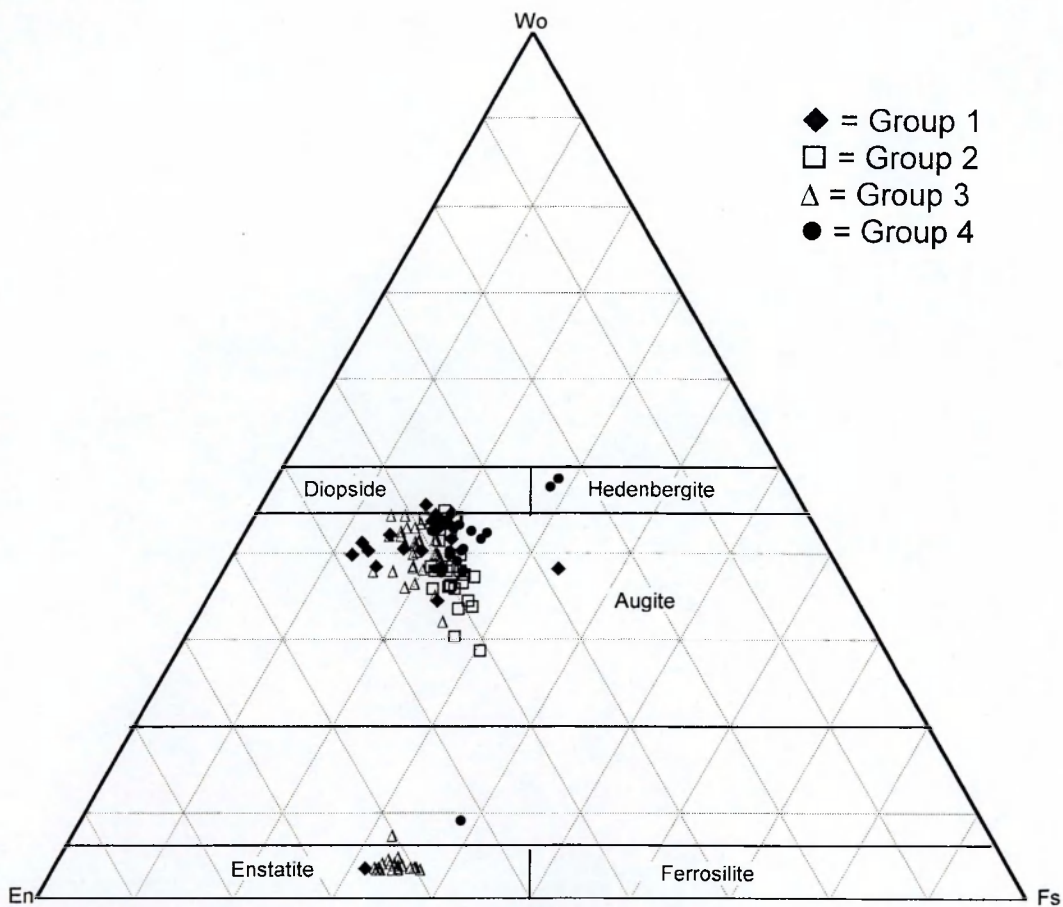


Figure 5.2. Ca_2SiO_6 (Wo) – $\text{Mg}_2\text{Si}_2\text{O}_6$ (En) – $\text{Fe}_2\text{Si}_2\text{O}_6$ (Fs) diagram showing the composition of the clinopyroxenes and orthopyroxenes from the Penmaenmawr Intrusion. Fields based on Morimoto (1988).

The clinopyroxenes from Groups 1 and 3 have broadly higher Mg contents and lower Fe contents than those from Groups 2 and 4, while clinopyroxenes from Group 2 have a wider range of Ca contents than the other groups. In addition, the clinopyroxenes from Group 2 also have lower SiO₂ and higher Al₂O₃ compositions than clinopyroxenes from the other groups.

Table 5.1. Typical Ca, Mg and Fe (as atomic %) values for clinopyroxenes from the different groups from the Penmaenmawr Intrusion.

	Ca	Mg	Fe
Group 1	41 - 44	38 - 44	15 - 20
Group 2	36 - 45	36 - 40	19 - 24
Group 3	38 - 43	38 - 43	15 - 20
Group 4	39 - 42	37 - 40	21 - 22

Studies of liquid/solid phase relationships of ferromagnesian minerals, which show Mg-Fe solid solution, demonstrate that when crystals are formed, they are enriched in Mg with respect to the composition of the original liquid (Hall, 1987). Fractional crystallisation of orthopyroxene and/or clinopyroxene will therefore result in a residual liquid composition enriched in Fe. During a fractional crystallisation process, therefore, ferromagnesian minerals should become progressively enriched in iron and depleted in magnesium. The data presented above shows that clinopyroxenes from Groups 2 and 4 have a slightly higher atomic percentage of iron and a slightly lower atomic percentage of magnesium than the clinopyroxenes from Groups 1 and 3. These differences could be the result of fractional crystallisation, and might suggest that rocks from Groups 2 and 4 represent more evolved magmas and that rocks from Groups 3 and 1 represent less evolved magmas.

5.6. Amphibole

The presence of amphibole characterises Group 3 rocks, in which it occurs as green, fibrous, elongate or rectangular crystals, which vary in size from 0.2 to 0.5 mm, although in many samples crystals up to 2 mm in length, occur. Seventy analyses were determined, six from Group 1, seventeen from Group 2, thirty-

seven from Group 3, and ten 10 from Group 4. The analyses are presented in Appendix 4.

Figure 5.3 shows the amphiboles classified according to the scheme proposed by Tindle & Webb (1994). In this scheme almost all of the amphiboles in Group 1 and 2 rocks are calcic amphiboles, with $(Ca + Na) > 1.34$ and $Na < 0.67$. Analyses from one sample in Group 2, however, plot as sodic-calcic amphiboles, with $(Ca + Na) > 1.34$. Amphiboles from Group 3, and most of the analyses from Group 4 tend to have lower $Ca + Na$ contents; in both groups 50% of the minerals analysed are calcic amphiboles and 50% are Fe-Mg-Mn amphiboles ($Ca + Na < 1.34$).

The calcic amphiboles from Group 1 rocks plot in the magnesio-hornblende to actinolite fields on the $Mg/(Mg+Fe)$ v silica diagram (Figure 5.4), whereas the calcic amphiboles from Group 3 and Group 4 rocks tend to plot in the tschermakitic-hornblende to hornblende fields. The amphiboles from Group 2 rocks have a very wide variation plotting from the tschermakite to the actinolitic-hornblende fields.

The Fe - Mg - Mn amphiboles plot in both the anthophyllite and the gedrite fields on the $Mg/(Mg + Fe)$ v silica diagram (Figure 5.5) but with a greater preponderance in the gedrite field. Some of the amphiboles from Group 3 rocks have a higher concentration of Mg than those from Group 4.

The amphiboles from Groups 1 and 2 and those with higher $Ca + Na$ contents from Group 4 tend to have higher K_2O and TiO_2 concentrations than the amphiboles from Group 3 (Figure 5.6).

In Chapter 4 it was shown that amphiboles in the Penmaenmawr Intrusion are likely to be of secondary origin, replacing primary orthopyroxene. However the compositions of the amphiboles vary widely; the amphiboles from Groups 3 and 4 tend to have lower contents of $Ca+Na$ and lower contents of K_2O and TiO_2 than the amphiboles from Groups 1 and 2. Ca , Na and K tend to be mobile elements and as rocks from Group 3 tend to be the least altered rocks whereas rocks from Groups 2 tend to be the most altered, these differences in composition could be

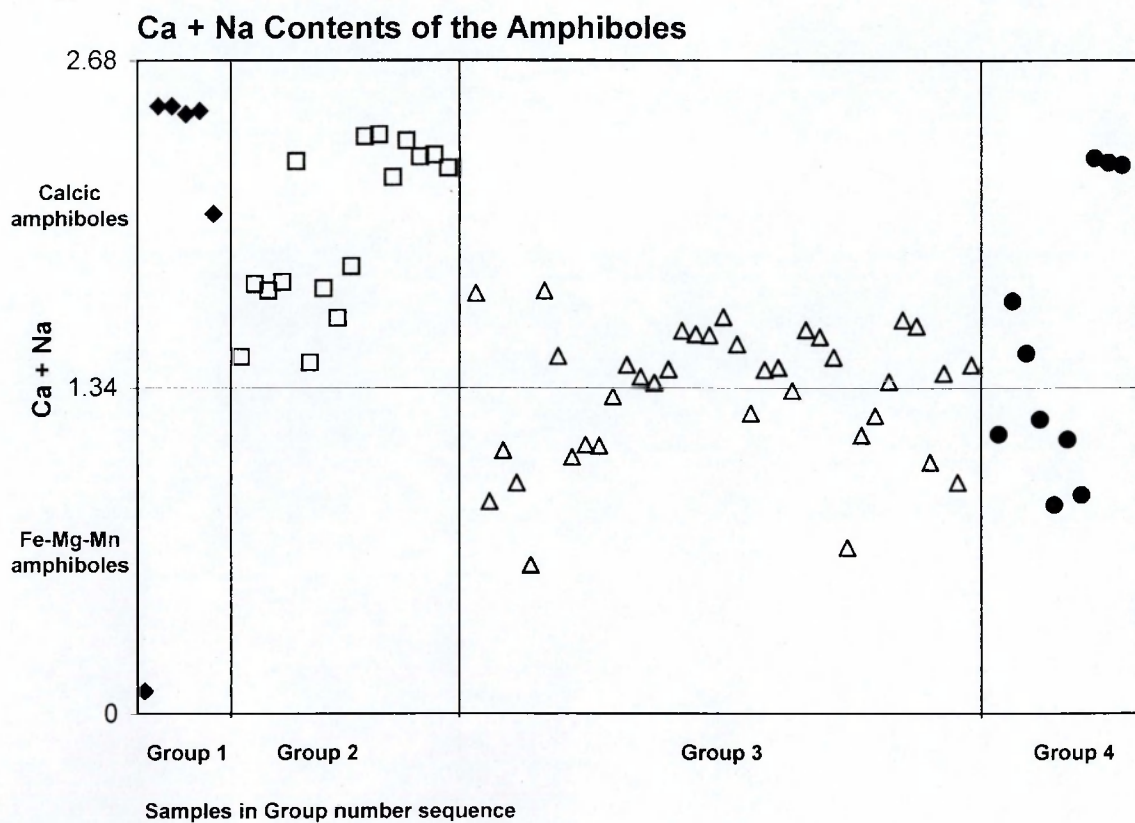


Figure 5.3. Plot of the Ca + Na content of Penmaenmawr amphiboles, showing the separation into calcic amphiboles and Fe-Mg-Mn amphiboles. Samples are separated according to their Groups (1-4).

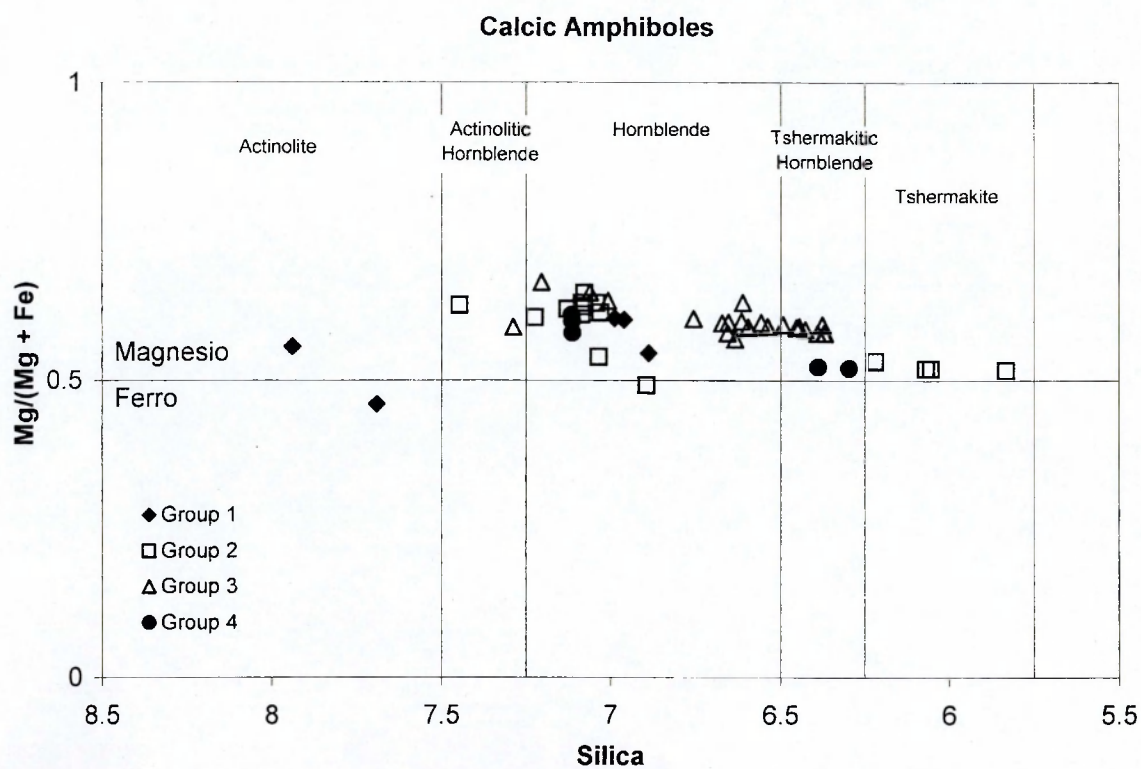


Figure 5.4. Plot of Mg/(Mg + Fe) against Silica (Si) for Penmaenmawr calcic amphiboles.

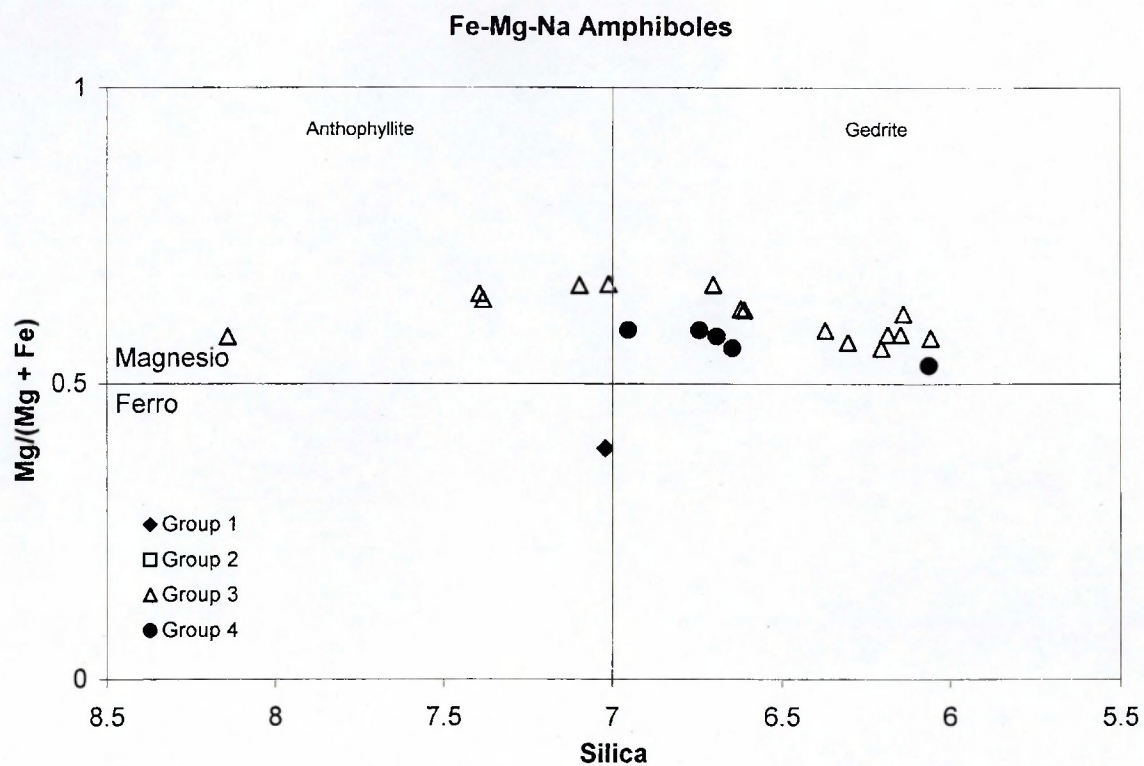


Figure 5.5. Plot of Mg/(Mg + Fe) against silica (Si) for Penmaenamwr Fe-Mg-Mn amphiboles.

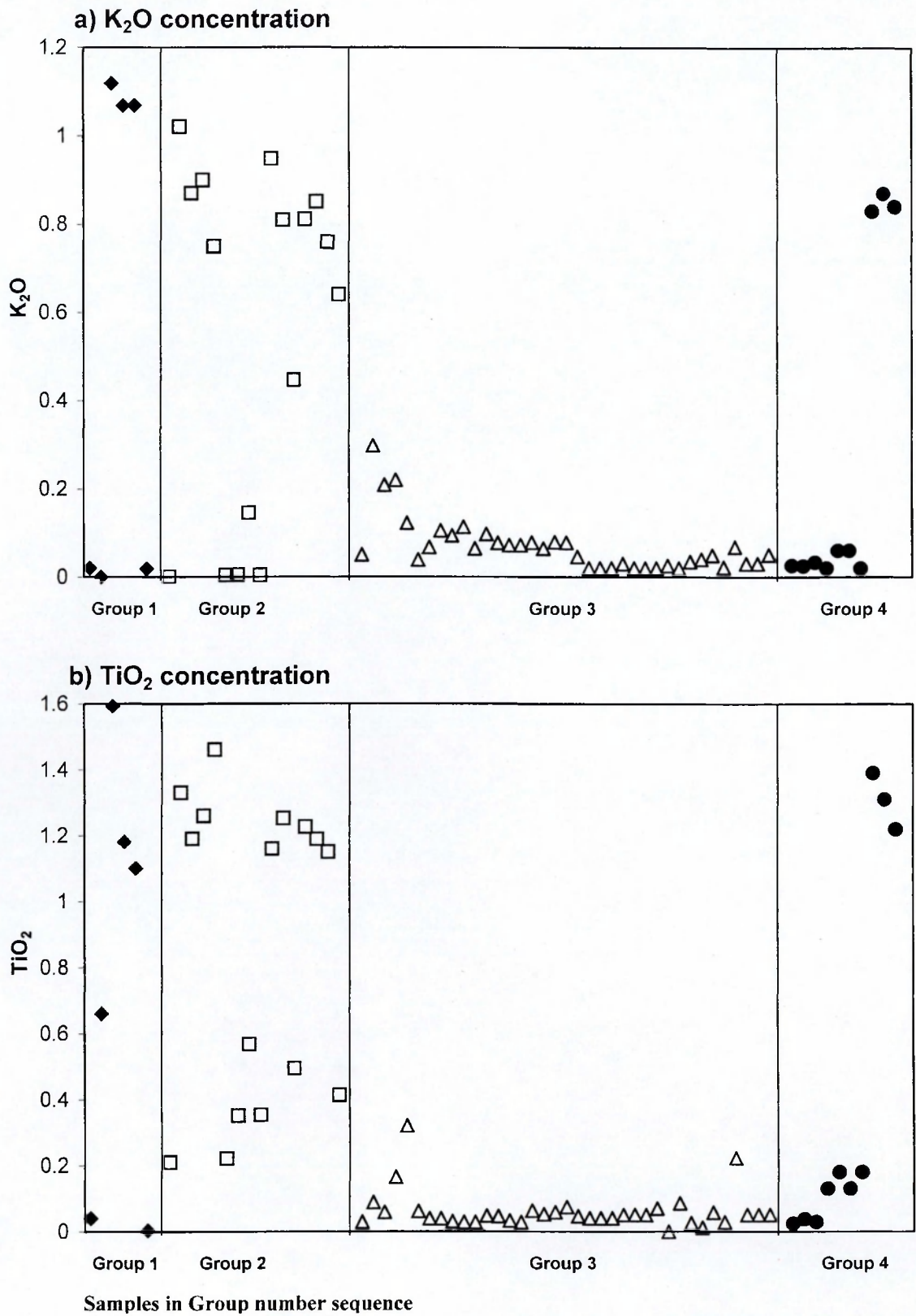


Figure 5.6. Plots of (a) K₂O and (b) TiO₂ concentrations of Penmaenmawr amphiboles, divided according to their groups.

related to the different degrees of alteration within the Penmaenmawr Intrusion and the release of Ca, Na and K with the increasing breakdown of plagioclase feldspar, biotite and possibly clinopyroxene. However the different amphibole compositions could also be due to their mode and temperature of formation; actinolitic amphiboles are likely to have formed at lower temperatures than tschermakitic amphiboles (Deer *et al.*, 1992). As the least altered rocks from Group 3 contain tschermakitic amphiboles and the most altered rocks from Group 2 contain the more actinolitic amphiboles, the contrasting amphibole compositions within similar rocks suggests that there may have been more than one alteration event, the first forming tschermakitic amphiboles and the second forming actinolitic amphiboles.

5.7. Iron and titanium minerals

Iron and titanium minerals occur in all samples, generally only in minor amounts (<1%), although in some samples they reach up to an estimated 2% of the mode. Twenty-seven analyses were determined, four from Group 1, five from Group 2, seventeen from Group 3 and one from the Group 4. The chemical analyses are presented in Appendix 4.

Analyses from Group 3 rocks show that the Fe-Ti minerals consist of intergrown crystals of magnetite and ilmenite. Ilmenite has a range in TiO₂ contents of 43.6-48.2 wt% and in FeO of 45.3-49.3 wt%, whereas magnetite has a range in TiO₂ contents of 2.7-9.1wt% and in FeO of 78.9-84.4 wt%. Although some ilmenite is present in Group 1 rocks, most of the opaque minerals in Group 1 and 2 have been altered to titanite, with variable amounts of Si and Ca incorporated into the structure.

5.8. Biotite

Biotite occurs only in the least altered rocks in Group 3 and only six analyses have been determined. Analyses are presented in Appendix 4. The MgO / (MgO + FeO) ratio varies from 0.42–0.58. There is wide variation in K₂O contents (4.14-9.34wt%), which is most likely due to varying amounts of alteration causing depletion. Biotite is considered to be a primary mineral and not a

product of metamorphism because it is seen partially altering to chlorite; in fact biotite may have been present in all of the groups originally, only surviving now in the least altered rocks from Group 3.

5.9. Chlorite

Chlorite occurs as a secondary mineral after orthopyroxene, amphibole and biotite. It is the main ferromagnesian mineral in Group 2 rocks and its abundant occurrence, greater than 30% modal estimate, is used to characterise rocks in this Group. It occurs in trace amounts in Group 3 rocks, where it partially or wholly replaces biotite, and in the more altered samples where it occurs as small fringes to amphibole crystals. Fifty-seven analyses were determined, nineteen from Group 1, twenty-nine from Group 2, five from Group 3, and four from Group 4. The chemical analyses are presented in Appendix 4.

The chemical compositions of chlorites from all analyses are fairly similar. The chemical proportions of interlayer cations Ca, K and Na are generally less than 0.1, except in a few isolated cases. The $\text{MgO} / (\text{MgO} + \text{FeO})$ ratio is between 0.28 and 0.39, the analyses from Group 3 rocks accounting for most of the higher values. Using the Fe v Si diagram of Hey (1954) (Figure 5.7) the chlorites can be seen to plot in a tight field that straddles the border between pycnochlorite and diabanite.

Chlorite and clinopyroxene are the two main ferromagnesian minerals in Group 2 rocks, which suggest that chlorite may have replaced primary orthopyroxene, biotite and secondary amphibole. The small range of chlorite compositions and the consistency of the chlorite $\text{MgO} / (\text{MgO} + \text{FeO})$ ratios, irrespective of whether the original mineral was orthopyroxene, amphibole or biotite, suggests that chlorite compositions equilibrated under similar conditions. The composition of chlorite on the Si versus Fe diagram of Hey (1954) are typical of chlorites in altered basic to intermediate rocks belonging to the prehnite and pumpellyite to greenschist facies grades of metamorphism (Bevins & Rowbotham, 1983; Bevins & Merriman, 1988).

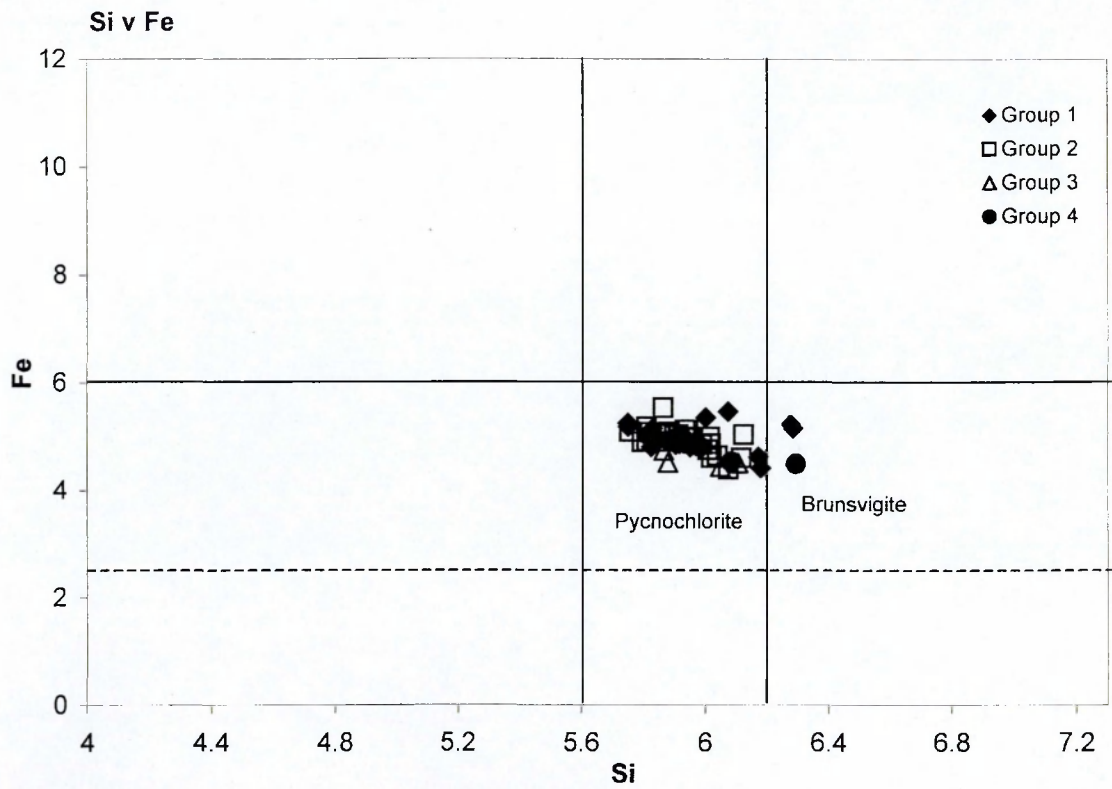


Figure 5.7. Fe versus Si concentration diagram for the Penmaenmawr samples from Groups 1 to 4. Plot after Hey (1954).

5.10. Apatite

Apatite occurs in most Penmaenmawr samples in trace amounts as small, needle-like crystals. Only five analyses were carried out on samples from Group 1, 2 and 3 rocks (see Appendix 4). The microprobe analyses show a consistent chemistry between all crystals analysed from the three groups.

5.11. Mineral chemistry - summary

The petrographic observations presented in Chapter 4, combined with the mineral analyses presented above, suggest that the primary mineralogy of the Penmaenmawr Intrusion consisted of plagioclase feldspar (30-60%), orthopyroxene (15-30%), clinopyroxene (10-20%), and minor amounts of accessory biotite, intergrown magnetite and ilmenite, apatite and quartz. However, there has been variable degrees of alteration of the Penmaenmawr Intrusion so that the mineralogy now consists of plagioclase feldspar, which has been altered in varying amounts; amphibole largely replacing orthopyroxene; chlorite partially replacing amphibole and biotite; and clinopyroxene, along with minor amounts of titanite, alkali feldspar, apatite, and quartz, and finally varying amounts of prehnite, pumpellyite, epidote and axinite.

The less-altered plagioclase feldspar crystals appear to change progressively, from labradorite to andesine and oligoclase, from Group 3 rocks to Group 2 and 4 rocks and there is a comparable progressive Fe enrichment in clinopyroxene crystals from Group 3 rocks to Group 2 and 4 rocks. These changes in primary mineral compositions suggest that the Penmaenmawr Intrusion may consist of an evolving suite of minerals formed by magmatic processes and that Group 2 and 4 rocks may have evolved from Group 3 rocks by fractional crystallisation.

However, the presence of chlorite, with a composition which is typical of prehnite and pumpellyite to greenschist facies grades of metamorphism, in the more altered Group 2 and 4 rocks and its absence in the less altered Group 3 rocks indicates that the chemical differences between minerals from rocks assigned to the different groups are due to alteration.

The presence of tschermakitic amphiboles in Groups 3 and 4 rocks and the presence of actinolitic amphiboles in Groups 1 and 2 rocks also shows that rocks from Groups 1 and 2 have been altered. Although the tschermakitic amphiboles may be primary minerals, it was reported in Chapter 4 that they were replacing primary orthopyroxene. The presence of two different amphibole compositions, both the result of alteration, suggests that there may have been more than one alteration event, the first at higher temperatures, altering orthopyroxene to tschermakitic amphibole and the second at lower temperatures, altering tschermakitic amphibole, and any orthopyroxene not affected by the first event, to actinolitic amphibole.

CHAPTER 6. MAGNETIC SUSCEPTIBILITY

6.1. Introduction

In Chapter 4, the texture of the rocks, their mineralogy, and their location were used to divide the intrusion into four petrographic Groups. In order to support this division using an additional and independent analytical procedure and to attempt to refine the boundaries, the magnetic susceptibility of all rock samples was measured. Williams-Thorpe & Thorpe (1993) recognised that magnetic susceptibility provides a rapid method of distinguishing some igneous rocks. The process is easy to use in the field and the values obtained from previously collected hand specimens were confirmed by measurements on site.

Magnetic susceptibility is a measure of the extent to which magnetism can be induced in a rock sample when a magnetic field is applied to that sample. The induced magnetism only lasts as long as the magnetic field is applied. It is normally represented by the letter K and expressed in SI units (Williams-Thorpe *et al.*, 1996). Most iron-rich minerals can contribute to the total magnetic susceptibility of a sample but magnetite is by far the most important. Other minerals, such as ilmenite, hornblende, and biotite can also contribute to a significant extent, particularly when the magnetite content of a sample is low (Bourne, 1993).

6.2. Application of magnetic susceptibility to the Penmaenmawr Intrusion

Magnetic susceptibility measurements of samples from the Penmaenmawr Intrusion were taken using an Exploranium G.S. Ltd model KT-5 meter maintained and monitored by the Open University. It is calibrated in SI units $\times 10^{-3}$ with a display resolution of 0.01×10^{-3} SI. Measurements were carried out in two stages. A first measurement was taken in the air, at least 30 mm away from any magnetic material, to set the background value and zero the display. A second measurement was then taken with the meter positioned against the sample.

The accuracy of the measurements depends on several key factors, including the sample size, the surface area in contact with the instrument, and the thickness of the sample; 90% of the measurement comes from the uppermost 2 cm below the surface. The measurements obtained depend heavily on the homogeneity of the sample, particularly near the surface, and any surface weathering that may have altered any magnetite present will also affect the accuracy of the readings (Williams-Thorpe & Thorpe, 1993). The manufacturer provides tables of corrections that need to be applied to the values obtained when the key properties do not satisfy optimum requirements; these are surface contact ideally 10 cm in diameter but certainly greater than 6 cm diameter, thickness of sample ideally 6 cm but greater than 2 cm, and any surface irregularities less than 5 mm.

Measurements are most accurate on flat surfaces, as rough surfaces require corrections to be applied for the air gap between the surface of the rock and the head of the instrument. The hand specimens from the Penmaenmawr Intrusion provided ideal samples for use with this equipment as they had been broken up to remove weathered surfaces and any visible veins or other irregularities. They also satisfied the size range requirements specified by the manufacturer, and in most cases the hand specimens had been cut, thus providing a flat surface. Where these properties were outside the required specifications, corrections were applied according to the tables supplied by the manufacturer. At least 5 measurements were taken on each sample; further measurements were taken if the range of measurements obtained was greater than 0.05×10^{-3} SI. The average value for each sample was then calculated.

6.3. Variations in magnetic susceptibility

The results obtained are presented in Table 6.1. and in Figure 6.1. These results readily divide the samples into at least two distinct sets, namely those samples that have a low magnetic susceptibility of less than 1×10^{-3} SI and those samples that have a magnetic susceptibility greater than 2.4×10^{-3} SI. The set with the higher values can also be divided into 3 sub-sets, which have magnetic susceptibility values in the ranges of 2.4 to 5.9×10^{-3} SI, 7.2 to 9.3×10^{-3} SI and 11.9 to 15.02×10^{-3} SI.

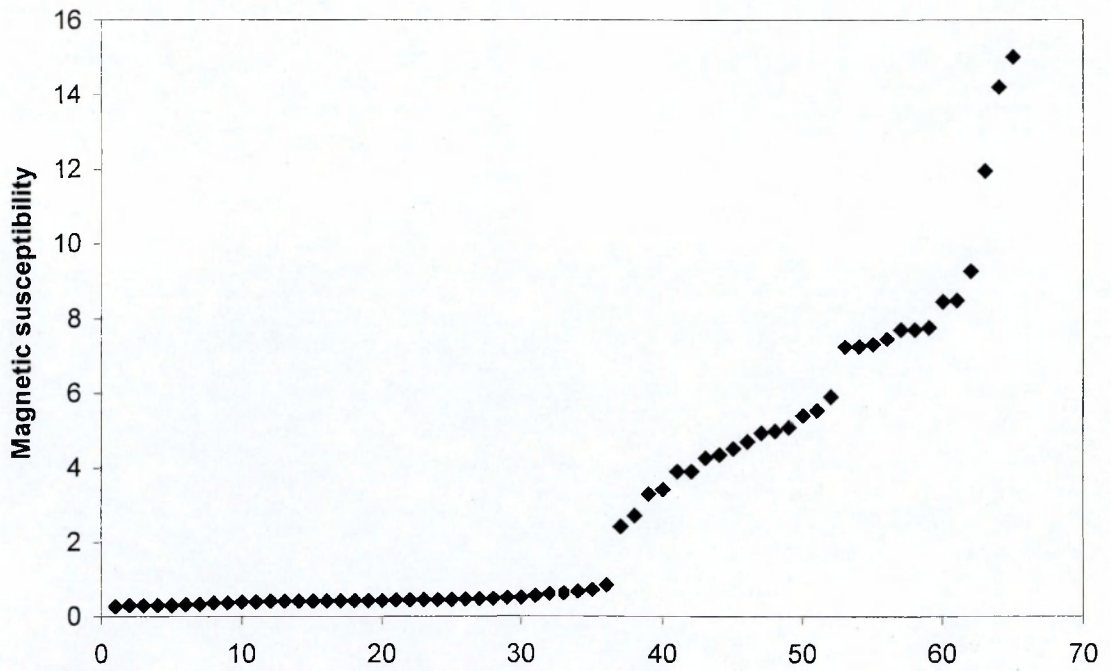


Figure 6.1. Magnetic susceptibility values for the samples from Groups 1-4 of the Penmaenmawr Intrusion, in ascending magnetic susceptibility value order.

Table 6.1. Magnetic susceptibility values for samples from the Penmaenmawr intrusion.

Sample	Mag sus	Sample	Mag sus	Sample	Mag sus
JD2901	0.29	JD2927	0.45	JD2949	7.77
JD2902	0.29	JD2928	0.5	JD2950	3.9
JD2903	0.39	JD2929	0.68	JD2951	4.93
JD2904	0.85	JD2930	0.45	JD2952	3.29
JD2905	0.4	JD2931	0.51	JD2953	0.5
JD2906	0.425	JD2932	0.48	JD2954	9.28
JD2907	0.555	JD2933	0.4	JD2955	5.9
JD2908	0.4	JD2934	0.46	JD2956	7.315
JD2909	7.71	JD2935	0.42	JD2957	0.33
JD2911	7.24	JD2936	2.715	JD2958	0.32
JD2912	0.465	JD2937	4.98	JD2959	2.42
JD2913	0.44	JD2938	4.51	JD2960	0.63
JD2914	0.44	JD2939	3.41	JD2961	8.465
JD2916	0.47	JD2940	0.4	JD2962	7.71
JD1917	0.39	JD2941	5.08	JD2963	5.53
JD2918	0.42	JD2942	4.7	JD2964	0.27
JD2919	0.41	JD2943	4.26	JD2965	0.29
JD2920	0.41	JD2944	7.25	JD2966	0.29
JD2921	4.35	JD2945	11.96	JD2967	0.36
JD2922	5.4	JD2946	15.02	JD2968	0.61
JD2923	0.72	JD2947	14.21	JD2969	0.36
JD2925	7.46	JD2948	3.9		

The variation in magnetic susceptibility within the intrusion is shown in Figure 6.2, which also shows the locations from where the samples were collected and their corresponding magnetic susceptibility values. Figure 6.3 presents a contour diagram for the magnetic susceptibility values using the Surfer for Windows, surface-mapping system. This shows that the highest values tend to be concentrated in the western and south-western part of the intrusion, and the values in the centre and in the east and the south tend to be low. However, there is a lack of data from the centre of the intrusion which may have caused the contour mapping system to make inappropriate suppositions.

6.4. Magnetic susceptibility and the petrographic groups

The magnetic susceptibility values for the different petrographic groups identified in Chapter 4 are presented in Figure 6.4. This figure shows that the magnetic susceptibility of the samples from Group 1 range from 0.27 to 0.85×10^{-3} SI, but with two anomalous measurements, JD2958 and JD2947 with values of 2.42 and 14.21×10^{-3} SI, respectively. Both these anomalous samples were collected from the central to western part of the southern margin of the intrusion. and tend to contain a higher proportion of phenocrysts and appear less altered than the other samples from Group 1. For example, JD2947 contains relatively unaltered orthopyroxene amongst its phenocrysts.

The magnetic susceptibility of the all samples from Group 2 is between 0.40 and 0.55×10^{-3} SI. The magnetic susceptibility of the samples from Group 4 is between 0.45 and 0.68×10^{-3} SI with one anomalous measurement at 8.5. This sample is one of the least altered in this group and has the mineralogical characteristics of samples from Group 3.

The magnetic susceptibility of the samples from Group 3 are more varied and range from 2.71 to 15.02×10^{-3} SI, with only two samples falling below 1. The two samples with low values are the most altered rocks from Group 3 and show biotite altering to chlorite along with amphiboles which lack the usual fibrous appearance.

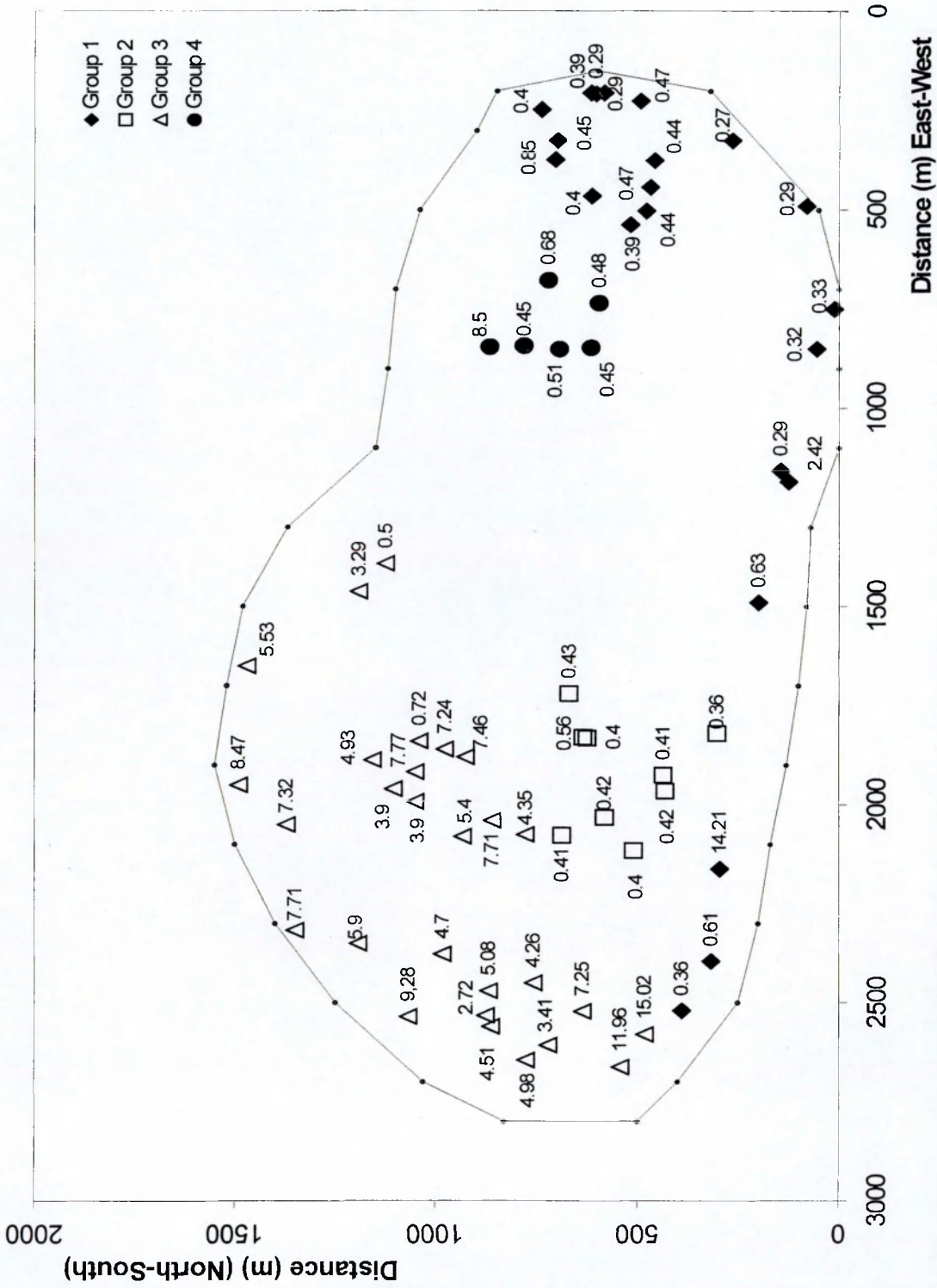


Figure 6.2. Plot of magnetic susceptibility values of the samples from Groups 1-4 from the Penmaenmawr intrusion, with respect to the location of the samples.

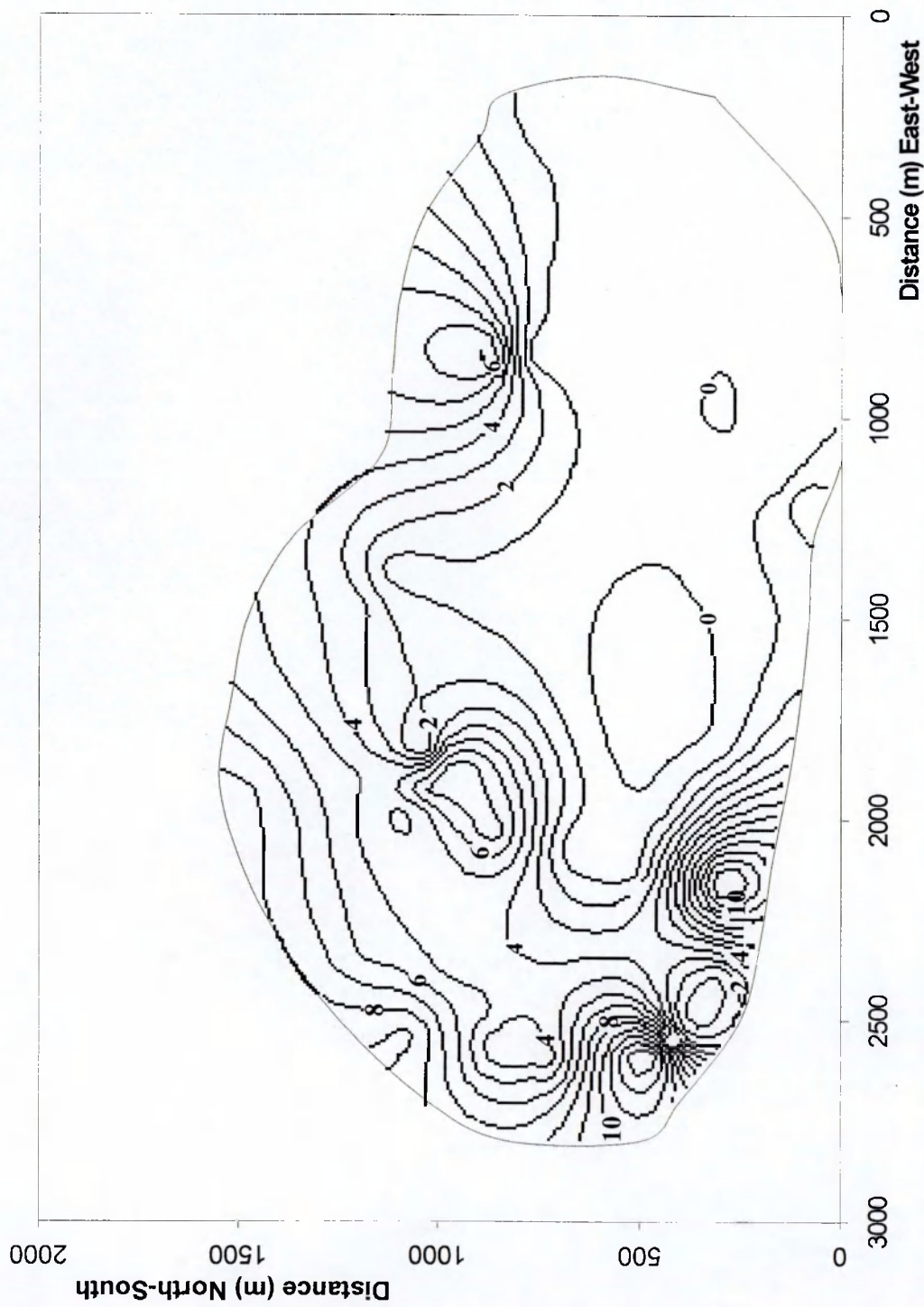


Figure 6.3. Contour plot for the magnetic susceptibility values from the Penmaenmawr Intrusion using Surfer for Windows, surface-mapping system.

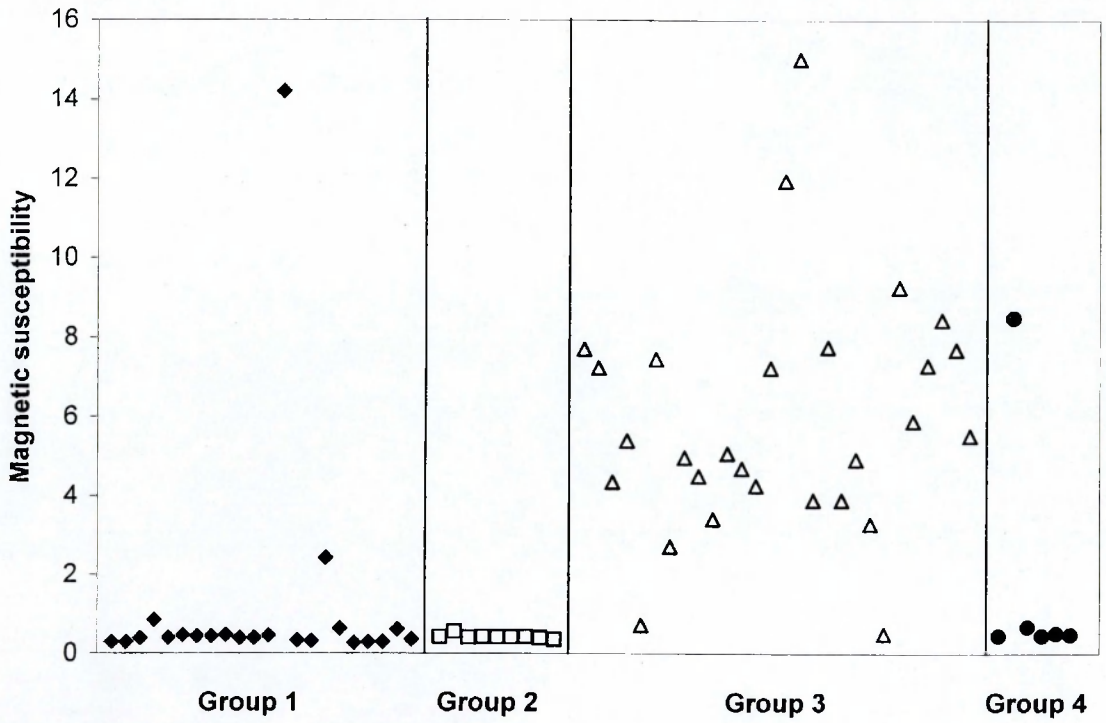


Figure 6.4. Magnetic susceptibility values for the Penmaenmawr samples from Groups 1-4, divided according to their groups.

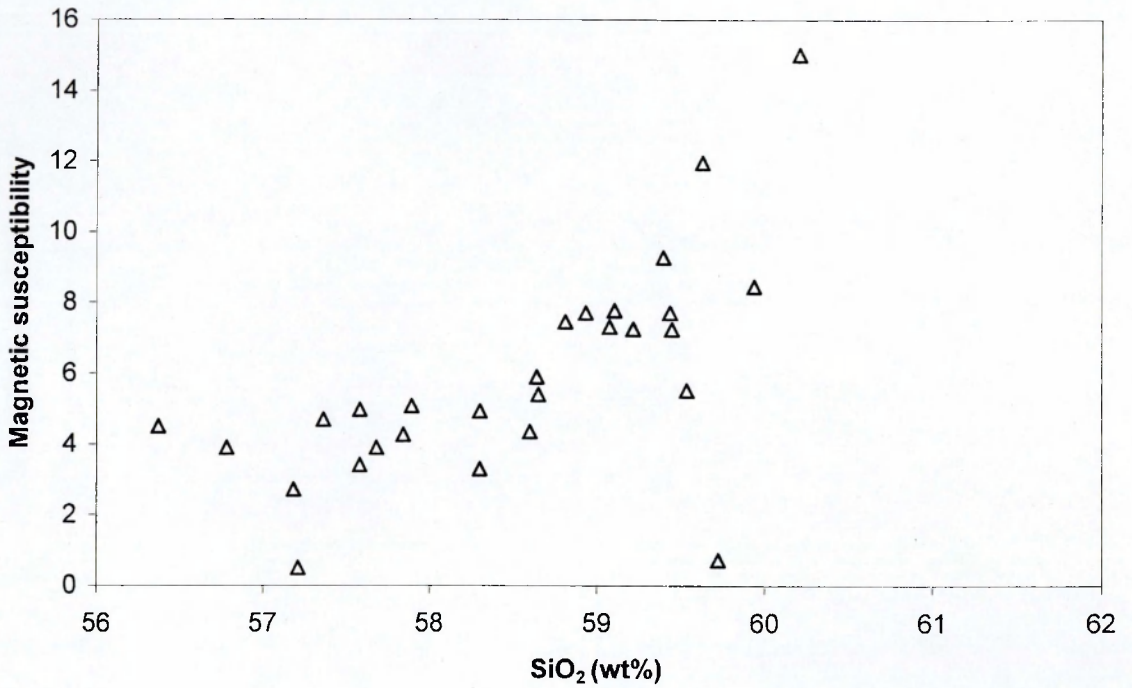


Figure 6.5. Magnetic susceptibility values for the Penmaenmawr samples from Group 3 against silica content (SiO₂) (wt%).

In order to investigate the magnetic susceptibility variation within Group 3 rocks in more detail, the magnetic susceptibility values were plotted against SiO₂ contents of the samples (details of the whole rock geochemistry are presented in Chapter 8). This plot is presented in Figure 6.5 and shows that the magnetic susceptibility tends to be constant, at between 3 and 4 x 10⁻³ SI, with SiO₂ compositions from 56% to 58.7% and then generally increases with increase in SiO₂ contents.

6.5. Magnetic susceptibility - interpretation and discussion

Results from the magnetic susceptibility studies tend to support some of the division of the rocks of the Penmaenmawr Intrusion into petrographic groups. Group 3 samples, in the western part of the intrusion tend to have high magnetic susceptibility values, above 2.4 x 10⁻³ SI, whereas samples from Groups 1, 2 and 4 tend to have magnetic susceptibility values below 1 x 10⁻³ SI. Magnetic susceptibility can, therefore, facilitate the division of Group 3 rocks from the other groups but does not distinguish between Group 1, 2 and 4 rocks.

In Chapter 4, it was shown that samples from Group 3 tend to be less altered than samples from the other Groups, and these results suggest that the magnetic susceptibility values may be associated with the extent of alteration. Where the extent of alteration is low then the magnetic susceptibility values are greater than 2.4 x 10⁻³ SI, but where there is significant alteration the magnetic susceptibility values are reduced to less than 1 x 10⁻³ SI.

Cameron & Carrigan (1987) listed three factors that are likely to exert a major influence the magnetic susceptibility of a sample:

- the primary magnetite content of the sample
- any secondary magnetite formed by the replacement of pre-existing minerals
- the loss of magnetite by late stage oxidation along faults and fractures

Bourne (1993) also included as a factor the magnetic anisotropy of the sample

and Williams-Thorpe *et al.* (1996) reported that lower susceptibilities can result from a decrease in the grain size of magnetic minerals such as titanomagnetite.

In Chapter 5 it was suggested that magnetite intergrown with ilmenite occurs as a primary, minor opaque mineral (<1%) in samples from Group 3. Magnetite is not present, however, in samples from Group 1 (with the exception of sample JD2947 which has an anomalously high magnetic susceptibility) Group 2 or Group 4. The opaque minerals in these Groups are either primary ilmenite or secondary titanite. In Group 2, the most altered group, all the opaque minerals analysed have a titanite composition.

As the magnetic susceptibility is mainly dependent on the presence of magnetite, the magnetic susceptibility data corroborate the mineralogical data presented in Chapter 4 for the medium-grained samples and supports the suggestion that the magnetic susceptibility values are related to alteration.

In Chapter 4, it was noted that the majority of samples from Group 1 are very fine-grained (< 0.01mm) and this together with the lack of magnetite may also account for the low magnetic susceptibility values for samples from this Group.

The increase in magnetic susceptibility with higher SiO₂ contents within Group 3 rocks suggests that at higher SiO₂ contents, there is a greater abundance of magnetite. However, Bourne (1993), on the basis of analyses from a number of granitic plutons, demonstrated that samples with the least magnetic susceptibility have the highest SiO₂ values. This is to be anticipated as primary magnetite tends to crystallise early during fractional crystallisation processes so that sequences of rocks with increasing SiO₂ contents produced by fractional crystallisation should have decreasing magnetic susceptibility values. The increase in magnetic susceptibility values with SiO₂ content in Group 3 rocks appears anomalous therefore and suggests that either this Group may not be linked through fractional crystallisation involving magnetite as a fractionating phase, and that in fact there is an increase in the proportion of magnetite at higher SiO₂ contents caused by another process.

Speer (1987, in Bourne 1993) showed that magmatic reactions in which pyroxenes are replaced by amphiboles or amphiboles by biotite commonly produce magnetite as a by-product. In Chapter 5 it was suggested that in some samples from Group 3, orthopyroxene has been replaced by amphibole whereas in the least altered samples, unaltered orthopyroxene is still present. The rise in magnetic susceptibility with SiO₂ content within the Group 3 rocks could therefore be due to an increase in the proportion of magnetite caused by an early alteration event, and that if this were the case then the various samples in Group 3 would still be related through a fractional crystallisation process.

CHAPTER 7. THE WHOLE ROCK GEOCHEMISTRY OF THE PENMAENMAWR INTRUSION

7.1. Introduction

This chapter presents details of the whole rock geochemistry of the rocks from the Penmaenmawr Intrusion and uses them to illustrate the variations within the intrusion, to classify the rock types according to well-established discrimination diagrams and to examine the mobility of elements during alteration.

Whole rock geochemical analyses were carried out on all seventy samples collected from the intrusion (details of the sample numbers and locations were presented in Chapter 3). The samples were prepared for XRF analysis following the standard procedures of the Department of Earth Sciences, Open University (detailed in Appendix 5). Major element compositions were obtained in weight percent of their oxides and trace element compositions were in parts per million. The major and trace element compositions of all samples are presented in Appendix 6.

7.2. Geochemical classification of the rocks from the Penmaenmawr Intrusion

The Penmaenmawr rocks can be classified on the total alkalis versus silica (TAS) diagram for plutonic rocks of Cox *et al.* (1979), adapted by Wilson (1989) (Figure 7.1). On this diagram the samples from Groups 2, 3 and 4 plot in the diorite field along a fairly tight trend whereas most Group 1 samples plot in the quartz diorite field with only a few plotting in the diorite field. However, because the rocks are sub-volcanic, and in order to be consistent with Ball and Merriman (1989) the samples were also plotted on the total alkalis versus silica (TAS) diagram for volcanic rocks of Le Maitre *et al.* (1989) (Figure 7.2). In this diagram the samples plot mainly in the andesite field, with a few samples from Group 3 rocks falling in the basaltic andesite field, and most samples from Group 1 rocks falling in the dacite field.

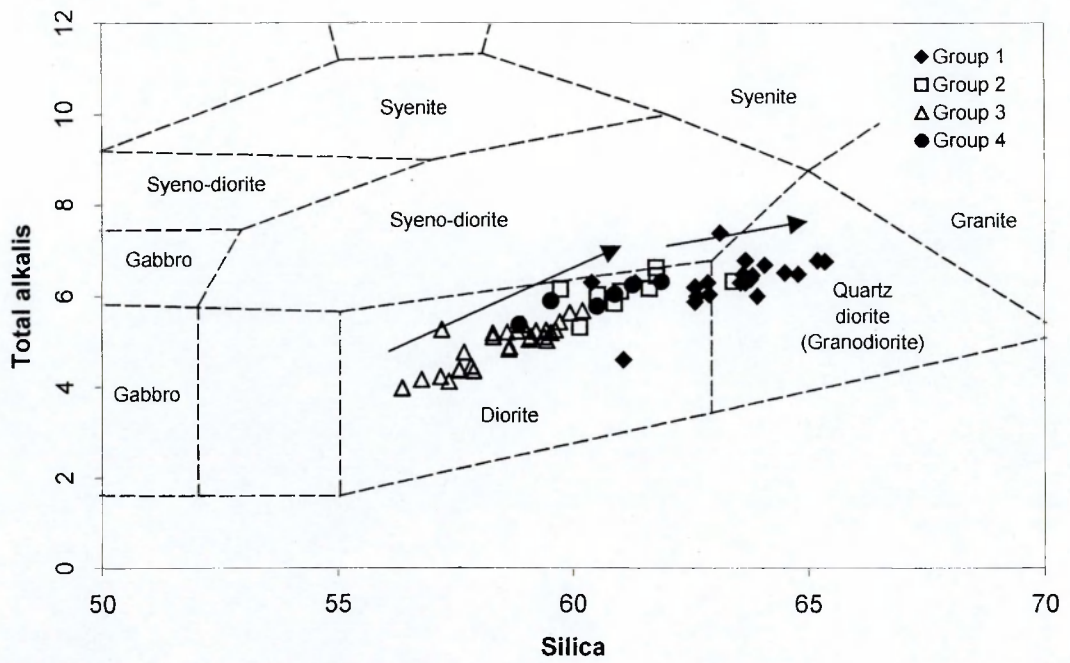


Figure 7.1. Total alkalis ($\text{Na}_2\text{O}+\text{K}_2\text{O}$) (wt%) versus silica (SiO_2) (wt%), TAS diagram for plutonic rocks (from Cox *et al.*, 1979, adapted by Wilson, 1989) showing the Penmaenmawr samples from Groups 1-4 with the fields for gabbro, diorite, quartz diorite, syenite, syeno-diorite and granite also depicted.

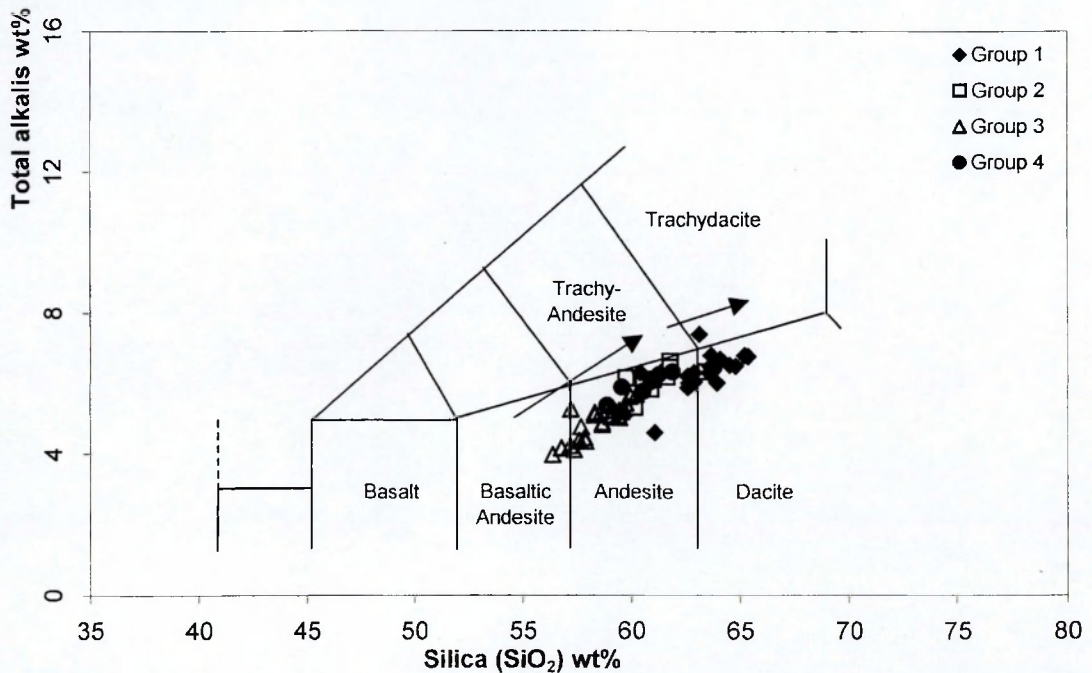


Figure 7.2. Total alkalis ($\text{Na}_2\text{O}+\text{K}_2\text{O}$) (wt%) versus silica (SiO_2) (wt%) (from Le Maitre *et al.*, 1987) for Penmaenmawr samples from Groups 1-4, with the basalt, andesite, basaltic andesite, dacite, trachy-andesite and trachydacite fields also depicted.

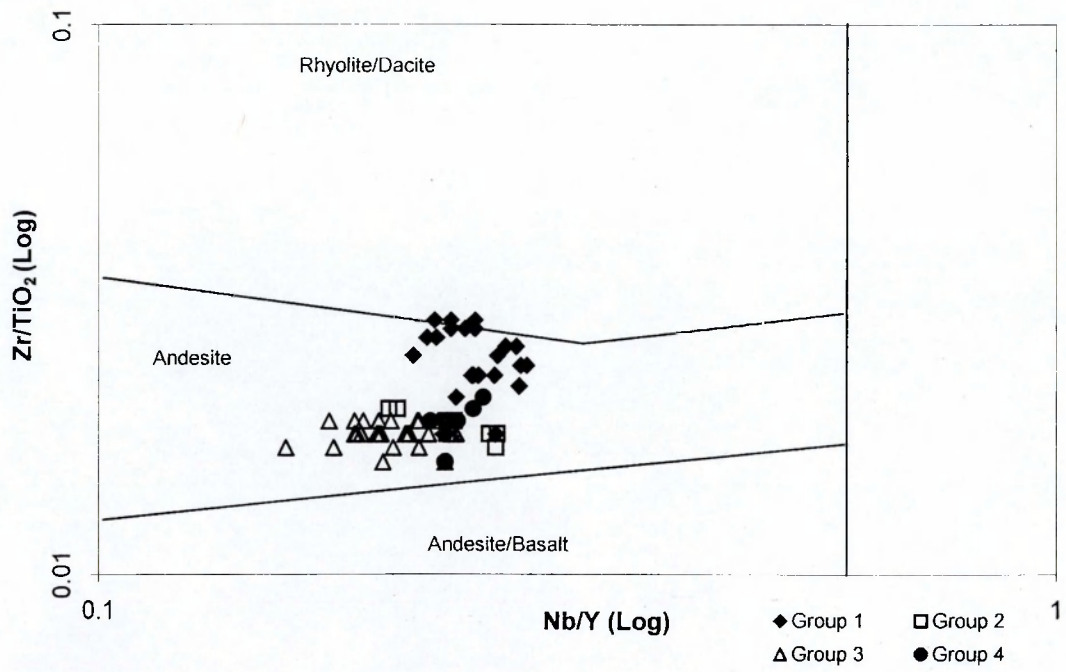


Figure 7.3. Log-log plot of Zr/TiO_2 versus Nb/Y (from Winchester & Floyd, 1987) for the Penmaenmawr samples from Groups 1-4, with the rhyodacite/dacite, andesite and andesite/basalt fields also depicted.

These plots show two tight linear trends, with the contents of total alkalis increasing with increase in SiO₂ content. Three data points (JD2917, JD2901 and JD2953), which are extensively altered samples, plot away from these major trends. The samples from Groups 2, 3 and 4 tend to show a single, positive linear trend on the TAS diagram. The samples from Group 3, with lower SiO₂ and total alkali contents, form the initial part of this trend, with two samples actually plotting in the basaltic andesite field, while the samples from Group 2, with higher SiO₂ and total alkali contents, form the later part of the trend. Samples from Group 1 plot mainly in the dacite field and form a separate linear trend to the other groups. Two samples from Group 1, which were collected close to the Group 4 area, plot near the high silica end of the first trend.

As the TAS diagram is only valid for classifying fresh volcanic rocks, and many of the samples from Penmaenmawr have been altered (see Chapter 4), the above classification may not be valid. Nevertheless when the Penmaenmawr samples are plotted on the Nb/Y versus Zr/TiO₂ diagram of Winchester and Floyd (1978) (Figure 7.3), which is based on elements that are considered to have low mobility during alteration, they plot in a tight area mainly within the andesite field but with a few samples from Group 1 plotting in the rhyodacite/dacite field. These results are consistent with the TAS diagram for volcanic rocks and suggests that there has been little mobility of the alkali elements during alteration and that the current contents of alkali elements in these samples are close to their original contents.

7.3. Main geochemical variation and spatial distribution

The range of geochemical variation within the intrusion can be demonstrated simply by the range of SiO₂ contents of the samples, the element with the highest concentration. In the Penmaenmawr Intrusion the range of SiO₂ contents varies continuously from 56% to 65%. However many of the samples from the Penmaenmawr Intrusion have been altered (see Chapter 4), and some of the variation may not be primary magmatic but due to later alteration processes. The trace elements Zr and Y are considered to be immobile during alteration (Pearce & Cann, 1973), and therefore the range of geochemical variation due to primary magmatic processes may be better demonstrated by the contents of these two

elements. The contents of Zr and Y vary continuously from 86 to 227 ppm and 28 to 62 ppm, respectively.

The range, median and average SiO₂, Zr and Y contents of the samples within the four Groups identified in Chapter 4 are presented in Tables 7.1, 7.2 and 7.3 respectively. The difference between the median and the average should give an indication of whether there is a bias in the distribution and whether the samples collected are representative of the group as a whole.

Table 7.1. SiO₂ contents of the 4 Groups from the Penmaenmawr Intrusion

	Range	Median	Average
Group 1	60.4% - 65.4%	62.9%	63.2%
Group 2	59.7% - 63.4%	61.6%	61.3%
Group 3	56.4% - 60.2%	58.3%	58.5%
Group 4	58.9% - 61.9%	60.4%	60.5%

Table 7.2. Zr contents of the 4 Groups from the Penmaenmawr Intrusion

	Range	Median	Average
Group 1	183-210 ppm	196 ppm	196 ppm
Group 2	147-227 ppm	187 ppm	181 ppm
Group 3	86-173 ppm	129 ppm	125 ppm
Group 4	147-181 ppm	164 ppm	166 ppm

Table 7.3. Y contents of the 4 Groups from the Penmaenmawr Intrusion

	Range	Median	Average
Group 1	47-53 ppm	50 ppm	50 ppm
Group 2	41-62 ppm	52 ppm	48 ppm
Group 3	28-47 ppm	37 ppm	36 ppm
Group 4	40-49 ppm	45 ppm	45 ppm

These data show that Groups 1 and 3 can be separated from each other by their SiO₂, Zr and Y contents. Samples from Group 1 have SiO₂ contents above 60.4%, Zr above 180 ppm and Y above 47 ppm, whereas samples from Group 3 have SiO₂ contents below 60.2%, Zr below 180 and Y below 47. However samples from Group 2 and Group 4 tend to be intermediate between Groups 1 and 3 and their SiO₂, Zr and Y contents overlap with those from the adjacent parts of Group 3 and Group 1.

7.3.1. Main geochemical variations with height

A plot of SiO₂ contents of the samples against height above sea level is presented in Figure 7.4 (see also Appendix 12). Group 1 rocks, which have the highest SiO₂ contents, are found at the highest levels and Group 2 rocks, with intermediate SiO₂ contents, tend to form a compact group at a high elevation of about 350–370 m above sea level. Group 3 rocks, which have the lowest SiO₂ contents and Group 4 rocks with intermediate SiO₂ contents are found at widely varying heights.

These data suggest that the Penmaenmawr Intrusion is not horizontally layered with respect to today's sea level. However, the Penmaenmawr Intrusion is only exposed down to sea level on the north-western boundary, where it rises above the north Wales coast and Group 3 rocks were found at all heights in this boundary area. The only other exposures at low level are in the small quarries northwest of Graig Lwyd where Group 4 rocks are found.

However, in Chapter 3 it was reported that the shales into which the Penmaenmawr Intrusion has been emplaced dip at about 40° to the southeast and that the intrusion may have been subjected to post solidification deformation during the Acadian phase of the Caledonian Orogeny. Any original vertical layering in the intrusion could therefore have been rearranged so that it no longer corresponds to present day heights. The Group 3 rocks on the north-western boundary of the intrusion show very little compositional variation with height, which would suggest that if the intrusion had been originally horizontally layered, it was subsequently rotated through 90° so that the layers are now vertical. As the country shales dip at 40°, it is considered unlikely that sufficient deformation to rotate the intrusion 90° could have occurred.

7.3.2. Geochemical variations across the intrusion

In order to determine the extent of the geochemical variation across the Penmaenmawr Intrusion, the SiO₂, Zr and Y contents of samples were plotted on simplified outlines of the intrusion (see Figures 7.5, 7.6 and 7.7). These diagrams show that samples with the highest SiO₂, Zr and Y contents occur along the

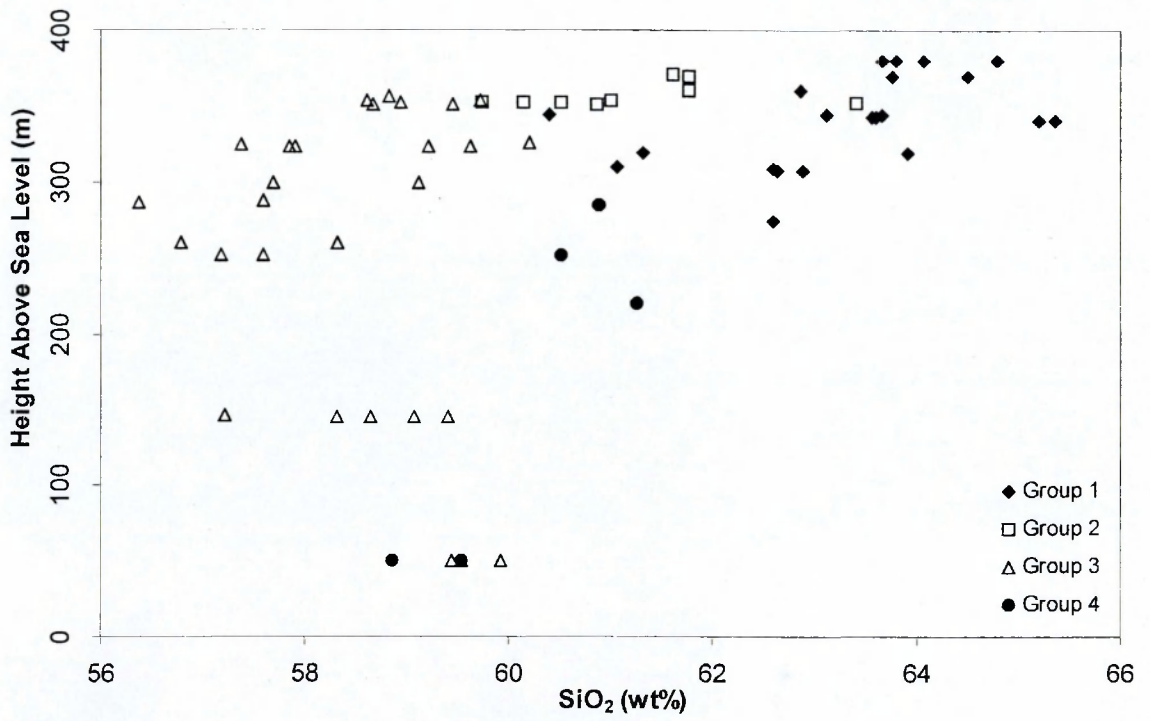


Figure 7.4. Plot of height above sea-level against silica (SiO₂) (wt%) for the Penmaenmawr samples from Groups 1-4.

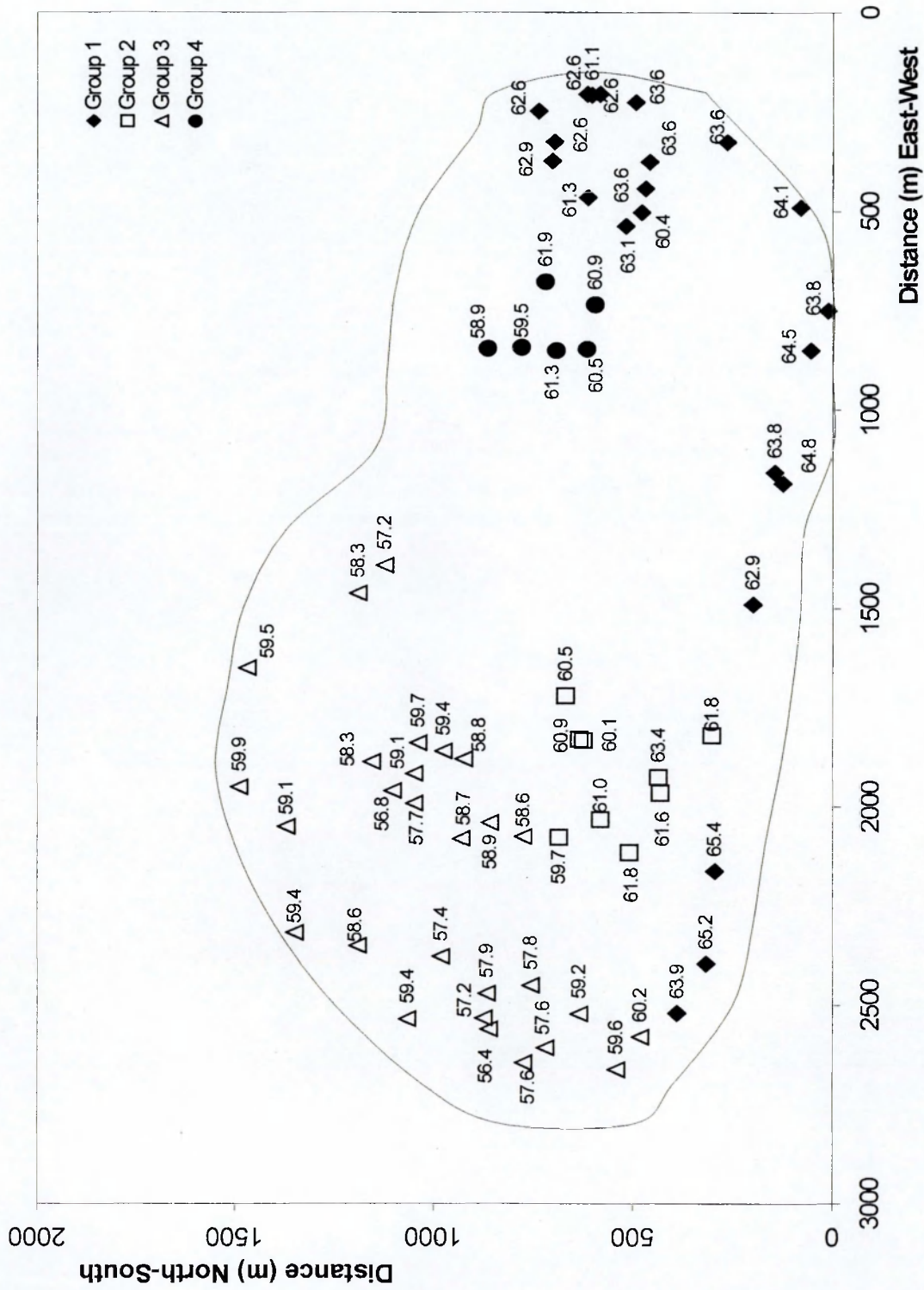


Figure 7.5. Plot of silica (SiO₂) (wt%) values of the Penmaenmawr samples from Groups 1-4, with respect to the location of the samples.

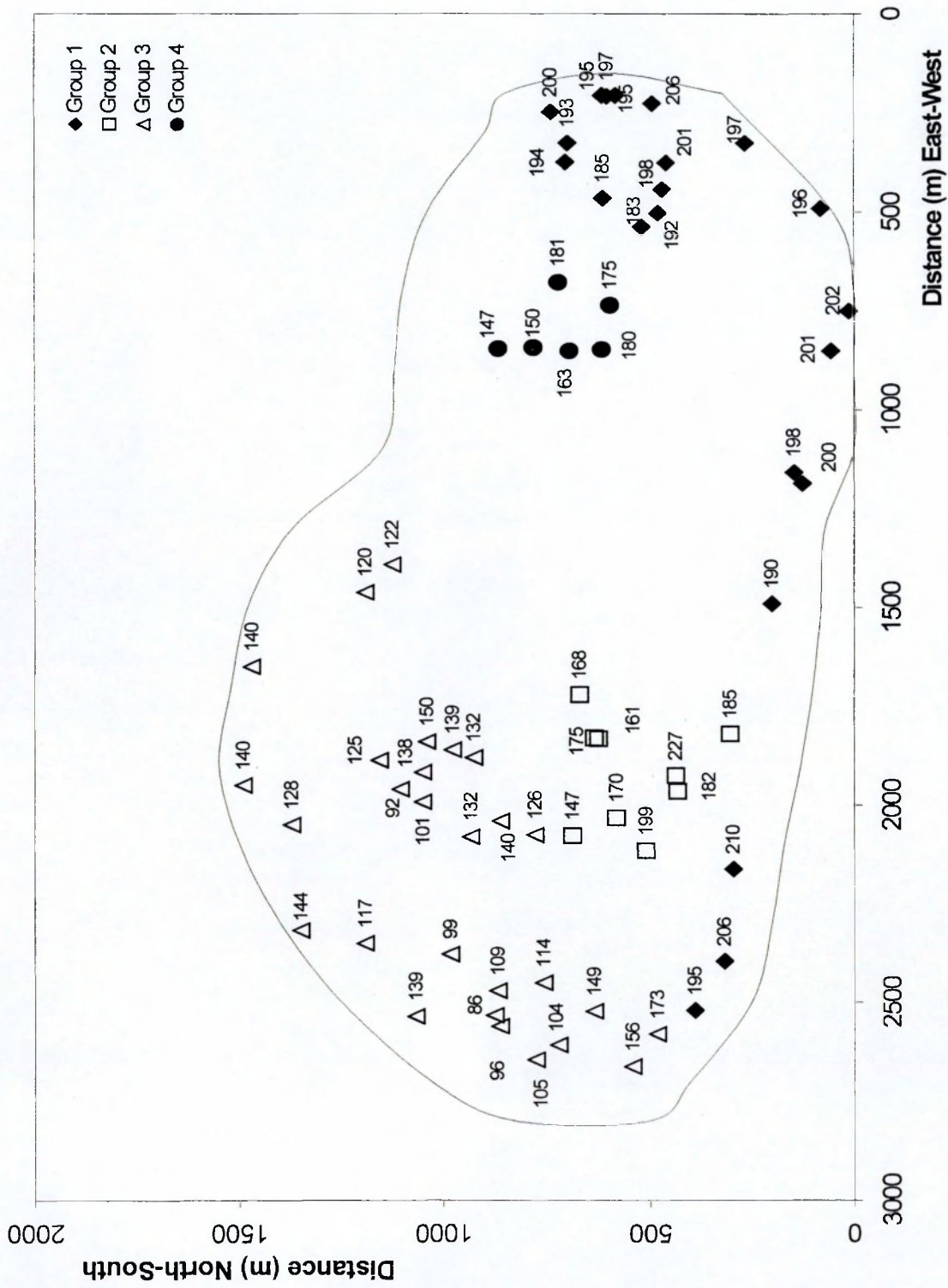


Figure 7.6. Plot of Zr (ppm) values of the Penmaenmawr samples from Groups 1-4, with respect to the location of the samples.

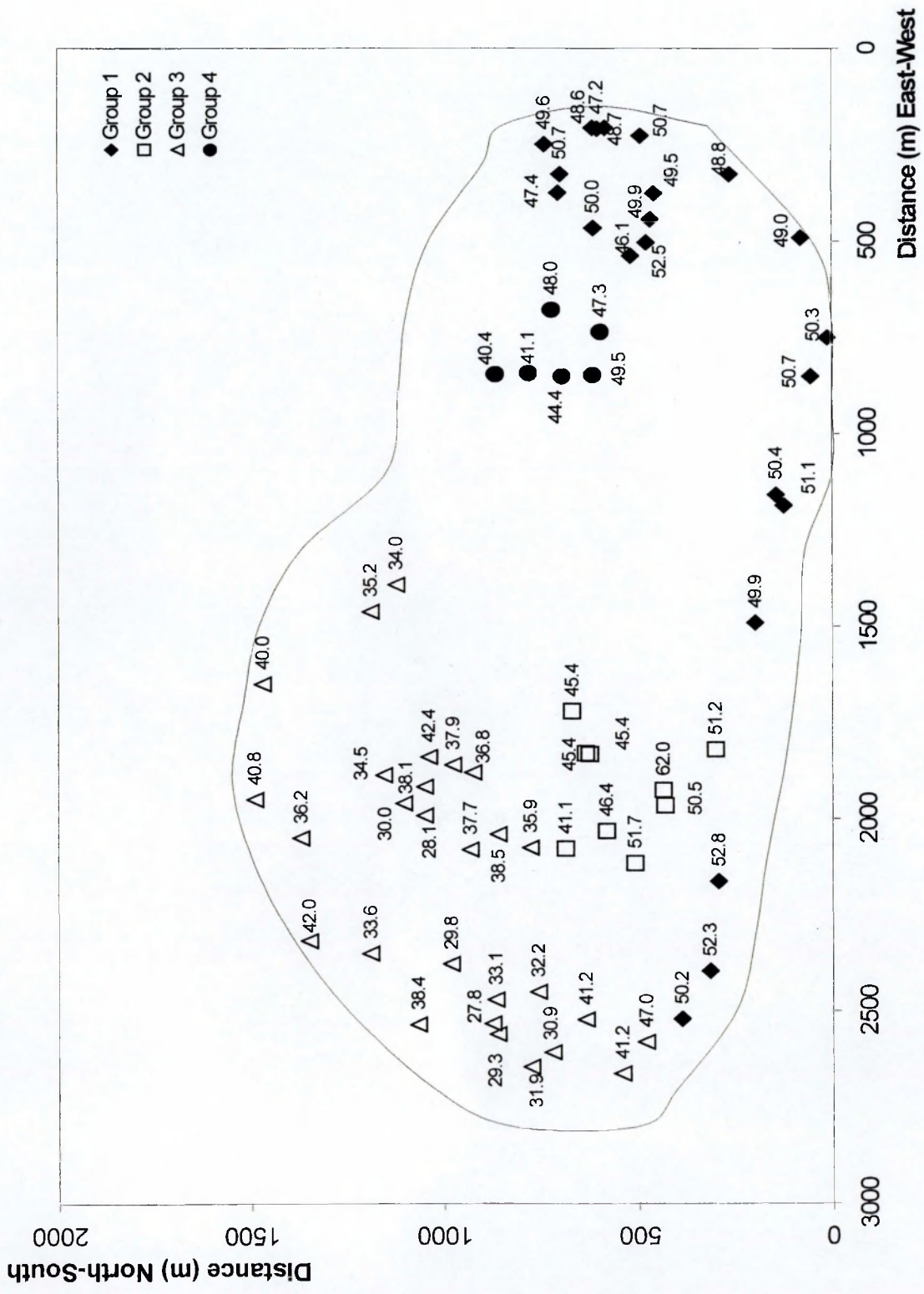
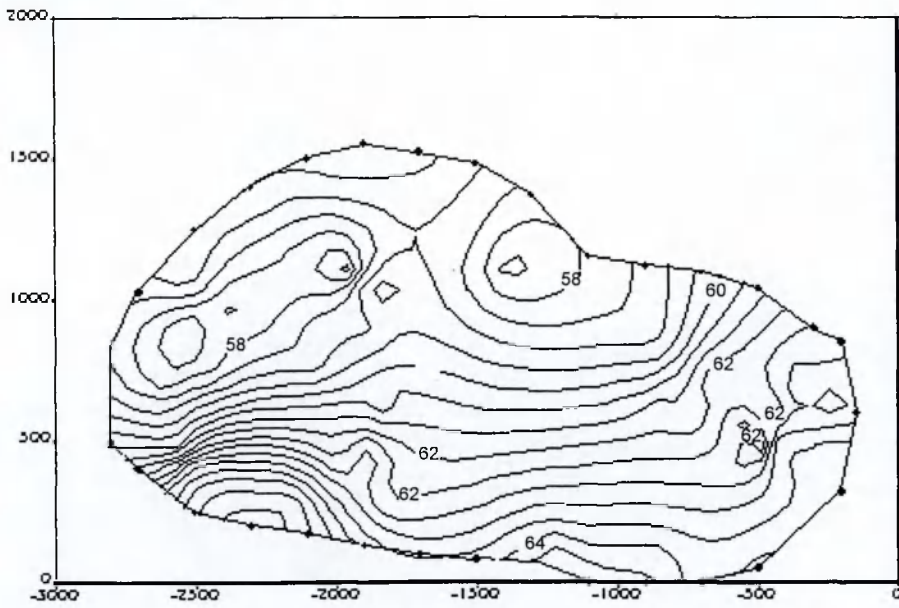
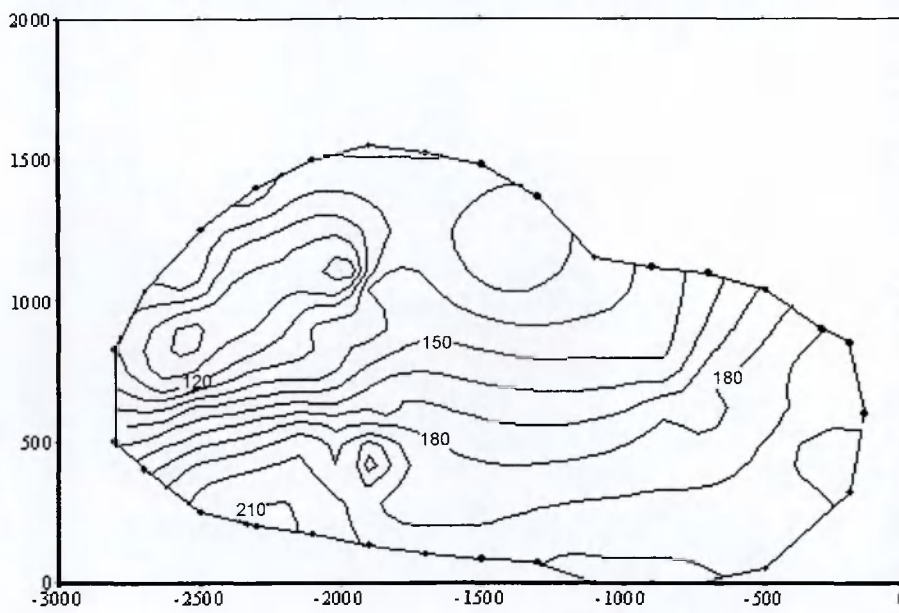


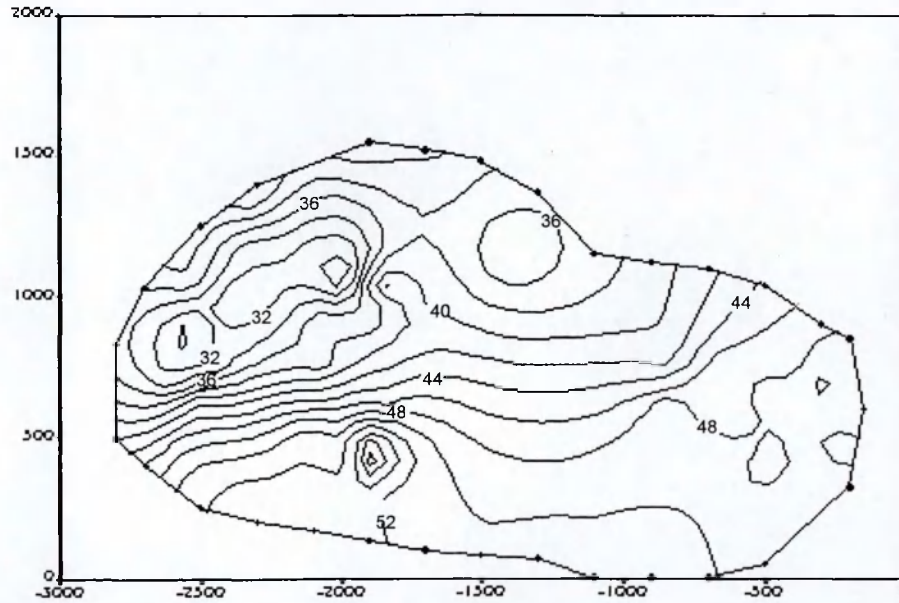
Figure 7.7. Plot of Y (ppm) values of the Penmaenmawr samples from Groups 1-4, with respect to the location of the samples.



a) SiO₂



b) Zr



c) Y

Figure 7.8. Contour plots of (a) SiO₂, (b) Zr and (c) Y contents across the Penmaenmawr Intrusion using the Surfer for Windows surface mapping program.

southern and eastern boundaries of the intrusion, the samples with the lowest SiO₂, Zr and Y contents occur close to but not at the north-western boundary of the intrusion, and between them are samples with intermediate SiO₂, Zr and Y contents.

In order to investigate this variation in more detail, contour diagrams for the SiO₂, Zr and Y contents were generated using Surfer for Windows, a surface-mapping system; these are presented in Figure 7.8. All three diagrams show consistent contour patterns, which suggests that the variation is most likely to be of primary magmatic origin and not the product of later alteration as Zr and Y are considered to be immobile during alteration. These diagrams show that the SiO₂, Zr and Y contents increase regularly across the intrusion with an approximately northwest to southeast trend. The contour lines tend to be closer together in the western part of the intrusion than in the eastern part. However, contour plots will tend to smooth out any sharp changes and will compensate for the areas where there is a lack of exposure and the geographic distribution of samples precludes a more detailed analysis of spatial variation in geochemistry.

7.4. Element mobility

Major elements such as Ti, P, and Al, high field strength (HFS) trace elements such as Zr, Y, and Nb, and the transition elements Co, Ni, V, and Cr are generally considered to be immobile during alteration, whereas Ca, Na, K, the incompatible elements Cs, Sr, Rb, and Ba, and the transition elements Mn, Zn, and Cu are generally considered to be mobile (Rollinson, 1993). This section examines the data from the Penmaenmawr Intrusion in order to determine the mobility of elements during alteration, findings which can then be taken into account when analysing the results of geochemical variations and petrogenetic modelling, presented later in this thesis.

7.4.1. Zr content plots

In order to examine the extent of element mobility within the intrusion the concentration of major and trace elements were plotted against Zr, an element that is considered to be immobile in most alteration processes (Rollinson, 1993).

Where strong linear correlations occur, it is likely that the changes in element contents are due to magmatic processes. However, where there are either a number of samples that plot away from the main trends or there is a scatter of points, it is likely that one or other element has been mobilised to some degree.

The plots showing major element contents plotted against Zr contents are presented in Figure 7.9, and plots showing the trace element contents plotted against Zr contents are presented in Figure 7.10.

The plots for Zr versus MgO, and the immobile elements Y and Ni, show tight linear trends whereas in contrast the plot for Zr versus Sr shows a considerable scatter of points. The plots for Zr versus TiO₂, Fe₂O₃, Co, V, and Zn all show reasonably tight trends for low values of Zr and a distinct change in slope at about 170 ppm Zr, which tends to coincide with the distribution of plots for samples from Group 1. The plot for SiO₂ is similar in that it shows a tight linear trend to about 170 ppm and then the points become more scattered, although there still appears to be a change in slope of the trend. The plots for Zr content versus Al₂O₃, TiO₂, P₂O₅, Nb, and Cr generally show tight trends although at higher Zr contents the points tend to scatter. The plots for Zr versus Fe₂O₃ and MnO show a number of points plotting above the main trend while the plot for Zr versus CaO shows a number of points plotting below the main trend, particularly at higher Zr values.

The plots for Zr versus Na₂O, K₂O, Ba, and Rb show a reasonably good correlation with Zr, although in all plots there are a number of points that plot above and below the main trends. The plots for Zr versus Sr, Pb, V, and Zn show a high degree of scatter.

The tight linear trends for the plots of MgO, Y and Ni strongly suggest that they were immobile during the alteration of the Penmaenmawr Intrusion and the considerable scatter of points in the plot for Zr versus Sr shows that Sr is highly mobile during alteration. In view of the fact that Sr tends to be concentrated in plagioclase feldspar, this apparent mobility suggests that even in the unaltered samples plagioclase feldspar is beginning to break down.

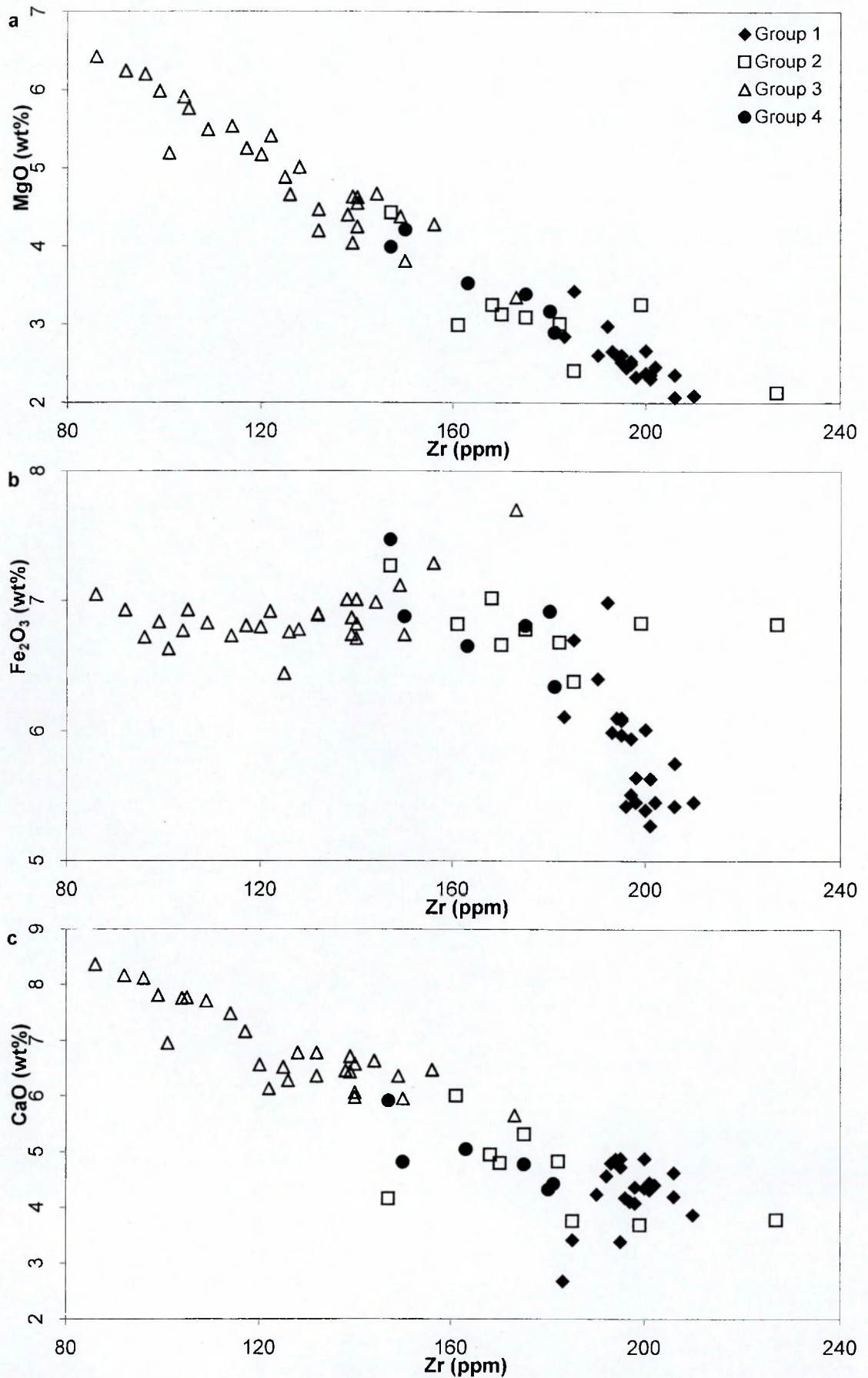


Figure 7.9. Plots of selected major elements (wt%) against Zr (ppm), for the Penmaenmawr samples from Groups 1-4, (Legend provided on plot (a)): (a) MgO, (b) Fe₂O₃ and (c) CaO (continued overleaf).

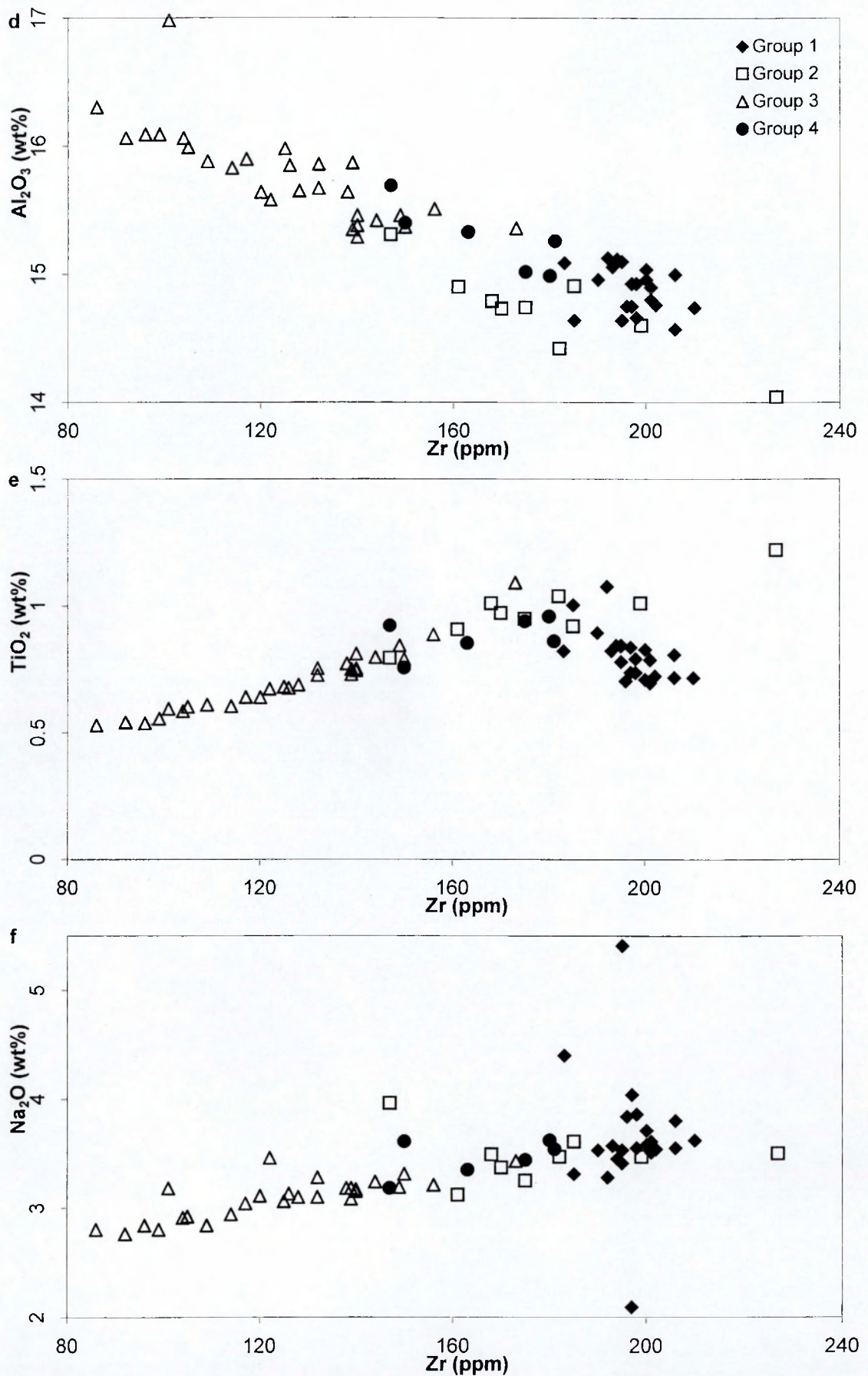


Figure 7.9 (continued). Plots of selected major elements (wt%) against Zr (ppm), for the Penmaenmawr samples from Groups 1-4 (Legend provided on plot (d)): (d) Al_2O_3 , (e) TiO_2 and (f) Na_2O , continued overleaf.

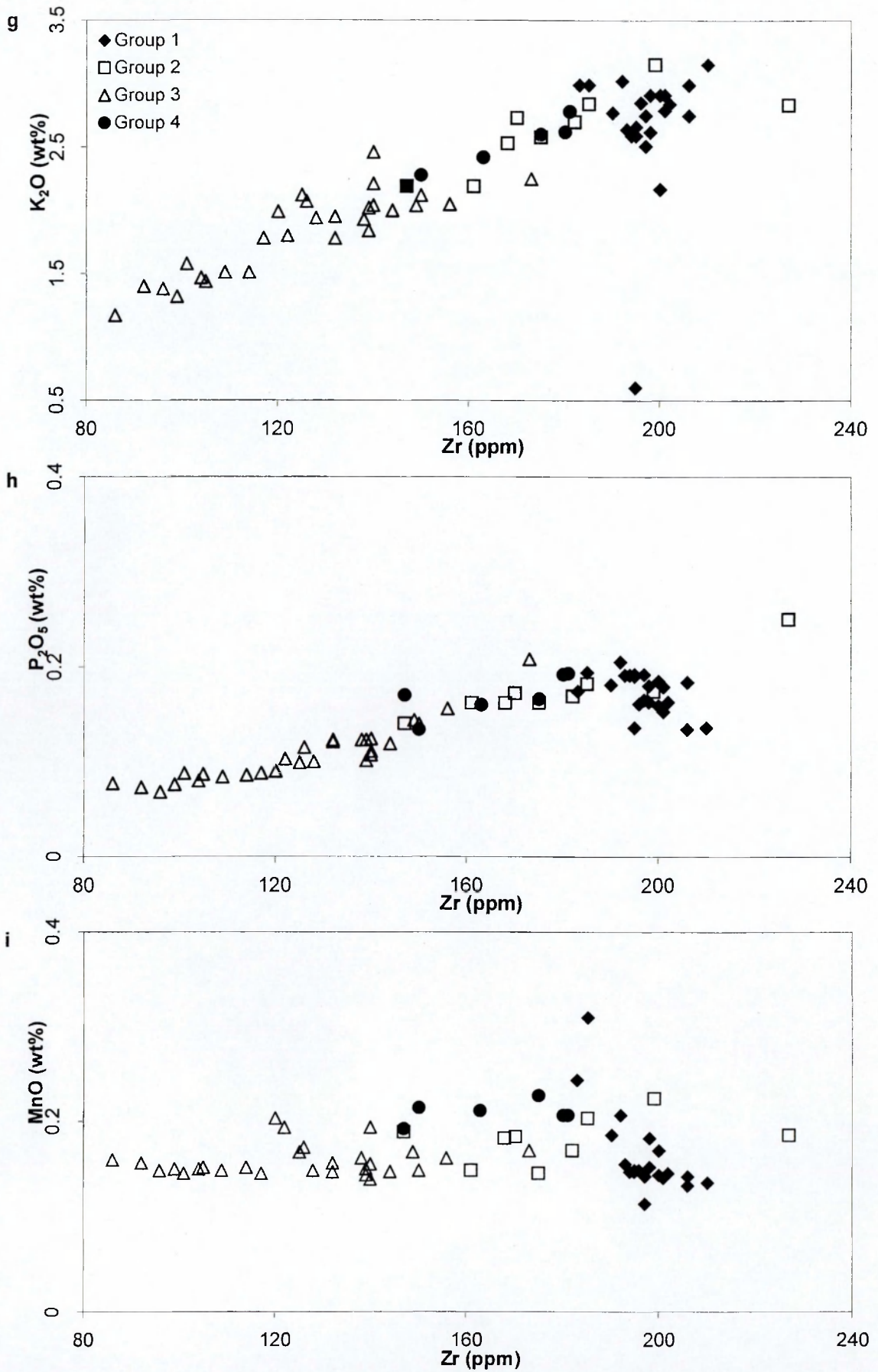


Figure 7.9. (continued). Plots of selected major elements (wt%) against Zr (ppm), for the Penmaenmawr samples from Groups 1-4 (Legend provided on plot (g)): (g) K_2O , (h) P_2O_5 and (i) MnO , continued overleaf.

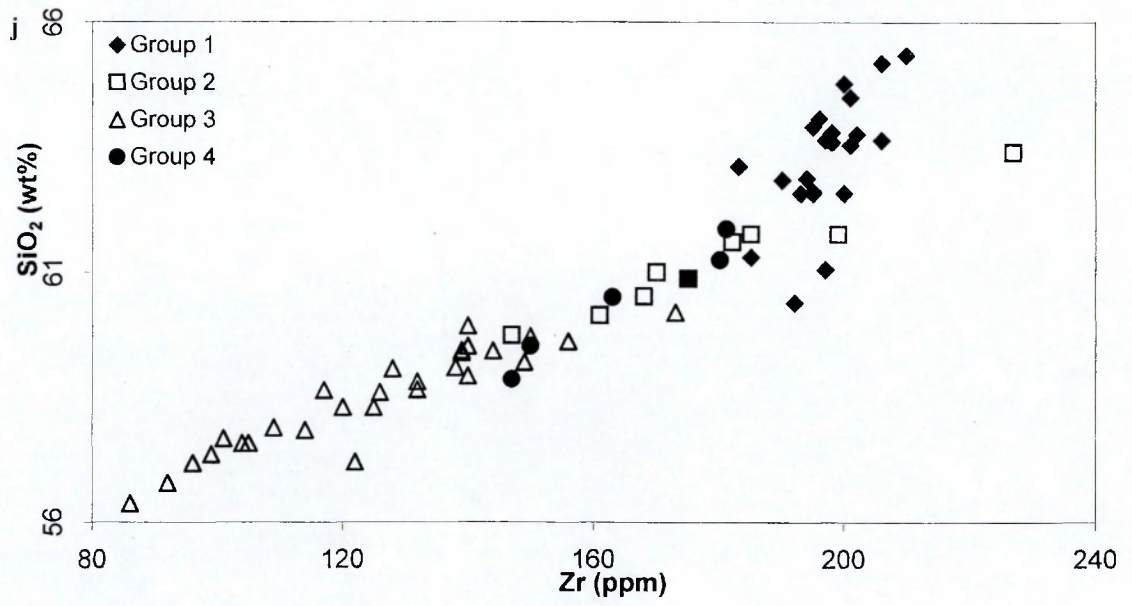


Figure 7.9 (continued). Plots of selected major elements (wt%) against Zr (ppm), for the Penmaenmawr samples from Groups 1-4, (Legend provided on plot (j)): (j) SiO₂.

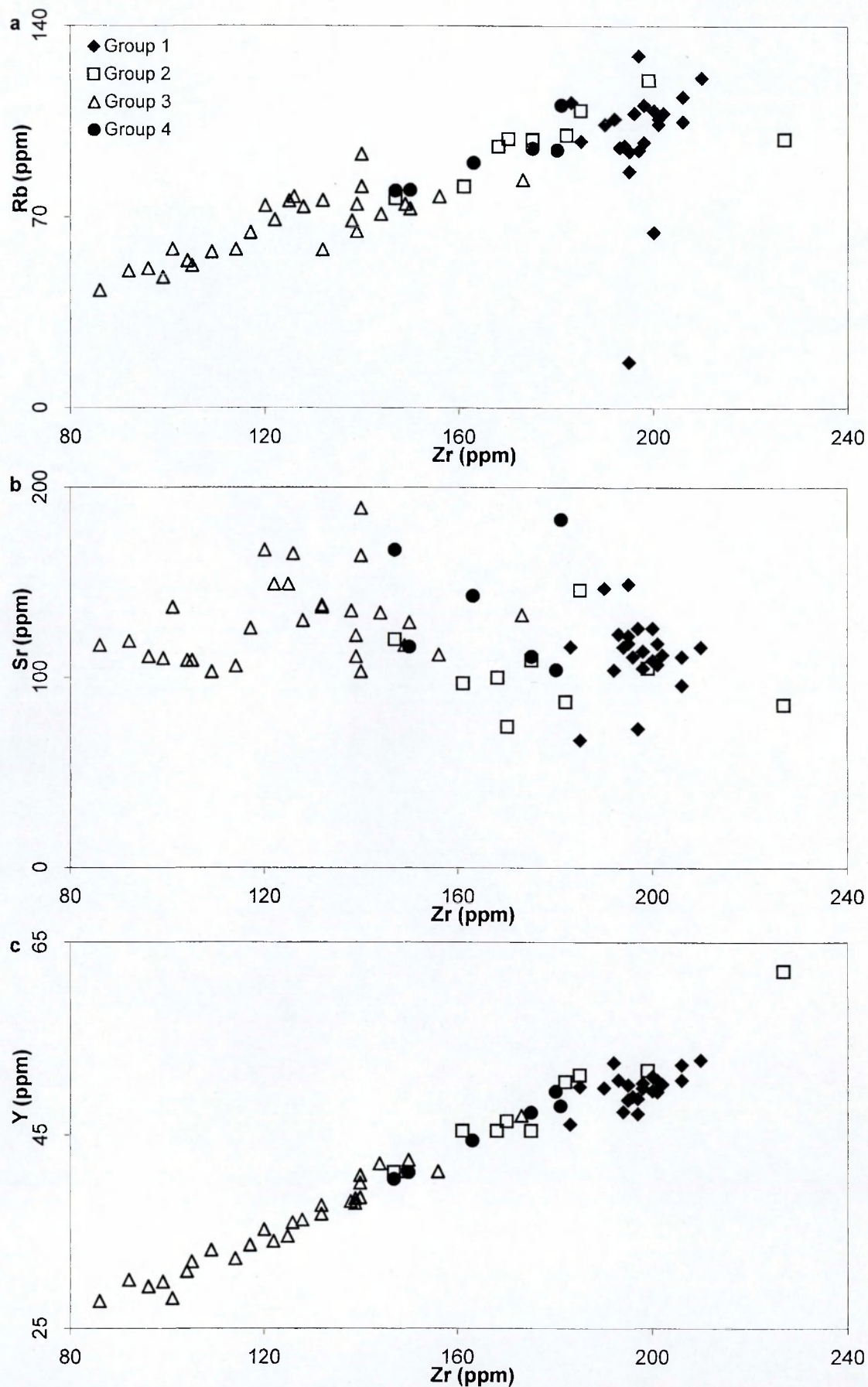


Figure 7.10. Plots of selected trace elements (ppm) against Zr (ppm), for the Penmaenmawr samples from Groups 1-4 (Legend provided on plot (a)): (a) Rb, (b) Sr and (c) Y (continued overleaf).

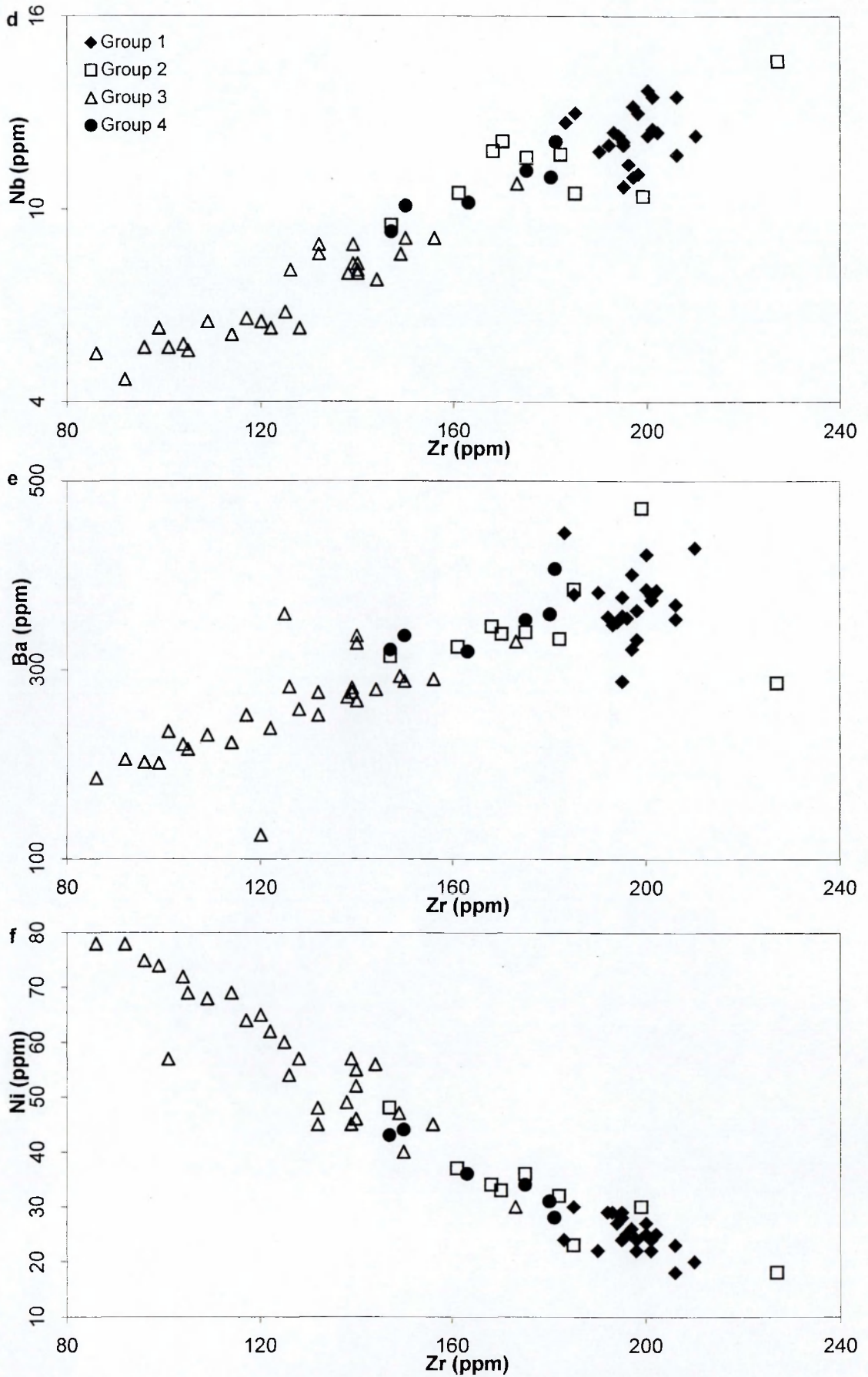


Figure 7.10 (continued). Plots of selected trace elements (ppm) against Zr (ppm), for the Penmaenmawr samples from Groups 1-4 (Legend provided on plot (d)): (d) Nb, (e) Ba and (f) Ni (continued overleaf).

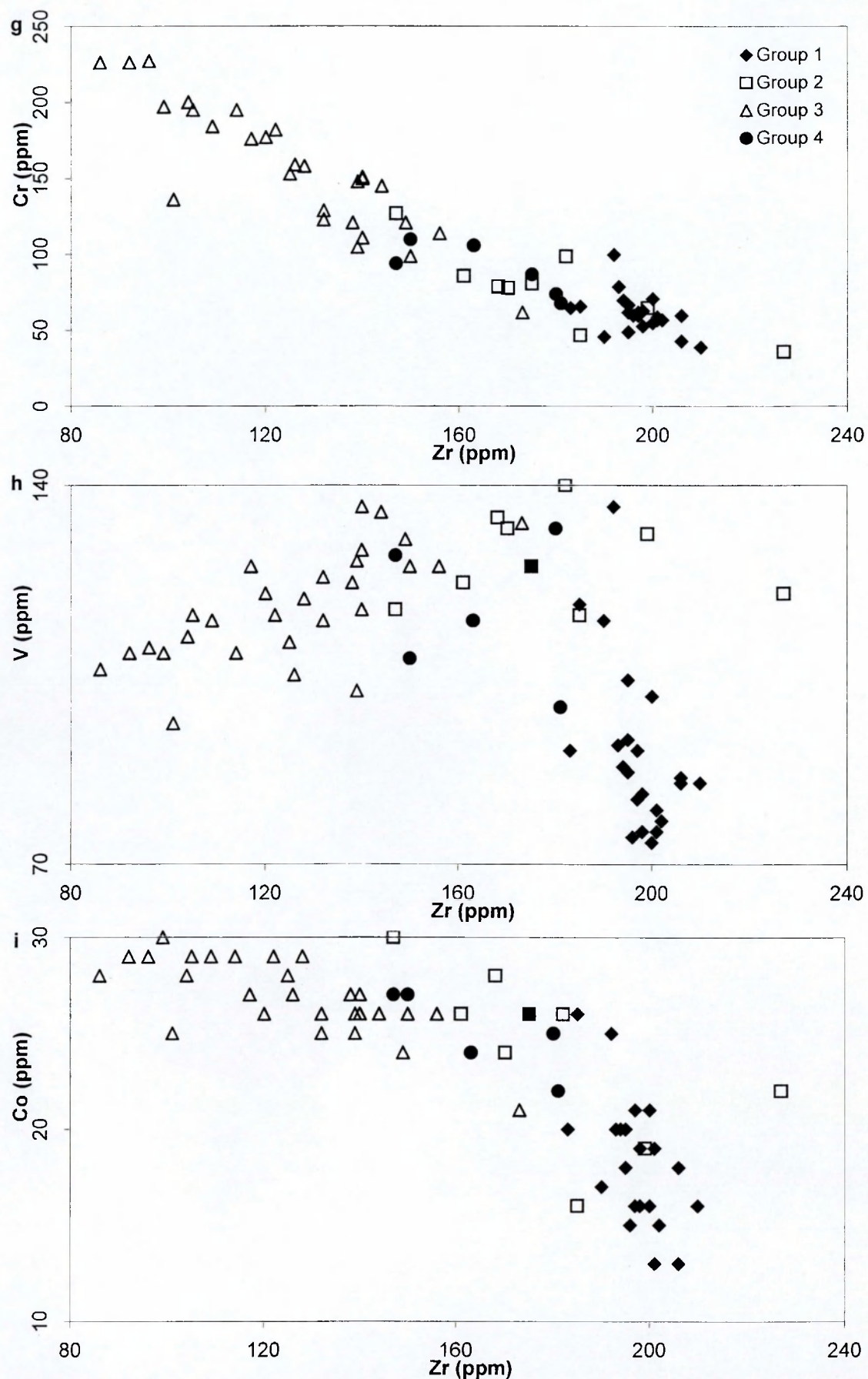


Figure 7.10 (continued). Plots of selected trace elements (ppm) against Zr (ppm), for the Penmaenmawr samples from Groups 1-4 (Legend provided on plot (g)): (g) Cr, (h) V and (i) Co (continued overleaf).

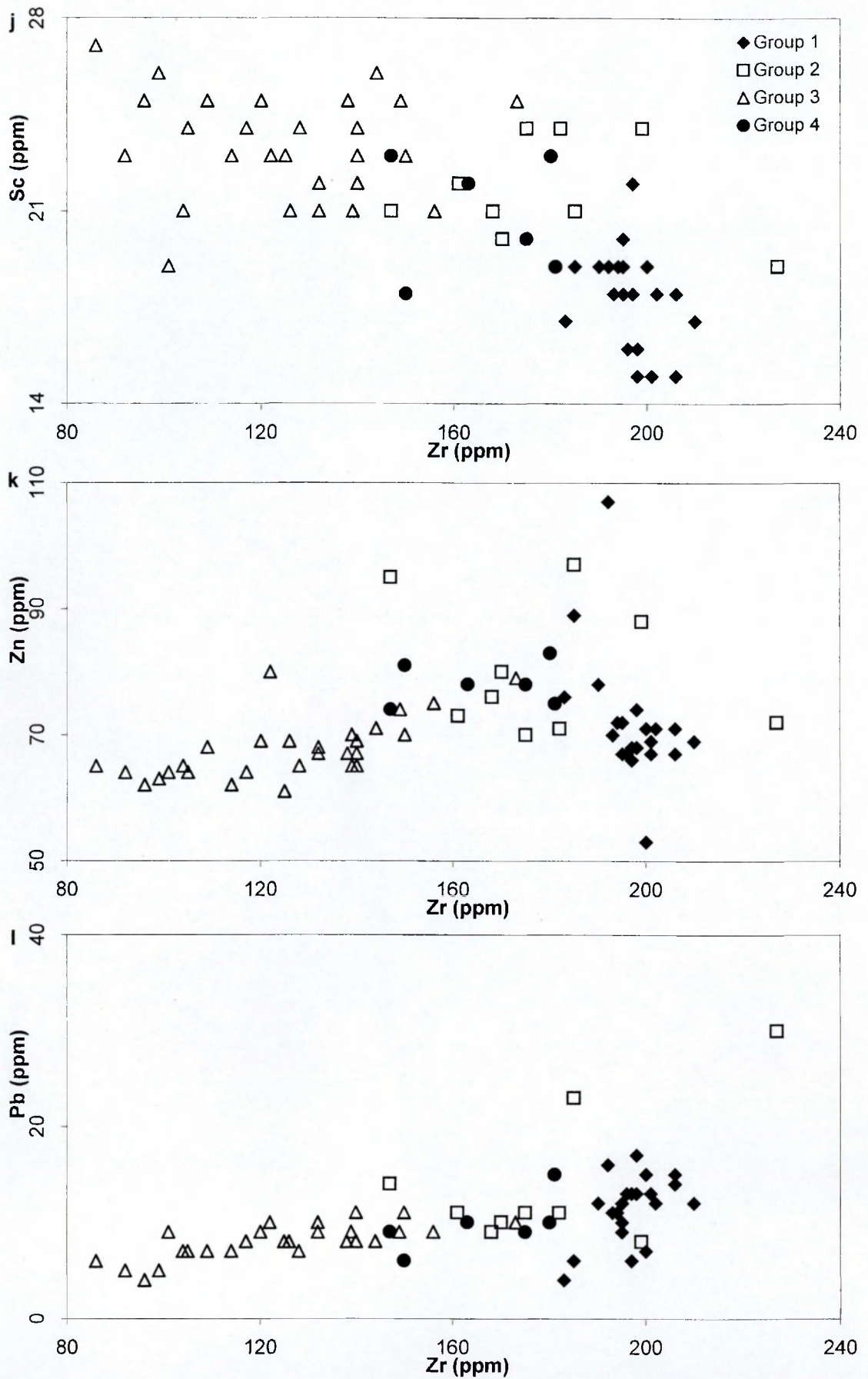


Figure 7.10 (continued). Plots of selected trace elements (ppm) against Zr (ppm), for the Penmaenmawr samples from Groups 1-4 (Legend provided on plot (j)): (j) Sc, (k) Zn and (l) Pb.

The change of slope in the plots for Zr versus TiO_2 , Co, V and Zn all occur at roughly the same Zr concentration and a possible cause may be related to a change in the primary magmatic process, such as a change in fractionating minerals; this will be examined in more detail in Chapter 10.

The initial tight trend on the plot of Zr versus SiO_2 suggests that SiO_2 is immobile for most samples within the Penmaenmawr Intrusion. However the scatter of points at higher concentrations of Zr suggests that in the area occupied by Group 1 rocks, alteration may have been more intense and SiO_2 became mobilised. Part of this Group is located along the southern boundary of the intrusion, in contact with poorly metamorphosed shales, and the source of the fluids could have been from dehydration reactions occurring in the shales during metamorphism. The silica mobilised during alteration could account for the presence of quartz veins in this part of the Penmaenmawr Intrusion, reported in Chapter 3.

The plots for Al_2O_3 , TiO_2 , P_2O_5 , Nb, and Cr also show a slight scatter of points at high Zr contents. The variation in Al_2O_3 contents could be related to the breakdown of primary plagioclase feldspar, leading to the formation of albite, coupled with the formation of alkali feldspar, and linked to the corresponding removal of Ca. The variation in Cr could be due to the alteration of amphibole to chlorite while the variation in TiO_2 and Nb could be linked to the alteration of ilmenite to titanite.

Variations in the plots for Fe_2O_3 and MnO suggest that these elements were, at least locally, highly mobile during alteration. This could also be due to the breakdown of amphibole and the formation of chlorite. Variations in the plots for CaO suggest that Ca was mobilised during alteration, most probably linked to the breakdown of plagioclase feldspar releasing Ca. Ca could then be taken up by the alteration of orthopyroxene to amphibole and the by the formation of prehnite and pumpellyite; the plots, however, suggest that, in some cases, Ca was apparently lost from the system.

Variations in the plots for the mobile elements Na_2O , K_2O , Ba, and Rb do not show a high degree of scatter, despite the amount of alteration that has taken place. As these elements were released by the breakdown of the primary minerals

plagioclase feldspar and biotite, this lack of scatter suggests that these elements were readily incorporated into secondary minerals such as albite and alkali feldspar and were not totally lost from the system.

The high degree of scatter on the plots for Pb, V, and Zn, may suggest that they were mobile during alteration and lost from the system but may be due to a lack of precision of the data. The scatter for the elements Pb and Zn may reflect a small amount of mineralisation despite care in avoiding veins during the preparation of samples.

7.4.2. Element Mobilisation, Summary

During alteration, major elements such as Fe, Ca, Al, Na, Mn, and K were mobilised while Mg and Ti remained relatively immobile. Si became mobile in the southern parts of the intrusion. Na, K, Fe, Mn and mostly all of the Al, and Ca were incorporated into secondary minerals, although some Ca appears to have been removed from the system. Trace elements Zr, Y, and Ni were generally immobile, whereas the trace element Sr appears to have been highly mobile. The trace elements Rb, Ba, Cr and Nb, were relatively immobile in most samples but became more mobile at higher Zr concentrations, perhaps related to the breakdown of plagioclase feldspar, orthopyroxene, ilmenite and biotite.

In Chapter 4 it was observed that Group 2 rocks, located in the Central Quarries, were the most altered rocks from the Penmaenmawr Intrusion and this observation is supported by the Zr plots which generally show a higher degree of scatter for Group 2 rocks. However there is also a high degree of scatter for Group 1 rocks, located at the Craig Lwyd Quarries and along the southern boundary of the intrusion, which suggests they are also highly altered but due to their very fine grain size is not immediately apparent from thin section observations.

CHAPTER 8. DISCUSSION AND POSSIBLE ORIGINS OF THE ALTERATION OBSERVED IN THE PENMAENMAWR INTRUSION

8.1. Introduction

In Chapters 4, 5 and 7 it was shown that the rocks of the Penmaenmawr Intrusion had undergone varying degrees of alteration and that certain elements had been mobilised during the alteration events. In Chapter 4, based on an examination of thin sections, five zones with varying amounts of alteration were identified and plotted on a plan of the intrusion. The greatest amounts of alteration appear to have taken place within the central part of the intrusion and along the southern boundary of the intrusion; in contrast, only about 750 m to the west of the central part, the rocks are relatively unaltered.

A number of post-emplacement processes could have caused this alteration, including early Devonian regional metamorphism and deformation, and the passage of hydrothermal fluids through the intrusion. This Chapter reviews these two key processes, evaluates their possible effects on the Penmaenmawr Intrusion and suggests possible processes responsible for the alteration observed in the intrusion.

8.2. Regional metamorphism

Rocks of the Lower Palaeozoic Welsh Basin were subjected to extensive folding and low grade metamorphism during the Acadian orogeny in early to mid Devonian times (Soper *et al.*, 1987). Bevins and Rowbotham (1983), in a study of mineral assemblages from the Paratectonic Caledonides of Wales, showed that metamorphism was predominantly within the prehnite - pumpellyite facies and that greenschist facies metamorphic assemblages occur only in the more central part of the region, a proposal supported by the subsequent investigation of Bevins and Robinson (1993).

Roberts (1981) studied metabasic rocks of Ordovician age from Llŷn and Snowdonia and divided the area into four metamorphic zones, the Penmaenmawr Intrusion being in the "clinozoisite zone" of the greenschist facies.

Subsequently, Roberts & Merriman (1985), using white mica crystallinity and clay mineralogy of pelitic rocks from the Llŷn and Snowdonia area, identified three stages of metapelite recrystallisation, corresponding to the “sub-pumpellyite zone”, the prehnite-pumpellyite facies, and the “clinozoisite” and “biotite” zones of the greenschist facies as defined in the metabasites studied by Roberts (1981). On their metamorphic map the boundary line between stage 2, the prehnite–pumpellyite facies and stage 3, the “clinozoisite” and “biotite zones” of the greenschist facies, terminates at the south-western margin of the Penmaenmawr Intrusion.

If this boundary line were to be extrapolated in a north-easterly direction, it would pass through the Penmaenmawr Intrusion, so that the western part of the intrusion, the least altered part, would be in their stage 2 (the prehnite–pumpellyite facies) and the central and eastern parts of the intrusion, the more altered part, would be in their stage 3 (the “clinozoisite” and “biotite zones” of the greenschist facies). Some of the differences in the alteration of the intrusion could, therefore, possibly be the result of different degrees of metamorphism in different parts of the intrusion.

However, the variation within the Penmaenmawr Intrusion is more complex than a simple bipolar division into two parts and may not necessarily imitate the variation in a different lithology. It is, therefore, necessary to take into account other factors, such as variation in primary mineralogy and the effect of whole rock composition on the secondary mineral assemblages.

Bevins & Merriman (1988), in a study of the Tal y Fan Intrusion, an altered olivine dolerite sheet approximately 5 km southeast of the Penmaenmawr Intrusion, and Bevins and Robinson (1993), in a study of sub-greenschist to greenschist metabasites of Ordovician age from the Welsh Basin, determined that whole rock $MgO/(MgO+FeO)$ ratios plays a crucial role in determining the mineral assemblage in transitional grade metabasites, and that whole rock $MgO/(MgO+FeO)$ ratios are closely mirrored by chlorite $MgO/(MgO+FeO)$ ratios. At these transitional grades, metabasites with an $MgO/(MgO+FeO)$ ratio <0.54 contain prehnite and pumpellyite while those with ratios >0.54 have actinolite with prehnite. Bevins and Robinson (1993) concluded that contrasting assemblages

present within a single intrusion can be controlled by whole rock composition, and thus do not necessarily indicate varying conditions of temperature and pressure.

Whole rock MgO/(MgO + FeO) ratios from the Penmaenmawr Intrusion range from 0.24 to 0.48, all falling below the 0.54 threshold (see Appendix 6). This is in keeping with observations made in this study, namely that prehnite and pumpellyite are present rather than actinolite and prehnite in the alteration zones 4 and 5 identified in Chapter 4. Actinolite has been found in only two samples from Group 1 in the far east of the intrusion where the whole rock MgO/(MgO + FeO) ratio is 0.30.

In the less altered parts of the intrusion, none of the metamorphic indicator minerals of Bevins and Robinson (1993) occur. The different degrees of alteration observed within the Penmaenmawr Intrusion are therefore unlikely to be a consequence of metamorphism of rocks with different compositions within the intrusion.

8.3. Hydrothermal fluids

From studies of Rb-Sr whole rock ages, Evans (1991) showed that the Penmaenmawr Intrusion has a re-set metamorphic age within the lower Devonian. She also suggested that the extent to which a metamorphic mineral assemblage is developed depends upon the amount of fluid with which the rocks have interacted and that the absence of fluid tends to preserve the primary mineralogy. The most obvious source of fluid was the sedimentary pile into which the original Penmaenmawr magma was intruded.

In Chapter 3 it was also shown that the Intrusion contains many thin, post magmatic veins of quartz and that there were very thin veins of axinite on joint surfaces, both of which tend to be more abundant within the very fine-grained rocks from the eastern quarries. It was also shown that within the central part of the Penmaenmawr Intrusion, where the rock is most heavily altered, there are vertical joint or fault planes and shear zones. These fault planes and shear zones could have provided critical pathways allowing the ingress of hydrothermal fluids. This could account for the variation in the extent of alteration seen within the

intrusion.

The faults and shear zones are most likely to have formed during the major period of deformation in North Wales, associated with the regional metamorphic event which is considered to have occurred in early to mid Devonian times. Howells *et al.* (1991) stated that faults are common throughout Snowdonia, they trend predominantly north, north-east and west-north-west and many were active during the Mid Devonian (Acadian) period of deformation. However, hydrothermal fluid generation and movement are generally associated with the emplacement of hot magma and will normally occur soon after emplacement. Howells *et al.* (1991) suggested that hydrothermal alteration was common within the marine-dominated volcanic and sedimentary rocks of Snowdonia and Bevins and Merriman (1988), in their study of the Tal y Fan Intrusion, suggested that alkali feldspar in the marginal and contact zones was due to early hydrothermal replacement of plagioclase microphenocrysts prior to subsequent regional metamorphism.

It was shown in Chapter 2 that the Penmaenmawr Intrusion was emplaced during Caradoc times, (late Ordovician) long before the major period of deformation, which suggests that if hydrothermal fluids were the major cause of the alteration, there were already zones of weakness along which the fluids could move within the intrusion shortly after emplacement. There was undoubtedly syn-volcanic tectonism during the Caradoc. Kokelaar (1988) suggested that Caradoc volcanism was controlled by east-west extension resulting in the Snowdon graben, and Howells *et al.* (1991) suggested that episodes of hydrothermal alteration of the Caradoc volcanic rocks were broadly contemporaneous with the magmatism. These zones of weakness, therefore, could have formed syn-emplacement of the intrusion and were later exploited during the Acadian deformation event to produce the faults and shear zones as now seen in the quarry.

These considerations suggest that there may have been two alteration events, the first being immediate post-magmatic, after initial crystallisation, involving the interaction between the cooling magma and sea water, and the second, much later, following the reactivation of the fault and shear zones as part of the regional metamorphic episode in early to mid Devonian times, the fluids being the result of dehydration reactions within the sediments during regional metamorphism. This

suggestion is supported by the analyses of mineral chemistry presented in Chapter 5 and the analyses of magnetic susceptibility presented in Chapter 6. The localised, thin veins of axinite within Group 1 rocks the southern boundary of the intrusion, may be indicative of the second stage of alteration as axinite is generally considered to be of metasomatic origin, often after alteration has already taken place (Deer *et al.*, 1992).

8.4. Alteration - summary

The mineralogy of the Penmaenmawr Intrusion presented in Chapter 4 suggests that it has undergone sub-greenschist metamorphism, probably as part of the Acadian metamorphic event that affected North Wales in early to mid Devonian times. However the characteristic metamorphic mineral assemblage associated with this degree of metamorphism did not develop throughout the intrusion and primary magmatic minerals, and amphiboles characteristic of higher temperature alteration, were preserved to varying degrees. The intrusion, however, was cut by a number of faults and shear zones which could have allowed hydrothermal fluids to enter the intrusion at certain places and to effect alteration to parts of it.

The faults and shear zones determined in this study have NNW-SSE and NNE-SSW trends and tend to enclose the central part of the intrusion, and in Chapter 4 it was shown that this part of the intrusion has experienced the greatest extent of alteration. It was also suggested in Chapter 7 that rocks from Group 1, which occur in the Craig Lwyd Quarries and along the southern boundary of the intrusion, also experienced a high degree of alteration

Alteration is considered to have taken place in two episodes, the first immediately following emplacement, with the alteration fluids originating from the cooling magma or possibly from the surrounding rocks influenced by the cooling magma. In this episode, orthopyroxene was altered to amphibole, biotite to chlorite and plagioclase feldspar became depleted in Na and in some instances was locally altered to alkali feldspar. The second alteration occurred as part of the Acadian metamorphic event of early to mid Devonian times, with the fluid originating from dehydration reactions linked to the de-watering of the sediment pile around the intrusion. Most of the alteration took place along the boundaries of the intrusion

and between the NNW-SSE and NNE-SSW trending faults and shear zones in the central part of the intrusion, which were probably re-activated during this deformation event.

During this second alteration episode amphibole and biotite were almost entirely altered to chlorite but locally, away from the main alteration centres, amphibole was enriched in Ca, Na and K to form actinolite. Any orthopyroxene not altered by the first alteration episode, was altered to actinolitic amphibole during the second alteration episode. Plagioclase feldspar was locally albitised and in certain places was almost completely albitised. Ilmenite and primary magnetite were locally altered to titanite; however, clinopyroxene, in the main, remained unaffected during both alteration episodes. In the more altered parts of the intrusion, metamorphic mineral assemblages developed and prehnite, pumpellyite and epidote now occur. In the southern parts of the intrusion veins of quartz with prehnite formed, along with a few thin veins of axinite.

CHAPTER 9. MAGMA CHAMBER PROCESSES THAT PRODUCE VARIATIONS IN GEOCHEMISTRY

9.1. Introduction

This chapter briefly reviews the major processes that occur within magmatic systems that result in variations in geochemistry of the rocks, which subsequently develop, and discusses how they might apply to the variations determined within the Penmaenmawr Intrusion.

Magmas will tend to rise within the crust due to the density difference between the magma and typical crust (Hall, 1987). The magma may either reach the surface and be erupted or collect in a magma chamber, dependent on density and temperature differences between the magma and the country rock as well as the local tectonic environment. Where a magma chamber is formed the liquid will begin to cool and eventually start to crystallise leading to a number of different processes.

9.2. Fractional crystallisation

Fractional crystallisation is a common cause of variations in whole rock geochemistry in igneous intrusions and studies of the fractional crystallisation of the Skaergaard Intrusion represent some of the most important works on igneous petrology (see Wager & Deer, 1939; Wager & Brown, 1968 and McBirney & Noyes, 1979). As a magma cools, crystals will begin to form and elements that have high partition coefficients for the minerals being formed will be concentrated in these crystals and depleted in the remaining liquid. If the crystals and the liquid become separated and the residual liquid continues to precipitate crystals, because the latter has a different composition, further crystallisation will produce crystals that contain different proportions of elements or even different minerals. When the magma chamber has completely solidified it will consist of a suite of rocks with a range of geochemical compositions.

The potential mechanisms by which crystals and liquid can be separated include: the removal of crystals from the site of crystallisation by gravity; removal by the movement of convection currents; or the removal of the liquid by filter pressing.

The crystals most likely to be separated by gravity are those having a large density contrast with the liquid and which are large in size at an early stage of cooling (McBirney, 1984), although, crystals less dense than the liquid may separate by flotation. McBirney & Noyes (1979), in a study of the Skaergaard Intrusion, suggested that plagioclase feldspar crystals had a minimal density difference with the host liquid which would prevent them being separated by gravity, while Marsh (1996), in a review of the role of solidification fronts in magmatic evolution, actually considered differentiation through crystal settling to be unrealistic. Sparks *et al.* (1984), in a review of fluid dynamic concepts in evolving magma chambers, also suggested that crystal settling is an inadequate mechanism for fractional crystallisation within a single system.

Convection currents are caused by differences in density within a liquid, which arise from compositional and temperature variations caused by a number of processes, including fractional crystallisation. Sparks *et al.* (1984) proposed that in fact convective fractionation is the dominant mechanism for crystal fractionation.

Filter pressing is the process by which buoyant residual liquid present in a mush of loosely packed crystals is expelled towards zones of lower pressure, effectively separating the liquid from partially crystalline horizons. Hall (1987) claimed that nearly all the possible models for filter pressing are open to serious question and it has yet to be demonstrated convincingly that filter pressing actually occurs in nature. However, he does suggest that filter pressing may form small patches of segregations of residual liquid found in lava flows and large sills formed by the Kilauea volcano.

Crystallisation is likely to begin along the side walls or roof of an intrusion, where cooling starts as hot melt comes into contact with cold country rock. Residual liquid, whatever the method of separation, would accumulate towards the centre of the intrusion and would eventually solidify to form a symmetrically zoned intrusion, with the least evolved rocks at the margins and the most evolved rocks towards the centre. Sparks *et al.* (1984) and McBirney *et al.* (1985) have suggested that residual liquids formed as a result of side-wall crystallisation would tend to rise as a laminar plume and pond at the top of an

intrusion. This may result in a vertically layered suite of rocks towards the centre of an intrusion, surrounded by rocks that solidified against the side-walls, enriched in cumulate minerals.

Fractional crystallisation processes will lead to a suite of rocks in which the composition varies in line with the composition of the residual liquid. The compositions of rocks related by fractional crystallisation can be plotted against any major elemental constituent, normally SiO_2 , as 'variation diagrams' so that trends on variation diagrams represent changes in composition of the residual liquid as crystals are formed and removed from the melt. The composition of the residual liquid depends on the composition and the proportions of the minerals being formed and in igneous suites most major rock forming minerals form solid solutions of different elements. Changes in the proportions of the different elements being incorporated into the crystals being formed causes trends on the variation diagrams to follow curves rather than straight lines (McBirney, 1984). The change in the proportion, type, or composition of the minerals crystallising will cause a change in direction of the trends reflecting liquid compositions.

9.3. Magma mixing

Residual liquids produced by fractional crystallisation will be less dense than the original magma from which they were derived. This density difference may cause them to rise above and sometimes through the more dense liquids. If the flow of the less dense liquid becomes turbulent it may entrain the less dense magma from the interior and mix with it, producing a range of intermediate compositions. The mixing of a derivative liquid with its parent is known as back-mixing (McBirney, 1984). A series of magma compositions produced by varying degrees of mixing will have compositions that have a linear variation between the two end members and will show as linear variations on elemental binary plots. However, McBirney (1984) suggested that a variety of compositions and textural features may result if either of the end member liquids are in equilibrium with crystallising phases and the mixed magmas cool before re-equilibration is complete.

In some magma chambers, convection currents may transfer heat and materials around the chamber very turbulently, which may very effectively mix the constituents producing a homogeneous magma. If this does not subsequently differentiate it may result in an intrusion with little or no geochemical variation.

Additional evidence for magma mixing may be the presence of crystals out of equilibrium with each other in the same rock (McBirney, 1984) or the occurrence of rounded inclusions of more basic material that represent portions of magma that were not completely incorporated into the hybrid magma and probably result from disruption at the interaction zones between the two end member magmas (Castro *et al.*, 1990).

9.4. Assimilation

Magma may melt the country rock into which it has intruded and incorporate the liquid produced, thus altering its composition. In order to melt country rock the intruding magma needs to supply sufficient heat, equivalent to the latent heat of fusion of the country rock. Hall (1987) suggested that the main limitation on the melting of country rocks is the need for the country rock first to be raised to its melting temperature, and that this is more likely to occur in deeper parts of the crust where they may already be approaching their solidus, and secondly where the magma body is very large.

Assimilation often occurs by incorporating country rock into the liquid and then dispersing xenoliths through the magma. As the magma is normally cooling and crystallising, this process is often incomplete and partially assimilated xenoliths are commonly found, generally in greater abundance close to the margins of the intrusion.

Where country rocks have been assimilated into the magma the resulting minerals formed may not differ in composition or appearance from minerals that would normally have formed from the original magma. Additionally, liquids, in terms of major element compositions and mineral phases will, in any case, tend to follow a line of descent that would be possible without assimilation, only the proportion of the products change (McBirney, 1984). However, Hall (1987)

suggests that it is the presence of xenoliths which are the most conspicuous indication of assimilation.

9.5. Complex magma chambers

Magma chambers are seldom composed of a single batch of magma that cools, crystallises and differentiates according to the processes outlined above. Many magma chambers will receive fresh injections of liquid from below and will lose liquid intermittently by eruption.

Fresh injections of liquid into an existing magma chamber may not mix with the existing magma because of differences in density or the existing magma may be partially solid, either due to crystallisation or due to the removal of the less viscous liquids by eruption. Where the individual injection is small it may solidify as a homogeneous unit. It may, however, undergo fractional crystallisation or magma mixing as outlined above and form a discrete unit within the intrusion with its own geochemical character.

The injected fresh liquid may intermingle and mix with the existing magma already in the chamber, forming either a range of liquids with compositions intermediate between the two end members or, if they mix thoroughly, a single homogeneous liquid with an intermediate composition. Sparks *et al.* (1984) suggested that when a new hot dense magma is injected beneath a cooler, lighter magma and begins to crystallise and differentiate, the resulting compositional change may lower its density until it is lighter than the overlying liquid and is able to rise and mix with it turbulently. It has also been suggested that following the injection of basic magma into acid magma the two magmas may mix thoroughly by vigorous convection and that this mixing is a common mechanism of triggering explosive eruptions (Sparks *et al.*, 1977).

A high-level magma chamber may be supplied from a single, larger magma chamber situated at some depth beneath it, which may be differentiating due to fractional crystallisation or magma mixing as described above. The larger, underlying magma chamber may, therefore, be layered, with less dense, more evolved liquids located on top of the more dense, less evolved liquids. Small

injections into the high level chamber may be supplied from the upper, more evolved, layers of the lower chamber and a series of consecutive injections, ejected from successive layers, will have different compositions. The variation in composition of each injection will be dependent on the time between each injection and the rate of differentiation taking place in the lower chamber. Hall (1987) suggested that replenishment is an important factor in magmatic evolution and that repeated injections into high-level magma reservoirs reduce the amount of differentiation.

Initial injections to the higher level may also be smaller, as a single body of magma cannot ascend very far because of the limited amount of heat that it can supply to the country rock, but if a magma ascends in successive batches the second and later batches can ascend more easily and may involve larger amounts of magma.

9.6. Applicability of magma chamber processes to the Penmaenmawr Intrusion

The Penmaenmawr Intrusion is considered to be a sub-volcanic intrusion (Ball & Merriman, 1989; Howells *et al.*, 1991). Ball & Merriman (1989) suggested that the Llewelyn Volcanic Group and its associated intrusives, which include the Penmaenmawr Intrusion, are consistent with an origin through high level storage and fractionation on the basis that: the fractionated phases are typical of low pressure crystallisation; there are no coarse-grained autoliths or xenocrysts consistent with plutonic crystallisation; thermal aureoles are poorly developed; and the most evolved rhyolitic rocks are sparsely phenocrystic. Merriman and Roberts (1985), in a study of white mica crystallinity of pelitic rocks, suggested that the mudstones at the contact with the sub-volcanic intrusions of Snowdonia indicate contact temperatures of 200-300°C supportive of a high level of emplacement for the intrusions.

High-level magma chambers in volcanic environments are unlikely to assimilate country rock due to their inability to provide sufficient heat to raise the temperature of the country rock to its melting point. Pitcher (1993) suggested that wall rock assimilation appears to be exceptional in upper crustal conditions as the operation of this process is likely to rapidly freeze the contact zones.

The Penmaenmawr Intrusion is emplaced into black Ordovician shales and during this study no xenoliths of these shales have been seen in the intrusion. This absence of xenoliths, the poorly evolved metamorphic aureole in the shales, and the high level of emplacement at relatively low temperatures suggest that the composition of the Penmaenmawr Intrusion has not been affected by assimilation of country rock.

Small batches of magma emplaced into high-level magma chambers will cool moderately quickly and are unlikely to undergo fractionation. The Penmaenmawr Intrusion is relatively small in volume and any variation in geochemistry is, therefore, unlikely to be due to *in-situ* fractional crystallisation. However, where a batch of magma has been supplied from an underlying, larger magma chamber it may exhibit differences due to the processes taking place in the larger chamber. Any geochemical variations observed within the Penmaenmawr Intrusion may, therefore, be due to the emplacement of a batch of magma that was differentiated by fractional crystallisation or magma mixing within an underlying, larger magma chamber.

High-level, sub-volcanic magma chambers are likely to be complex magma chambers, receiving injections of fresh magma and losing magma by eruption. Any variation within the Penmaenmawr Intrusion may, therefore, be due to the emplacement and interaction of a number of injections of magma with varying characteristics. Tremlett (1997) suggested that the variations within the Penmaenmawr Intrusion were the result of a number of pulses of magma from an underlying magma chamber undergoing differentiation. If this is so, successive injections of magma should show trends indicating the evolution of the underlying magma chamber. Where there is a time interval between injections of magma there may be breaks in the trends and observable margins between the injections. However, if there is sufficient time for cooling, successive injections of magma may completely or partially mix with each other, producing a variety of compositions which may blur any original trends. Additionally, the variation in composition could also be affected by eruptions of magma, which could remove all or some of the various magma compositions.

In Chapter 7 it was demonstrated that the Penmaenmawr Intrusion was not horizontally layered and that the lateral variation in SiO₂, Zr and Y contents increases regularly across the intrusion with an approximately northwest to southeast trend. These elemental variation distributions are inconsistent with the crystallisation and differentiation of a single body of magma as discussed above which supports the suggestion that the Penmaenmawr Intrusion is not the result of the emplacement and *in-situ* fractional crystallisation of a single batch of magma.

The variation in geochemistry across the Penmaenmawr Intrusion could therefore be due to the single emplacement of magma from an already differentiated magma chamber or alternatively it could be due to successive injections of magma from an underlying larger magma chamber, each injection having a progressively different composition from the previous one. As the main geochemical variation appears to increase regularly across the intrusion and no sharp contacts were identified within the intrusion, the former suggestion seems most likely.

CHAPTER 10. WHOLE ROCK GEOCHEMICAL VARIATION PATTERNS

10.1. Introduction

This Chapter presents diagrams showing variations in the major and trace element contents plotted against the SiO₂ contents and discusses the patterns in relation to the igneous processes that were outlined in Chapter 8. This chapter uses the Groups identified in Chapter 4, which are based on field and petrographic features and, in general, this is separate from petrogenetic considerations.

10.2. Description of the variation patterns

The variation diagrams presented in Figure 10.1 show the major element contents plotted against SiO₂ contents and the diagrams presented in Figure 10.2 show the trace element contents plotted against SiO₂ contents, for all rocks analysed. Generally, these diagrams show tight linear, or possibly curved trends, with a compositional continuity, which together, suggest that the samples are linked genetically. However in almost all of the plots, the samples from Group 1 show a divergence from the trend exhibited by the samples from Group 3.

The plots show that the contents of MgO, Fe₂O₃, CaO, Al₂O₃, Ni, Cr and Co generally decrease with increasing SiO₂ contents, whereas Na₂O, K₂O, Rb, Zr, Y, Nb, Ba tend to increase with increasing SiO₂ contents. MnO shows a more constant content with increasing SiO₂ contents and the diagrams for Sc, Th and Cu have insufficient analytical accuracy to determine any trends.

The distributions form tight trends with few data points plotting away from main trends, however some plots, notably CaO, Fe₂O₃, MnO, Rb, Sr, Zn show some scatter of data points confirming the mobility of these elements reported in Chapter 7. The degree of scatter tends to be greater between SiO₂ contents of 59% to 63%, tending to give the diagrams a slight bulge in the mid to high SiO₂ range. The samples within this range of SiO₂ contents are mainly from Groups 2 and it was noted earlier (Chapters 4 and 7) that samples from this Group are the most altered, with an alteration index of between 3 and 5 (the value of 5 being the most altered).

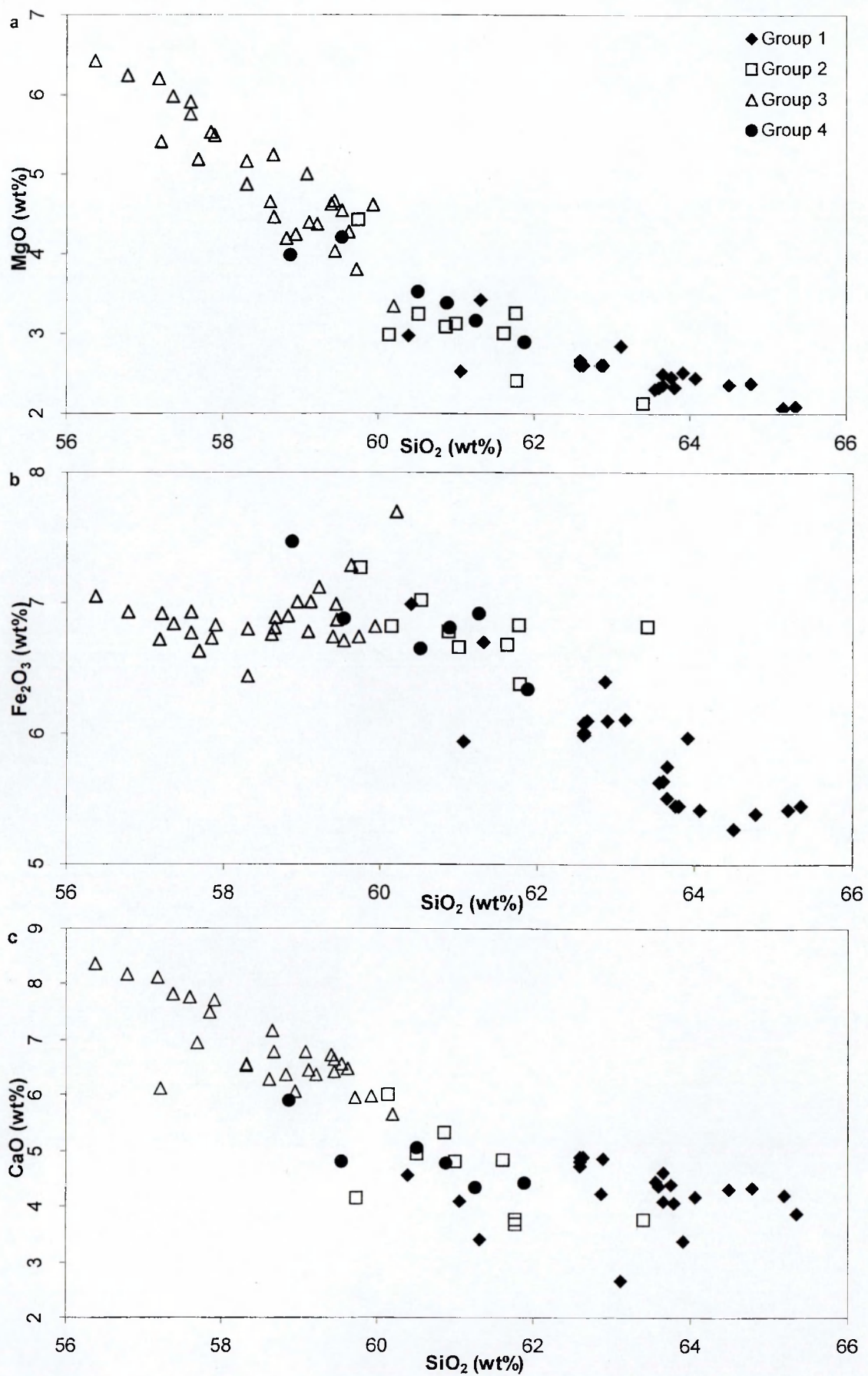


Figure 10.1. Plots of selected major elements (wt%) against silica (SiO_2) (wt%), for the Penmaenmawr samples from Groups 1-4, (Legend provided on plot (a)): (a) MgO , (b) Fe_2O_3 and (c) CaO (continued overleaf).

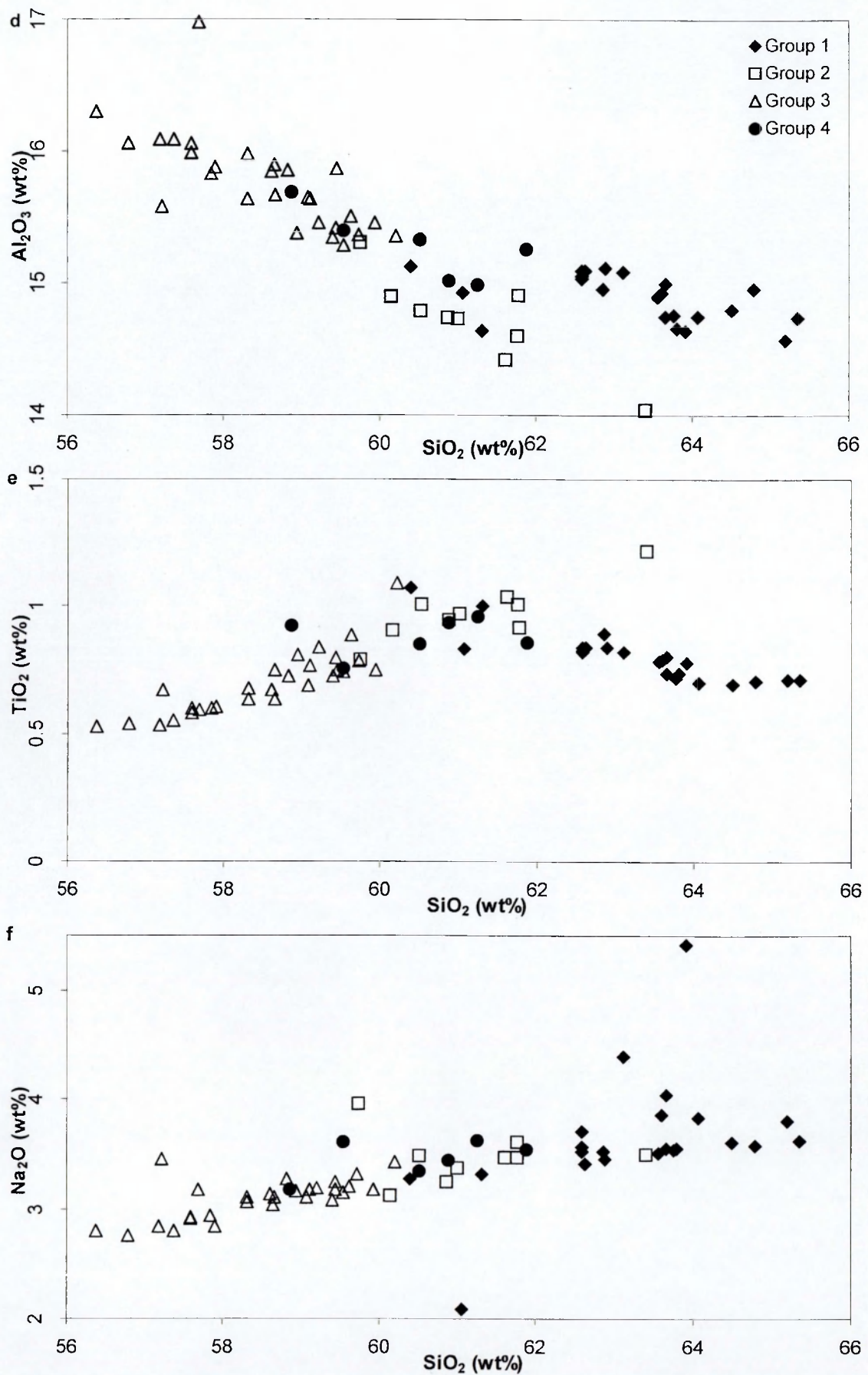


Figure 10.1. (continued). Plots of selected major elements (wt%) against silica (SiO_2) (wt%), for the Penmaenmawr samples from Groups 1-4 (Legend provided on plot (d)): (d) Al_2O_3 , (e) TiO_2 and (f) Na_2O (continued overleaf).

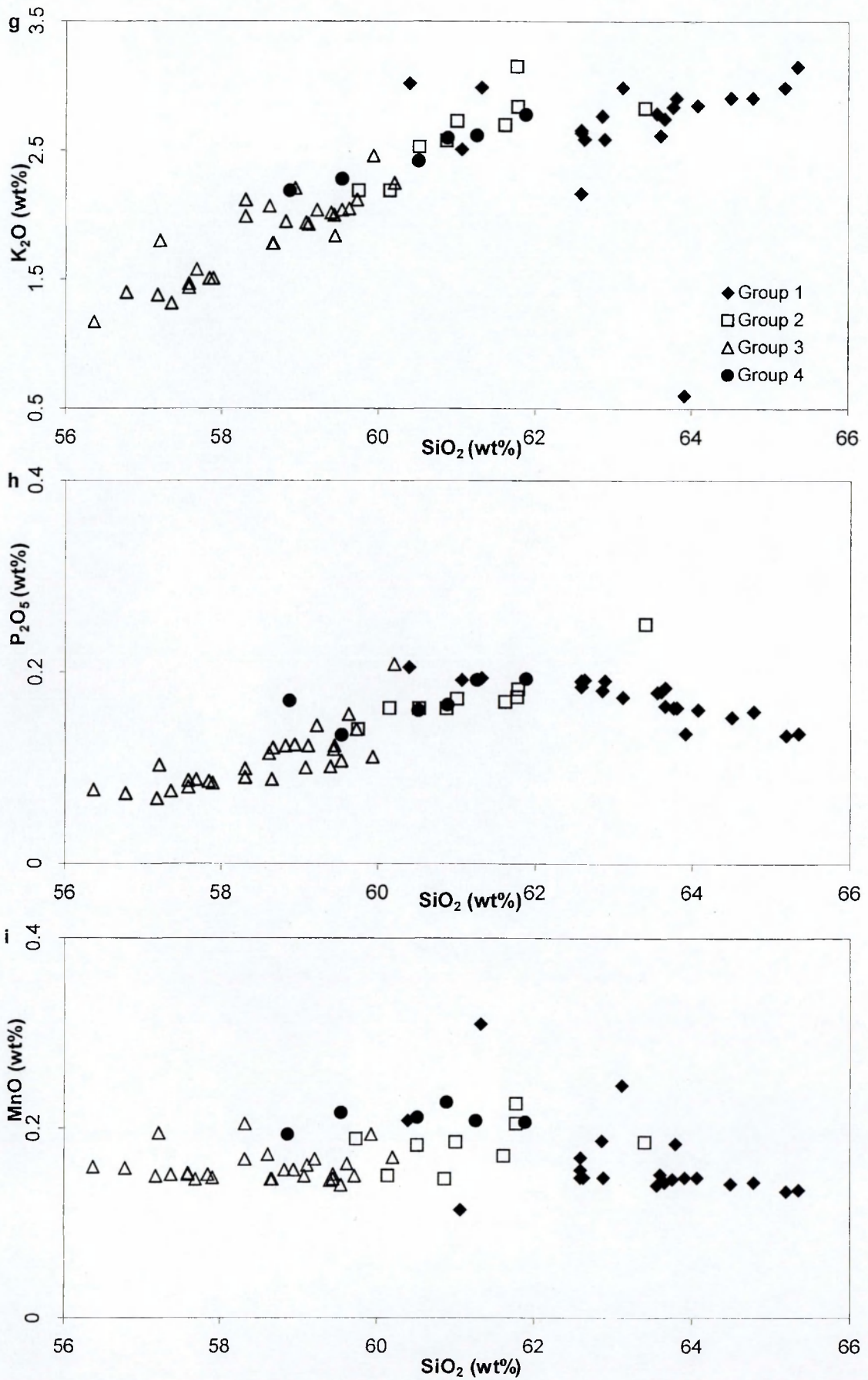


Figure 10.1. (continued). Plots of selected major elements (wt%) against silica (SiO₂) (wt%), for the Penmaenmawr samples from Groups 1-4 (Legend provided on plot (g)): (g) K₂O, (h) P₂O₅ and (i) MnO.

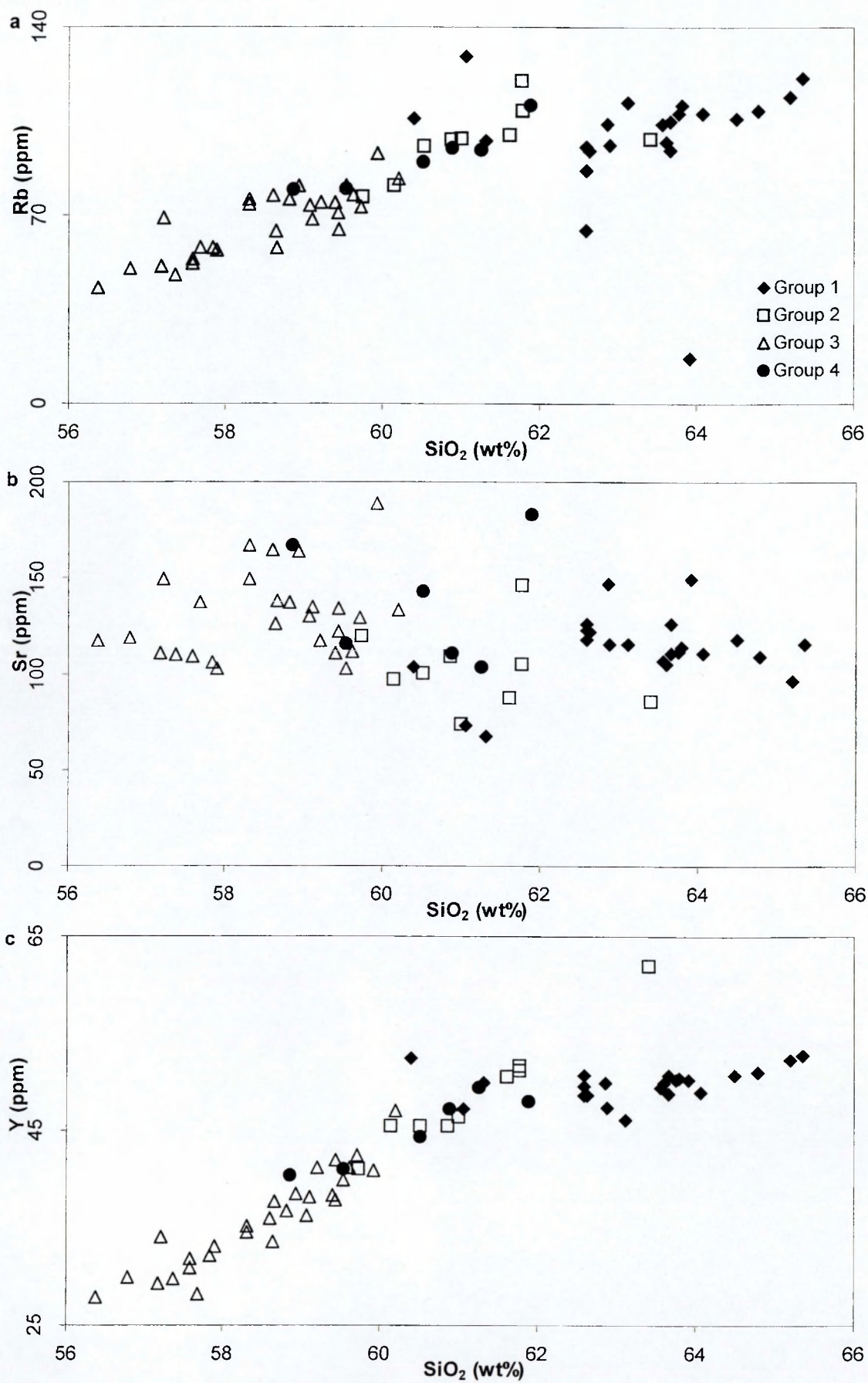


Figure 10.2. Plots of selected trace elements (ppm) against silica (SiO₂) (wt%), for the Penmaenmawr samples from Groups 1-4 (Legend provided on plot (a)): (a) Rb, (b) Sr and (c) Y (continued overleaf).

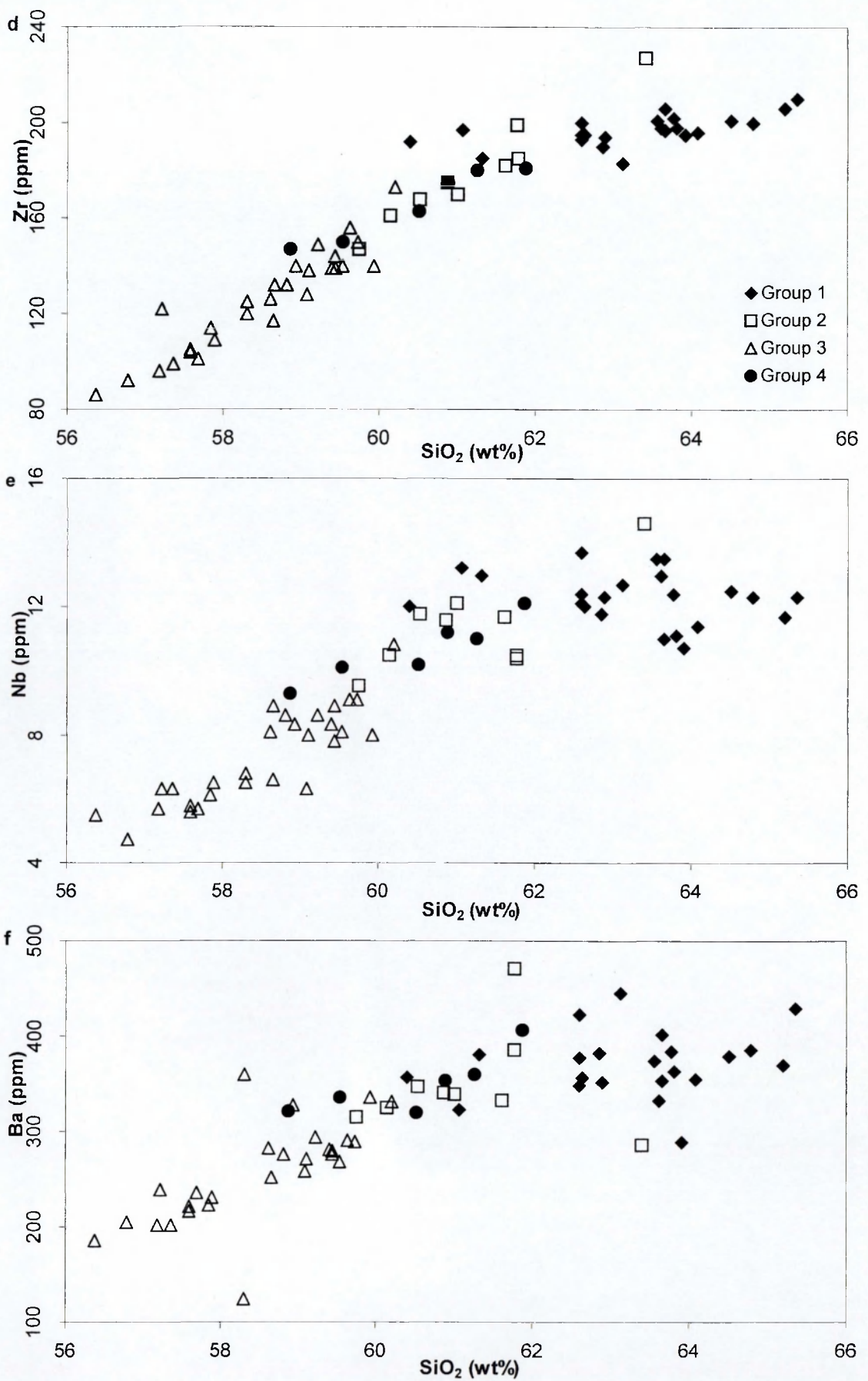


Figure 10.2. (continued). Plots of selected trace elements (ppm) against silica (SiO_2) (wt%), for the Penmaenmawr samples from Groups 1-4 (Legend provided on plot (d)): (d) Zr, (e) Nb and (f) Ba (continued overleaf).

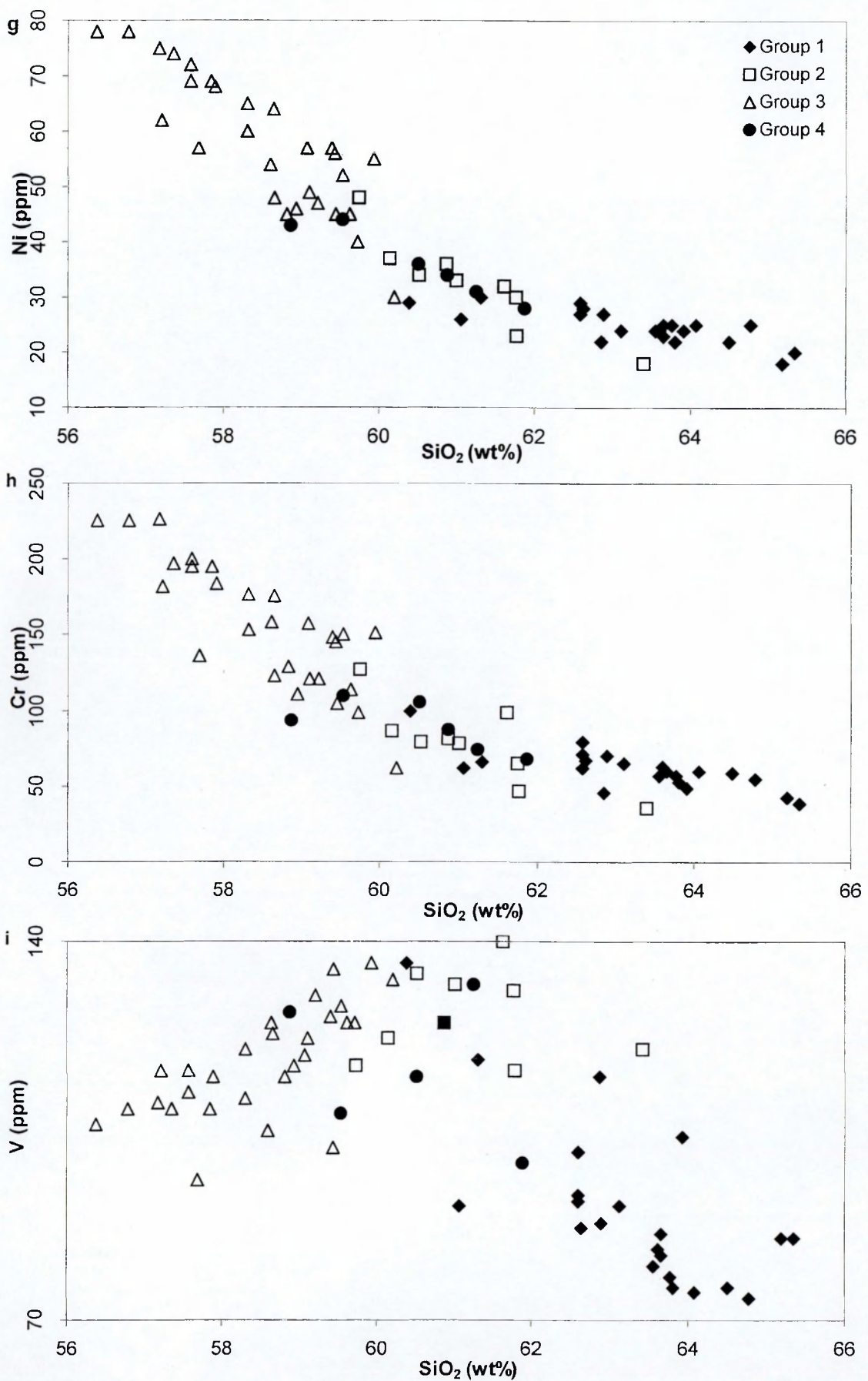


Figure 10.2. (continued). Plots of selected trace elements (ppm) against silica (SiO_2) (wt%), for the Penmaenmawr samples from Groups 1-4 (Legend provided on plot (g)): (g) Ni, (h) Cr and (i) V (continued overleaf).

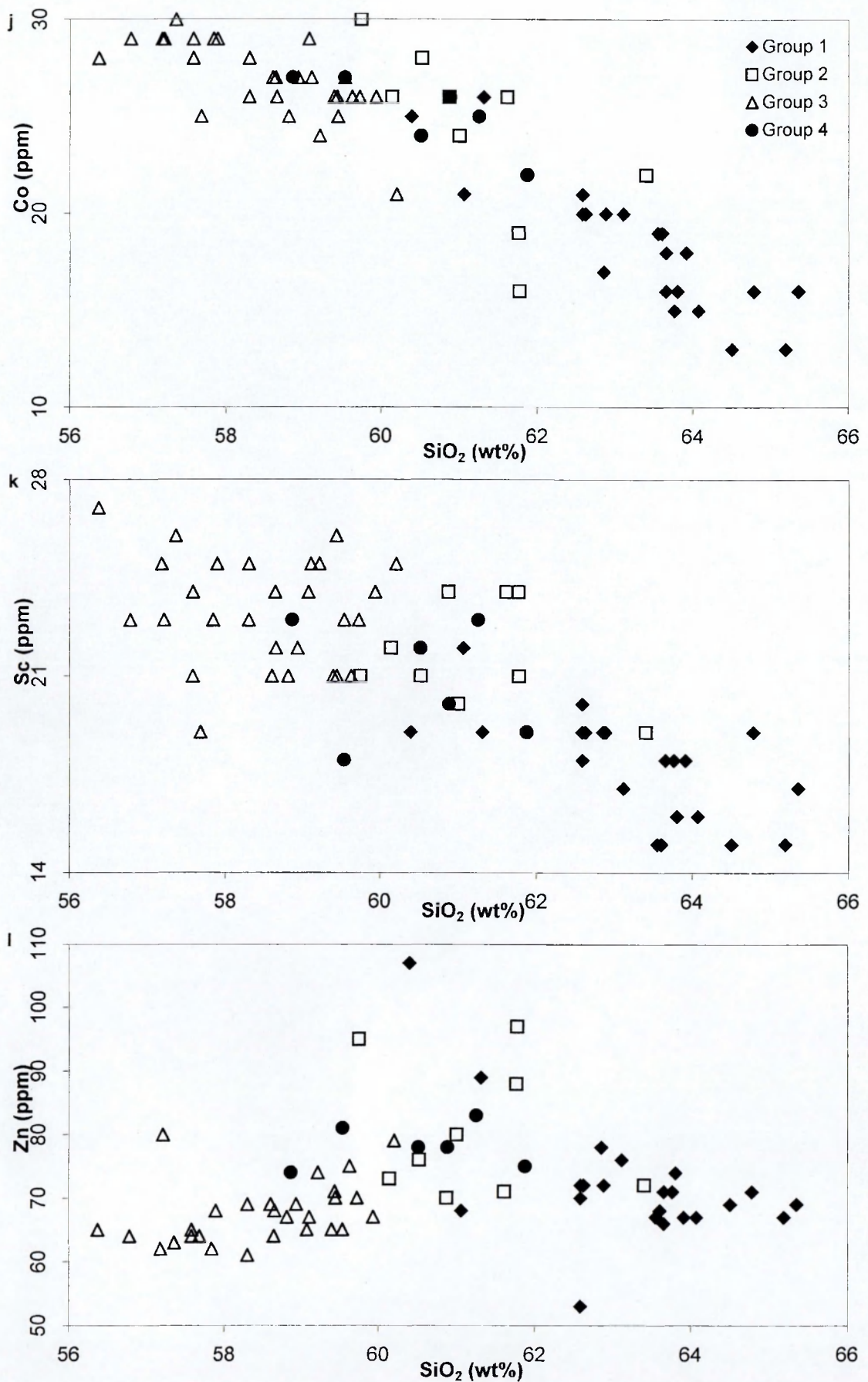


Figure 10.2. (continued). Plots of selected trace elements (ppm) against silica (SiO_2) (wt%), for the Penmaenmawr samples from Groups 1-4 (Legend provided on plot (j)): (j) Co, (k) Sc and (l) Zn (continued overleaf).

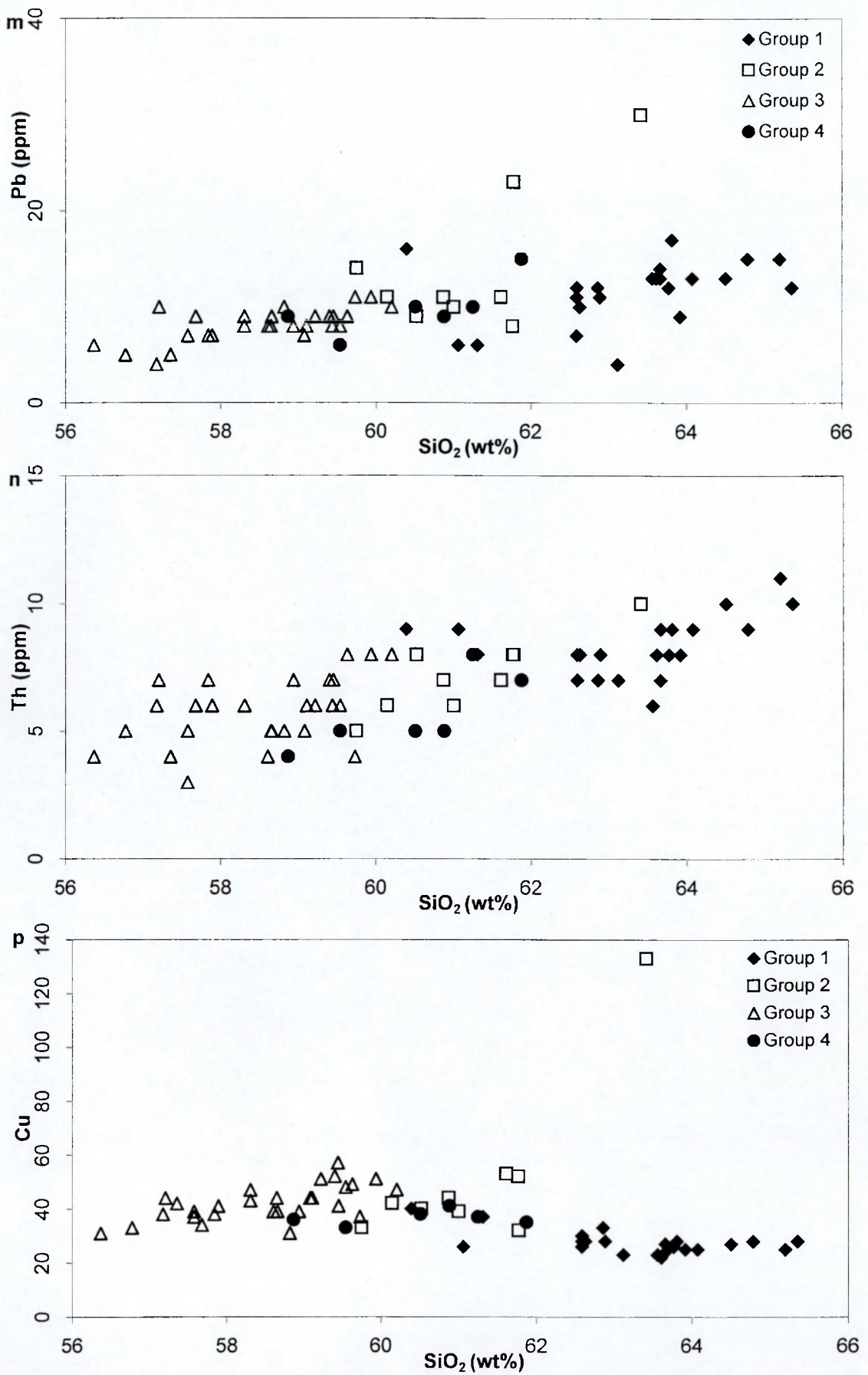


Figure 10.2. (continued). Plots of selected trace elements (ppm) against silica (SiO_2) (wt%), for the Penmaenmawr samples from Groups 1-4 (Legend provided on plot (m)): (m) Pb, (n) Th and (p) Cu.

The scatter of data points in the mid to high SiO₂ contents is therefore likely to be due to post-magmatic alteration rather than to a number of superimposed but differing magmatic trends. The samples whose data points plot away from the main trends are not used in any subsequent modelling.

Group 3 rocks, with SiO₂ contents between 56.4% and 60.2%, form a distinct compositional group with tight linear trends in all plots. Group 1 rocks, with SiO₂ contents between 60.4% and 65.4%, also tend to form a distinct group with linear trends, and in all plots the slopes of the trends for Group 1 rocks are different from the slopes of the trends for Group 3 rocks. The rocks from Groups 2 and 4, with SiO₂ contents intermediate between Groups 3 and 1 rocks, form loose clusters of data points between these two trends. In most cases it is not clear whether they represent a continuation of the trend of the Group 3 rocks or the beginning of the trend for Group 1 rocks. However, the plots for Al₂O₃, Y and Zr show Group 2 rocks forming a continuation of the trend for Group 3 rocks and one sample from Group 2 (JD2919), which has a higher SiO₂ content than the other samples in Group 2, plots on all diagrams as a linear extension to the trends shown by Group 3 rocks.

The linear trends for Group 3 rocks tend to meet the linear trends for Group 1 rocks at about 61% SiO₂ giving the diagrams a distinct change in slope and also contributing to the scatter of data points between SiO₂ contents of 59% and 63% noted above. The change in slope is most marked in the plots for Fe₂O₃, TiO₂, P₂O₅ and V. In the first of these, the Fe₂O₃ content for Group 3 rocks remains approximately constant with increasing SiO₂ content but for Group 1 rocks decreases with increasing SiO₂ content. In the latter three plots, the TiO₂, P₂O₅ and V contents for Groups 3 rocks increase with increasing SiO₂ content, and then decrease with increasing SiO₂ content in Group 1 rocks.

10.3. Interpretation of the variation patterns

In Chapter 9 it was shown that two common processes that can cause variations in geochemistry during the cooling of a magma are fractional crystallisation and magma mixing and that these processes can be reflected by trends on variation diagrams for a suite of igneous rocks. For fractional crystallisation, the trends on

variation diagrams represent the changes in composition of the residual liquid as crystals form and are removed from the liquid melt, and generally follow curves. A change in slope, in most cases, reflects a change in the minerals that were crystallising. For magma mixing a series of rocks are produced that have a linear variation between their two end members, which produces straight-line trends on the variation diagrams.

The variation diagrams for the Penmaenmawr Intrusion as a whole appear to be curved but this may be due to the intersection of two straight-line trends and the scatter of some data points in the plots, between 59% to 63% SiO₂, discussed in Section 10.2. above. However, the clear separation between Group 3 and Group 1 rocks, both of which plot as linear trends on all plots, suggests that geochemical variation in the Penmaenmawr Intrusion can be considered as two trends, represented by the rocks from Group 3 and Group 1. Rocks from Group 2 could represent a continuation of the trend shown by the Group 3 rocks. However, the relationship between Group 4 rocks and the rocks of the rest of the intrusion is not clear.

These straight-line trends could be the result of either fractional crystallisation or magma mixing.

10.4. Variation diagrams and fractional crystallisation

In Chapters 4 and 5 it was shown that the main primary minerals present in the samples from the Penmaenmawr Intrusion are orthopyroxene, clinopyroxene and plagioclase feldspar with trace amounts of primary biotite, iron-titanium oxides and apatite. This section reviews the variation diagrams presented in Figures 10.1. and 10.2 and discusses whether they are broadly compatible with the fractional crystallisation of these primary minerals.

Orthopyroxene and clinopyroxene from the Penmaenmawr Intrusion contain between 19-23% and 12-16% MgO respectively, and between 19-23% and 9-15% FeO respectively (Appendix 4). The liquid/solid phase relationships of ferromagnesian minerals, which show Mg-Fe solid solution, demonstrate that when crystals are formed, they are enriched in Mg with respect to the

composition of the original liquid (Hall, 1987). Fractional crystallisation of orthopyroxene and/or clinopyroxene will therefore result in a residual liquid composition enriched in Fe relative to Mg.

The variation diagram for MgO shows that the whole rock MgO contents decrease with increase in SiO₂ contents, the Group 3 rocks showing a steeper slope than the Group 1 rocks, which would be consistent with the fractionation of orthopyroxene and/or clinopyroxene, the change of slope suggesting that there is a change in the proportion of the minerals being fractionated. The variation diagram for Fe₂O₃ shows that the whole rock Fe₂O₃ contents remain approximately constant with increase in SiO₂ contents for Group 3 rocks and decrease with increasing SiO₂ contents for Group 1 rocks. The approximately constant Fe₂O₃ contents and the decreasing MgO contents over the same range of SiO₂ contents suggests that the residual liquid became enriched in Fe with respect to Mg which would be consistent with the fractionation of orthopyroxene and/or clinopyroxene for Group 3 rocks.

Further evidence to support the fractional crystallisation of orthopyroxene and/or clinopyroxene could be obtained from the Mg/Fe ratio of crystals from the Penmaenmawr Intrusion, which should show progressive Fe enrichment in the more evolved rocks. Unfortunately fresh orthopyroxene is found only in the least altered rocks of Group 3 and is in insufficient samples to determine whether the Mg/Fe ratio of the crystals has changed with whole rock SiO₂ contents. However, clinopyroxene is found in all samples and mineral chemistry analyses (discussed in Chapter 5) shows that it does indeed become slightly enriched in Fe in the more evolved rocks from Groups 2 and 4.

If orthopyroxene and/or clinopyroxene were also fractionating phases for Group 1 rocks, the decrease in whole rock Fe₂O₃ contents with increase in SiO₂ contents suggests that some other minerals began fractionating and removing Fe from the residual liquid. Other primary phases that contain significant amounts of FeO are the iron-titanium oxides. These minerals are only present in trace amounts and in the more evolved rocks they have been altered to titanite with low FeO contents. However analyses of fresh magnetite crystals from Group 3 rocks show FeO contents of between 80-85%.

The fractionation of iron-titanium oxides would cause the residual liquid to be depleted in both Fe and Ti and the variation diagram for TiO_2 shows the whole rock contents of TiO_2 increasing with increase in SiO_2 contents for Group 3 rocks but decreasing slightly with increasing SiO_2 contents in Group 1 rocks. This diagram therefore supports the suggestion that iron-titanium oxides could be additional fractionating phases for Group 1 rocks.

Plagioclase feldspar is found in all samples from the Penmaenmawr Intrusion and contains between 19-30% Al_2O_3 . Relatively unaltered plagioclase feldspars from Group 3 rocks contain between 11-15% CaO and between 3-5% Na_2O but the more evolved samples tend to be progressively altered, and the CaO contents reduce to less than 1% whereas the Na_2O contents increase to up to 12%. However, it was reported in Chapter 5 that during fractional crystallization, residual liquids become enriched in Na.

The variation diagram for Al_2O_3 shows that the whole rock Al_2O_3 contents decrease with increase in SiO_2 contents, the Group 3 rocks showing a steeper slope than the Group 1 rocks, and could be due to the fractionation of plagioclase feldspar, the different trends for the Group 3 and Group 1 rocks could reflect different proportions of plagioclase feldspar fractionating.

The variation diagram for CaO shows that the whole rock CaO contents decrease with increase in SiO_2 contents, and again the Group 3 rocks show a steeper slope than the Group 1 rocks. This trend could also be due to the fractionation of plagioclase feldspar. However clinopyroxene contains between 16-21% CaO and this whole rock CaO trend could be affected by the fractionation of clinopyroxene.

The variation diagram for Na_2O shows the whole rock Na_2O contents increasing with increase in SiO_2 contents but there does not appear to be a significant difference in slope between the Group 3 and the Group 1 rocks. The increase in Na_2O contents with a corresponding decrease in CaO contents would be consistent with the fractionation of plagioclase feldspar. However, the lack of a significant difference in slope between the Group 3 and the Group 1 rocks for the whole rock Na_2O variation diagram is not compatible with the variation

diagrams for both CaO and Al₂O₃ contents, and suggests that some other phase could be fractionating in the Group 1 rocks which changes the Ca/Na ratio of the residual liquid.

Apatite, although only present in trace amounts, contains between 53% and 56% CaO and the fractionation of apatite would slightly affect the CaO content of the residual liquid. Apatite also contains approximately 40% P₂O₅ and the fractionation of apatite would remove P₂O₅ from the residual liquid and cause it to become progressively depleted in P₂O₅. The variation diagram for P₂O₅ shows the whole rock P₂O₅ contents increasing with increase in SiO₂ contents for Group 3 rocks and decreasing with Group 1 rocks. The fractionation of apatite in Group 1 rocks could therefore account for the decrease in the whole rock P₂O₅ contents in Group 1 rocks and the lack of a significant difference in slope between the Group 3 and the Group 1 rocks for whole rock Na₂O contents.

The variation diagrams for the compatible trace elements show that the contents of Ni, Cr, Co, and Sc decrease with increase in SiO₂ contents, which would be consistent with the fractional crystallisation of ferromagnesian minerals. The variation diagrams for the incompatible trace elements Rb, Y, Zr, Nb, and Ba increase with increasing SiO₂ contents and show a distinct change in slope between the Group 3 and Group 1 rocks. As incompatible trace elements tend to remain in the residual liquids during fractional crystallisation, these diagrams are also consistent with such a process. The separate trends for Group 1 and Group 3 rocks support the suggestions above, that the combined effect minerals fractionating in Group 3 rocks is different from that of the minerals fractionating in Group 1 rocks.

The variation diagram for V shows the whole rock V contents for Groups 3, 2 and 4 rocks plotting as distinct field, separated from the whole rock V contents for Group 1 rocks, and, although there is a degree of scatter, the whole rock V contents tend to increase with increase in SiO₂ contents for Groups 3 and 2 and decrease with SiO₂ contents for Group 1. V substitutes in magnetite and also tends to concentrate in apatite and micas and therefore this diagram would be consistent with the fractionation of iron titanium oxides and apatite in Group 1 rocks.

The variation diagrams, therefore, appear to be consistent with a two-stage fractional crystallisation process, the first involving the fractionation of plagioclase feldspar and orthopyroxene and/or clinopyroxene and the second involving the fractionation of plagioclase feldspar, orthopyroxene and/or clinopyroxene, iron titanium oxides and apatite.

10.4.1. Summary of variation diagrams according to the fractional crystallisation model

The variation diagrams show tight linear, or possibly curved trends, with a compositional continuity, which suggests that the samples are linked genetically and that the geochemical variation could be due to fractional crystallisation. However, the different trends for Group 3 and Group 1 rocks suggest that the variation could be consistent with a two-stage fractional crystallisation process within a single body of magma. The first, involving the fractionation of plagioclase feldspar and orthopyroxene and/or clinopyroxene resulted in the Group 3 rock trend and the second, involving the fractionation of plagioclase feldspar, orthopyroxene and/or clinopyroxene, iron-titanium oxides, apatite and possibly biotite, resulted in the Group 1 rock trend.

Group 2 rocks tend to plot as a linear extension to the trends shown by Group 3 rocks and could therefore represent a continuation of the fractionation of Group 3 rocks. Group 4 rocks plot sometimes overlapping the trend of Group 3 rocks and sometimes as a backward extension of Group 1 rocks and their evolution is not clear.

However, extending the trend from Group 3 rocks to include Group 2 rocks and extending backwards the trend from Group 1 rocks to include some of Group 4 rocks would produce two trends that crossed each other at 61% SiO₂, which would not be consistent with a two-stage fractionation process of a single body of magma. It would suggest, instead, that the geochemical variation could be due to two bodies of magma, one represented by rocks from Groups 2 and 3 and the other by some rocks from Group 1 and some rocks from Group 4 rocks that fractionated independently of each other. This suggestion would be consistent with the emplacement models proposed in Chapter 9, namely that

the Penmaenmawr Intrusion could have been emplaced by a single injection of magma from an already differentiated, and possibly layered, magma chamber or alternatively it could be due to successive injections of magma from an underlying larger magma chamber, each injection having a progressively different composition from the previous one.

10.5. Variation diagrams and magma mixing

In Chapter 4 it was shown that rounded mafic inclusions are present in Group 2 rocks from the Central Quarries and in some of the samples from Group 4 rocks. Their occurrence is a well-known feature of magma mixing and locally, at least, mixing of magmas could have taken place. Unfortunately the degree of alteration of critical minerals, particularly in the rocks from Group 2 with SiO₂ contents of between 59% and 63%, has destroyed any evidence of compositional zoning in those minerals, which could have provided additional evidence for magma mixing.

The tight linear trends for Group 3 and Group 1 rocks on the variation diagrams could represent two straight-line trends, which individually would be consistent with magma mixing trends. The Penmaenmawr Intrusion could therefore consist of two batches of magma, one represented by Group 1 rocks and the other by Group 3 rocks each of which evolved separately by the mixing of two magmas represented by the samples with the lowest SiO₂ contents and the highest SiO₂ contents from each group. The rocks of Groups 2 and 4, which plot between these two trends on the variation diagrams, could be the result of magma from these two, already part mixed, batches intermixing and producing rocks with a range of intermediate compositions.

10.6. Variations in compatible and incompatible trace element contents

To examine the processes that could lead to the geochemical variation in the Penmaenmawr Intrusion in more detail, the variation of compatible trace elements with incompatible trace elements were compared.

During fractional crystallisation, incompatible trace elements will tend to concentrate in residual magmas whereas compatible elements will be preferentially

concentrated in the crystals being formed, so that compatible elements will tend to be removed from the magma at greater rates than incompatible trace elements. As fractional crystallisation progresses these differences become emphasised and linear plots of incompatible trace elements against compatible trace elements will produce a curved trend (The Open University, 1990).

Log/log plots of compatible trace elements versus incompatible trace elements should show a straight-line trend if fractional crystallisation is the major process taking place, and a change in slope will indicate a change in the minerals being crystallised and removed (The Open University, 1990).

If, on the other hand, the variation in composition is the result of the mixing of two different magmas, the resultant magma will have a concentration of compatible and incompatible trace elements that will be intermediate between the two initial magmas. Where a range of resultant magmas exist, composed of different proportions of each initial magma, plots of incompatible against compatible elements will show as a straight line trend between the two initial magma compositions (The Open University, 1990).

10.6.1. Variation in compatible and incompatible trace element contents for the Penmaenmawr Intrusion

Plots showing the contents of incompatible against compatible trace elements for all the samples from the Penmaenmawr Intrusion are shown in Figure 10.3. The plots for Zr v Ni, Zr v Cr, Y v Ni, and Y v Cr show reasonably good straight-line trends whereas the plots for Ba v Ni, Ba v Cr, Nb v Ni and Nb v Cr show curved trends. The plots for Zr v V, Zr v Co, Y v V and Y v Co show two straight-line trends that intersect. However, all plots involving V and Co show a degree of scattering and the high degree of scatter in the plots of Ba v V, Ba v Co, Nb v V and Nb v Co make it impossible to identify any clear trends in these plots.

In all the diagrams in Figure 10.3, the samples from Group 3 and from Group 1 plot as a distinct groups and, apart from the plots that show a high degree of scatter identified above, have tight linear trends. The samples from Group 2 and Group 4 tend to plot between the trends for Groups 3 and 1.

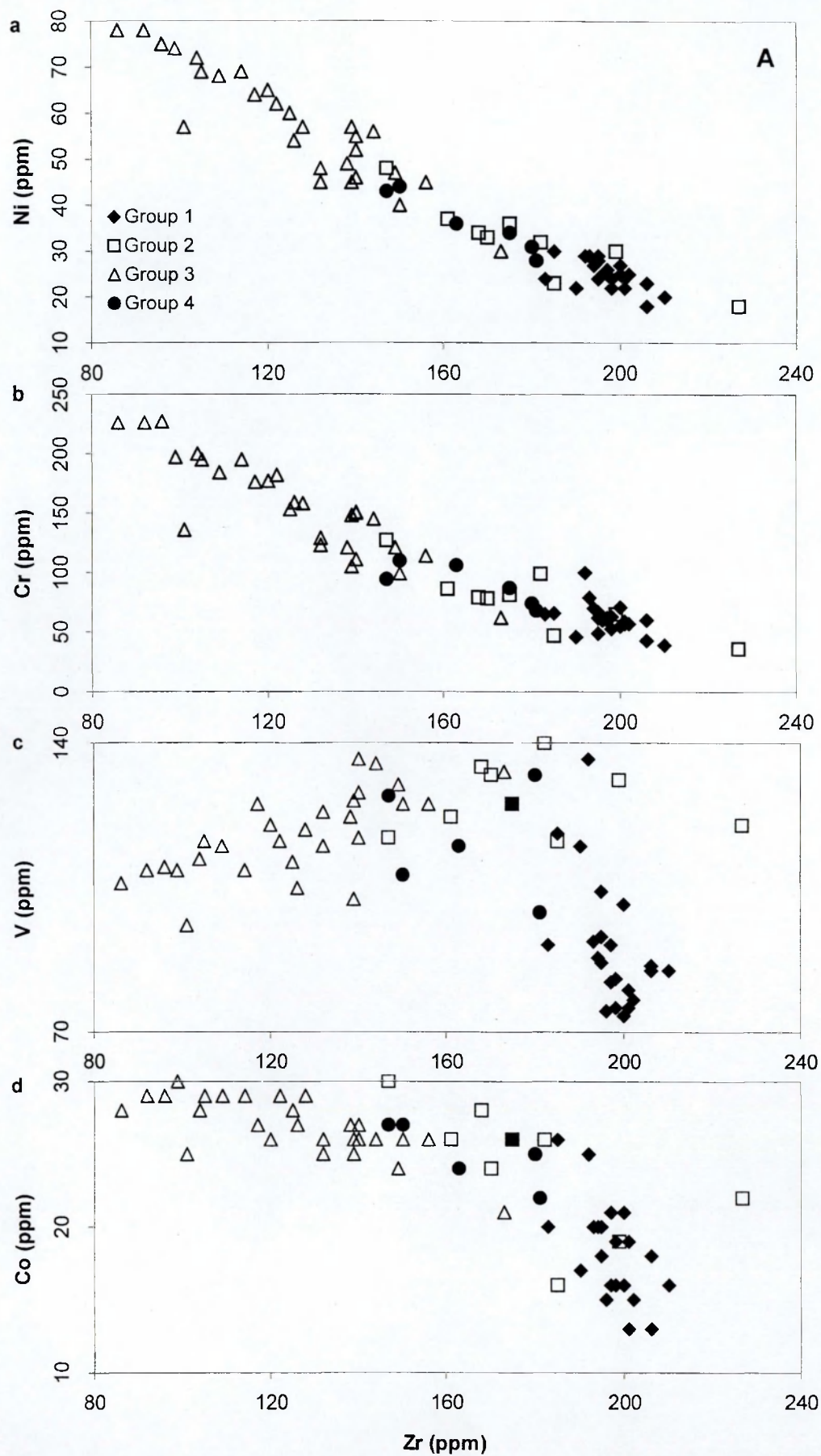


Figure 10.3. Plots showing the contents of compatible against incompatible elements (ppm) for the Penmaenmawr samples from Groups 1-4 (Legend provided on plot (a)). (A) The incompatible element Zr: (a) Ni, (b) Cr, (c) V and (d) Co, (continued overleaf).

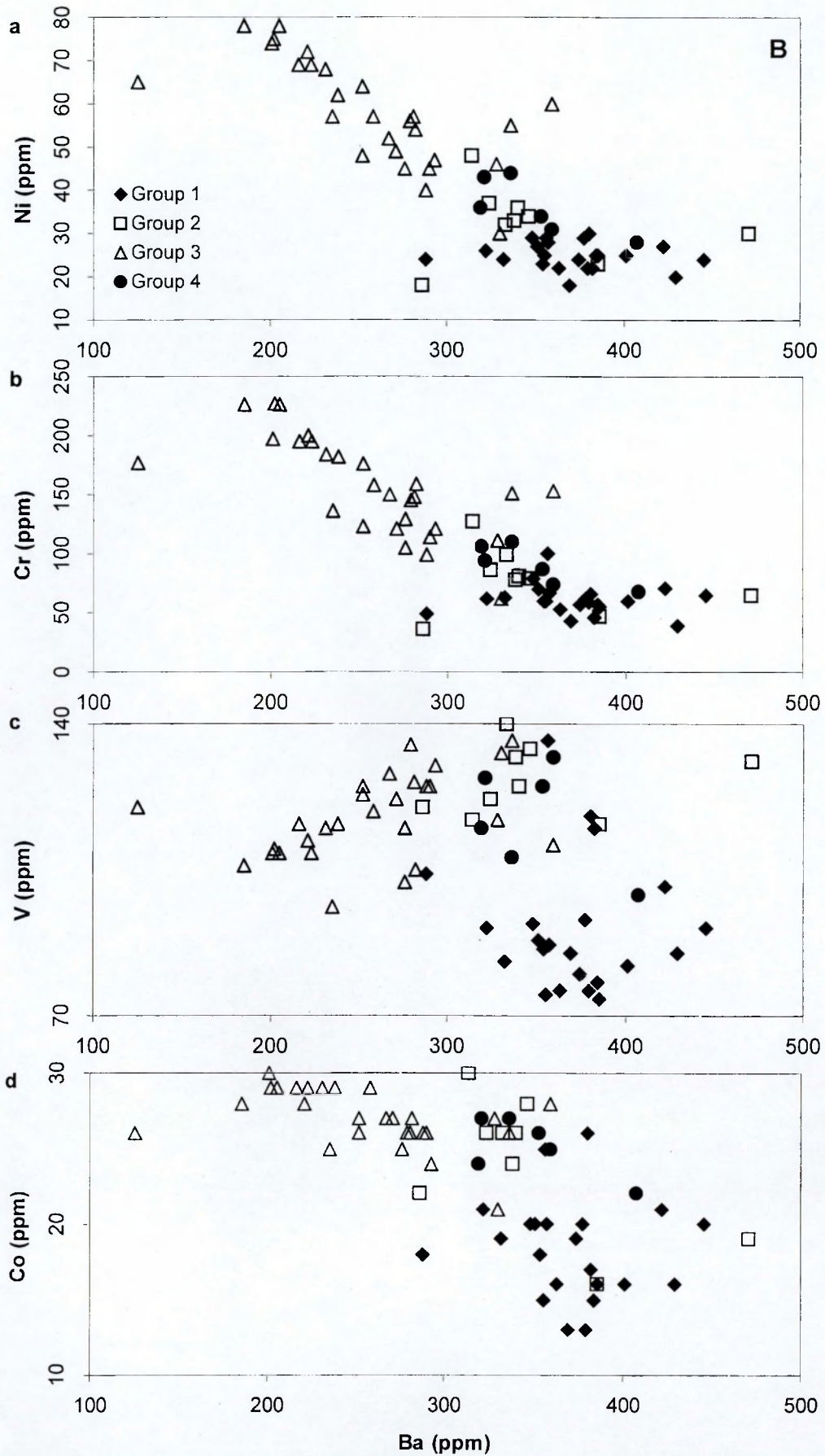


Figure 10.3. (continued). Plots showing the contents of compatible against incompatible elements (ppm) for the Penmaenmawr samples from Groups 1-4 (Legend provided on plot (a)). (B) The incompatible element Ba: (a) Ni, (b) Cr, (c) V and (d) Co, (continued overleaf).

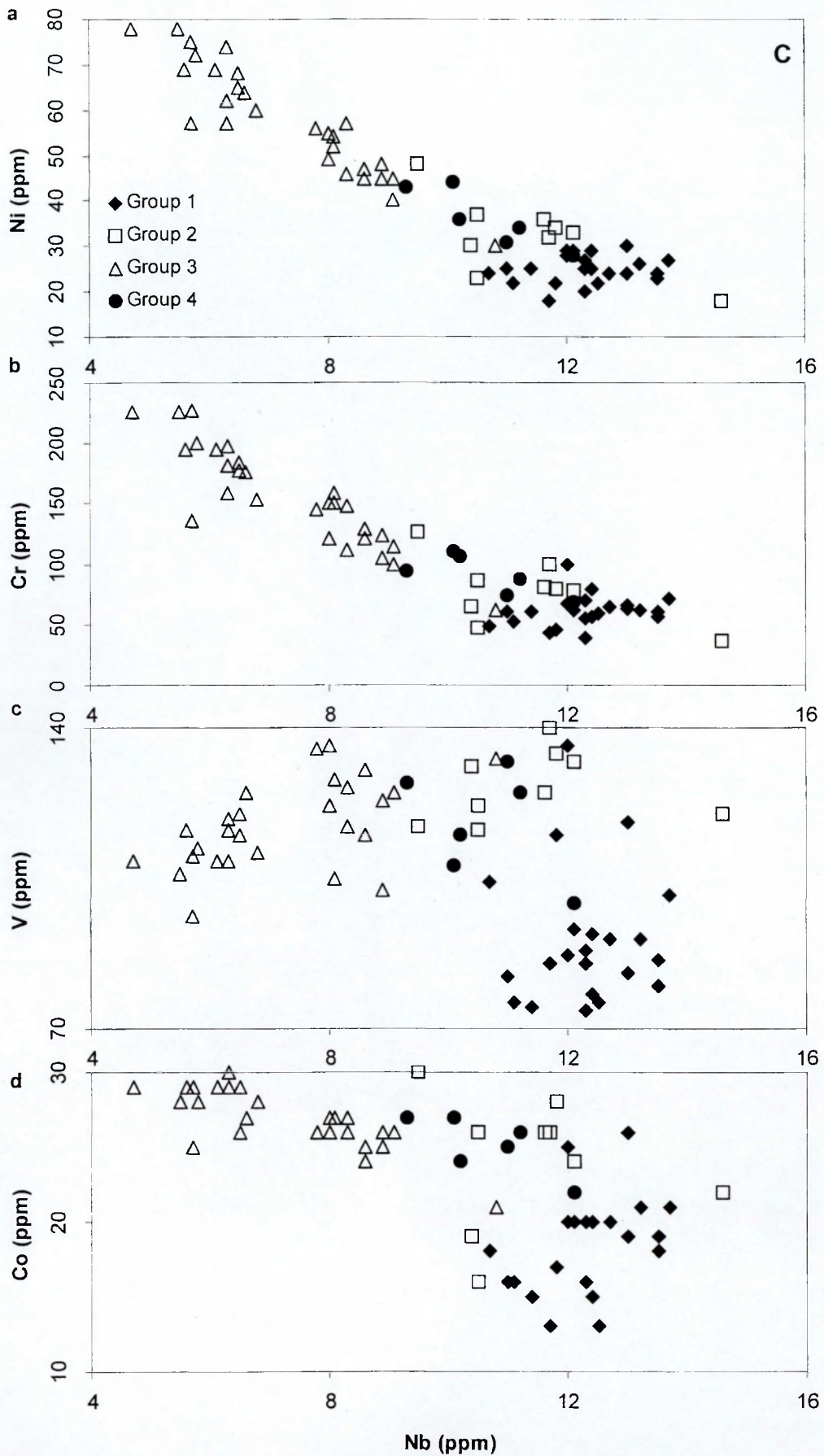


Figure 10.3. (continued). Plots showing the contents of compatible against incompatible elements (ppm) for the Penmaenmawr samples from Groups 1-4 (Legend provided on plot (a)). (C) The incompatible element Nb: (a) Ni, (b) Cr, (c) V and (d) Co, (continued overleaf).

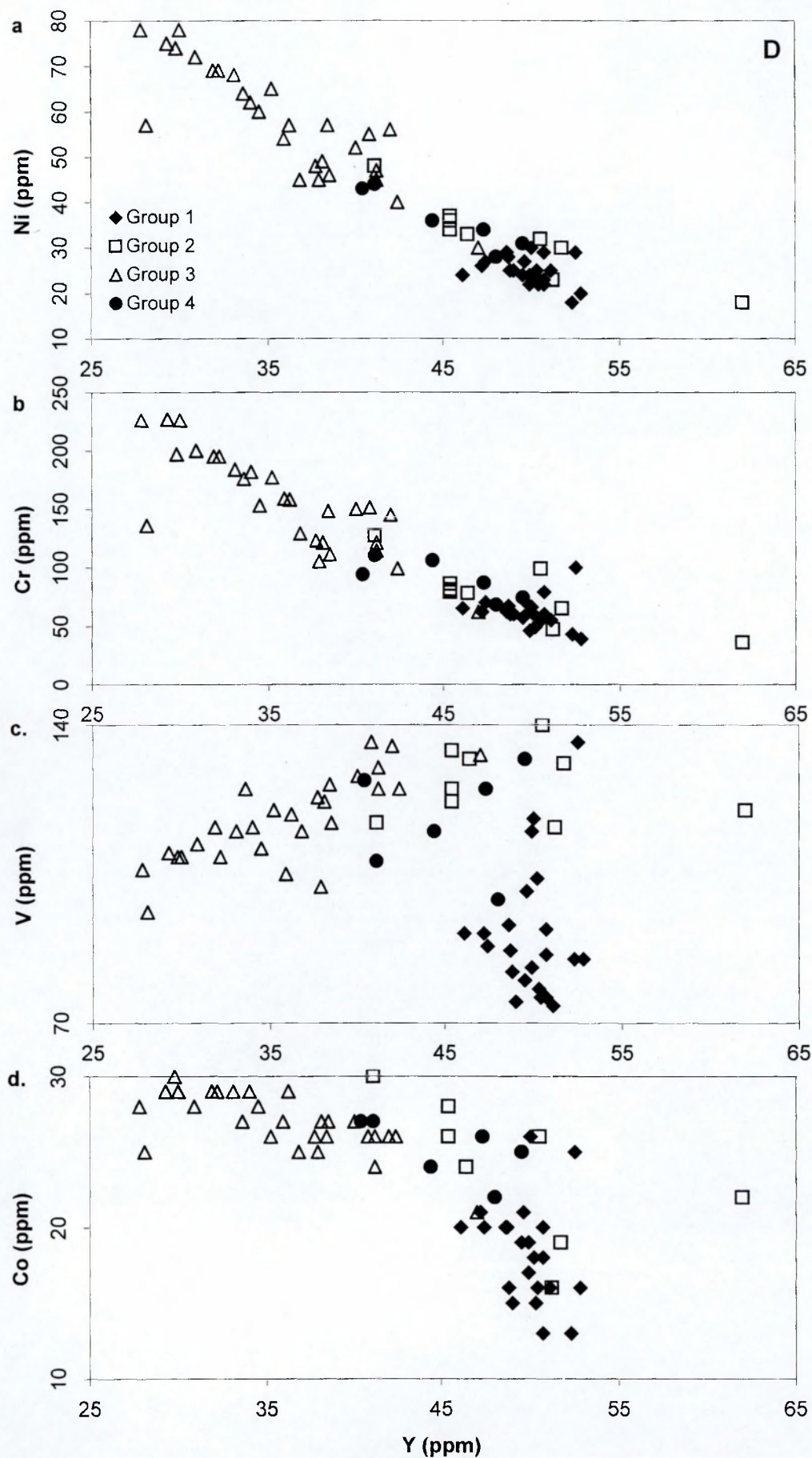


Figure 10.3. (continued). Plots showing the contents of compatible against incompatible elements (ppm) for the Penmaenmawr samples from Groups 1-4 (Legend provided on plot (a)). (D) The incompatible element Y: (a) Ni, (b) Cr, (c) V and (d) Co.

In most plots, Group 2 rocks continue the trend for Group 3 rocks, with one sample (JD2919), with high incompatible trace elements contents, consistently plotting as an extension to the Group 3 trend. Group 4 rocks in most cases tend to plot with Group 2 rocks but in certain other cases they plot with Group 1 rocks.

Log/log plots of incompatible trace elements against compatible trace elements are presented in Figure 10.4. All plots involving the compatible trace elements Ni and Cr plot as tight linear trends with, in most cases, a slight curvature. The plots involving compatible trace elements V and Co show two intersecting straight-line trends, with the rocks from Groups 3, and most of Group 2 and Group 4 rocks forming one linear trend, and the rocks from Group 1, with some rocks from Groups 2 and 4, forming the other linear trend.

10.6.2. Interpretation of the variations in compatible and incompatible trace element contents

The straight line trends on the linear plots for Zr v Ni, Zr v Cr, Y v Ni, and Y v Cr suggest that magma mixing could account for the geochemical variation in the Penmaenmawr Intrusion, but the curved trends on the linear plots for Ba v Ni, Ba v Cr, Nb v Ni, Nb v Cr suggest that the geochemical variation could be due to fractional crystallisation. However, the curved trends could be due to two intersecting straight-line trends, which would be comparable with the plots for Zr v V, Zr v Co, Y v V and Y v Co and which would support the suggestion that the Penmaenmawr Intrusion is not the result of a single magmatic process.

These plots could support the suggestion in section 10.5 above, namely, that both Group 3 and Group 1 rocks were the result of two magma batches that evolved separately by magma mixing. However, the range of trace element contents may not be large enough for curved trends within each Group to be perceptible and the change in slope could support a fractional crystallisation process with a change in fractionating assemblage between Groups 3 and 1, as suggested in section 10.4.1 above. Group 2 rocks could share a common origin with Group 3 rocks but the origin of Group 4 rocks is still unclear.

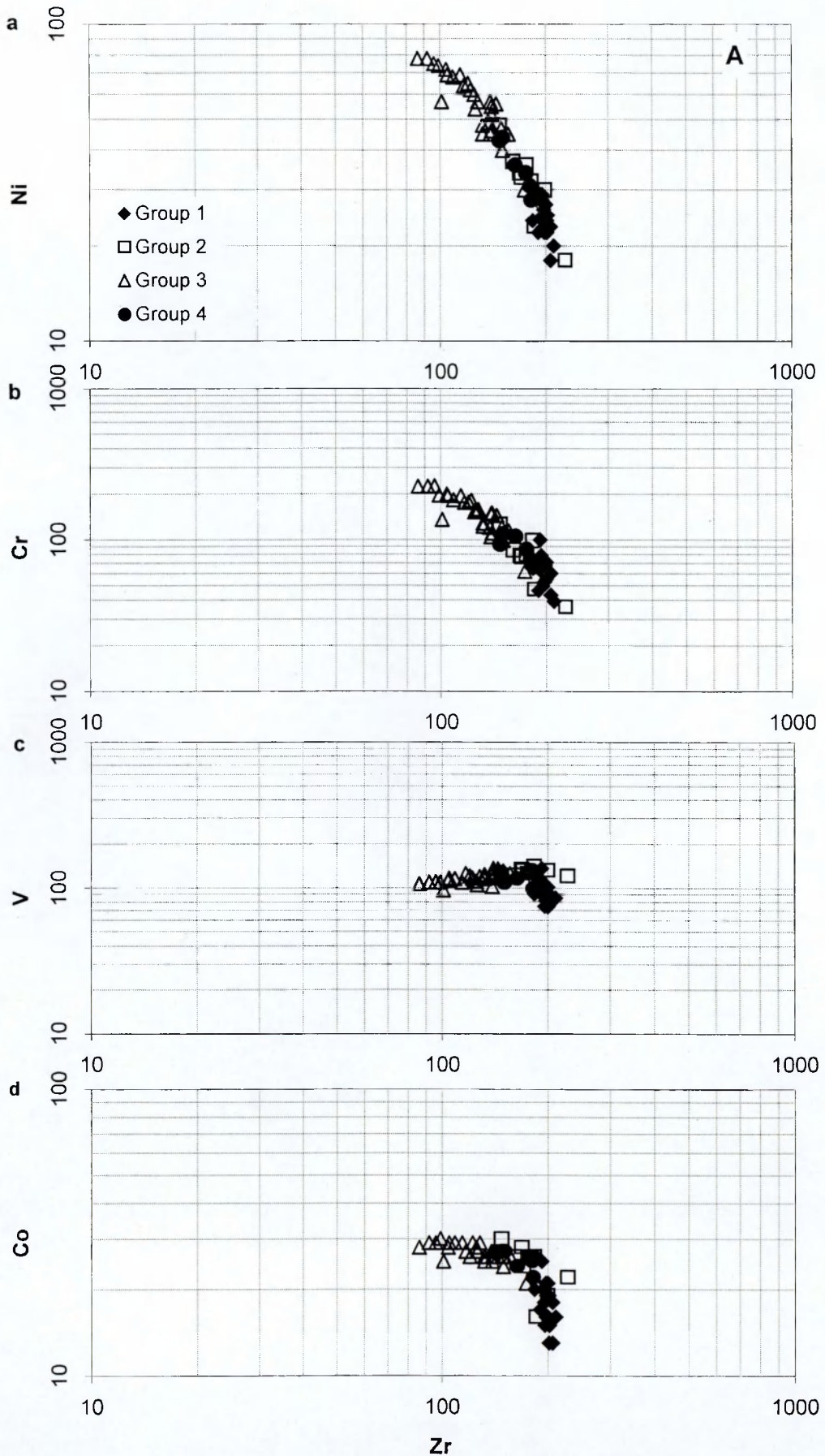


Figure 10.4. Log-log plots of compatible against incompatible elements for the Penmaenmawr samples from Groups 1-4 (Legend provided on plot (a)). (A) The incompatible element Zr: (a) Ni, (b) Cr, (c) V and (d) Co, (continued overleaf).

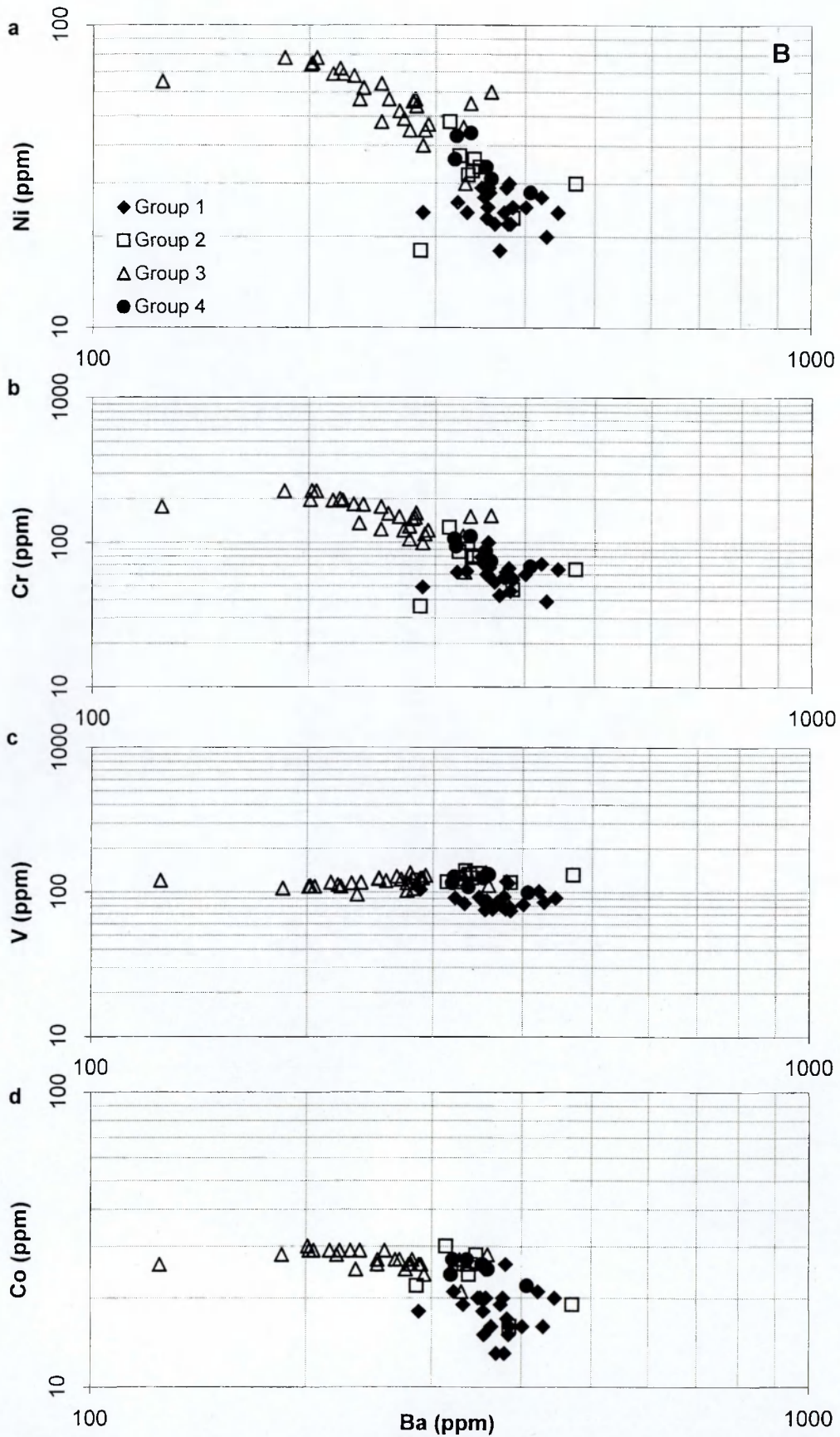


Figure 10.4. (continued). Log-log plots of compatible against incompatible elements (ppm) for the Penmaenmawr samples from Groups 1-4 (Legend provided on plot (a)). (B) The incompatible element Ba: (a) Ni, (b) Cr, (c) V and (d) Co, (continued overleaf).

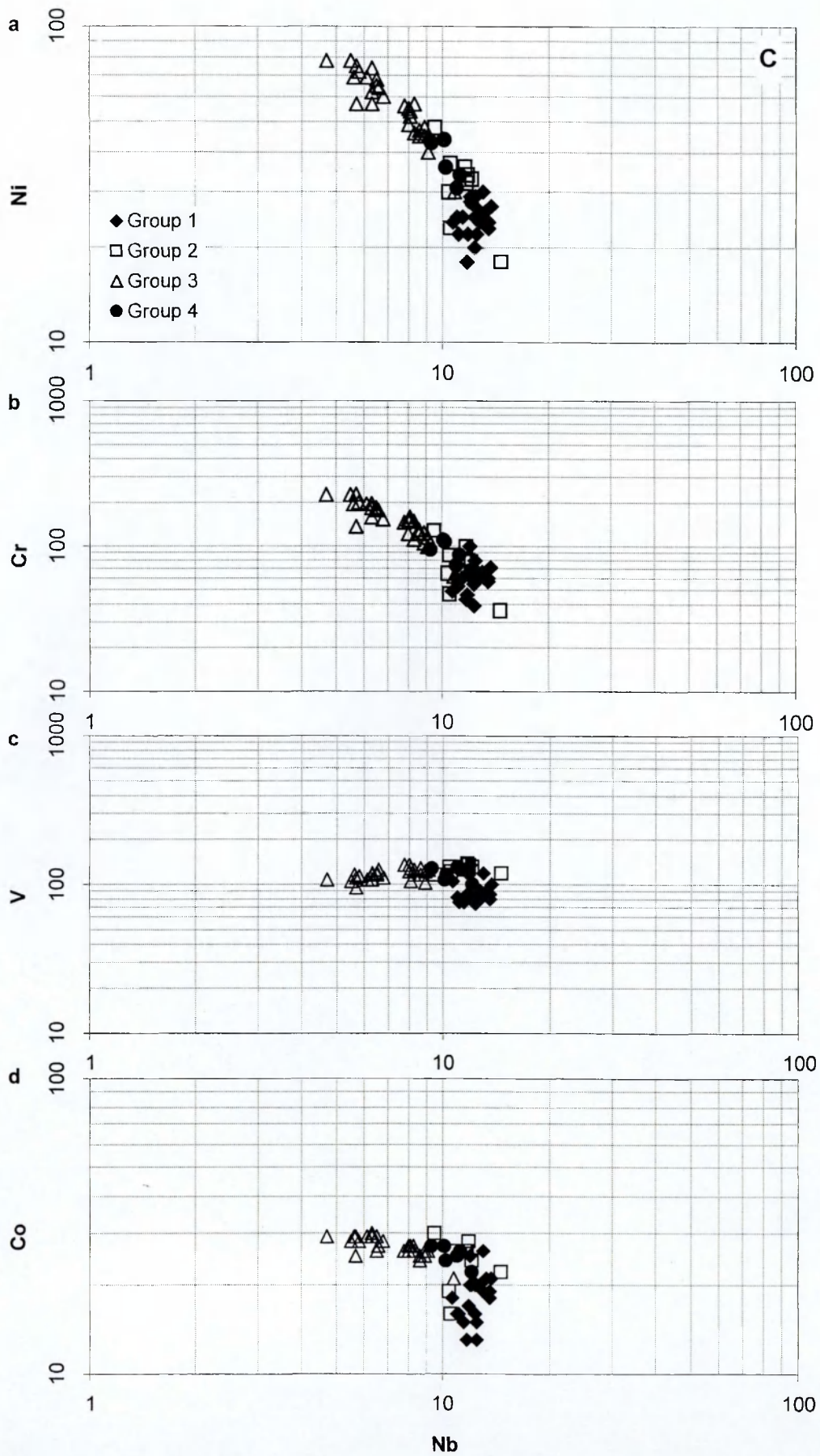


Figure 10.4. (continued). Log-log plots of compatible against incompatible elements (ppm) for the Penmaenmawr samples from Groups 1-4 (Legend provided on plot (a). (C) The incompatible element Nb: (a) Ni, (b) Cr, (c) V and (d) Co, (continued overleaf).

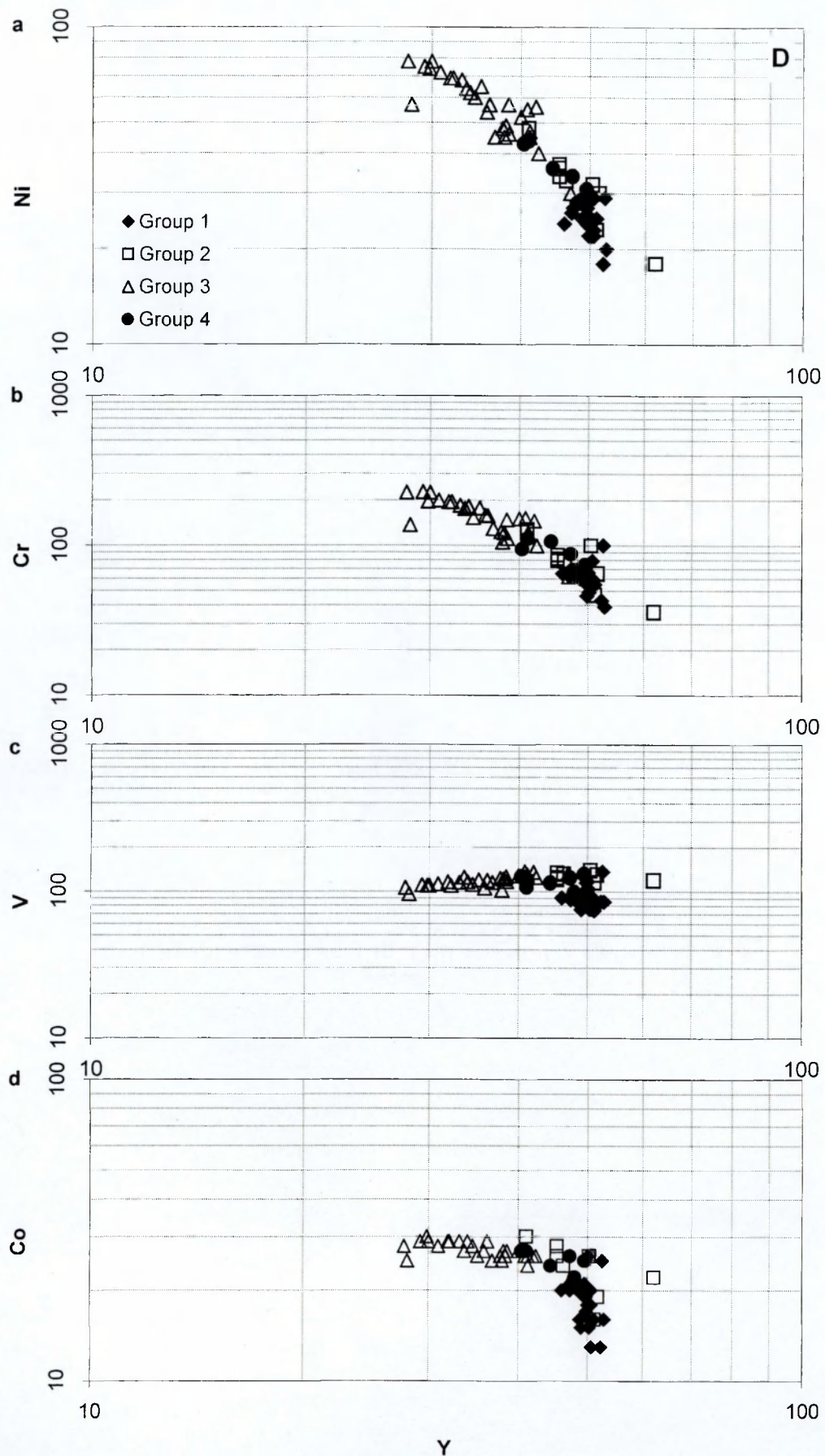


Figure 10.4. (continued). Log-log plots of compatible against incompatible elements (ppm) for the Penmaenmawr samples from Groups 1-4 (Legend provided on plot (a)). (D) The incompatible element Y: (a) Ni, (b) Cr, (c) V and (d) Co.

The linear trends of the log/log plots support the suggestion that fractional crystallisation could be the main process causing the geochemical variation, the slightly curved trends on the plots involving the trace elements Ni and Cr could be due to a varying fractionating assemblage. The change in slope on the plots involving the compatible trace elements V and Co supports the suggestion that fractional crystallisation could have operated on a two-stage process with a significant change in fractionating assemblage of minerals. As these trace elements tend to be compatible with the fractionation of iron titanium oxides and apatite, these plots are consistent with the two-stage fractional crystallisation process suggested in section 10.4.1.

10.7. Mineral fractionation vector diagrams for the Penmaenmawr Intrusion

If fractional crystallization was the main process causing the geochemical variation in the Penmaenmawr Intrusion, an indication of the minerals being formed and removed and the amount of crystal fractionation occurring within the intrusion can be obtained by calculating and displaying vector diagrams for groups of minerals on log/log plots of different trace elements. The combination of calculated trends can then be compared with the observed trends from samples collected from the intrusion.

During fractional crystallisation, the trace element concentration of the residual liquid due to the crystallisation and removal of each mineral can be calculated from the Rayleigh equation;

$$C_L/C_0 = F^{(D-1)} \quad (1)$$

where C_L is the concentration of a trace element in the residual magma, C_0 is the concentration of a trace element in the parental magma, F is the fraction of the melt remaining and D is the partition coefficient for the mineral concerned.

The calculated concentration of trace elements for different fractions of the melt remaining for each fractionating mineral can be plotted as a set of vectors on log/log bivariate plots. The variation in trace element concentrations observed in the intrusion can then be plotted as a vector on the same diagram which will provide an indication of the combination of minerals and the amount of fractionation that are likely to have been the dominant controls on the evolution of

the magma.

10.7.1. Calculation of mineral vectors

The least evolved sample from the Penmaenmawr Intrusion, considered to be the sample with the lowest SiO₂ content (JD2938), was used as the parental magma, and vectors showing the change in trace element concentrations in the daughter residual or daughter liquids were calculated for different fractions (0.9, 0.7 and 0.5) of melt remaining following the crystallisation of plagioclase feldspar, orthopyroxene, clinopyroxene, biotite and magnetite. The mineral-melt partition coefficients used are from Rollinson (1993) and are presented in Table 10.1

A range of plots was prepared for different pairs of trace elements and the trace element concentrations from samples from the Penmaenmawr Intrusion were plotted on the same diagrams for comparison. These plots are presented at Figures 10.5 and 10.6.

Table 10.1. Mineral-Melt partition coefficients for andesitic liquids. The biotite mineral-melt partition coefficients are for dacitic and rhyolitic liquids (from Rollinson, 1993).

Trace Element	Orthopyroxene	Clinopyroxene	Plagioclase feldspar	Biotite	Magnetite
Rb	0.022	0.013	0.07	3.2	0.01
Ba	0.013	0.04	0.16	6.36	0.01
Zr	0.046	0.162	0.013	1.2	0.2
Y	0.45	1.5	0.01	1.23	0.5
Ni	8	6	0.01		10
Cr	13	30	0.01	19	32
Co	6	3	0.01	88	8

10.7.2. Description of the vector diagrams

The plots for incompatible trace elements against incompatible trace elements, Zr v Y, Zr v Rb, Y v Rb and Y v Ba are presented in Figure 10.5. The plots for Zr v Y, Y v Rb and Y v Ba show the trends of the variations in trace element contents of the Penmaenmawr rocks close to and in most cases falling between the plagioclase feldspar, orthopyroxene and magnetite vectors. The plots for Zr v Rb show that the vectors for plagioclase feldspar, orthopyroxene, magnetite, and clinopyroxene, have similar trends and that they are concurrent with the trend of the Penmaenmawr rocks. In all plots the vectors for biotite appear to be in opposition to the trend of the Penmaenmawr rocks. The magnitude of the Penmaenmawr vector in these plots is comparable with the magnitude of the mineral vectors at approximately 50% fractionation.

The plots for incompatible trace elements against compatible trace elements Zr v Co, Zr v Cr, Y v Co and Y v Cr are presented in Figure 10.6. All plots show the trends of the variations in trace element contents of the Penmaenmawr Intrusion plotting between the vectors for plagioclase feldspar and orthopyroxene and plotting closer to the plagioclase feldspar vector than the orthopyroxene vector. The plots for Zr v Co shows the clinopyroxene vector plotting between the trend of the Penmaenmawr rocks and the orthopyroxene vector, however the plots for Y v Co and Y v Cr show the clinopyroxene vectors in the opposite direction to the trend of the Penmaenmawr rocks. In all plots, the vectors for biotite tend to be approximately perpendicular to the trend of the Penmaenmawr rocks and the magnetite vectors tend to plot close to the orthopyroxene vector.

The magnitude of the Penmaenmawr resultant vector in all plots tends to be less than the magnitude of the mineral vectors at 50% melt fraction remaining. The trends of the Penmaenmawr rocks on the plots for Zr v Co and Y v Co show a change of slope becoming more in line with the orthopyroxene vector at higher trace element concentrations.

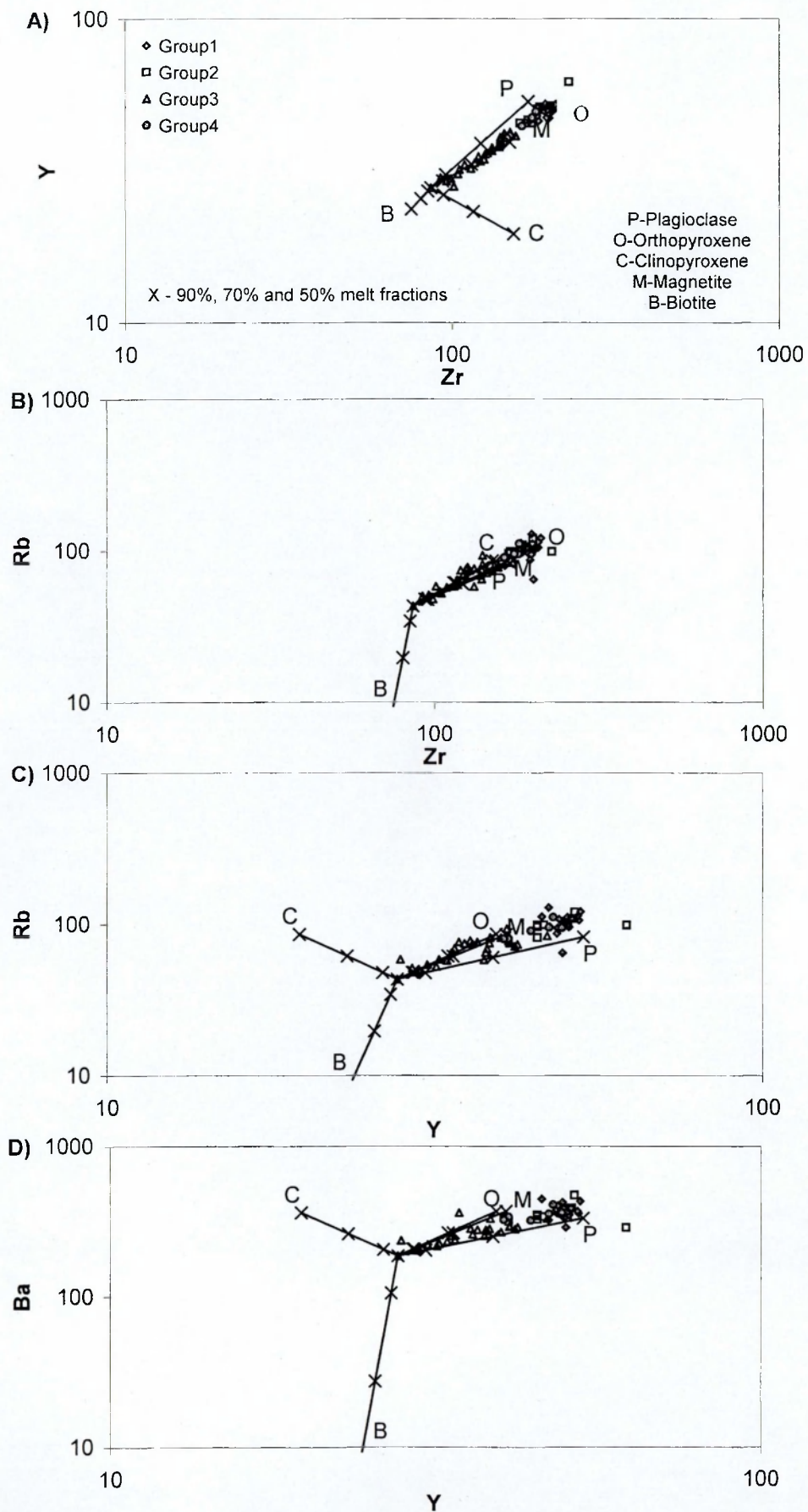


Figure 10.5. Vector diagrams for the Penmaenmawr rocks from all 4 Groups (legend provided on plot A.): Incompatible trace elements against incompatible trace elements, (A) Y against Zr, (B) Rb against Zr, (C) Rb against Y and (D) Ba against Y.

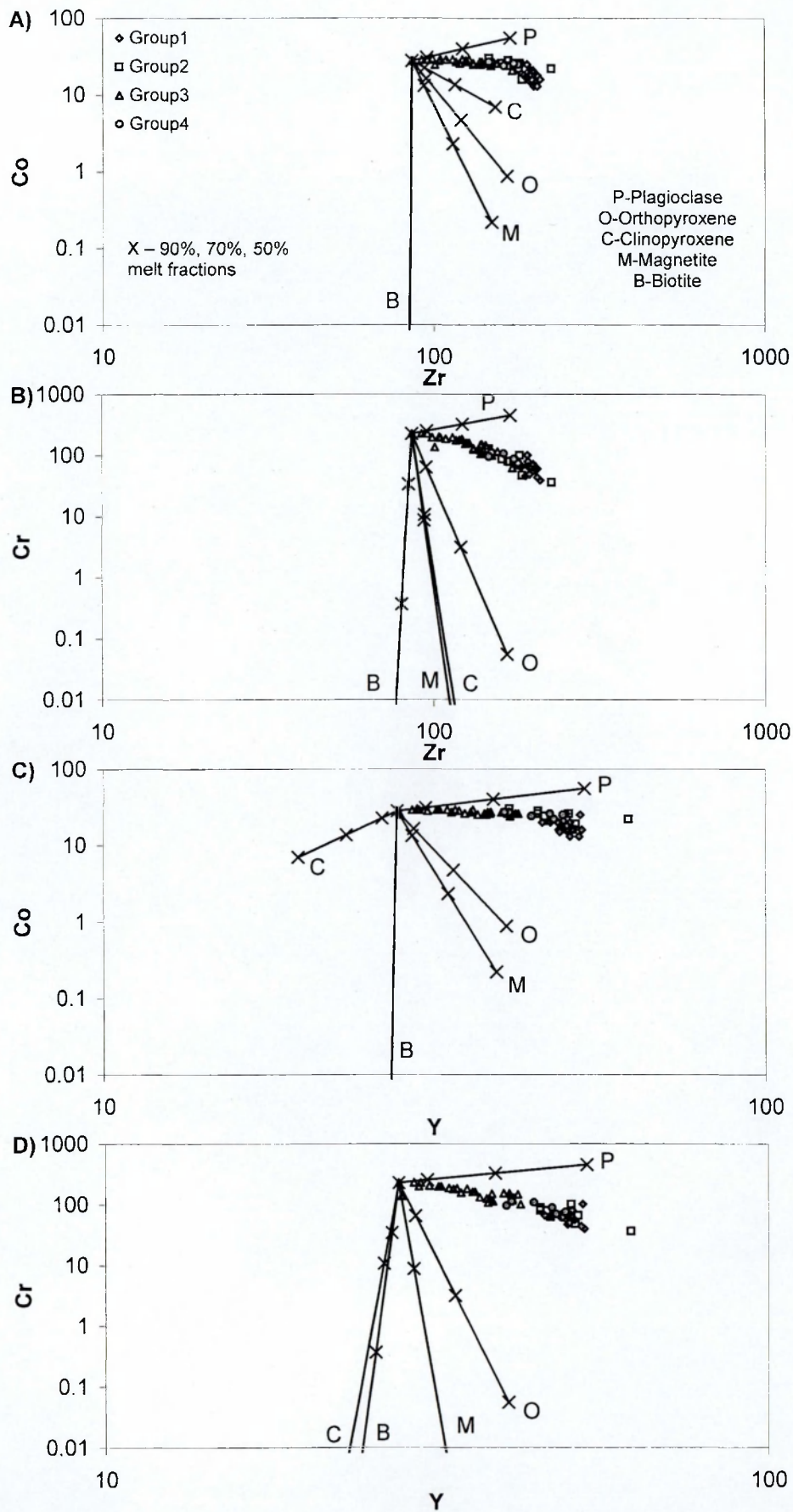


Figure 10.6. Vector diagrams for the Penmaenmawr rocks from all 4 Groups (legend provided on plot A.): Compatible trace elements against incompatible trace elements, (A) Co against Zr, (B) Cr against Zr, (C) Co against Y and (D) Cr against Y.

10.7.3. Interpretation of the vector diagrams

In all the vector diagrams of Figures 10.5 and 10.6, the trends of the variations in trace element contents of the Penmaenmawr rocks plot between the plagioclase feldspar and orthopyroxene vectors, which suggests that, if fractional crystallisation were the main cause for the geochemical variation in the Penmaenmawr Intrusion, the dominant phases crystallising and being removed were plagioclase feldspar and orthopyroxene. The vectors for clinopyroxene in the plots for Zr v Rb and Zr v Co suggest that this mineral could also have contributed to the resultant trend of the Penmaenmawr rocks; however, in the other diagrams the clinopyroxene vector is in opposition to the trend of the Penmaenmawr rocks. Clinopyroxene is present as a primary mineral in all samples from the Penmaenmawr Intrusion (see Chapter 5) it is therefore suggested that although it crystallised, it was not removed from the melt to any great extent and therefore did not contribute to the variations in trace element contents of the residual melt.

The vectors for biotite are generally in opposition to the trend of the Penmaenmawr rocks and it is therefore unlikely that the formation and removal of this mineral contributed to the observed variations in trace element contents. The magnetite vectors, however, in all plots are close to the orthopyroxene vectors and the formation and removal of magnetite could have contributed to the observed variation in trace element contents. It was shown in Chapter 5 that iron titanium oxides are only present in trace amounts in the rocks from the Penmaenmawr Intrusion and therefore the formation and removal of magnetite would only have had a small effect on the resultant trends of the variations in trace element contents.

In the plots of incompatible versus compatible trace elements (Figure 10.6) the trend of the Penmaenmawr rocks is closer to the plagioclase feldspar vector than the orthopyroxene vector, which suggests that the fractionation of the former mineral had a greater effect on the variation in trace element contents than the latter. An estimate of the proportions of these two minerals can be made by considering the Penmaenmawr trend as simply the resultant vector of the plagioclase and orthopyroxene vectors, constructing a vector parallelogram and

comparing the magnitude of the mineral vectors forming the two sides of the parallelogram. This construction suggests that the ratio of plagioclase feldspar to orthopyroxene fractionating is between 1.5 and 2.4 to 1.

The change in slope in the trend of the Penmaenmawr rocks in the plots for Zr v Co and Y v Co supports the suggestions made in Section 10.4.1 that fractional crystallisation could be a two-stage process. The change in slope, towards the orthopyroxene vector, could suggest that, at higher SiO₂ contents (Group 1 rocks), the ratio of plagioclase feldspar to orthopyroxene being formed and removed decreases. However, the direction of the change in slope is also towards the magnetite and biotite vectors and could be therefore suggest that at higher SiO₂ contents magnetite and/or biotite began to fractionate.

The vector diagrams for incompatible trace elements versus incompatible trace elements for the intrusion as a whole suggest that the fraction of melt remaining following fractionation would be approximately 50% whereas the vector diagrams for incompatible trace elements versus compatible trace elements suggest that the fraction of melt remaining is greater than 50%. This slight difference between the two sets of diagrams may suggest that in detail, the trace elements are not acting typically in their preferences for incorporation into minerals and are remaining in the melt or that the partitions coefficients used in these models differ from the values that may apply in the actual magma.

CHAPTER 11. FRACTIONAL CRYSTALLISATION MODELLING

11.1. Introduction

In Chapter 7 it was demonstrated that there is a variation in whole rock major and trace element contents across the Penmaenmawr Intrusion. It was suggested that the close correlation between the elements, seen on the variation diagrams in Chapter 10, and the coherence of the trends for both major and trace elements, indicate that the rocks of the intrusion are related genetically and that a two-stage fractional crystallisation process could have caused the observed geochemical variation.

In order to investigate in more detail whether fractional crystallisation could have caused the geochemical variation, theoretical mathematical modelling was undertaken. Initial modelling, based on the intrusion as a whole, produced inconsistent results. However, it was also suggested in Chapter 10 that the different petrographic groups, defined in Chapter 4, may represent batches of magmas that fractionated independently of each other and subsequent modelling was carried out within the petrographic groups.

Both major element and trace element data from selected, geochemically coherent samples from Groups 3, 2 and 1 were used to model fractional crystallisation. Samples from Group 4 were not included as the range of geochemical compositions within Group 4 was considered insufficient to produce any meaningful results. The results obtained from the modelling were then compared with the variations observed in each group. A good match between the modelled variations and the observed variations would not only provide support for fractional crystallisation having taken place but also demonstrate which minerals were involved.

This Chapter uses mineral geochemistry data and whole rock geochemistry data from the Penmaenmawr Intrusion, presented in Chapters 5 and 7, to investigate both major and trace element fractional crystallisation modelling.

11.2. Major element modelling - theoretical considerations

Major element modelling for fractional crystallisation is based on quantifying the proportions of the phases being formed during the crystallisation process which leads to changes in the chemical composition of the remaining melt. During fractional crystallisation a melt with a major element composition A will evolve to a composition B by the crystallisation and removal of different proportions of minerals of different compositions. This can be expressed by the equation:-

$$\text{Rock A} = f \text{ Rock B} + (x \text{ mineral X} + y \text{ mineral Y} + z \text{ mineral Z} \dots) \quad (\text{Rollinson, 1993})$$

where Rock A represents the major element composition of the parent melt, Rock B represents the major element composition of the daughter melt, f represents the proportion of parent melt remaining and x , y and z represent the proportions of minerals X, Y, Z being crystallised and removed from the system.

In a series of rocks with coherent variation in compositions, the most mafic member can be used to represent the original or parent magma and the most felsic member can be used to represent the fractionated or daughter magma. By using the major element contents of the fractionating minerals for each element in turn, it is possible to prepare a set of simultaneous equations, which can be solved using a least squares, best-fit mathematical method to estimate the proportion of evolved magma and the proportions of the different minerals involved in generating it from the proposed parent magma.

The proportions obtained from the best-fit calculations can be substituted in the equation above to produce the major element composition of a modelled parent magma. This composition can be compared with the major element composition of the rock that was used to represent the parent magma and the differences between them provide a measure of the acceptability of the model. The differences in composition between the modelled parent magma and the sample used to represent the parent magma is normally denoted by R^2 , the sum of the squares of the differences for each major element oxide.

11.3. Major element modelling - constraints and assumptions

For mathematical modelling the major element whole rock compositions of selected samples from the Penmaenmawr Intrusion were recalculated to remove the LOI (loss on ignition) so that the sum of the 10 major element oxides was 100%. The samples selected as parent and daughter magmas in major element modelling and their major element compositions are presented in Table 11.1 and Figure 11.1.

It was suggested in Chapters 4 and 5 that, although many of the mineral grains found in the Penmaenmawr Intrusion have been altered and that there are many secondary minerals present, the primary mineralogy consisted mainly of plagioclase feldspar (30-60%), orthopyroxene (15-30%) and clinopyroxene (10-20%), with minor amounts of biotite, ilmenite, apatite and quartz.

The compositions of the fractionating minerals used in the modelling (presented in Table 11.2) were based on the mineral chemistry from representative samples from the Penmaenmawr Intrusion (presented in Chapter 5 and Appendix 4), in particular the average mineral compositions from Group 3 rocks. These compositions were used because the primary mineral compositions of the more evolved samples were either unavailable or unreliable; in particular, orthopyroxene and biotite in these rocks have been completely replaced by secondary minerals and the compositions of plagioclase feldspar and ilmenite have been partially changed by post emplacement alteration. For the calculations the compositions of the minerals, with the exception of biotite, which contains integral (OH)⁻ ions, were recalculated so that the sum of the 10 major element oxides was 100%.

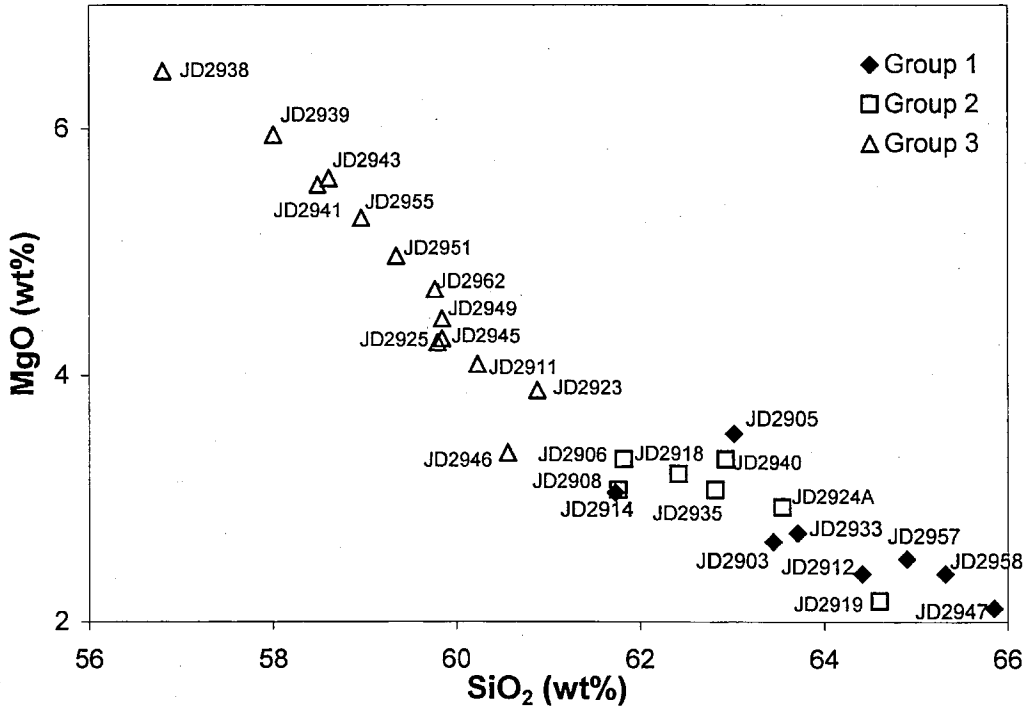
In carrying out this modelling two further major assumptions were made which need to be taken into account when assessing the validity of the results.

1. The chemistry of the minerals used in this modelling does not change during the process.

Table 11.1. Major element compositions of Penmaenmawr samples used for fractional crystallisation modelling, normalised to 100% after the removal of the LOI (loss on ignition).

Group 1								
	<u>JD2914</u>	<u>JD2933</u>	<u>JD2912</u>	<u>JD2905</u>	<u>JD2957</u>	<u>JD2958</u>	<u>JD2947</u>	<u>JD2903</u>
SiO ₂	61.73	63.71	64.41	63.01	64.90	65.32	65.85	63.56
TiO ₂	1.10	0.84	0.82	1.03	0.73	0.70	0.72	0.86
Al ₂ O ₃	15.46	15.31	15.18	15.05	15.02	14.99	14.85	15.34
Fe ₂ O ₃	7.14	6.12	5.82	6.89	5.55	5.34	5.49	6.18
MnO	0.21	0.17	0.14	0.32	0.15	0.14	0.14	0.15
MgO	3.05	2.72	2.39	3.53	2.51	2.39	2.11	2.65
CaO	4.66	4.96	4.68	3.50	4.48	4.36	3.89	4.79
Na ₂ O	3.35	3.78	3.59	3.40	3.60	3.66	3.65	3.59
K ₂ O	3.09	2.21	2.78	3.07	2.89	2.95	3.17	2.70
P ₂ O ₅	0.21	0.18	0.19	0.20	0.17	0.15	0.13	0.18
TOTAL	100.00	100.00	100.00	100.00	100.00	100.00	100.00	100.00
Group 2								
	<u>JD2908</u>	<u>JD2906</u>	<u>JD2918</u>	<u>JD2935</u>	<u>JD2940</u>	<u>JD2924A</u>	<u>JD2919</u>	
SiO ₂	61.76	61.82	62.41	62.81	62.92	63.54	64.60	
TiO ₂	0.93	1.03	0.99	1.06	1.03	1.08	1.24	
Al ₂ O ₃	15.30	15.11	15.07	14.70	14.87	14.76	14.31	
Fe ₂ O ₃	7.00	7.17	6.81	6.81	6.96	6.74	6.95	
MnO	0.15	0.19	0.19	0.17	0.23	0.15	0.19	
MgO	3.07	3.32	3.20	3.07	3.32	2.93	2.17	
CaO	6.16	5.05	4.90	4.91	3.75	3.82	3.84	
Na ₂ O	3.20	3.57	3.45	3.54	3.54	3.57	3.57	
K ₂ O	2.25	2.58	2.79	2.75	3.21	3.22	2.88	
P ₂ O ₅	0.18	0.16	0.19	0.18	0.17	0.19	0.25	
TOTAL	100.00	100.00	100.00	100.00	100.00	100.00	100.00	
Group 3								
	<u>JD2939</u>	<u>JD2941</u>	<u>JD2943</u>	<u>JD2955</u>	<u>JD2951</u>	<u>JD2962</u>	<u>JD2925</u>	<u>JD2945</u>
SiO ₂	58.00	58.48	58.60	58.96	59.34	59.76	59.79	59.84
TiO ₂	0.59	0.62	0.61	0.64	0.69	0.80	0.74	0.89
Al ₂ O ₃	16.18	16.04	16.04	15.99	16.27	15.51	16.12	15.57
Fe ₂ O ₃	6.82	6.90	6.82	6.85	6.55	7.03	7.01	7.32
MnO	0.15	0.15	0.15	0.15	0.17	0.15	0.16	0.16
MgO	5.95	5.55	5.60	5.28	4.97	4.70	4.27	4.30
CaO	7.82	7.79	7.58	7.20	6.64	6.67	6.47	6.49
Na ₂ O	2.93	2.87	2.98	3.05	3.11	3.26	3.33	3.22
K ₂ O	1.48	1.53	1.53	1.79	2.16	2.01	1.98	2.06
P ₂ O ₅	0.08	0.07	0.09	0.09	0.10	0.11	0.13	0.15
TOTAL	100.00	100.00	100.00	100.00	100.00	100.00	100.00	100.00
Group 3								
	<u>JD2949</u>	<u>JD2911</u>	<u>JD2946</u>	<u>JD2923</u>	<u>JD2938</u>			
SiO ₂	59.84	60.23	60.56	60.88	56.80			
TiO ₂	0.78	0.76	1.10	0.80	0.53			
Al ₂ O ₃	15.84	16.08	15.45	15.67	16.42			
Fe ₂ O ₃	7.10	6.96	7.75	6.87	7.10			
MnO	0.16	0.15	0.17	0.15	0.16			
MgO	4.46	4.09	3.37	3.88	6.47			
CaO	6.53	6.52	5.68	6.07	8.43			
Na ₂ O	3.22	3.22	3.45	3.37	2.82			
K ₂ O	1.95	1.86	2.26	2.16	1.18			
P ₂ O ₅	0.12	0.13	0.21	0.15	0.08			
TOTAL	100.00	100.00	100.00	100.00	100.00			

a) MgO v SiO₂



b) Zr v SiO₂

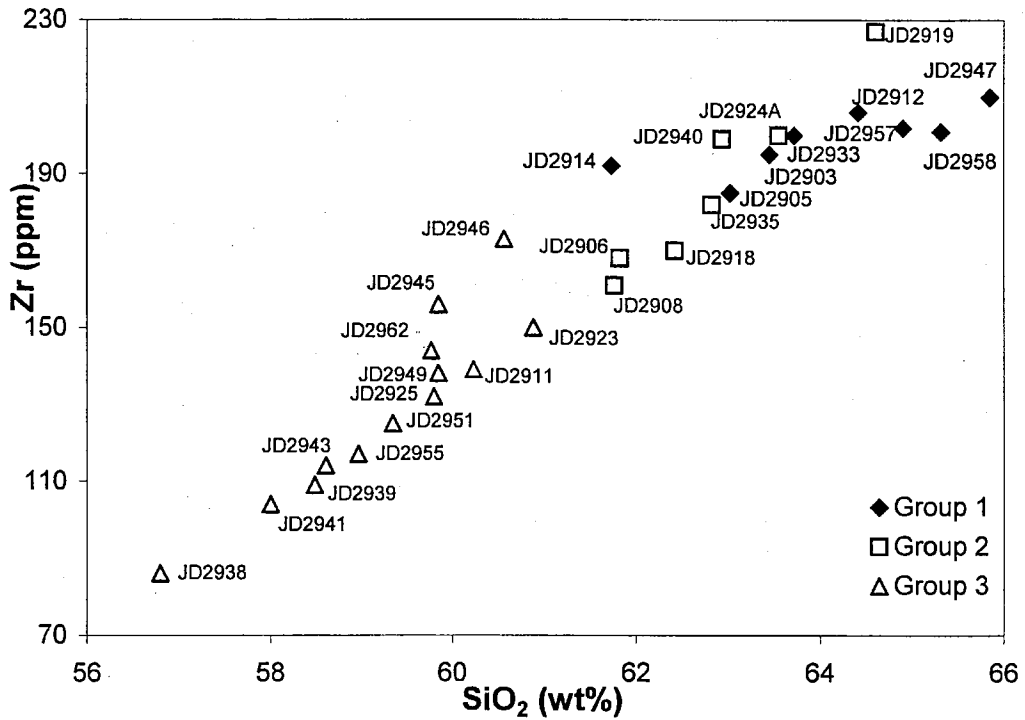


Figure 11.1. Plots of (a) MgO versus SiO₂ and (b) Zr versus SiO₂ for the 30 samples used for fractional crystallization.

2. The compositions of the samples used as parent and daughter represent magma compositions and do not contain any cumulate minerals.

The mathematical, least squares, best-fit modelling was carried out, for convenience, using the optimiser function on a Quatro Pro spreadsheet. Trial results using this procedure were compared with those produced by XLFRAC (Excel) - a program for the interactive testing of magmatic differentiation models, based on Stomer and Nichols (1978) - at the Open University, and the two methods were found to produce identical results.

Table 11.2. The mineral compositions used for major element modelling based on the average mineral chemistry determined by electron probe mineral analysis from Group 3 rocks (See Chapter 5 and Appendix 4).

Wt. % oxide	Plagioclase	Orthopyroxene	Clinopyroxene	Biotite	Ilmenite	Apatite
SiO ₂	55.15	52.93	51.94	36.67	0.13	0.31
TiO ₂	0.06	0.34	0.52	3.20	29.82	0.01
Al ₂ O ₃	27.59	0.91	1.54	12.96	0.61	0.00
Fe ₂ O ₃	0.47	21.35	11.08	17.17	67.00	0.17
MnO	0.01	0.55	0.38	0.15	2.33	0.04
MgO	0.02	21.69	14.28	15.59	0.02	0.04
CaO	10.92	2.18	19.97	0.18	0.04	57.25
Na ₂ O	5.45	0.03	0.27	0.08	0.01	0.15
K ₂ O	0.31	0.02	0.01	7.44	0.00	0.01
P ₂ O ₅	0.01	0.00	0.01	0.00	0.00	42.01
Total	99.99	100.00	100.00	93.41	100.00	99.99

11.4. Trace element modelling – theoretical considerations, constraints and assumptions

Proportions of minerals and melt derived from major element modelling were tested for feasibility by using them in trace element modelling. Trace element modelling uses the Rayleigh equation (equation 1, Section 9.6)

$$C_L/C_O = F^{(D-1)}$$

which describes the partitioning of a trace element between minerals and melt during fractional crystallisation. It enables the potential trace element concentration in a residual or daughter melt to be calculated after a known proportion of the original or parent melt has crystallised as a particular assemblage of minerals.

In the Rayleigh equation: C_L is the concentration of the trace element in the daughter magma; C_O is the concentration of the trace element in the parent magma; F is the fraction of the melt remaining; D is the bulk partition coefficient for the minerals being crystallised and removed. The bulk partition coefficient for each trace element is the sum of the mineral/melt partition coefficients for that trace element in each mineral phase fractionating, multiplied by the proportion of that mineral in the fractionating, crystallising assemblage.

The results from major element modelling provide an estimate of the proportion of liquid remaining and the proportions of the different minerals fractionating. These values can then be used to calculate trace element concentrations for respective daughter magmas, which can then be compared with the actual trace element concentrations observed in the evolved samples. A close correlation between calculated concentrations and observed concentrations would support the results from the major element modelling and hence the suggestion that a fractional crystallisation process could have caused the elemental variations in the intrusion.

The elements used for trace element modelling were Rb, Y, Zr, Nb, Ba, Cr and Co as these elements showed reasonably tight trends on the variation diagrams (see Chapter 10) and were shown to be relatively immobile during alteration (see Chapter 7). The trace element partition coefficients applicable to andesitic liquids, (for biotite, dacitic and rhyolitic liquids) were from Rollinson, (1993), and were presented in Table 10.1.

As the trace element modelling employs the results of the major element modelling, the assumptions listed in Section 11.3 above need to be taken into account when assessing the results. Additionally, the accuracy of the results relies on the use of appropriate mineral/melt partition coefficients. Rollinson (1993) points out that partition coefficients can vary extensively according to the

temperature and pressure conditions, the composition and oxygen activity of the melt. Although a good approximation, the rocks from Group 1 are more evolved than the rocks from Group 3 and so the values used may not be accurate and are an acknowledged source of error in the modelling.

11.5. Modelling the less evolved rocks (Group 3)

Group 3 rocks have the lowest SiO₂ contents and comprise the least evolved rocks from the intrusion. Sample JD2938, with the lowest SiO₂ content within Group 3 rocks (See Table 11.1 and Figure 11.1) was used to represent the parent magma composition for the modelling and a selection of more evolved samples from both Group 3 and Group 2 were chosen to represent the daughter magmas.

11.5.1. Major element modelling for the less evolved rocks (Group 3)

The detailed results of the modelling are presented in Appendix 7. The R² values are generally high, above 0.3, for daughter samples with SiO₂ contents >59.5% which questions whether fractional crystallisation with JD2938 as the parent magma could account for the geochemical variation within all Group 3 rocks or that Group 2 rocks represent daughter magmas evolved from sample JD2938. However, the R² values are low from 0.04 to 0.13 for five daughter samples from Group 3 that are close to JD2938 both geographically and compositionally. The data for these five samples are summarised in Table 11.3.

These data also show that the amount of fractionation would range from 27.7% to 48.8% and that during the fractionation process plagioclase feldspar, orthopyroxene, clinopyroxene and biotite would be removed from the melt in fairly consistent proportions ranging from 57.4% to 58.2% plagioclase feldspar, 23% to 24.8% orthopyroxene, 13% to 17.1% clinopyroxene and 0.1% to 4.1% biotite.

These models require clinopyroxene and small amounts of biotite to be crystallised and removed from the melt but it was suggested in Chapter 10, from an analysis of vector diagrams, that, if fractional crystallisation were the main process that caused the geochemical variation, the dominant phases being

formed and removed from the melt were most likely to have been plagioclase feldspar and orthopyroxene with a minor, if any, contribution from magnetite and that clinopyroxene was not involved to any great extent.

Table 11.3. A summary of the results of major element modelling for five Group 3 daughter samples using JD2938 (SiO₂ content 56.8%) as the parent magma.

Sample	JD2939	JD2941	JD2943	JD2955	JD2951
SiO ₂	58.00	58.48	58.6	58.96	59.34
R ²	0.046	0.056	0.075	0.124	0.133
% Fractionation	27.3	34.8	35.5	42.7	48.8
% plag	57.9	58.2	57.5	58.1	57.4
% opx	23.8	24.8	23.0	24.3	23.4
% cpx	15.3	13.5	15.4	15.7	17.1
% ilm	0.25	0	0	0	0
% apa	0.01	0	0	0	0
% bio	2.8	3.4	4.1	1.9	0.13

However, it was reported in Chapters 5 and Chapter 7 that crystals of plagioclase feldspar in the more altered rocks tend to become albitised and that both Na and Ca had become mobilised during alteration, although most of these elements had been incorporated into secondary minerals. Differing Na/Ca ratios in plagioclase feldspar crystals and whole rock compositions could cause the equations used in the modelling to apportion more of the whole rock CaO into clinopyroxene, thus overestimating the proportion of clinopyroxene being crystallised and removed from the melt. As this modelling would also apportion whole rock FeO and MgO contents into clinopyroxene, there would be less FeO and MgO apportioned to orthopyroxene and therefore the proportion of orthopyroxene being crystallised and removed from the melt would be correspondingly underestimated.

These data suggest that the modelling may be a good approximation for a few samples within Group 3 and that fractional crystallisation could account for the geochemical variation within a small group of samples which are geographically and compositionally close. However, the high R² values for daughter samples

with SiO₂ contents >59.5% suggest that major element fractional crystallisation modelling cannot be used to account for the geochemical variation within all Group 3 rocks or that Group 2 rocks represent daughter magmas evolved from a parent magma represented by sample JD2938.

Group 3 rocks cover a large area and could be made up of two or more batches of magma that, although related through a common parent magma, underwent fractional crystallisation independently. In order to examine this hypothesis, major element modelling was carried out using sample JD2925 as the parent magma and other more evolved samples from Group 3 as the daughter magmas. Sample JD2925 was chosen as the parent magma because it was the least evolved sample in Group 3 to show a high R² value (0.35) on modelling as a daughter of JD2938, reported above and presented in Appendix 7, and therefore it is unlikely to have evolved from sample JD2938. Additionally, it was collected towards the centre of the intrusion, close to the Central Quarries, whereas sample JD2938 was collected from the Western Quarries (see Figures 3.6 and 4.1).

The detailed results for the major element modelling using JD2925 as the parent magma and four more evolved Group 3 samples from the Central Quarries as the daughter magmas are presented in Appendix 8 and summarised in Table 11.4.

The accuracy of this modelling using R² is generally good with values of 0.01 to 0.04, with one poor value of 0.54. Excluding this sample, these data show that the amount of fractionation would range from 2.0% to 13.7% and that during the fractionation process plagioclase feldspar, orthopyroxene, clinopyroxene and biotite would be removed from the melt in a variety of proportions ranging from 100% plagioclase feldspar in one model to 42.5% plagioclase feldspar, 3.8% orthopyroxene, 1.7% clinopyroxene and 51.8% biotite in another.

The low values of R² from this modelling support the suggestion that the geochemical variation within this batch of Group 3 rocks could be due to fractional crystallisation. The one sample (JD2946) with a high R² value (0.54) is located towards the southern boundary of the intrusion, some distance away

from the other samples modelled in this sub-group and is, therefore, not considered to be part of the same batch.

Table 11.4. A summary of the results of major element modelling for four Group 3 daughter samples using JD2925 (SiO₂ content 59.70%) as the parent magma.

Sample	JD2949	JD2911	JD2946	JD2923
SiO ₂	59.84	60.23	60.56	60.88
R ²	0.047	0.028	0.54	0.010
% Fractionation	2.0	2.9	17.3	13.7
% plag	100	42.5	67.6	63.9
% opx	0	3.8	19.0	22.6
% cpx	0	1.7	13.3	6.6
% ilm	0	0	0	1.1
% apa	0	0.08	0	0
% bio	0	51.9	0	5.7

However, modelling for two samples (JD2949 and JD2911) show very small amounts of fractionation (2.0% and 2.9%) and variable proportions of different minerals being formed. As the crystallising minerals only make a small contribution to the calculation in these models, any small analytical or sampling errors in the compositions of the samples and minerals involved or invalid assumptions in the modelling could produce large variations in the amount of fractionation and the mineral proportions calculated.

Modelling using sample JD2923 as the daughter magma, on the other hand produces a low R² value (0.01) and 13.7% fractionation, fits the model well and could reflect fractional crystallisation. This modelling requires plagioclase feldspar, orthopyroxene, clinopyroxene and biotite as fractionating phases, which is at variance with the vector diagrams for Group 3 rocks, presented in Chapter 10. However, these differences could be due to the assumptions made or to the effects of alteration discussed above.

Major element modelling therefore, suggests that Group 3 rocks could represent two separate, fractionating batches of magma, one represented by the least

evolved rocks from the Western Quarries, and another, by rocks from the Central Quarries.

11.5.2. Trace element modelling for the less evolved rocks (Group 3)

In order to investigate the validity of the suggestion that there were two separate fractionating batches of magma within Group 3 rocks, the results obtained from the major element fractionation modelling were used in trace element modelling based on the Rayleigh fractionation equation (see Section 11.4). The calculated values of trace element compositions obtained from the modelling were then compared with the trace element compositions of potential daughter samples from the intrusion.

Trace element modelling was carried out using JD2938 as the parent magma and the five samples geographically and compositionally close to it as the daughter magmas. Further trace element modelling was carried out using JD2925 as the parent magma and JD2923 as the daughter magma, as this sample fitted the major element model well.

Results of the trace element modelling using JD2938 as the parent magma are presented in Table 11.5. The calculated contents of incompatible elements, Rb, Y, Zr, and Nb in the daughter magma are mostly slightly higher than the observed contents and the calculated contents for the compatible elements, Cr and Co, in the residual liquid are all much lower than the observed contents.

The differences between the calculated contents and the observed contents using incompatible trace elements mostly show a reasonable fit, which supports the evidence from the major element modelling. However there are significant differences between the calculated contents and the observed contents using compatible trace elements, which questions the validity of the modelling.

Table 11.5. Results of trace element modelling using sample JD2938 as the parent magma and five samples as daughter magmas.

Daughter magma, sample JD2939

Trace element	Bulk D	Parent magma JD2938 ppm	Calculated daughter contents ppm	Observed contents JD2939 ppm	Difference ppm	% Difference
Rb	0.1337	43.10	56.82	53.90	2.92	5.42
Y	0.3785	27.80	33.90	30.90	3.00	9.70
Zr	0.0756	86.00	115.50	104.00	11.50	11.05
Nb	0.3149	5.50	6.84	5.80	1.04	17.99
Ba	0.2727	185.00	233.31	221.00	12.31	5.57
Cr	8.2290	226.00	22.52	200.00	-177.48	-88.74
Co	4.2580	28.00	9.90	28.00	-18.10	-64.63

Daughter magma, sample JD2941

Trace element	Bulk D	Parent magma JD2938 ppm	Calculated daughter contents ppm	Observed contents JD2941 ppm	Difference ppm	% Difference
Rb	0.1579	43.10	61.74	57.20	4.54	7.93
Y	0.3643	27.80	36.47	33.10	3.37	10.17
Zr	0.0821	86.00	127.24	109.00	18.24	16.74
Nb	0.3610	5.50	7.22	6.50	0.72	11.14
Ba	0.3203	185.00	247.26	231.00	16.26	7.04
Cr	7.9420	226.00	11.68	184.00	-172.32	-93.65
Co	4.9269	28.00	5.24	29.00	-23.76	-81.93

Daughter magma, sample JD2943

Trace element	Bulk D	Parent magma JD2938 ppm	Calculated daughter contents ppm	Observed contents JD2943 ppm	Difference ppm	% Difference
Rb	0.1780	43.10	61.80	58.10	3.70	6.37
Y	0.3927	27.80	36.28	32.20	4.08	12.68
Zr	0.0921	86.00	128.05	114.00	14.05	12.33
Nb	0.4013	5.50	7.15	6.10	1.05	17.23
Ba	0.3609	185.00	244.84	223.00	21.84	9.79
Cr	8.4019	226.00	8.80	195.00	-186.20	-95.49
Co	5.4424	28.00	3.99	29.00	-25.01	-86.23

Table 11.5 continued.

Daughter magma, sample JD2955

Trace element	Bulk D	Parent magma JD2938 ppm	Calculated daughter contents ppm	Observed contents JD2955 ppm	Difference ppm	% Difference
Rb	0.1084	43.10	70.80	64.30	6.50	10.10
Y	0.3756	27.80	39.35	33.60	5.75	17.12
Zr	0.0668	86.00	144.57	117.00	27.57	23.57
Nb	0.2666	5.50	8.27	6.60	1.67	25.34
Ba	0.2223	185.00	285.21	252.00	33.21	13.18
Cr	8.2320	226.00	4.04	176.00	-171.96	-97.71
Co	3.5917	28.00	6.62	27.00	-20.38	-75.49

Daughter magma, sample JD2951

Trace element	Bulk D	Parent magma JD2938 ppm	Calculated daughter contents ppm	Observed contents JD2951 ppm	Difference ppm	% Difference
Rb	0.0521	43.10	81.15	76.00	5.15	6.77
Y	0.3793	27.80	42.07	34.50	7.57	21.94
Zr	0.0483	86.00	162.32	125.00	37.32	29.86
Nb	0.1625	5.50	9.62	6.80	2.82	41.46
Ba	0.1101	185.00	335.07	359.00	-23.93	-6.67
Cr	8.4503	226.00	1.56	153.00	-151.44	-98.98
Co	2.1529	28.00	12.97	28.00	-15.03	-53.68

Trace element modelling for the second batch of magma within Group 3 using JD2925 as the parent magma and JD2923 as the daughter magma is presented in Table 11.6. The calculated contents of incompatible elements Y, Zr, Nb and Ba are good being within 5% of the observed values and the calculated contents for the compatible elements Cr and Co are poor being 40ppm and 15ppm lower respectively.

In all models there is a divergence between the results for incompatible and compatible trace elements, which could be due to the use of inappropriate partition coefficients for the compatible trace elements in the modelling as discussed in Section 11.4 above.

In some models, the differences in both major and trace element contents between the samples used as the parent magmas and the samples used as the daughter magmas are generally small and the very small differences between

the calculated and observed values may not be statistically significant. However, trace element modelling generally supports the evidence from the major element modelling that fractional crystallisation could account for the geochemical variation within batches of magma in the Group 3 rocks.

Table 11.6. Results of trace element modelling using sample JD2925 as the parent magma and sample JD2923 as the daughter magma.

Trace element	Bulk D	Parent magma JD2925 ppm	Calculated daughter contents ppm	Observed contents JD2923 ppm	Difference ppm	% Difference
Rb	0.23307	76.1	85.20	73.2	12.00	16.40
Y	0.28462	36.8	40.89	42.4	-1.51	-3.56
Zr	0.10000	132	150.72	150	0.72	0.48
Nb	0.48897	8.6	9.27	9.1	0.17	1.90
Ba	0.47045	276	298.40	288	10.40	3.61
Cr	6.35939	129	58.57	99	-40.43	-40.84
Co	6.66439	25	10.85	26	-15.15	-58.26

11.5.3. Less evolved rocks (Group 3) - summary

The major element modelling of Group 3 rocks suggested that this Group does not represent a single, coherent body of magma that underwent fractional crystallisation. The rocks from this group cover a wide geographic area and the subsequent major element modelling suggests that it may contain two or more batches of magma that underwent fractional crystallisation involving mainly plagioclase feldspar and orthopyroxene with minor amounts of clinopyroxene and biotite, but independently. The results from the major element modelling are supported by the trace element modelling.

The relationship between the two samples used as parent magmas in the modelling (JD2938 and JD2925) is unclear. The high R^2 value obtained from the major element modelling with JD2938 as the parent and JD2925 as the daughter (see Appendix 7) suggests that they are not directly related by fractional crystallisation. Sample JD2925 could be a parent magma and sample JD2938 could represent a cumulate enriched in the fractionating phases and in Chapter 4 it was shown that JD2938 contains a higher estimated modal percentage of plagioclase feldspar than JD2925. However the estimated modal percentages, for

both samples, of orthopyroxene/secondary amphibole are similar and estimates of the composition of a cumulate, based on the sum of the compositions and proportions of the minerals being removed during the proposed fractionation of sample JD2925, failed to provide a close match with the composition of sample JD2938 (See Appendix 9).

11.6. Modelling the intermediate rocks (Group 2)

Group 2 rocks have a composition intermediate between Group 3 and Group 1 rocks and are altered. For major element modelling, initially the sample from Group 2 with the lowest SiO₂ contents, from the suite of selected samples in Table 11.1 (JD2908, SiO₂ - 61.76) was taken as the parent magma and six samples from the central part of the intrusion with progressively higher SiO₂ compositions were used as the daughter magmas. As Group 2 rocks have been altered, problems in using JD2908 as the parent magma were found and further major element modelling was carried out using the sample with the next lowest SiO₂ composition, (JD2906, SiO₂ - 61.82) as the parent magma, which was less altered than JD2908. The mineral compositions used in the modelling were taken from Table 11.2 and are based on Group 3 rocks because of the amount of alteration of the minerals in Group 2 rocks. Therefore, this modelling does not take into account any change in mineral geochemistry between Group 3 and Group 2 rocks and could affect the proportions of the different minerals required by the modelling.

11.6.1. Major element modelling for the intermediate rocks (Group 2)

The detailed results of the major element modelling are presented in Appendix 10 and are summarised in Table 11.7.

These results show that the amount of fractionation modelled ranges from 4.5% to 21.9% and that during fractionation plagioclase feldspar, orthopyroxene, clinopyroxene, ilmenite and, in two samples biotite, would be removed from the melt. Plagioclase feldspar is removed in fairly similar proportions (between 57.5%-64.6%) but the proportions of the other minerals removed are variable.

Table 11.7. A summary of the results of major element modelling for Group 2 samples using JD2906 (SiO₂ content 61.82%) as the parent magma.

Sample	JD2918	JD2935	JD2940	JD2024A	JD2919
SiO ₂	62.41	62.81	62.92	62.54	64.60
R ²	0.036	0.031	0.230	0.092	0.029
% Fractionation	4.51	8.15	11.43	15.09	21.88
% plag	57.87	63.93	59.73	59.48	57.48
% opx	27.48	23.62	0	11.77	16.64
% cpx	4.32	0.	26.12	24.08	12.67
% ilm	10.33	5.37	4.15	4.66	0.29
% apa	0	0	0	0	0
% bio	0	7.07	0.	0	12.92

The accuracy of this major element modelling based on values of R² is generally good, at between 0.029 and 0.092, with one poor value of 0.23.

This modelling, apart from one sample, produces reasonably consistent results with low R² values. The model that has a poor value of R² uses sample JD2940 as the daughter magma and does not require orthopyroxene as fractionating phase. Sample JD2940 was collected from the southern boundary of the intrusion, some distance away from the parent sample and may not be part of a fractionating batch of magma centred on the parent sample JD2906. The models using the two least evolved samples as daughter magmas (JD2918 and JD2935) show low amounts of fractionation (4.5% and 8.15%) and may be prone to effects of analytical and sampling errors. The models using the two most evolved samples as daughter magmas (JD2924A and JD2919) show 15.1% and 21.9% fractionation but require clinopyroxene and JD2919 requires biotite as well as plagioclase feldspar and orthopyroxene as fractionating phases, which is at variance with the vector diagrams presented in Chapter 10. However, Group 2 rocks are altered and it was suggested in Section 11.5.2. above that alteration, coupled with the assumptions made could cause major element modelling to overestimate the proportions of clinopyroxene and underestimate the proportions of orthopyroxene. These models could therefore represent a batch of fractionating magma.

11.6.2. Trace element modelling for the intermediate rocks (Group 2)

In order to investigate the validity of the suggestion that within the Group 2 rocks, a batch of magma underwent fractional crystallisation, the results from the major element fractionation modelling were used in trace element modelling. Trace element modelling was carried out using sample JD2906 as the parent magma and the two most evolved samples, JD2919 and JD2924A, as the daughter magmas.

The results of the trace element modelling are presented in Table 11.8. When using sample JD2924A as the daughter magma, the differences between the calculated contents and the observed contents of incompatible trace elements Rb, Y, Zr are generally good, the Ba content is lower than the observed value and the Nb content is higher than the observed value. The difference between the calculated and observed contents for the compatible elements is poor, the calculated contents for Cr is considerably lower than the observed value whereas for the calculated contents for Co is higher than the observed value. The results of the trace element modelling using JD2919 as the daughter magma (Table 11.8) are also generally good with differences of less than 18% for all incompatible elements, except Ba, but there are considerable differences for the compatible elements Cr and Co.

As with the Group 3 rocks, the differences in SiO₂ contents of the samples used as parent and daughter magmas are small, 1.72% and 2.78% respectively, and there are some correspondingly small differences between their trace element contents. In some cases, therefore, the results may not be statistically significant. However, the results from the trace element modelling generally support the suggestions from the major element modelling that fractional crystallisation could account for the variation in geochemistry of some samples within Group 2 rocks.

Table 11.8. Results of trace element modelling using sample JD2906 as the parent magma and samples JD2924A and JD2919 as daughter magmas.

Daughter magma sample JD2924A.

Trace element	Bulk D	Parent magma JD2906 ppm	Calculated daughter contents ppm	Observed contents JD2924A ppm	Difference ppm	% Difference
Rb	0.04785	95.8	111.83	122	-10.17	-8.33
Y	0.44584	45.4	49.68	49.4	0.28	0.56
Zr	0.06161	168	195.68	200	-4.32	-2.16
Nb	0.17548	11.8	13.49	10.7	2.79	26.09
Ba	0.10684	346	400.05	483	-82.95	-17.17
Cr	10.274	79	17.50	60	-42.50	-70.83
Co	1.81295	28	24.53	18	6.53	36.30

Daughter magma sample JD2919.

Trace element	Bulk D	Parent magma JD2906 ppm	Calculated daughter contents ppm	Observed contents JD2919 ppm	Difference ppm	% Difference
Rb	0.45838	95.8	109.60	98.5	11.10	11.27
Y	0.43285	45.4	52.27	62	-9.73	-15.69
Zr	0.19109	168	205.40	227	-21.60	-9.52
Nb	0.93531	11.8	11.99	14.6	-2.61	-17.87
Ba	0.91971	346	352.97	286	66.97	23.42
Cr	8.52075	79	12.19	36	-23.81	-66.13
Co	12.7588	28	1.51	22	-20.49	-93.15

11.6.3. Intermediate rocks (Group 2) - summary

Major element modelling for Group 2 rocks using JD2908 as the parent magma produced results that were inconsistent with a fractional crystallising magma. However, when sample JD2906 was used as the parent magma the major element modelling produced results that could reflect a batch of magma that underwent fractional crystallisation involving the removal of plagioclase feldspar, orthopyroxene and minor amounts of clinopyroxene and biotite and these results were broadly supported by trace element modelling using the fractionation and mineral proportions from the major element modelling. Group 2 rocks occur within the Central Quarries and are the most altered samples from the intrusion. Alteration has precluded the use of many samples from Group 2 for modelling and could be the cause of the poor results obtained using JD2908 as the parent

magma. It is therefore possible that all Group 2 rocks could represent a batch of magma that underwent fractional crystallisation.

11.7. Modelling the more evolved rocks (Group 1)

Group 1 rocks have the highest SiO₂ contents in the intrusion and as a group they tend to plot with a separate trend from the other samples on the variation diagrams (see Chapter 10). Major element modelling for Group 1 rocks was based on sample JD2914, the sample with the lowest SiO₂ content (61.76%) as the parent magma, and selected samples from Group 1 with progressively higher SiO₂ compositions as the daughter magmas. However, poor results were obtained using sample JD2914 as the parent magma and further major element modelling was carried out using sample JD2903 as the parent magma, a very fine-grained sample, located close to the eastern margin of the intrusion with SiO₂ content of 63.01% (see Figures 3.6 and 4.1).

11.7.1. Major element modelling for the more evolved rocks (Group 1)

The detailed results of the major element modelling are presented in Appendix 11 and summarised in Table 11.9

Modelling with sample JD2903 as the parent magma and four samples along the southern boundary as daughter magmas (Table 11.9) produced results with R² values between 0.005 and 0.026. The amount of fractionation ranged from 5.5% to 15.2% and during the fractional crystallisation, plagioclase feldspar, orthopyroxene and ilmenite would be removed from the melt in fairly consistent proportions and clinopyroxene and biotite are required to be formed and removed from the melt by two models.

The low R² values and the generally uniform proportions for plagioclase feldspar, orthopyroxene and ilmenite modelled as fractionating phases suggest that this modelling could represent a batch of magma that underwent fractional crystallisation. The requirement for ilmenite to be crystallised and removed from the melt in these models is in line with the change of slope in the vector diagrams for Group 1 rocks reported in Chapter 10 and could explain the

change in slope in the variation diagrams (see Chapter 10). The small but variable proportions of clinopyroxene and biotite modelled could be due to alteration of the samples and the assumptions used in the major element modelling as discussed in Section 11.5.1 above.

Table 11.9. A summary of the results of major element modelling for Group 1 samples using JD2903 (SiO₂ content 63.01%) as the parent magma.

Sample	JD2912	JD2957	JD2958	JD2947
SiO ₂	64.41	64.90	65.32	65.85
R ²	0.005	0.017	0.0258	0.008
% Fractionation	5.55	8.05	10.41	15.23
% plag	57.45	66.87	64.27	63.64
% opx	24.18	21.11	23.72	20.69
% cpx	0	0	0.35	8.86
% ilm	6.20	11.53	10.73	5.97
% apa	0	0.49	0.92	0.84
% bio	12.17	0	0	0

11.7.2. Trace element modelling for the more evolved rocks (Group 1)

To verify the suggestion above, trace element modelling was carried out using the results from the major element modelling and sample JD2903 as the parent magma and two samples JD2958 and JD2947 as the daughter magmas. These two samples have the highest SiO₂ contents within Group 1 and provide relatively large compositional differences in trace element concentrations for modelling when compared with sample JD2903, the assumed parent magma. This would help to ensure a realistic model that would produce significant results.

The results from the trace element modelling are presented in Table 11.10. The model using JD2958 as the daughter magma are generally good and shows that differences between the calculated and the observed contents of the incompatible trace elements Rb, Y, Zr, Nb, Ba are less than 9.5% of the observed values; the calculated content for Rb is less than the observed

content whereas the calculated contents for the other incompatible trace elements are greater than the observed contents. The calculated contents of the incompatible trace elements Cr and Co are lower and higher, respectively, than the observed contents.

The model using JD2947 as the daughter magma is also generally good and produces differences between the calculated and the observed contents of the incompatible trace elements of less than 16.3%, the calculated contents for Rb being lower than the observed contents whereas the calculated contents for the other incompatible trace elements are higher than the observed contents. The calculated contents for the compatible element Cr is lower than the observed contents but the calculated contents for Co is only slightly higher than the observed contents.

These results show a reasonable to good fit between the calculated trace element contents and observed trace element contents and support the suggestion from the major element modelling that the variation in geochemistry of the Group I rocks that occur along the southern boundary of the intrusion could be the result of fractional crystallisation. The largest differences were obtained with Cr, which could be due to the use of inappropriate mineral/melt partition coefficients for this trace element.

Table 11.10. Results of trace element modelling using sample JD2903 as the parent magma and samples JD2947 and JD2958 as daughter magmas.

Daughter magma sample JD2958.

Trace element	Bulk D	Parent magma JD2903 ppm	Calculated daughter contents ppm	Observed contents JD2958 ppm	Difference ppm	% Difference
Rb	0.05133	86.8	95.92	106	-10.08	-9.51
Y	0.17301	48.6	53.02	50.7	2.32	4.58
Zr	0.04115	195	215.73	201	14.73	7.33
Nb	0.20693	12.1	13.15	12.5	0.65	5.24
Ba	0.10715	377	414.19	379	35.19	9.28
Cr	6.60143	62	34.36	59	-24.64	-41.76
Co	2.29343	20	17.45	13	4.45	34.25

Daughter magma sample JD2947.

Trace element	Bulk D	Parent magma JD2903 ppm	Calculated daughter contents ppm	Observed contents JD2947 ppm	Difference ppm	% Difference
Rb	0.05081	86.8	101.28	121	-19.72	-16.30
Y	0.26292	48.6	54.78	52.8	1.98	3.76
Zr	0.04385	195	227.78	210	17.78	8.47
Nb	0.17375	12.1	13.84	12.3	1.54	12.51
Ba	0.10856	377	435.77	429	6.77	1.58
Cr	7.22536	62	22.54	39	-16.46	-42.20
Co	1.98436	20	17.04	16	1.04	6.52

11.7.3. The more evolved rocks (Group 1) - summary

The major element modelling for Group 1 rocks suggests that the some of the variation in geochemistry within this Group, particularly the rocks along the southern boundary of the intrusion, could be the result of the fractional crystallisation and this was supported by the results obtained from the trace element modelling.

In Chapter 10 it was suggested that there could be a change in the fractionating assemblage between Group 3 and Group 1 rocks and the fractional crystallisation modelling supports this suggestion. Modelling with Group 3 rocks requires plagioclase feldspar and orthopyroxene as the main fractionating phases whereas modelling with Group 1 rocks requires plagioclase feldspar, orthopyroxene and ilmenite as the main fractionating phases.

However, modelling does not support fractional crystallisation for the whole of Group 1 rocks. The results using JD2914 as the parent magma were unsatisfactory and could not be reliably used to support fractional crystallisation. Group 1 samples, located towards the centre of the intrusion, tend to have lower SiO₂ contents than the samples from the southern boundary and, although the modelling difficulties could be due to alteration and compositions used, or to analytical errors or to the assumptions used in the modelling it may also suggest that the rocks towards the centre of the intrusion are not part of the same batch of magma as the rocks along the southern boundary or that they have been affected by some other process.

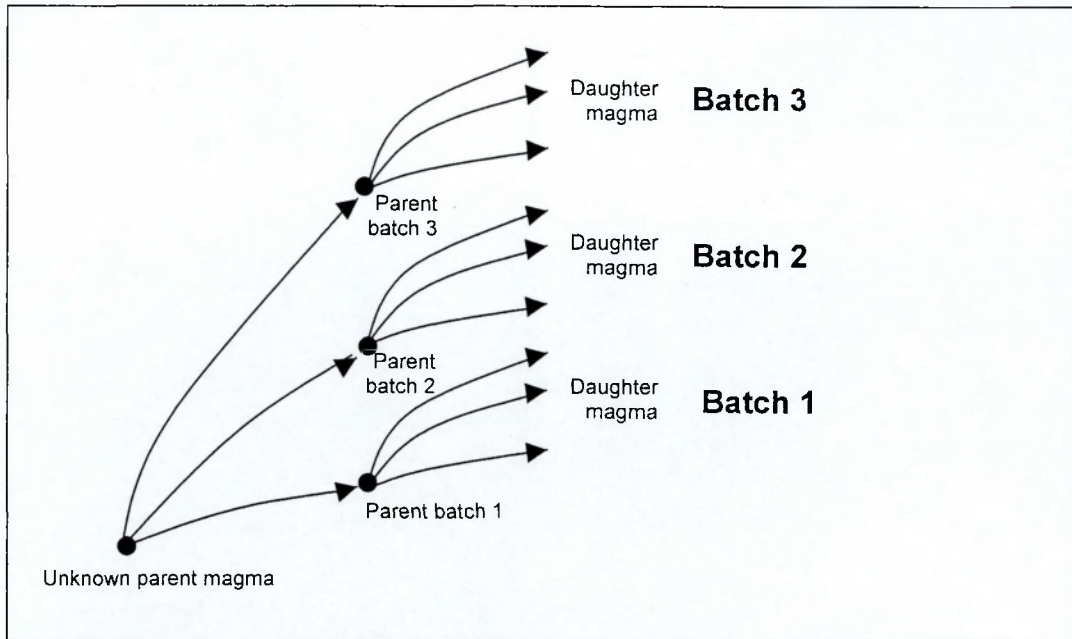
11.8. Fractional crystallisation modelling - summary

Fractional crystallisation modelling presented in this chapter supports a change in the assemblage of fractionating minerals between Groups 3 and 2, and Group 1 and suggests that rocks in Group 3 and Group 2 evolved largely by the fractionation of plagioclase feldspar and orthopyroxene whereas the rocks from Group 1 evolved largely by the fractionation of plagioclase feldspar, orthopyroxene and ilmenite.

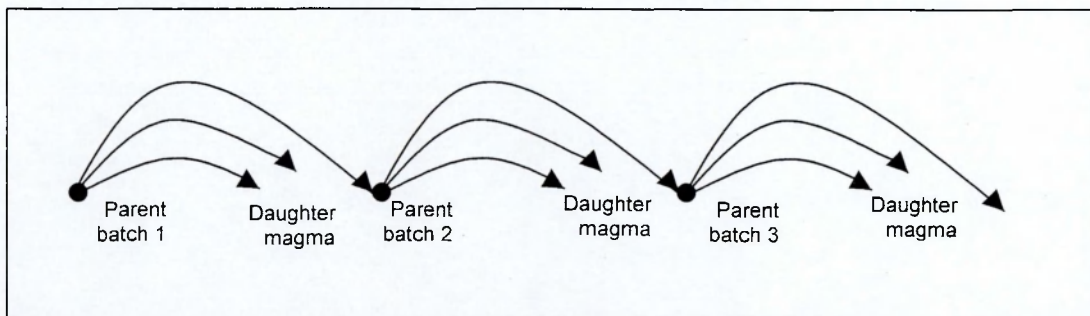
Fractional crystallisation modelling further suggests that the Penmaenmawr Intrusion could be composed of several batches of magma, each of which underwent fractional crystallisation independently. However, although the trends on both the major and trace element variation diagrams, presented and discussed in Chapter 10, indicate that the rocks from the Penmaenmawr Intrusion are genetically related, the relationship between the batches of magma is not clear from the modelling carried out.

The batches of magma could have evolved from a common, unknown parent and then separated to evolve by fractional crystallisation independently of each other. Alternatively, they could have evolved as a progression of fractionating batches of magma in which the daughter magma of one fractionating batch of magma became the parent magma of the next batch and so on. A simple diagram illustrating these two alternative models, called in this study 'the separate batches of magma model' and the 'progressive fractionation model', is presented in Figure 11.2.

One possible mechanism for the separate batches of magma model would be the successive emplacement of batches of magma from an underlying evolving magma chamber, each batch then undergoing further fractionation. However, in Chapter 9 it was proposed that the Penmaenmawr Intrusion was a high-level magma chamber and, due to its small size and the rapidity of cooling, it was unlikely that there had been any in-situ fractional crystallisation. Therefore, the separate batches of magma model would require the separation and subsequent fractional crystallisation of batches of magma to have taken place in an underlying, larger magma chamber prior to emplacement. It was



a. Separate batches of magma model.



b. Progressive fractionation model

Figure 11.2. Diagrams illustrating the alternative fractional crystallisation models for the Penmaenmawr Intrusion.

suggested in Chapter 10 that the Penmaenmawr Intrusion could be composed of two bodies of magma, one represented by rocks from Groups 2 and 3 and the other by some rocks from Group 1 and some rocks from Group 4 which fractionated independently of each other and were then emplaced as successive batches of magma from an underlying magma chamber so that each batch of magma would have a different composition from the previous one. This suggestion would be consistent with separate batches of magma model.

As in-situ fractionation is considered unlikely, the progressive fractionation model would require the underlying magma chamber to have been compositionally layered as a result of fractional crystallisation and for the Penmaenmawr Intrusion to have been emplaced by a single injection of magma with the layering preserved. In Chapters 9 and 10, based on the lack of sharp contacts and the regular increase in geochemical variation across the intrusion, it was considered possible that the Penmaenmawr Intrusion could have been emplaced by a single injection of magma from an underlying, layered magma chamber. This suggestion would be consistent with the progressive fractionation model in which the layers in the underlying magma chamber evolved progressively from each other prior to emplacement.

CHAPTER 12. MAGMA MIXING (HYBRIDISATION) MODELLING

12.1. Introduction

In Chapter 10 it was suggested that the variation in geochemistry in the Penmaenmawr Intrusion could be due to either a two-stage fractional crystallisation process within a single body of magma or the independent fractionation of two related but separate bodies of magma. In Chapter 11, based on fractional crystallisation modelling, it was suggested that the Penmaenmawr Intrusion could be composed of several batches of magma that underwent fractional crystallisation independently within a single large underlying magma chamber and two possible fractionating models were proposed.

However, in Chapter 10 it was also noted that the straight-line trends on both the major element variation and the compatible and incompatible trace element diagrams could be indicative of magma mixing or hybridisation. In this process two or more magmas undergo varying degrees of mixing and produce rocks with a range of compositions intermediate between the two end members. In order to investigate the possibility that some of the variations in geochemistry of the Penmaenmawr Intrusion could be due to magma mixing, this chapter presents the results of magma mixing modelling. Initial modelling was carried out using selected samples from across the whole intrusion as potential products of mixing. However, it was suggested in Chapter 10 that the Penmaenmawr Intrusion could consist of two batches of magma that evolved separately by magma mixing, and subsequent modelling was carried out using data sets from groups of samples from the intrusion identified in Chapter 4.

12.2. Magma mixing modelling - theoretical considerations

Magma mixing modelling was carried out based on a linear compositional variation between two magma sources. Where two magmas of different compositions mix together they produce a new magma with an intermediate composition and dependent on the proportions of the two magmas involved. Mixing different proportions of the two end members produces a series of magmas with a range of intermediate compositions. The element contents of the

resultant magmas will vary linearly between the element contents of each end member involved.

In order to model this process, the most and least evolved samples from a group of samples were selected as potential end member samples. The concentrations of each element in the intermediate samples were then scaled for plotting, in proportion to the concentrations of the two end members using the following equation:-

$$\frac{\text{Concentration (sample)} - \text{Concentration (Least evolved end member)}}{\text{Concentration (Most evolved end member)} - \text{Concentration (Least evolved end member)}}$$

Where mixing has occurred, the resulting scaled concentration of each element in an intermediate magma produced by mixing are the same, so that plotting the scaled concentrations calculated from the above equation for one sample, on a multi-element diagram should produce a horizontal straight line. Plotting a series of samples produced by mixing different proportions of the two end members should produce a series of straight horizontal lines.

12.3. Whole intrusion magma mixing modelling

In Chapters 7 and 10, it was shown that the concentrations of both major and trace elements vary regularly across much of the whole intrusion. The most felsic samples occur around the eastern and southern boundaries of the intrusion, whereas the most mafic samples occur towards the western boundary. The intermediate samples between these two end members could arguably be the result of mixing of these two magmas. In order to test this hypothesis, initial modelling of magma mixing was carried out for the intrusion as a whole.

The most felsic sample from the eastern boundary, sample JD2912, was selected as one end member, and JD2938, the most mafic sample from the western quarries, was selected as the other end member. These samples were selected as end members to be geographically separated by as great a distance as possible. Intermediate samples, representing the potential results of

the mixing, were selected at roughly equal distances along from the main trends on the variation diagrams and therefore they are not identical to the samples selected for fractional crystallisation modelling. Variation diagrams for SiO₂ v MgO and SiO₂ v Zr, showing the selected intermediate samples, are presented in Figure 12.1.

Elements used in this modelling were thought to be relatively immobile during alteration (see Chapter 7) and were selected to provide as wide a range of elements as possible. They include major elements (SiO₂, MgO) incompatible trace elements (Rb, Y, Zr, Nb and Ba) and compatible trace elements (Cr and Ni).

12.3.1. Whole intrusion modelling - results and interpretation

The results for modelling the intrusion as a whole are presented in multi-element diagrams in Figure 12.2. The plots for samples from Group 3: JD2939, JD2955 and JD2949, show nearly horizontal plots becoming progressively nearer to the more felsic end member. These plots, however, show a consistent trough for Nb and peak for Ba and sample JD2949 shows scaled concentrations for the compatible elements Cr and Ni nearer the more evolved end member. The plots for samples from Group 4: JD2927, JD2930 and JD2929, tend to be more variable; sample JD2929 showing peaks for both Rb and Ba, and show scaled concentrations for Cr and Ni nearer to the more evolved end member. The plots for the samples from Group 2, JD2906, JD2940 and JD2924A and one sample from Group 1, JD2933 are extremely variable. However, one sample from Group 1, JD2904, shows a near horizontal plot.

The magma mixing modelling does not provide a consistent set of results for the intrusion as a whole. The highest degree of variability occurs for the elements Rb, Nb, Ba, Cr and Ni. The variability of Ba and Nb could be due mobility as a result of alteration, particularly of the more felsic end member, as the variation diagrams for Ba and Nb (see Chapters 7 and 10) show a degree of scatter for samples with higher SiO₂ contents.

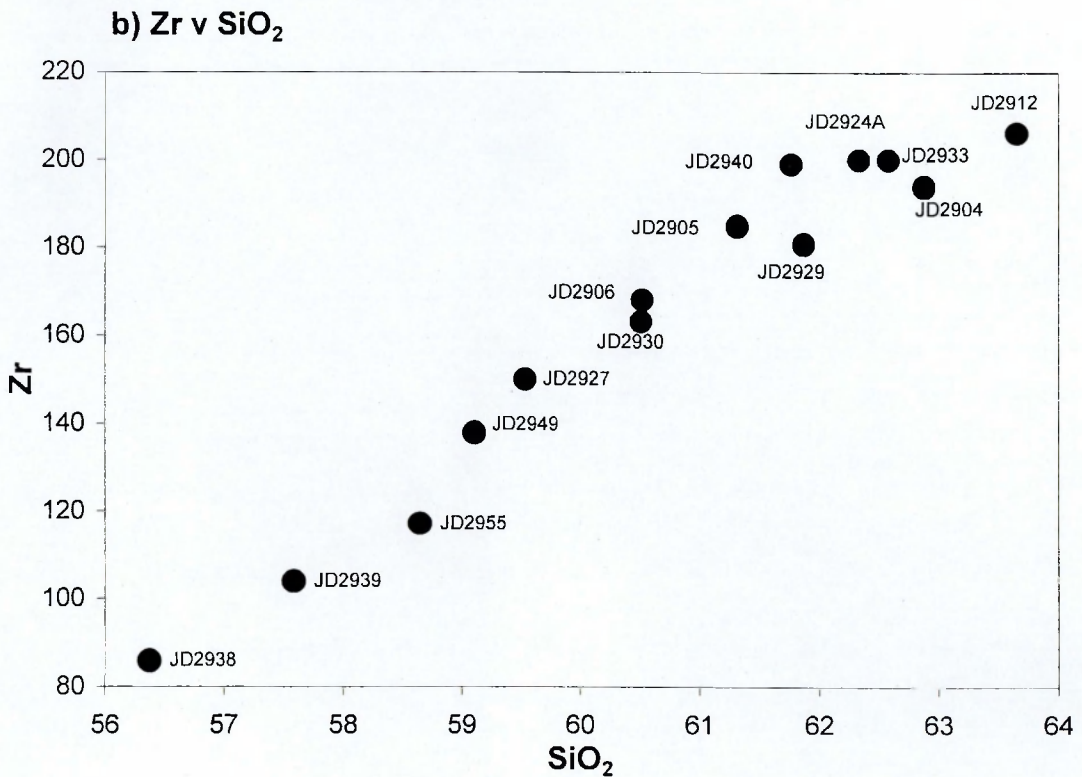
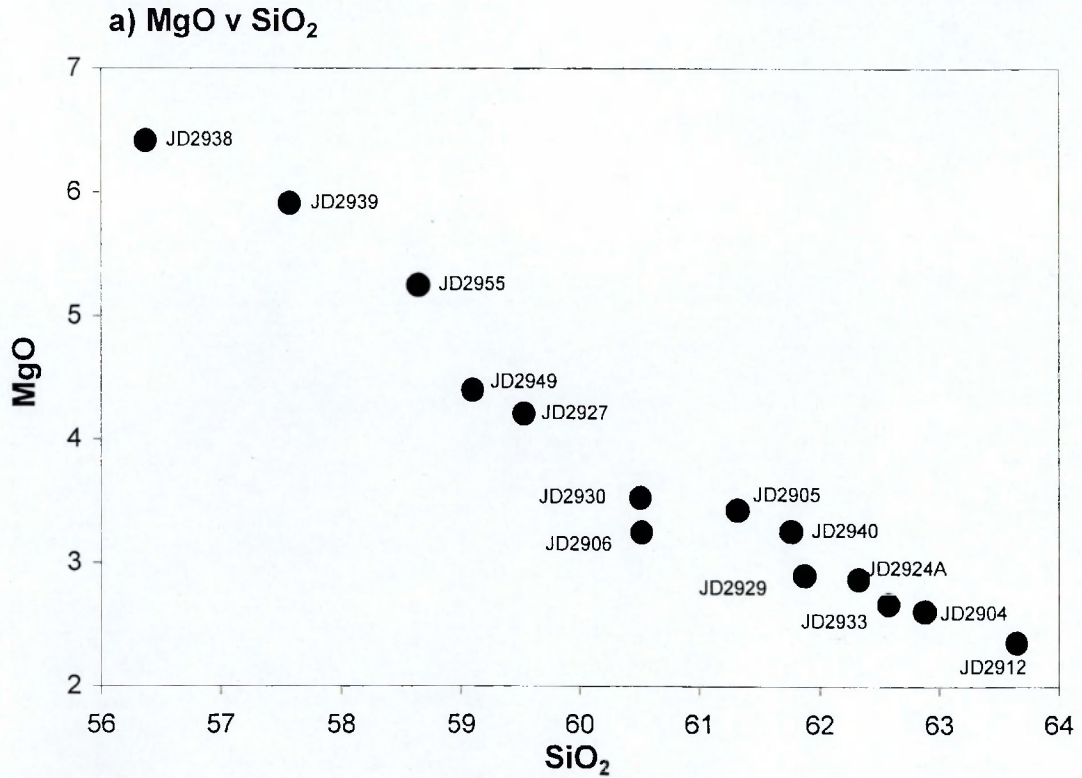


Figure 12.1. Plots of (a) MgO against SiO₂ and (b) Zr against SiO₂ for the 14 Penmaenmawr Intrusion samples JD2912, JD2904, JD2905, JD2933, JD2924A, JD2940, JD2906, JD2938, JD2939, JD2955, JD2949, JD2930, JD2927, JD2929, selected for whole intrusion magma mixing models.

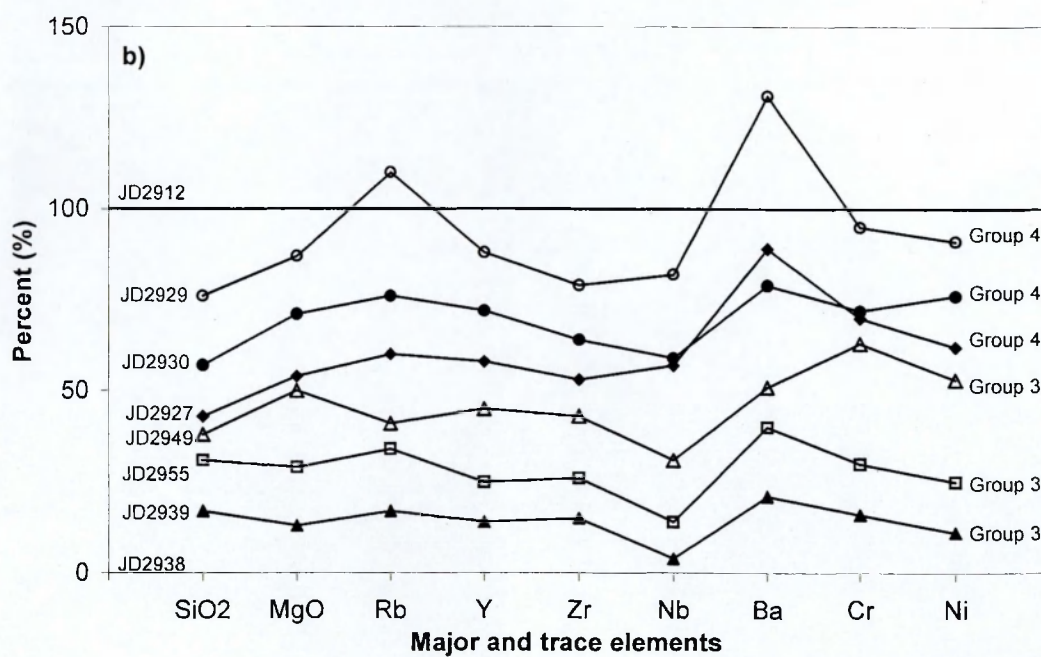
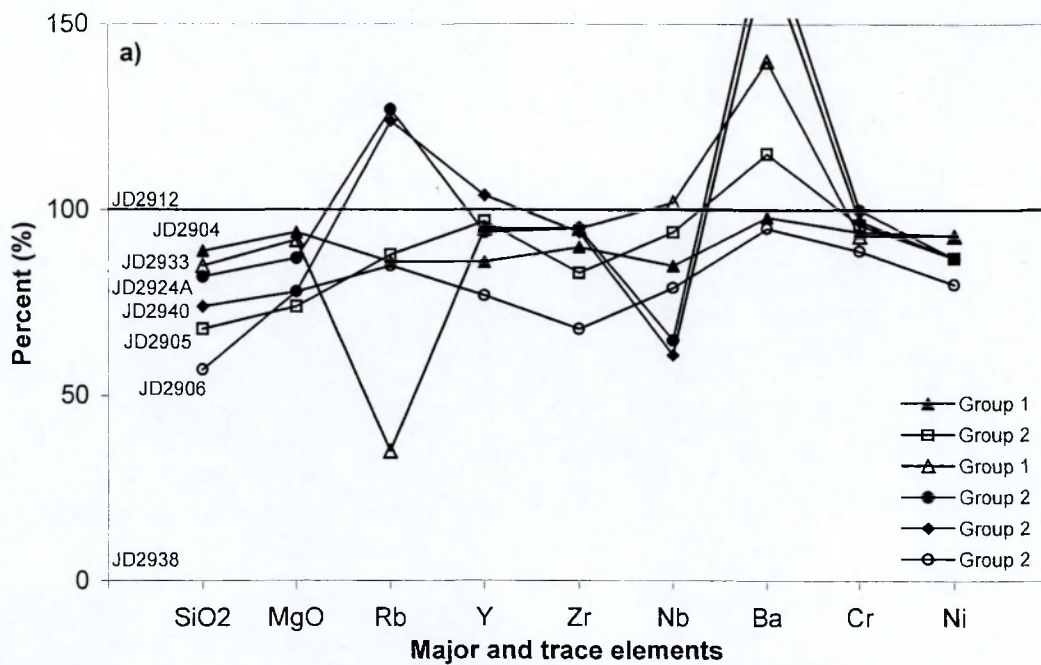


Figure 12.2. Plots of magma mixing for the whole intrusion using Penmaenmawr samples JD2912 and JD2938 as end members: (a) samples JD2904, JD2905, JD2933, JD2924A, JD2940, and JD2906, and (b) samples JD2939, JD2955, JD2949, JD2930, JD2927 and JD2929.

The variable results suggest that the variation in geochemistry in the intrusion as a whole is unlikely to be due to the mixing of two different magmas represented by samples from the east and from the west of the intrusion. However, the similarity of plots for the samples within some groups, particularly the Group 3 samples, suggest that there may have been some magma mixing within groups.

12.4. Group 3 rocks magma mixing modelling

Initial modelling for Group 3 rocks was carried out using sample JD2938, the most mafic sample within Group 3, as the basic end member and sample JD2923 as the felsic end member. These samples were chosen because JD2938 was located towards the west of the intrusion and JD2923 was the most easterly sample from Group 3 and thus the modelling would cover a wide geographical area. The intermediate samples were selected if they plotted on the main trend of the variation diagrams. Two sets of intermediate samples were used in the modelling, the first based on intermediate samples located in the western quarries, reasonably close to the most mafic end member and the second based on intermediate samples located towards the centre of the intrusion. In order to reduce the geographical spread further, additional modelling, involving a sub-group of samples from just the Western Quarries, using sample JD2936 as the basic end member and JD2946 as the felsic end member, and a sub-group from just the central part of the intrusion, using sample JD2948 as the basic end member and JD2923 as the felsic end member, was carried out.

12.4.1. Group 3 rocks magma mixing modelling - results and interpretation

The results from the magma mixing modelling for Group 3 rocks are presented in Figure 12.3. Figure 12.3a shows the modelling involving intermediate samples from the Western Quarries and Figure 12.3b shows the modelling involving intermediate samples from near the centre of the intrusion.

In Figures 12.3a and 12.3b most data points plot within the field defined by the end members, with only Rb, Zr and Ba occasionally plotting outside. The plots on Figure 12.3a show a series of near horizontal lines, with a little deviation, mainly due to peaks for Ba and Rb and troughs for Nb values.

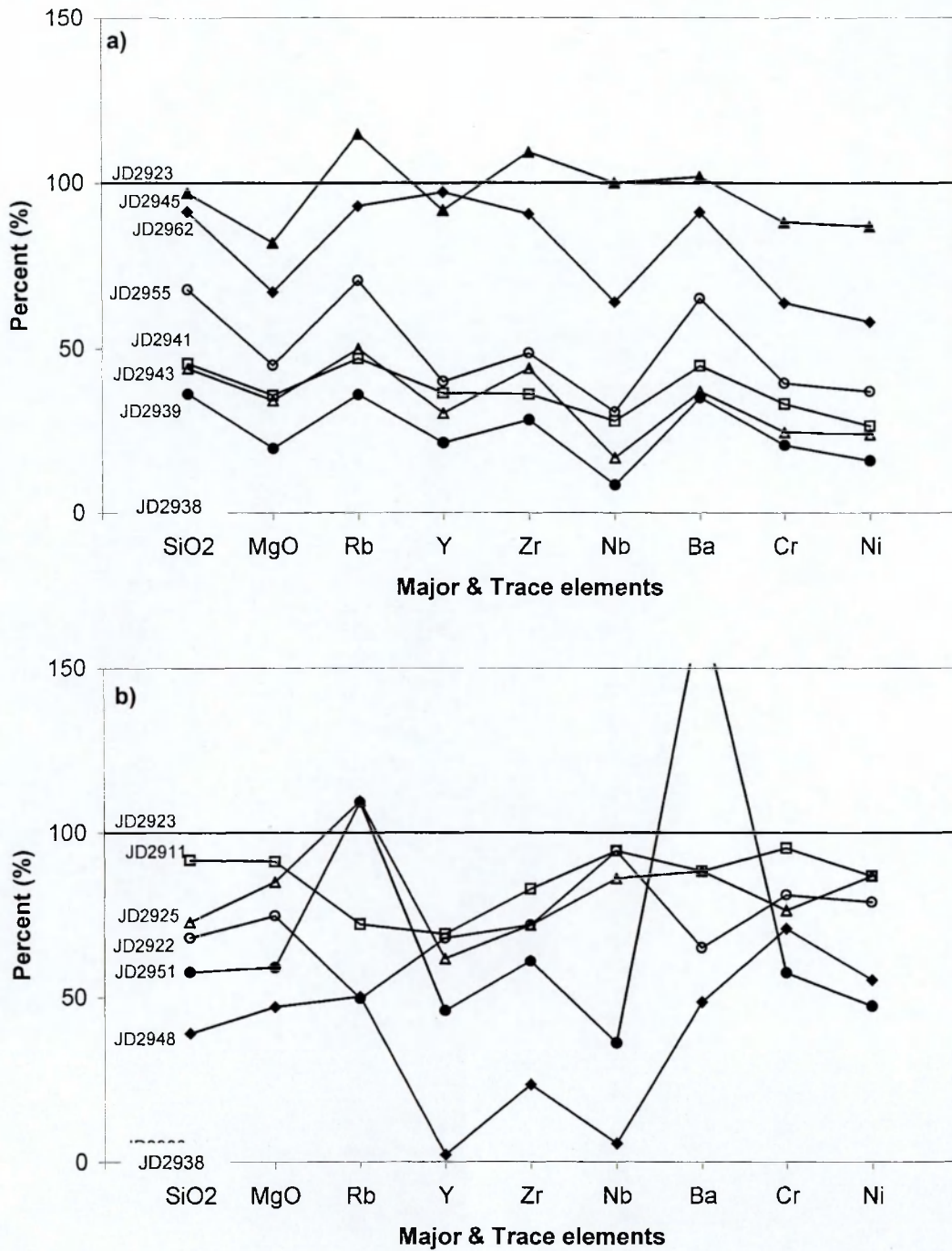


Figure 12.3. Magma mixing plots for Group 3 Penmaenmawr samples, using the end members JD2938 and JD2923, with (a) showing the samples from the western area of the intrusion (JD2945, JD2962, JD2955, JD2941, JD2943, and JD2939), and (b) showing the samples from the centre of the intrusion (JD2911, JD2925, JD2922, JD2951 and JD2948).

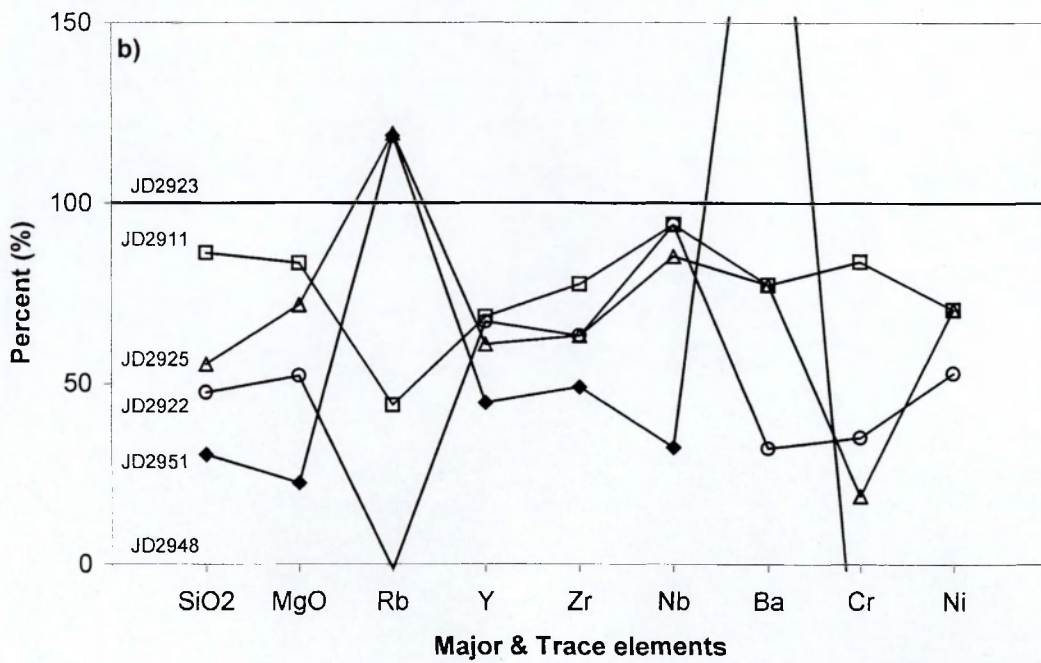
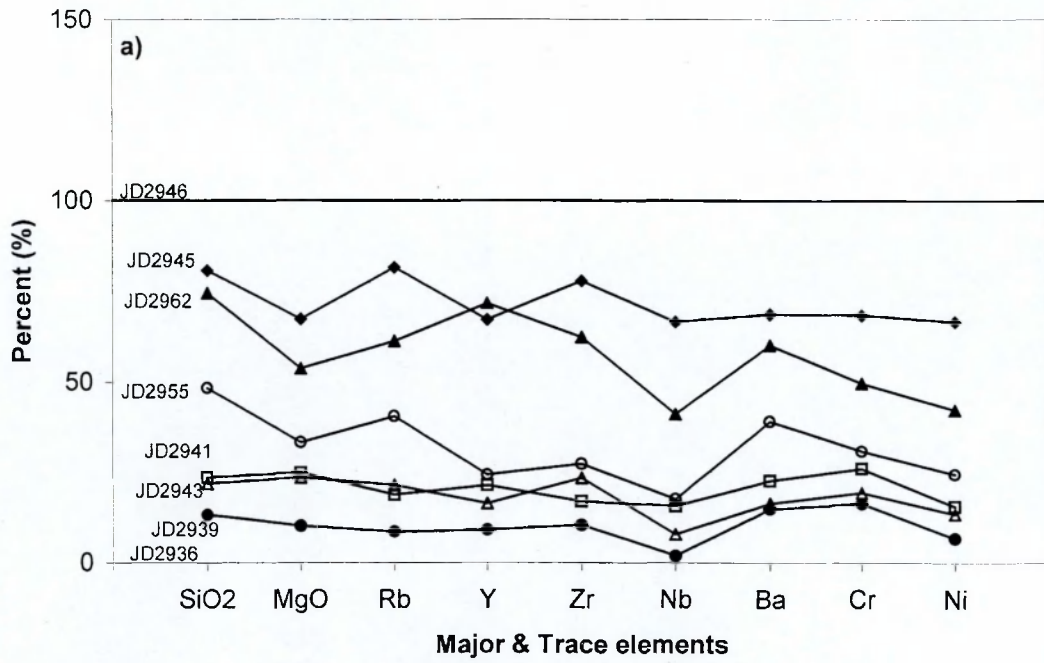


Figure 12.4. Magma mixing plots for Group 3 Penmaenmawr samples, using (a) the end members JD2936 and JD2946, with the samples from the western area of the intrusion (JD2945, JD2962, JD2955, JD2941, JD2943, and JD2939), and (b) the end members JD2923 and JD2948, with the samples JD2911, JD2922, JD2925 and JD2951.

The plots on Figure 12.3b show a large amount of deviation from the horizontal and only two samples, JD2911 and JD2922, approach reasonable horizontal lines. The peaks for Rb and Ba could be due to alteration and the troughs for Nb, which are consistent across all plots, including the modelling of the intrusion as a whole (Section 12.3 above) could be due to sample JD2938 having an anomalously high Nb content.

The plots for Group 3 to produce variable results, and although a good number of samples from the Western Quarries (Figure 12.3a) with compositions close to the most mafic end member and with small variations in SiO₂ contents tend to produce fairly straight horizontal lines, there are greater deviations from the horizontal line for the plots using samples located towards the centre of the intrusion (Figure 12.3b). The disparity between the plots for Group 3 rocks suggests that the compositional variation for the whole of Group 3 is unlikely to be a product of magma mixing.

Figure 12.4 shows the modelling using samples from the sub-groups of Group 3, Figure 12.4a showing the sub-group from the Western Quarries and Figure 12.4b the sub-group from the central part of the intrusion. The modelling for the sub-group from the Western Quarries (Figure 12.4a) produces a reasonable series of horizontal lines whereas the modelling for the sub-group from the central part of the intrusion (Figure 12.4b) shows many deviations from the horizontal.

The good horizontal lines obtained from the Western Quarries' sub-group modelling may be due to the small differences in both major and trace element contents between the samples used as the end members; however there are equally small differences in both major and trace element between the end members of the magma mixing model for the other sub-group. This sub-group therefore could represent a batch of magma that formed by magma mixing with the basic and felsic end members represented by samples JD2936 and JD2946 respectively. The plots for the sub-group from the central part of the intrusion (Figure 12.4a) however, do not support magma mixing for this sub-group.

Magma mixing modelling suggests that Group 3 rocks do not represent a coherent body of magma that underwent a single mixing process, thus supporting

the suggestions from the fractional crystallisation modelling presented in Chapter 10 that Group 3 rocks may consist of two or more batches of magma. However, in this case, modelling suggests that the origin for the geochemical variation in the least evolved sub-group from the Western Quarries could be due magma mixing.

12.5. Group 2 rocks magma mixing modelling

It was reported in Chapter 3 and 4 that Group 2 rocks from the Central Quarries contain dark-grey, rounded inclusions. Rounded inclusions are often associated with magma mixing (Castro *et al.*, 1990; Poli and Tommasini, 1991). For Group 2 modelling, the most mafic sample, JD2908 (SiO₂ composition 60.18%) and the most felsic sample, JD2924A (SiO₂ composition 62.33%), were used to represent the end members and other selected intermediate samples from Group 2 taken as the products of mixing.

The results of the mixing modelling for Group 2 samples are presented in Figure 12.5. They show a very high degree of variation for all elements in the samples, with many data points falling outside the field defined by the end members; the largest variation being for Rb and Ba proportions.

The high degree of variation within this group, suggests that magma mixing, as modelled, is unlikely to be the cause of the variation within this group. However, this group contains the most altered samples from the intrusion and this could account for some of variation seen in the modelling; nevertheless, elements that were considered to be relatively immobile were used and although both Nb and Ba show a degree of scatter on the variation diagrams presented in Chapters 7 and 10, alteration is unlikely to account for the amount of variation shown by all elements on the plots.

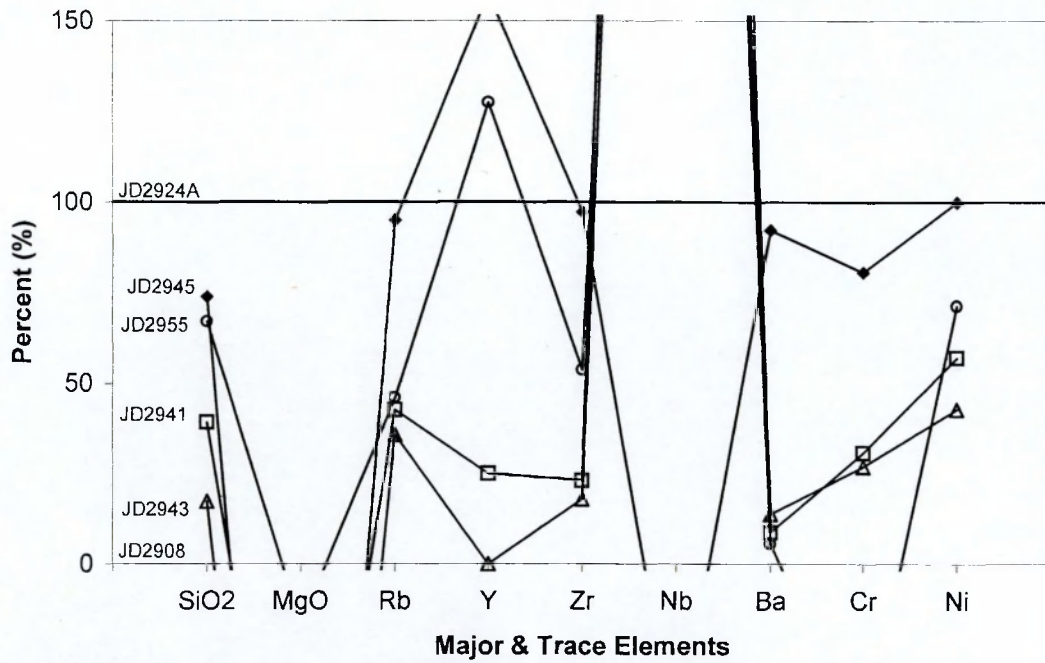


Figure 12.5. Magma mixing plot for Group 2 Penmaenmawr samples JD2945, JD2955, JD2941, and JD2943, using samples JD2908 and JD2924A as the end members.

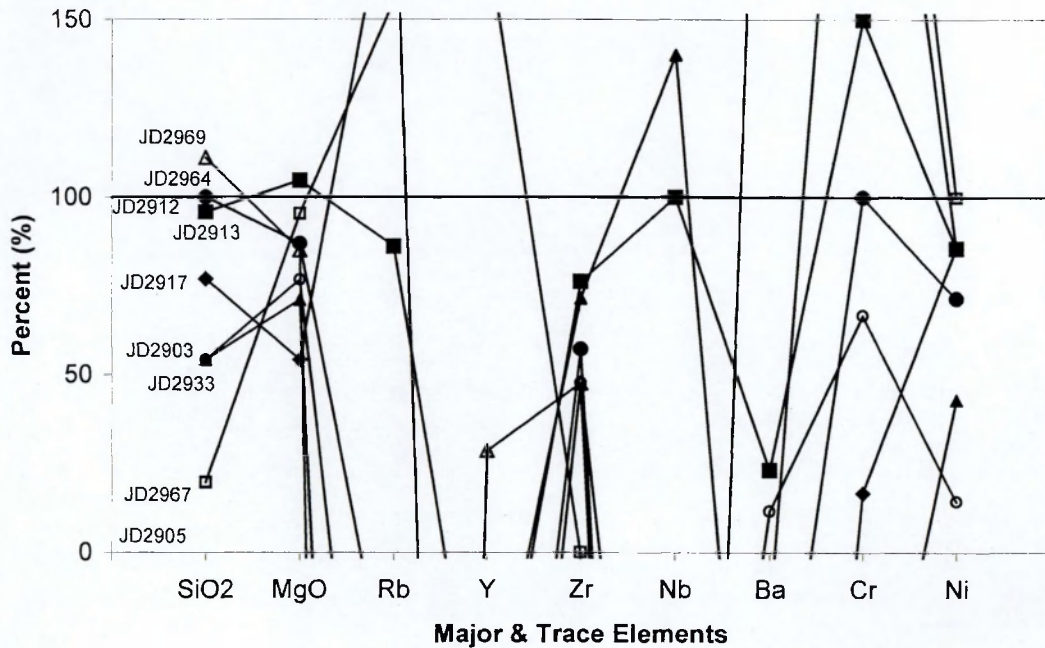


Figure 12.6 Magma mixing plot for Group 1 Penmaenmawr samples JD2903, JD2913, JD2917, JD2933, JD2964, JD2967 and JD2969, using samples JD2905 and JD2912 as the end members.

12.6. Group 1 rocks magma mixing modelling

In Chapter 8 it was suggested that the variation in geochemistry of Group 1 samples from the southern boundary of the intrusion could be due to fractional crystallisation but that this process was unlikely to account for the variation in the other samples from Group 1, situated away from the boundary. Magma mixing modelling was therefore carried out on a group of samples away from the boundary to determine whether the variation in geochemistry could be due to magma mixing.

For this modelling, Group 1 samples JD2905 (SiO₂ composition 61.31%) and JD2912 (SiO₂ composition 63.65%) were chosen as the felsic and mafic end members and compositions of samples collected away from the margin of the intrusion were used as the intermediate rocks to test magma mixing.

The results of this modelling are presented in Figure 12.6 and show a very high degree of variation for all elements. It is therefore extremely unlikely that magma mixing, as modelled, could be the cause for the variations observed.

12.7. Group 4 rocks magma mixing modelling

For this group, the most mafic sample (JD2928, SiO₂ 58.86%) and most felsic sample (JD2929, SiO₂ 61.87%) were chosen as the end members. This Group is located geographically close to Group 1 samples; between Group 1 and the centre of the intrusion. However, it was reported in Chapter 4 that different samples from this Group contain mineralogical characteristics of other group and some samples contain small rounded inclusions of finer-grained minerals. So magma mixing modelling was also carried out using sample JD 2913 from Group 1 as one end member and sample JD2953 from Group 3 as the other end member. These samples were chosen on the basis of their location and composition; they had to be reasonably close to the Group 4 samples in order to act as end members, and their SiO₂ contents had to be, respectively, greater than and less than the SiO₂ content of the samples from Group 4. Samples from Group 2 were ruled out as end members on the basis of the fact that in general their SiO₂

contents were too high to be the mafic end member and their compositions tended to be too similar to the samples from the Group 4.

12.7.1. Group 4 rocks magma mixing modelling - results and interpretation

The results of the magma mixing modelling using just the samples from Group 4 are presented in Figure 12.7a. They show a high degree of variability with some data points plotting outside the field defined by the end members. The plots for MgO, Rb, Ba and Cr tend to be closer to the least evolved end member than the other elements, whereas the plots for Y, and in some samples Zr and Nb, tend to be closer to the more evolved end member.

The results using samples selected from Groups 1 (JD2913) and 3 (JD2953) as end members are presented in Figure 12.7b. This modelling produced a more consistent, flatter set of plots, although Ba, and Cr tend to plot nearer the more evolved end member. One sample, JD2929, tends to produce anomalous mixing values for Rb and Ba, while sample, JD2931, produces an anomalous value for Y.

The anomalous values for Rb and Ba in JD2929 could be due to alteration of that sample and the plots for MgO, Cr, and Ni could be due to the small mafic inclusions affecting the whole rock geochemistry of some Group 4 rocks; however the variation diagrams presented in Chapters 7 and 10 do not indicate that Group 4 samples are enriched in these elements. Nevertheless, the flatness of many of the plots suggest that some Group 4 rocks could be the result of magma mixing between Group 1 rocks and Group 3 rocks.

12.8. Magma mixing modelling - summary

Magma mixing modelling, based on the intrusion as a whole, suggests that a simple mixing of two magmas could not account for the variation in geochemistry in the Penmaenmawr Intrusion. However, further modelling, with samples from the different Groups from within the intrusion suggests that some mixing of magmas could have occurred, in particular in a sub-group of Group 3 rocks in the Western Quarries and in Group 4 rocks.

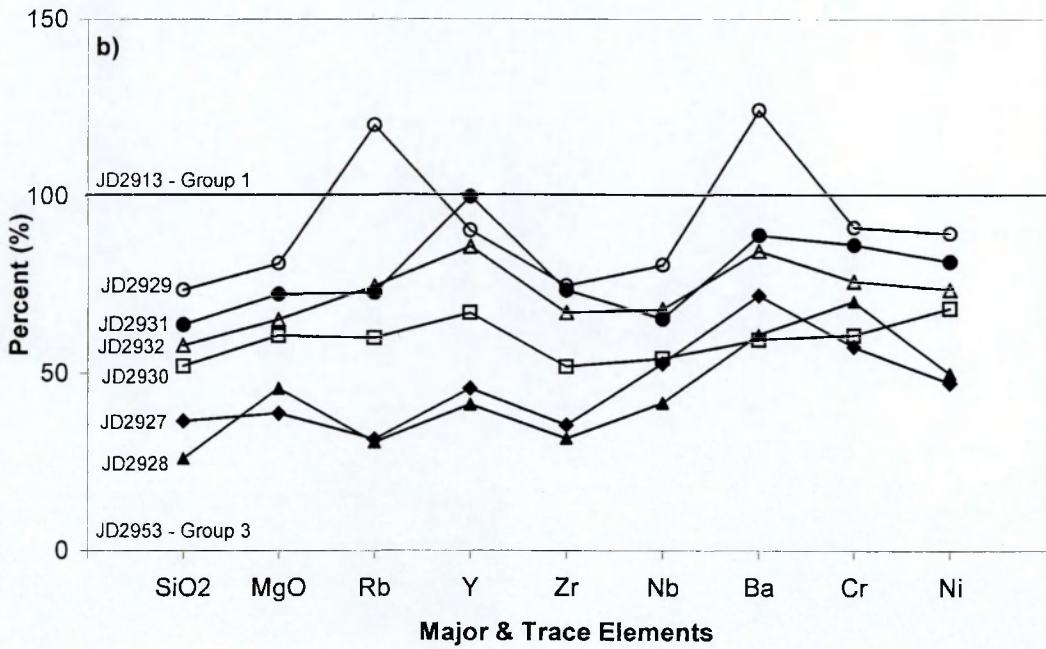
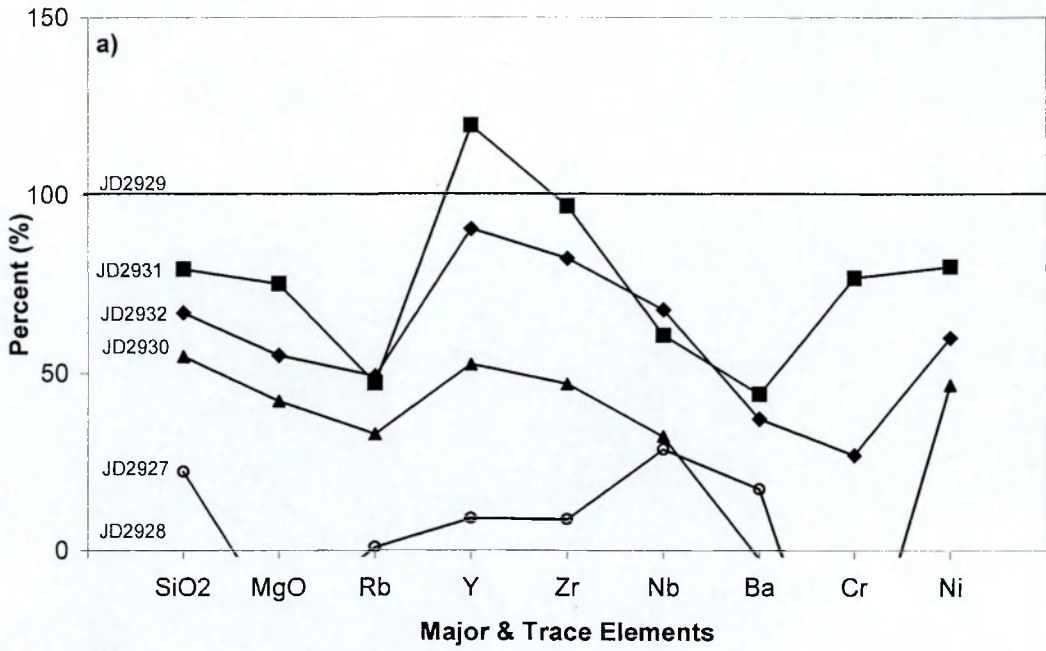


Figure 12.7. Magma mixing plots for Group 4, Penmaenmawr samples JD2927, JD2930, JD2931, and JD2932, using (a) JD2928 and JD2929 as the end members, and (b) JD2913 (Group 1) and JD2953 (Group 3) as end members.

The origin of the two end members in the sub-group from the Western Quarries is not clear. Sample JD2946 could have evolved by fractional crystallisation from sample JD2936 or another unknown parent magma or both samples could have evolved from the same or different unknown parent magmas. Fractional crystallisation modelling in Chapter 10 suggested that Group 3 rocks may contain batches of magma that underwent fractional crystallisation independently, therefore, conceivably the two end members from the magma mixing modelling could represent parent and daughter magmas from a fractional crystallisation process that then mixed to form the linear range of compositions observed.

It was suggested in Chapter 10 that Group 1 and Group 3 rocks could represent different batches of magma that underwent fractional crystallisation independently. Group 4 rocks could therefore represent a boundary zone between these two batches of magma in which some Group 3 magma mixed with some Group 1 magma to produce a volume of magma with the compositional variation represented by Group 4 rocks.

Magma mixing modelling supports the suggestion that the Penmaenmawr Intrusion could represent a number of batches of magma and suggests that one batch represented by the sub-group of Group 3 rocks in the Western Quarries could have been developed by the mixing of a magma, evolved by fractional crystallisation with its parent magma. Magma mixing modelling also suggests that the batches of magma represented by Group 3 rocks and Group 1 rocks could have mixed forming a zone of magma between them with intermediate compositions.

CHAPTER 13. SEGREGATIONS AND INCLUSIONS

13.1. Introduction

In Chapter 3 it was reported that rocks from the central part of the intrusion, mainly comprising Group 2 rocks, contain pale segregations comprising of irregularly shaped veins and pods, and small, rounded inclusions consisting of fine-grained equigranular crystals. The segregations and inclusions are often associated with each other. These segregations and inclusions are described in Chapter 3 and their mineralogy is described in Chapter 4. This chapter details their geochemistry, both major and trace elements, and presents variation diagrams showing how they differ from the other samples from the intrusion and considers possible processes which could have led to their formation.

A segregation sample was separated from its source rock for analysis, although in some places the boundary between the segregation and the surrounding rock was indistinct. Similarly, a group of inclusions occurring close together was separated from their source rock and prepared for a whole rock analysis. Major and trace element compositions were obtained for the segregation, the group of inclusions and the host rock containing the inclusions using the XRF spectrometer at the Open University and the analyses are presented in Appendix 6.

13.2. Variation diagrams

Variation diagrams showing the composition of the segregation, the inclusions and the source rock, plotted along with the other samples from the intrusion are presented in Figures 13.1 and 13.2. Figure 13.1 shows the concentration of major elements plotted against SiO₂ contents and Figure 13.2 shows the concentration of trace elements plotted against SiO₂ contents.

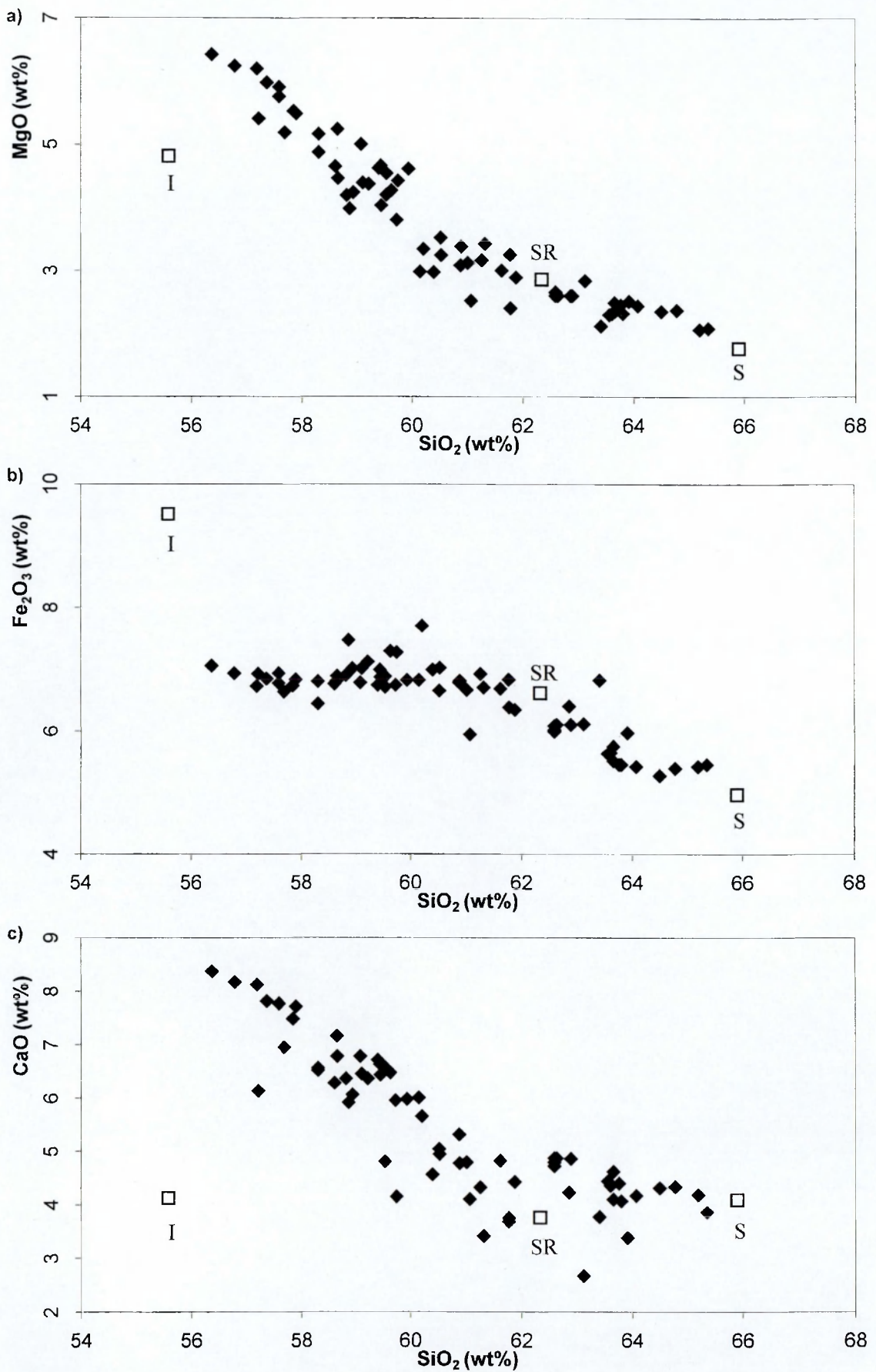


Figure 13.1. Plots of selected major elements (wt%) against Silica (SiO_2) (wt%), for the Penmaenmawr samples from groups 1-4, and the segregation (S), the inclusion (I) and the source rock (SR) containing the inclusion (shown by the open squares): (a) MgO , (b) Fe_2O_3 and (c) CaO , continued overleaf.

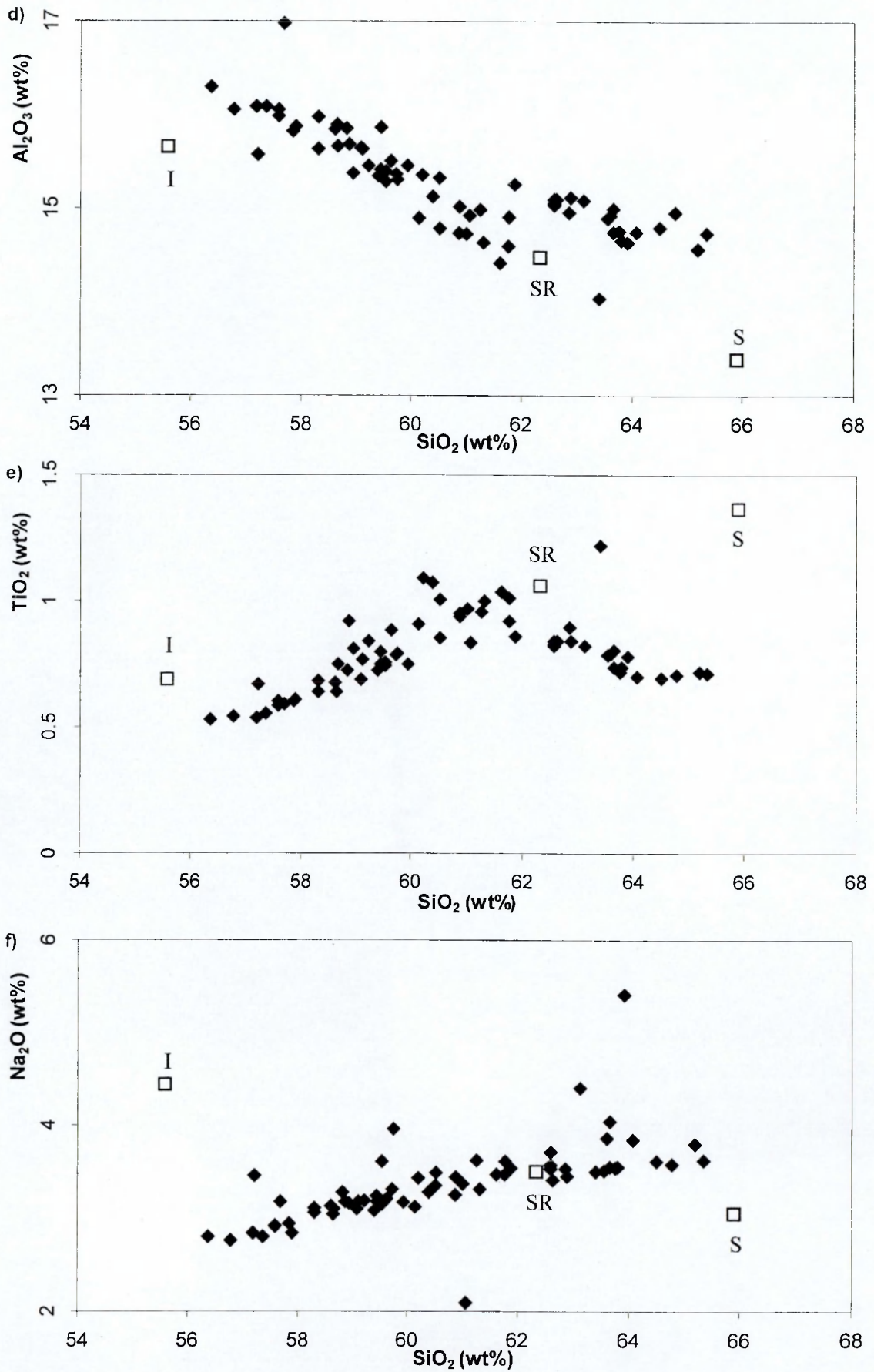


Figure 13.1 (continued). Plots of selected major elements (wt%) against Silica (SiO_2) (wt%), for the Penmaenmawr samples from Groups 1-4 and the segregation (S), the inclusion (I) and the source rock (SR) containing the inclusion (shown by the open squares): (d) Al_2O_3 , (e) TiO_2 and (f) Na_2O , continued overleaf.

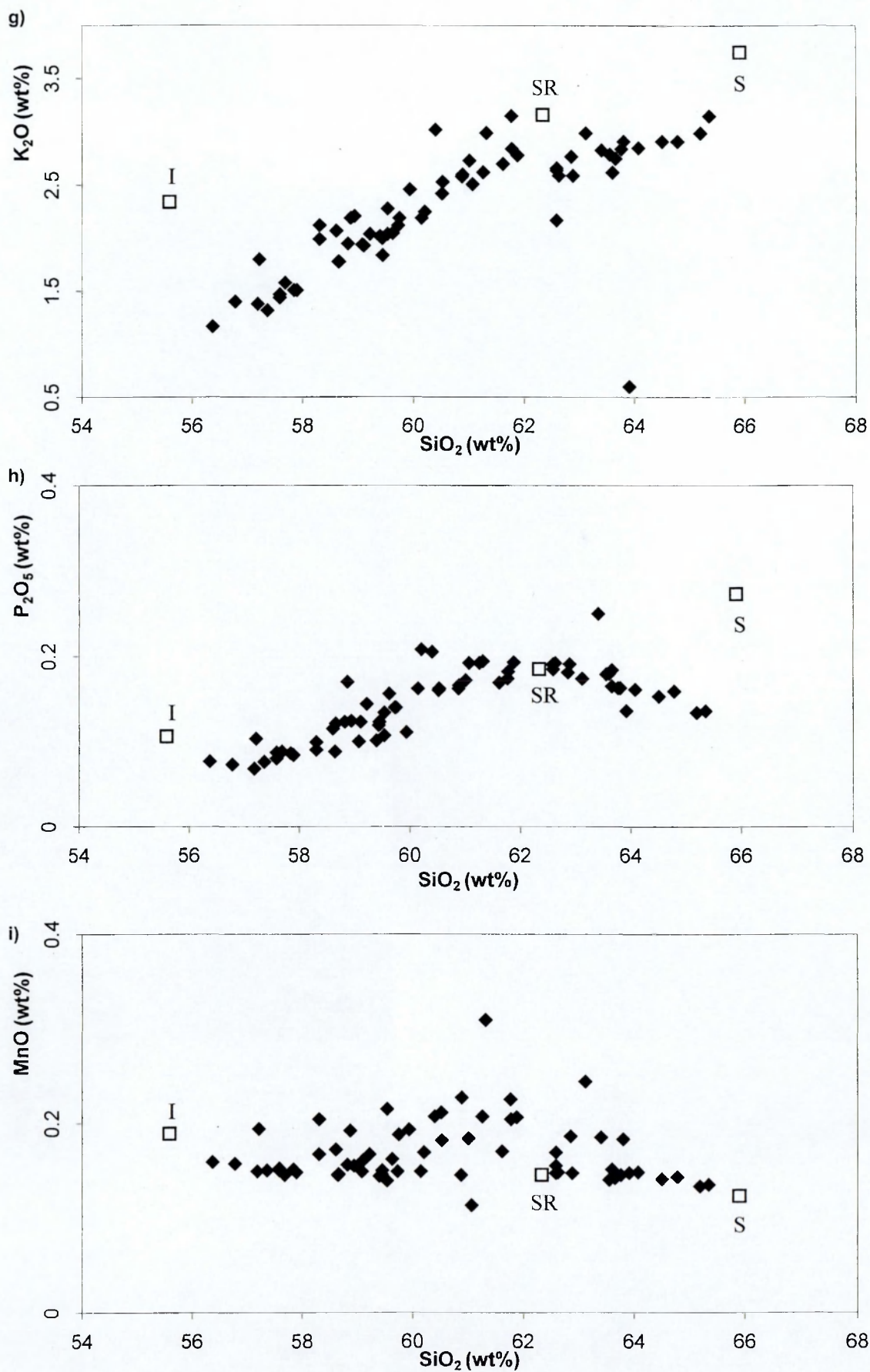


Figure 13.1 (continued). Plots of selected major elements (wt%) against Silica (SiO₂) (wt%), for the Penmaenmawr samples from Groups 1-4, and the segregation (S), the inclusion (I) and the source rock (SR) containing the inclusion (shown by the open squares): (g) K₂O, (h) P₂O₅ and (i) MnO.

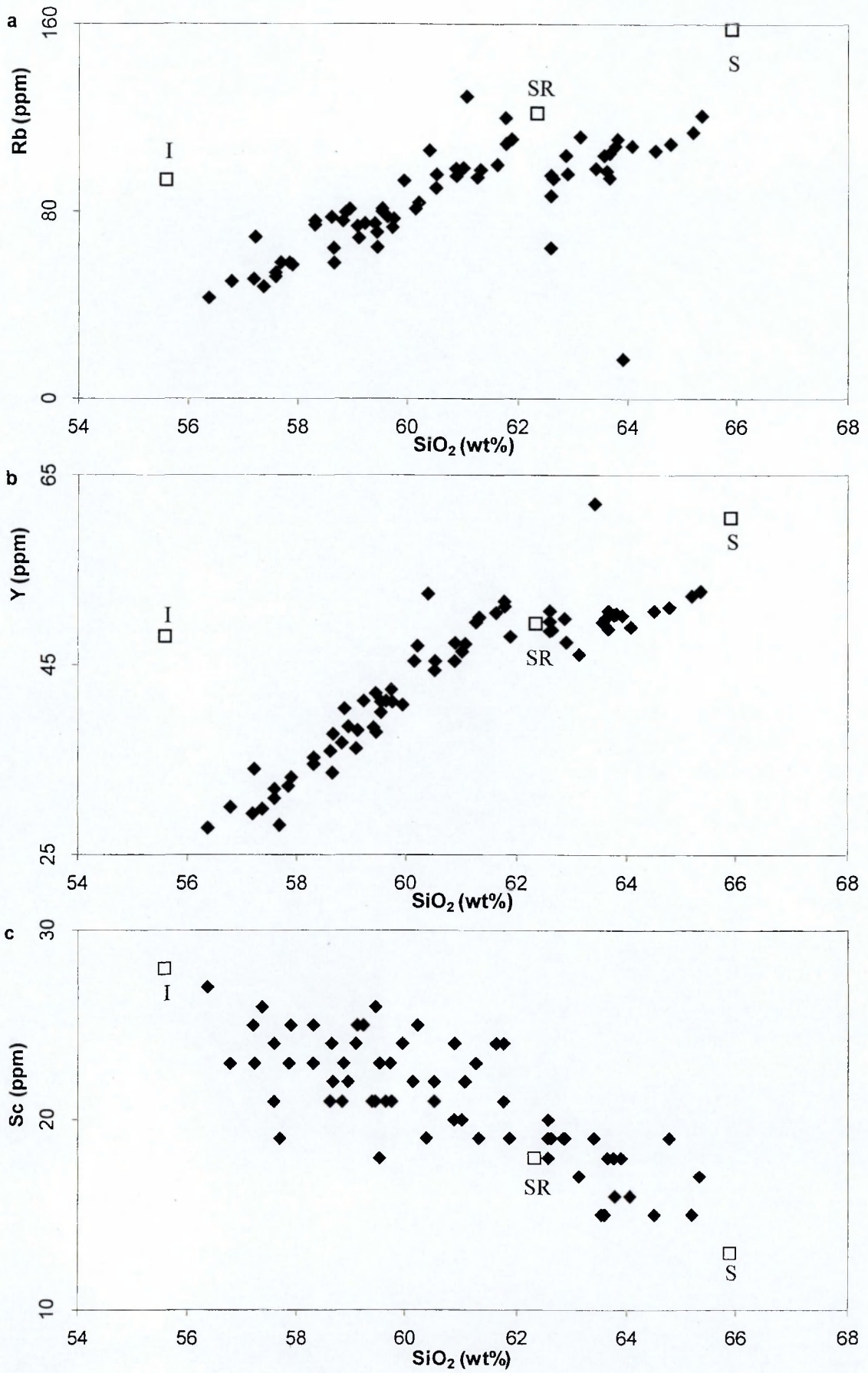


Figure 13.2. Plots of selected trace elements (ppm) against Silica (SiO_2) (wt%), for the Penmaenmawr samples from Groups 1-4 and the segregation, the inclusion and the source rock, containing the inclusion (shown by the open squares): (a) Rb, (b) Y and (c) Sc (continued overleaf).

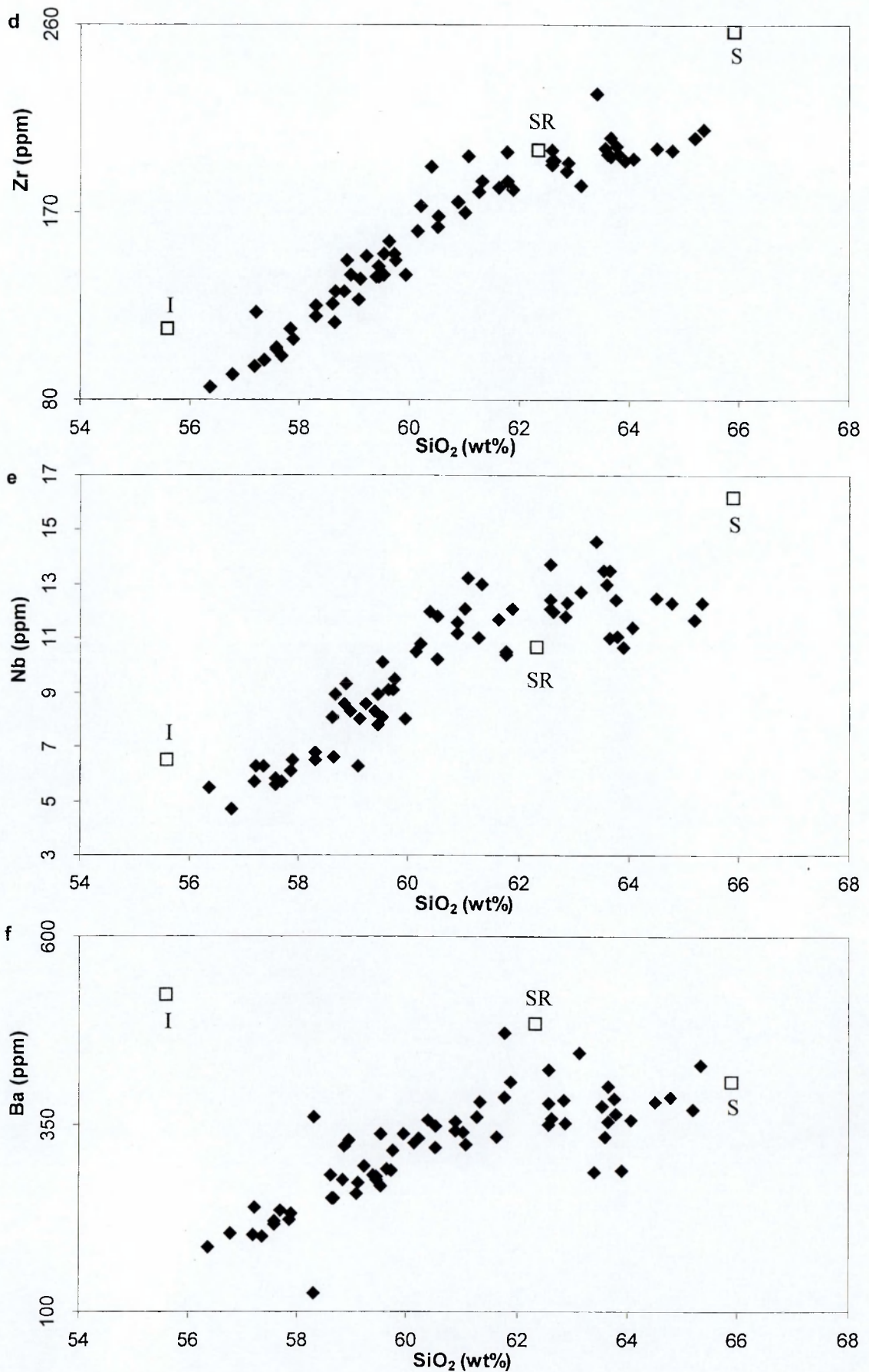


Figure 13.2 (continued). Plots of selected trace elements (ppm) against Silica (SiO_2) (wt%), for the Penmaenmawr samples from Groups 1-4, and the segregation (S), the inclusion (I) and the source rock (SR) containing the inclusion (shown by the open squares): (d) Zr, (e) Nb and (f) Ba (continued overleaf).

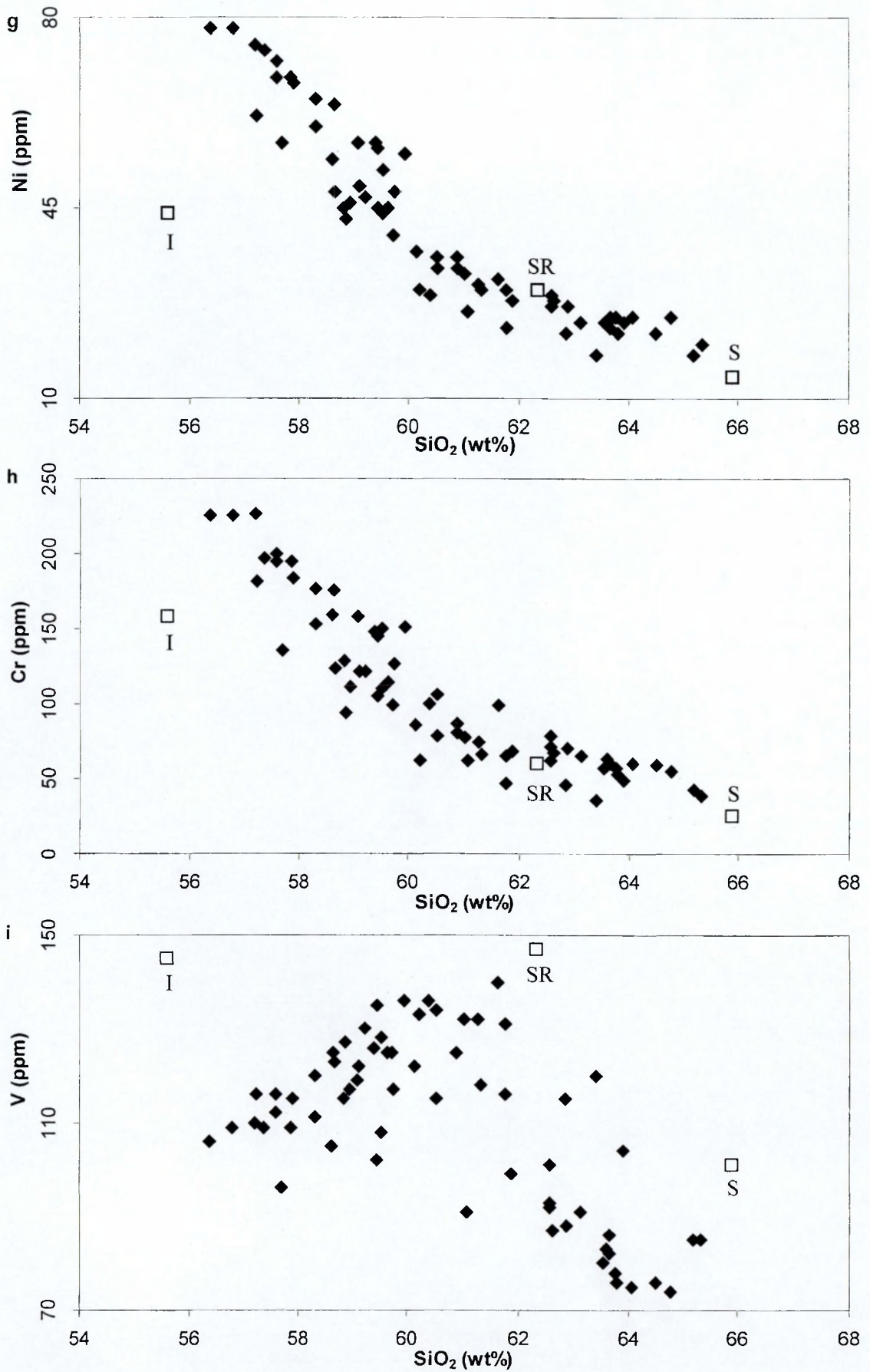


Figure 13.2 (continued). Plots of selected trace elements (ppm) against Silica (SiO_2) (wt%), for the Penmaenmawr samples from Groups 1-4 and the segregation, the inclusion and the source rock, containing the inclusion (shown by the open squares): (g) Ni, (h) Cr and (i) V.

13.3. Variation diagrams - description

The source rock was classified as Group 2 and plots on all variation diagrams as a typical Group 2 rock. The SiO₂ content of the segregation is 65.9wt%, which is higher than any other sample collected from the Penmaenmawr Intrusion and it plots on the variation diagrams for MgO, Fe₂O₃, CaO, MnO, Sc, Ni, Cr and Co as a continuation of the major trend of the Penmaenmawr Intrusion as a whole. However in the diagrams for Al₂O₃, TiO₂, K₂O, P₂O₅, Rb, Y, Zr, Nb, where there is a distinct change in slope (discussed in Chapter 7), it tends to plot with a major compositional gap as a continuation of the trend for Group 2 and 3 rocks.

The SiO₂ composition of the inclusion is 55.50%, which is lower than any other sample from the Penmaenmawr Intrusion and on the variation diagrams it plots away from the other samples. However, with the exception of the variation diagrams for TiO₂, Na₂O, P₂O₅, Zr and Nb, it appears to plot as a backward extension from the trend for Group 1 rocks.

The inclusion, segregation and source rock samples appear to plot with remarkable consistency with a linear relationship on almost all diagrams.

13.4. Variation diagrams- interpretation

The plots on the variation diagrams of the segregation suggest that it could be the result of fractional crystallisation of Group 3 magma. However in Chapter 11 it was suggested that the Penmaenmawr Intrusion could be composed of several batches of magma, which underwent fractional crystallisation independently. The segregations, therefore, could have evolved by fractional crystallisation from the Group 2 batch of magma. The mineralogy of the segregations, presented in Chapter 4, shows that they consist of large crystals, generally 2 mm in size, of mainly granophyric quartz and chlorite (after amphibole and biotite), with small amounts of plagioclase feldspar and clinopyroxene. The size of these crystals and the compositional gap between Group 2 rocks and the segregation on the variation diagrams suggest that the segregations could be the result of late stage fractionation and that the residual or daughter magma was

enriched with volatiles. This suggestion is supported by Sargent (1925) who suggested that the segregations were generated by volatiles in the later stages of cooling, which carried silica- and water-rich residual magma to areas of decreased pressure.

The inclusions appear to plot, on most of the variation diagrams, as backward extensions of the trend shown by Group 1 rocks. This observation suggests that the composition of the inclusion could represent a parent magma to Group 1 rocks or alternatively a cumulate of crystals removed during the fractional crystallisation of an evolving batch of magma represented by Group 1 rocks. It was reported in Chapter 4 that the inclusions contained a greater proportion of ferromagnesian minerals than other samples from the Penmaenmawr Intrusion, which would support the latter suggestion. However the mechanism that placed the rounded cumulates from a batch of magma that ended up in the eastern part of the intrusion into another batch of magma in the Central Quarries is unclear.

Rounded inclusions are often associated with magma mixing (Castro *et al.*, 1990; Poli and Tommasini, 1991) and the linear relationship between the inclusion, host sample and segregation could suggest magma mixing. However the inclusion plots away from the trend for Group 2 and 3 rocks and the magma mixing modelling presented in Chapter 13 rejected a magma mixing process for all but small groups of rocks from the intrusion.

The geochemical data considered above apply to a single segregation and a single group of inclusions that were analysed as one sample. The data, therefore, may not be representative of the segregations or the inclusions as a whole. Additionally, due to their method of extraction, the data may be contaminated by traces of the source rocks. Any interpretation above, therefore, can only be speculative and provide a starting point for additional work on the origin of the inclusions and segregations.

CHAPTER 14. DISCUSSION OF THE MAGMATIC PETROGENESIS OF THE PENMANMAWR INTRUSION

14.1. Introduction

This chapter reviews the data and the conclusions, presented in the previous chapters, discusses their implications and proposes a preferred model for the magmatic petrogenesis of the Penmaenmawr Intrusion.

In Chapter 4 it was shown that the Penmaenmawr Intrusion could be divided into four petrographic groups based on texture and mineralogy (numbered 1, 2, 3 and 4 in this study). In Chapter 5, on the basis of differences in primary mineral chemistry, it was suggested that although rocks from Groups 2 and 4 may have evolved from Group 3 rocks by fractional crystallisation the major petrographical differences between the groups are due to varying degrees of alteration, the origin of which was discussed in Chapter 8. However, in Chapter 7 it was shown that the geochemistry of the intrusion varied regularly across the intrusion with an approximately northwest to southeast trend and that rocks from Groups 1 and 3 could be separated from each other by their geochemistry and that rocks from Groups 2 and 4 tended to have a geochemical composition that was intermediate between the rocks from Groups 1 and 3.

In Chapter 9, following a review of magma chamber processes, it was suggested that the variation in geochemistry within the Penmaenmawr Intrusion is unlikely to be the result of the emplacement and fractional crystallisation of a single batch of magma and in Chapter 10, following an analysis of variation diagrams, it was suggested that the variation in geochemistry would be consistent with a two-stage fractionation process and that, possibly, the intrusion consisted of two batches of magma, one represented by rocks from Groups 2 and 3 and the other represented by rocks from Group 1 and some rocks from Group 4. However, the geochemical variation within the intrusion as a whole suggests that the intrusion has a common petrogenesis and, additionally, that although fractional crystallisation appears to be the main cause of the variations observed, magma mixing between batches of magma cannot be ruled out.

Subsequent fractional crystallisation modelling, presented in Chapter 11, suggested that the Penmaenmawr Intrusion could be composed of several batches of magma that underwent fractional crystallisation independently of each other and two possible models, described in this study as the separate batches of magma model and the progressive fractionation model, were proposed to account for the results of the modelling. Magma mixing modelling presented in Chapter 12 supported the suggestion that the Penmaenmawr Intrusion could have evolved as a number of independent fractionating batches of magma and that some of those batches could have mixed producing a zone of rocks with compositions that are intermediate between two end members.

14.2. Fractional crystallisation

The case for fractional crystallisation to be the main cause of the geochemical variation within the Penmaenmawr Intrusion is supported by other studies. Howells *et al.* (1991) reported that the predominant volcanic rock compositions within the Caradoc Volcanic sequence are bimodal basalt-rhyolite and they suggested that the basalts are mantle-derived parental magmas and that the acidic magmas are generated by fractional crystallisation. Croudace (1982), in a study of granitoids of Caradoc age on Llŷn, proposed that they had evolved from tholeiitic magma by crystal fractionation. Ball and Merriman (1989) proposed that the Llewelyn Volcanic Group, including the Penmaenmawr Intrusion, evolved by crystal fractionation and that the Penmaenmawr intrusives represent intermediate rocks in the evolution of a low-Zr series of volcanic rocks. Tremlett (1997) proposed that the Penmaenmawr Intrusion was the result of successive emplacements from a parental magma body undergoing crystallization differentiation at depth.

However, the review and analysis of geochemical variations presented in Chapters 7 and 10 suggested that although the rocks from the Penmaenmawr Intrusion could be related by fractional crystallisation, the geochemical variation is not the result of simple, *in situ* fractional crystallisation and therefore the Penmaenmawr Intrusion cannot be considered as a simple emplacement of intermediate rocks derived from an evolving suite of volcanic rocks.

Ball and Merriman (1989) used fractional crystallisation modelling to suggest that the rhyolites in the Llewelyn Volcanic Group had evolved by a two stage fractional crystallisation process, the first involving the removal of olivine, plagioclase and ilmenite to produce a trachyandesite and the second involving the removal of plagioclase, augite, ilmenite and apatite to form rhyolite.

Fractional crystallisation modelling for the Penmaenmawr Intrusion, presented in Chapter 11, involved the removal of plagioclase and orthopyroxene. The different assemblages of fractionating phases obtained by the different models may be the result of different modelling assumptions, but could also indicate that the Penmaenmawr Intrusion, although part of an overall, evolving trend for the Llewelyn Volcanic Group, evolved differently.

14.3. Other possible mechanisms

In Chapter 7 it was shown that the SiO₂, Zr and Y contents of rocks from the Penmaenmawr Intrusion increase regularly across the intrusion from approximately northwest to southeast. In addition it was shown that the rocks with the highest SiO₂, Zr and Y contents, the most evolved rocks, occur as fine-grained rocks along the southern boundary of the intrusion while rocks with the lowest SiO₂, Zr and Y contents, the least evolved rocks, occur as an elongate area close to the north-western boundary. In Chapter 9, in a review of possible magma chamber processes, it was reported that *in-situ* fractional crystallisation processes tend to produce a symmetrically zoned intrusion, with the least evolved rocks at the margins and the most evolved rocks towards the centre. The geochemical variation in the Penmaenmawr Intrusion is, therefore, more comparable to a reversely zoned intrusion where the most fractionated portion of magma occupies the outermost part of an igneous body.

Janousek *et al.* (1997), in a study of reverse zoning in the Ricany granite, Czech Republic, suggested that reverse zoning could be formed by three possible mechanisms.

1. Mixing (including assimilation and, or, periodic influx of fresh, little fractionated magma into the centre of the intrusion)

2. Emplacement of the granite magma in several separate batches possibly associated with cauldron subsidence
3. Emplacement of an essentially single pulse of magma from a deeper level magma chamber with a vertical compositional gradient.

As the simple, *in situ* fractional crystallisation model has been rejected as the cause of the overall geochemical variation within the Penmaenmawr Intrusion, the reverse zoning mechanisms above are considered valid alternatives to be examined.

14.3.1. Mixing (including assimilation and/or periodic influx of fresh magma)

Along the southern boundary, the Penmaenmawr Intrusion consists of very fine-grained rocks in contact with the country rock, which is indicative of rapid cooling, and, in Chapter 9, it was argued the Penmaenmawr Intrusion had not been affected by any significant assimilation of wall rock because of the absence of country rocks xenoliths, the poorly evolved metamorphic aureole in the shales, and the high level of emplacement. More substantial evidence would require isotopic analysis (e.g. $^{87}\text{Sr}/^{86}\text{Sr}$ ratios) from the intrusion and the shales, which is outside the remit of this study.

Any mixing, therefore, would have to be between periodic influxes of magma. Marshall and Sparks (1984), in a study of some mixed-magma and net-veined ring intrusions, proposed that a range of basic compositions can be produced by the periodic replenishment of a magma chamber.

However, linear variation, magma mixing modelling, presented in Chapter 12, suggested that a simple mixing of two magmas could not account for the overall variation in geochemistry in the Penmaenmawr Intrusion and that magma mixing could, in theory at least, only account for some local mixing of magmas within the Group 3 rocks while Group 4 rocks could be the result of the mixing between Group 3 and Group 1 rocks.

Additional evidence for magma mixing could come from the inclusions. Fine-grained, rounded inclusions are generally considered to be indicators of

hybridisation (Castro *et al.*, 1990; Poli and Tommasini, 1991). Janousek *et al.* (1997) suggested that magma mixing would be viable if microgranular enclaves plotted on extensions of trends defined by the host rocks. However, the composition of the fine-grained rounded inclusion, present in Group 2 rocks of the Penmaenmawr Intrusion, presented in Chapter 13 (Figures 13.1 and 13.2), plots away from the main trends shown by the other samples and, although in some plots the inclusion could be interpreted as a backward extension of the trend for Group 1 rocks, subsequent magma mixing modelling suggested that it was unlikely to represent the mafic end member of a magma mixing process. The origin of the inclusions is unclear but it is considered unlikely that they represent the composition of a basic magma that was emplaced into, and hybridised with, an existing acidic magma to produce the geochemical variation observed within the intrusion.

Magma mixing or hybridisation cannot account for the overall trends within the Penmaenmawr Intrusion. However, Blake and Campbell (1986) suggested that fluid dynamic instabilities at the boundaries between different magma compositions could lead to localised mixing that would smooth out the compositional differences between the magmas. Magma mixing between adjacent bodies of magma, therefore, could account for localised variations in geochemistry, blurring their contacts and producing small volumes of hybrid rocks. This suggestion which would be consistent with the results of the magma mixing modelling presented in Chapter 12 where it was suggested that Group 4 rocks could be the result of the mixing between some Group 3 magma with some Group 1 magma.

14.3.2. Emplacement in several separate batches

Tindle *et al.* (1988), in a study of the Cairnsmore of Carsphairn Intrusion in the Southern Uplands, used observed sharp contacts between rock types in the field, gaps in compositional variations, and rapidly varying compositional gradients to suggest that the intrusion was the result of a number of emplacements of magma that developed from a single batch of evolving magma below the level of emplacement.

Although no sharp contacts between rock types were observed in the Penmaenmawr Intrusion, the lack of clear contacts between the groups of rocks, described in Chapter 4, could be due to localised magma mixing, blurring the sharp contacts between adjacent magma bodies, as discussed above, combined with the lack of suitable exposure.

It was shown in Chapter 7 that geochemical compositions varied regularly across the Penmaenmawr Intrusion in a northwest to southeast direction without any sudden jumps. However, a possible exception to this general pattern is observed in the southwest corner of the intrusion where Group 1 rocks, with high SiO₂, Zr and Y contents, are in contact with Group 3 rocks, with notably low SiO₂, Zr and Y contents. Additionally, Figure 3.6, presented in Chapter 3, shows a large area where there is a lack of exposure between Group 1 rocks, occurring in the Graig Lywd quarries, and the Group 2 rocks, in the central quarries. This lack of exposure may have resulted in the contour mapping programme, used to produce the contour plots presented in Chapter 7, smoothing out and concealing any abrupt changes in composition between Group 1 and Group 2 rocks. The boundary between Group 1 rocks and the other groups in the intrusion could therefore be denoted by a sharp change in composition.

The variation diagrams for the Penmaenmawr Intrusion, presented in Chapter 10, generally show a continuum of values without any obvious gaps. However it was observed in almost all of the plots that Group 3 rocks and Group 1 rocks form distinct groups with tight linear trends with contrasting gradients, which intersect at between 61% and 62% SiO₂. Additionally, in most plots Group 2 rocks tend to form a continuation of the trend for Group 3 rocks. It was suggested in Chapter 10 that Group 3 rocks were derived from a separate injection of magma from the Group 1 rocks and the fractional crystallisation modelling, presented in Chapter 11, demonstrated that Group 1 rocks could have evolved independently of Group 3 rocks.

Throughout this study it has been observed that Group 1 rocks have different properties from the other rocks of the intrusion. They are very fine-grained, occur in a continuous arc along the southern boundary of the intrusion and have

different geochemical characteristics. The possible sharp boundary, the different compositional gradient and the different properties of Group 1 rocks suggest that they could represent a separate emplacement of magma from the rest of the intrusion.

Tremlett (1997) proposed that the variation in geochemistry of the Penmaenmawr Intrusion is due to the emplacement of magma in pulses from an underlying magma chamber, itself undergoing fractional crystallisation. He presented a geochemical distribution pattern within the Penmaenmawr Intrusion and geochemical variation diagrams, with major and trace element contents plotted against SiO_2 contents, that are broadly consistent with this study. However, although he found that most of the acid rocks occur at the eastern margin of the intrusion, he found one sample with a high SiO_2 content on the western margin and did not analyse as many samples from along the southern margin of the intrusion as this study.

He interpreted the geochemical distribution pattern and the variation diagrams as being the result of two original intrusions of quartz-microdiorite, represented by the least evolved rocks from the intrusion, (some of the Group 3 rocks and some of the Group 4 rocks in this study) which were then joined and flanked by the emplacement of progressively more acid rocks derived from a fractional crystallisation process taking place at depth. He observed that the continuous nature of the geochemical trends makes it impossible to indicate separate pulses of magma emplacement, but that the continuous nature of the chemical variation suggests that there may have been as many phases of magma emplacement as there are analyses. He also suggested that the small crystal size of the rocks, in areas where there is little change in composition, indicated that there may, in fact, have been many pulses of intrusion.

In Tremlett's (1997) model, progressively more evolved rocks are emplaced from an underlying magma chamber. However, it was reported in Chapter 9 that the fractional crystallisation within a magma chamber is likely to result in a magma that has a vertically layered composition, the more evolved rocks being above the less evolved rocks. Any initial emplacement would be from the top of the underlying magma chamber and hence consist of the more evolved portion

of magma. For subsequent emplacements of magma to be progressively more evolved than preceding emplacements of magma would require the underlying magma chamber to continue to fractionate for significant time periods between emplacements. However, It was demonstrated in Chapter 9 that the Penmaenmawr Intrusion is a high level intrusion and, therefore, the already emplaced magmas would begin to cool rapidly during the time periods between emplacements, particularly at the margins, forming sharp boundaries with subsequent incoming emplacements of magma. Many emplacements of progressively more evolved magma would, therefore, form many sharp boundaries between the emplacements and although some of the boundaries may be hidden by lack of exposure, as argued above, no such boundaries have been identified in areas where there is good exposure during this or other studies.

Additionally, it was observed from the variation diagrams, presented in Chapter 10 and by Tremlett (1997), that the geochemical variation within the Penmaenmawr Intrusion is continuous and it is unlikely that the degree of fractionation taking place in the underlying magma chamber between successive emplacements would be just sufficient to produce a magma of exactly the right composition, prior to each emplacement, to produce the continuous trend observed. Tremlett's (1997) model of batches of progressively more evolved magma being emplaced from an underlying magma chamber itself undergoing fractional crystallisation must therefore be rejected.

14.3.3. Emplacement of an essentially single pulse of magma from a deeper level magma chamber with a vertical compositional gradient

Janousek *et al.* (1997) showed that the Ricany granite has a gradational boundary between the central and marginal parts of the intrusion and used this and other evidence to suggest that the origin of the reverse zoning in the Ricany granite is due to the high level emplacement of a single batch of magma from a deeper level, vertically graded magma chamber. They suggested that progressively less evolved magma from successively deeper levels rose into the core displacing more evolved magma toward the margins.

The Penmaenmawr Intrusion is not reversely zoned, but has a composition that becomes more evolved across the intrusion with an approximately northwest to southeast trend. The emplacement of a single batch of magma would, therefore, require the less evolved magma to displace the more evolved magma toward the southeast, which could be due to differences in stress regimes in the country rocks and structures at the site of emplacement. An alternative mechanism to account for a unidirectional, compositional variation has been put forward by Blake and Campbell (1986) and Preston (2001) who suggested that a range of compositions could be obtained by tapping a series of magma compositions simultaneously from a zoned magma chamber. Preston (2001) suggested that a dyke could intersect a zoned magma chamber in such a way as to withdraw magma from more than one layer in the system simultaneously.

It was reported, in Chapter 7, that the variation in composition across the Penmaenmawr Intrusion was gradual and that the compositional variation between Group 3 and Group 2 rocks is small. The Penmaenmawr Intrusion could therefore be the result of the emplacement of a single body of magma that simultaneously tapped a range of magma compositions from an underlying, magma chamber that was itself compositionally zoned due to fractional crystallisation.

However, the fractional crystallisation modelling, presented in Chapter 11, suggested that although there could be a common parent magma, groups of magma fractionated independently of each other. Therefore in order to accept the single emplacement model for the Penmaenmawr Intrusion, it is necessary to establish whether processes within an underlying magma chamber could produce batches of magma that fractionated independently of each other.

In order for the underlying magma chamber to produce groups of magma that fractionated independently it would be necessary for it to be compositionally zoned. McBirney (1984) suggested that as a magma cools, differences in temperature and in composition may cause convection currents to be produced in the magma chamber. He described convection as a major process affecting the ways in which magmas cool, crystallise and differentiate. Thermally-driven convection takes place due to intrusions losing heat to the roof, wall and floor.

Compositionally-driven convection takes place due to changes in concentrations of different elements by fractional crystallisation or other processes. Collectively they are known as double diffusive convection. Huppert and Sparks (1984) suggested that once compositional gradients are established, double diffusive layers can be formed and each layer can subsequently evolve as a chemically independent system. This process suggests that local fractionation within layers of a magma chamber can take place prior to subsequent emplacement at a higher level. The Penmaenmawr Intrusion could therefore be the result of an emplacement of a single batch of magma from an underlying, vertically graded magma chamber.

14. 4. Evidence for magma emplacement processes from segregations

Ball and Merriman (1989) suggested that the Llewelyn Volcanic Group, which includes Penmaenmawr was stored and fractionated at high crustal levels and Merriman *et al.* (1986) suggested that a horizon of ferrodolerite in the Tal y Fan olivine dolerite intrusion, intruded into the Snowden Volcanic Group approximately 5 km southeast of the Penmaenmawr Intrusion, fractionated *in situ*.

In Chapter 13, it was shown that the composition of a felsic segregation, found in Group 2 rocks, plots as a continuation of the trends shown by the rocks from Groups 2 and 3. It was proposed that the compositional gap between the most evolved rocks from Group 2 and the segregation, the larger size of the crystals and the assemblage of minerals present in the segregation could be due to a volatile rich layer formed by a later stage fractional crystallisation of magma represented by the composition of Group 2 rocks, a suggestion that is supported by Sargent (1925). The segregations could, therefore, represent the results of late stage fractional crystallisation after emplacement.

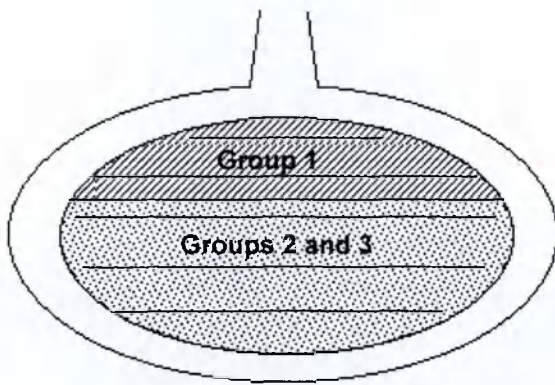
However, Preston (2001) suggested that during movement and emplacement of magmas, viscosity differences between the magmas could result in the less viscous, more basic magmas, encapsulating the more silicic magmas, leading to an intrusion with basic margins and a silicic centre. In Chapter 2 it was reported that the segregations within the Penmaenmawr Intrusion occur as irregularly shaped veins and pods within the central part of the intrusion. The

simultaneous movement and emplacement of a thin, viscous layer of silicic magma together with a large volume of underlying less viscous more basic rock could produce the irregularly-shaped vein and pod structures observed in the Penmaenmawr Intrusion. Therefore, any late stage fractionation process that produced the segregations is more likely to have occurred in an underlying magma chamber.

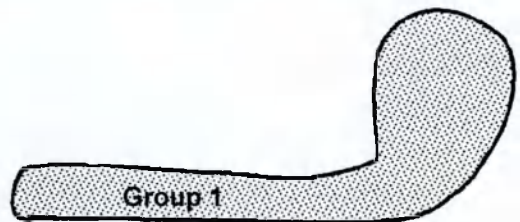
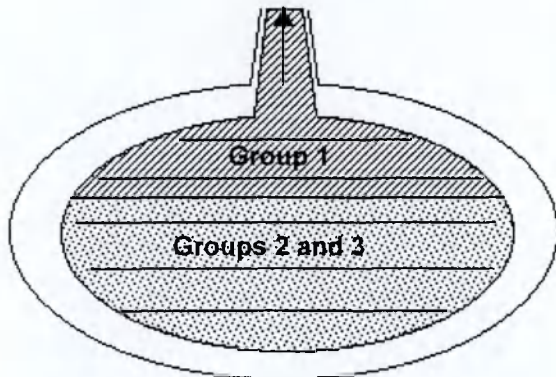
14.5. The preferred model for the magmatic petrogenesis of the Penmaenmawr Intrusion

A preferred model for the petrogenesis of the Penmaenmawr Intrusion has been prepared based on the data and the conclusions, presented in the previous chapters, and the discussions above. A diagram showing the preferred model is presented in Figure 15.1. In this preferred model the primary geochemical variation within the Penmaenmawr Intrusion is due to two major emplacements of magma, represented by Group 1 rocks, and Group 2 and 3 rocks respectively, from a larger underlying magma chamber undergoing fractional crystallisation. The underlying magma chamber was layered, with more evolved magma on top of less evolved magma and thermally driven and compositionally driven convection had formed double diffusive layers in which magmas were evolving by fractional crystallisation independently of each other.

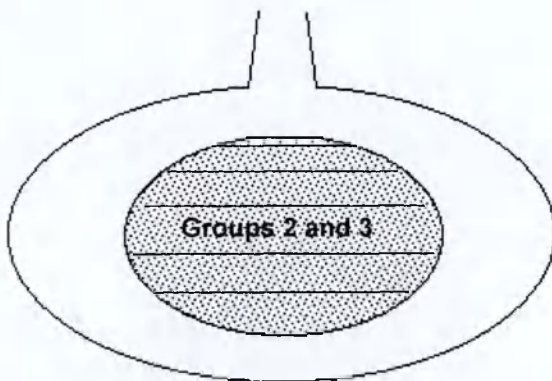
The initial emplacement consisted of the most evolved magma from the upper layer of the underlying magma chamber represented by Group 1 rocks, which are very fined-grained and the most evolved rocks from the intrusion. This magma was ejected and emplaced in a sheet form, forming what is now the southern margin of the Penmaenmawr Intrusion. The two plugs at Dinas and Garreg Fawr have a similar composition to Group 1 rocks and therefore it is likely that they were emplaced within a similar time frame, suggesting that the underlying magma chamber was probing and exploiting lines of weakness. At Graig Lwyd, in the eastern quarries, a greater volume of magma was emplaced than elsewhere in the intrusion.



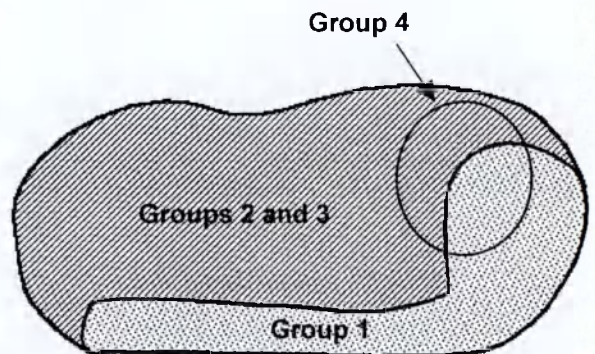
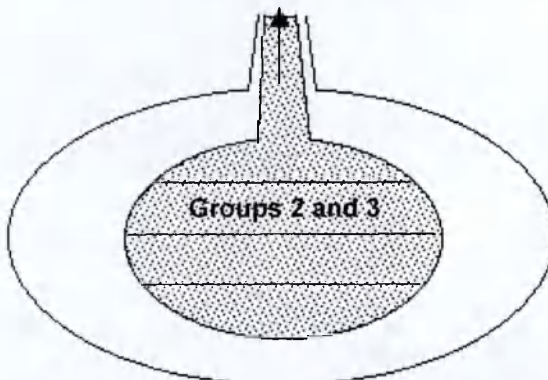
1. The underlying layered magma chamber, showing the magma represented by Group 1 rocks on top of the magma represented by Groups 2 and 3 rocks. Each group consists of several compositional layers, which are fractionating independently of one another.



2. The first emplacement of magma represented by Group 1 rocks, forming the rocks at the Graig Lwyd quarries and along the southern margin of the intrusion.



3 After the first emplacement a thin volatile layer formed by fractionation and the concentration of volatiles collects on the top of the magma chamber.



4. The second emplacement of magma represented by Groups 2 and 3 rocks forming the main part of the intrusion entraining the volatile rich layer and causing localised mixing between layers. At the margins of the two emplacements in the east of the intrusion local mixing occurs, forming the Group 4 rocks.

Figure 14.1. The preferred model for the magmatic petrogenesis of the Penmaenmawr Intrusion.

Where these emplacements were confined and in contact with cold country rock, as along the southern margin of the Penmaenmawr Intrusion they cooled quickly, preserving the geochemical variation from the underlying magma chamber. At Graig Lywd the larger volume of magma was insulated by the chilled margin and cooled more slowly.

Following the initial emplacement, a thin volatile rich layer, formed by fractional crystallisation and the concentration of volatiles, collected on the top of the deeper level magma chamber. The second emplacement, represented by Group 2 and 3 rocks, involved a larger volume of magma and was made up of several layers, including the volatile rich layer, that were tapped simultaneously from the underlying magma chamber. Some of the magma of the initial emplacement at Graig Lwyd was still molten, and mixed or hybridised with the incoming magma to form the Group 4 rocks. The movement and emplacement of magma entrained the thin, volatile rich layer breaking it up and forming the felsic segregations now present as irregularly shaped veins and pods within the central part of the intrusion. During transport and emplacement of the magma, fluid dynamic instabilities at the boundaries of the individual layers led to localised *in situ* mixing, smoothing out of the differences in magma compositions but preserving much of the original differences between the layers.

CHAPTER 15. CONCLUSION

15.1. Introduction

The objectives of this study were to use mineralogical and geochemical data from the Penmaenmawr Intrusion and to examine their variations within the intrusion in order to investigate its petrogenesis. This Chapter reviews and summarises the information and findings presented in the previous chapters.

15.2. Mineralogical differences within the Penmaenmawr Intrusion

The primary magmatic mineralogy of the Penmaenmawr Intrusion, presented in Chapters 4 and 5, includes plagioclase feldspar, orthopyroxene and clinopyroxene with accessory amounts of quartz, biotite, ilmenite and apatite. Petrographic examination shows that the rocks within the intrusion are variably altered, the most altered rocks occurring in the Central Quarries, the Graig Lwyd Quarries and along the southern border of the intrusion. In the most altered rocks plagioclase feldspar is completely albitised, orthopyroxene has altered to chlorite but clinopyroxene, although embayed, remains relatively unaltered. Accessory secondary minerals include quartz, alkali feldspar, titanite, prehnite, pumpellyite, epidote and axinite.

Differences in the mineralogy and the texture of samples collected from the intrusion have allowed the intrusion to be divided into four distinct petrographic groups, identified in this study as Groups 1, 2, 3 and 4. Rocks from Group 1 are very fine-grained and occur in the east of the intrusion and along the southern boundary. Rocks from Group 2 are fine- to medium-grained, contain more than 25% modal chlorite and occur in the central part of the intrusion. Rocks from Group 3 are also fine- to medium-grained, contain more than 15% modal orthopyroxene /amphibole and occur in the western and the northern part of the intrusion. Rocks from Group 4 contain both chlorite and fibrous amphibole, and some samples show characteristics of Group 2 rocks while others show characteristics of Group 3 rocks and occur in a small area in the north east of the intrusion.

Differences in mineral chemistry, presented in Chapter 5, support the division of the intrusion into the four groups. It also shows that, although differences in the compositions of unaltered plagioclase feldspar crystals of the least altered rocks of Group 3 and clinopyroxenes from most samples, could be indicative of primary magmatic processes, the main differences between the groups are largely due to alteration.

Further analysis, using magnetic susceptibility data, supports the separation of Group 3 rocks but the analysis was not able to distinguish between rocks from Groups 1, 2 and 4. It was suggested in Chapter 6 that the magnetic susceptibility values obtained in this investigation were associated with the degree of alteration of the rocks, confirming that Group 3 rocks are relatively unaltered whereas rocks from Groups 1, 2 and 4 are variably altered.

15.3. Alteration

The mineral data shows that alteration was most intense in the central part of the intrusion between NNW-SSE and NNE-SSW trending faults and shear zones, and along the southern boundary of the intrusion. The whole rock major and trace element suggests that although extensive alteration has taken place, the elements involved must have been relatively immobile on the scale of the whole rock sample and were generally incorporated into secondary minerals rather than being lost from the system.

Further analysis of the alteration phases and possible processes that could have caused the alteration suggests that the alteration took place in two episodes. The first episode occurred immediately following emplacement of the intrusion, when hot fluids originating from the cooling magma moved along the faults and shear zones locally altering orthopyroxene to tschermakitic amphibole, biotite to chlorite and depleting plagioclase feldspar in Na and in some instances completely altering it to alkali feldspar.

The second episode occurred as part of the Acadian metamorphic event of early to mid Devonian times when sub-greenschist facies conditions prevailed. In this episode amphibole and biotite were almost entirely altered to chlorite, plagioclase

feldspar was almost completely albitised, ilmenite and primary magnetite were altered to titanite, and prehnite, pumpellyite and epidote were formed; however, clinopyroxene remained largely unaffected. In the southern parts of the intrusion veins of quartz with prehnite formed, along with a few thin veins of axinite. The variable degree of alteration within the intrusion suggested that during the second alteration episode the NNW-SSE and NNE-SSW trending faults and shear zones were reactivated, allowing the ingress of fluids and that the source of the fluids was the dewatering of the sediments into which the intrusion had been emplaced.

15.4. Whole rock geochemical variation within the Penmaenmawr Intrusion

The main whole rock geochemical variation within the Penmaenmawr Intrusion is predominantly from north-west to south-east, with the more mafic rocks being located in the north-west and the more felsic rocks to the south-east. Additionally there does not appear to be any significant vertical geochemical variation within the intrusion. However, the geographic distribution of samples precludes a proper analysis of spatial variation in geochemistry.

Analysis of the major and trace element variation diagrams suggests that although the samples from the Penmaenmawr Intrusion are likely to be petrogenetically related, they are unlikely to be the result of the simple fractionation of a single body of magma. It was suggested in Chapter 10 that the trends would be consistent with two bodies of magma that fractionated independently of each other. The first body, represented by Group 2 and Group 3 rocks and involved the fractionation of plagioclase feldspar and orthopyroxene and/or clinopyroxene, while the second, represented by Group 1 and Group 4 rocks, involved the fractionation of plagioclase feldspar, orthopyroxene and/or clinopyroxene, iron-titanium oxides, apatite and possibly biotite.

The compatible and incompatible trace element plots support the suggestion that the intrusion could be separated into two evolving bodies of magma and that fractional crystallisation was the most likely cause of the geochemical variation observed in the Penmaenmawr Intrusion, although it did not completely rule out magma mixing. Vector diagrams indicate that plagioclase feldspar and orthopyroxene were the main phases being formed and removed

from the melt in an approximate ratio of 2:1 for Group 2 and 3 rocks and that plagioclase feldspar, orthopyroxene, possibly in different proportions, and probably magnetite/ilmenite were formed and removed from the melt for Group 1 rocks.

Subsequent major and trace element fractional crystallisation modelling, presented in Chapter 11, support the suggestion that the Penmaenmawr Intrusion is not the result of the crystallisation and differentiation of a single batch of magma. However, analysis of the fractional crystallisation modelling suggests that the Penmaenmawr Intrusion could be composed of several batches of magma that underwent fractional crystallisation autonomously and two possible models, described in this study as the separate batches of magma model and the progressive fractionation model, were proposed to account for the results of the modelling.

Modelling of magma mixing, presented in Chapter 12, confirm that magma mixing could not be a major cause of variations in geochemistry in the Penmaenmawr Intrusion but may account for some local variations. Analysis of the magma mixing models suggests that the variation in geochemistry of a sub-group of Group 3 rocks in the Western Quarries could have been developed by the magma mixing of two magmas, one more fractionally evolved than the other and that the variation in Group 4 rocks may be due to the mixing of Group 3 and Group 1 rocks.

A discussion of possible magmatic mechanisms and the data presented in this study allowed a preferred model for the magmatic evolution of the Penmaenmawr Intrusion to be developed, which is presented in Chapter 14. This model proposes that the primary variation in geochemistry within the Penmaenmawr Intrusion is due to the emplacement of two batches of magma from a larger underlying magma chamber undergoing fractional crystallisation where layered zones of different compositions had formed.

The initial emplacement, represented by the more evolved Group 1 rocks composed of a range of compositions, may have been, in part, in sheet form, forming the southern boundary of the intrusion and a larger mass in the east represented by rocks from the Graig Lwyd Quarries. The second emplacement,

represented by Group 2 and 3 rocks, was also composed of a range of compositions, from the underlying magma chamber. Some local mixing between the two batches of magma took place in the east, along the common boundary with the larger mass in the eastern part of the intrusion, resulting in the Group 4 rocks. Some localised mixing may also have taken place between the layered zones during the transport and emplacement of the second batch of magma.

It should be noted that the Groups used throughout this thesis are based on field and petrographic features and, that in general, this is separate from petrogenetic considerations.

15.5. The petrogenesis of the Penmaenmawr Intrusion

The Penmaenmawr Intrusion was emplaced into Lower Ordovician shales in early Caradoc times at about 450Ma. The intrusion is associated with the Llewelyn Volcanic Group, which erupted and formed a series of volcanic rocks in a back arc basin associated with the closure of the Iapetus Ocean.

The initial injections of magma, from an underlying, already fractionated magma chamber, were intruded into the planes of weakness within the country rocks and are represented by the very fine-grained rocks along the southern boundary of the Penmaenmawr Intrusion and the larger mass of very fine- to medium-grained rocks in the Graig Lwyd Quarries. The similar small plugs at Garreg Fawr and Dinas suggest that there may have been two or three small injections from the underlying magma chamber into the overlying shale country rocks. A subsequent, larger emplacement, probably following the path already prepared by the initial injection, took place at Penmaenmawr and locally mixed with the initial injection. Turbulence during emplacement also caused some localised internal mixing.

During the Caradoc volcanic episode, contemporaneous tectonic movement resulted in the development of faults and shear zones within the intrusion which were exploited by hydrothermal fluids generated from the cooling magmas and which locally altered the mineralogy of the adjacent intrusion rocks. A second episode of alteration occurred during the Acadian metamorphic event of early to

mid Devonian times, which reactivated the faults and shear zones and locally developed sub-greenschist facies mineral assemblages.

15.6. Future Work

Following the completion of this project three lines of investigation have been identified for any future study.

1. The variation in geochemistry within the Penmaenmawr Intrusion is due, in most parts, to processes taking place in an underlying magma chamber. The relationship between changes taking place in the underlying magma and the subsequent effect of those changes on a higher magma chamber could form a useful extension to this project. This could either involve a study of other high level intrusions, or collecting and analysing more samples from the Penmaenmawr Intrusion concentrating on boundary areas between the Groups and sub-groups identified during this project.
2. The major differences in mineralogy identified within the intrusion are due to different degrees of alteration. The alteration is considered to be associated with the faults and shear zones within the intrusion. In order to determine the relationship between fluid pathways and the degree of alteration a more detailed field investigation into the distribution and orientation of these faults and shear zones and the degree of alteration in the adjacent rocks could form a useful extension to this project.
3. It was reported in this thesis that rocks from the Penmaenmawr Intrusion contain segregations and inclusions. Samples were collected and analysed during this study; however, they were difficult to extract and analyse, and the discussion in Chapter 13 is based on a single example of each. In order to examine their role, if any, in the petrogenesis of the Penmaenmawr Intrusion a further investigation based on a more extensive examination of the segregations and inclusions could be carried out.

Appendix 1a. Model mineralogy.

(Size = average grain size (mm); %Ph = % of phenocrysts; Tot = total.

Alteration index: 1 = clear in plane light, good clear multiple twinning in cross polars; 2 = slightly turbid in plane light, clear multiple twinning in cross polars; 3 = turbid in plane light, clear outline in cross polars, multiple twinning visible but not clear; 4 = turbid in plane light, outline in cross polars but multiple twinning vague; 5 = very turbid in plane light, outline of mineral vague, no multiple cross twinning visible.

Group 1		Very fine-grained rocks							
		Average size (mm) of phenocryst minerals present							
Sample		Size	% Ph	Plag	Cpx	Amph	Chlor	Qtz	Opx
JD2912		0.05	< 10	1 (ghost)	0.5	0.1			
Observations	Calcite present in groundmass								
JD2901		0.04	< 5	0.5	0.5		0.5		
Observations	Calcite replacing								
JD2902		0.04	< 5	1.5	0.5				
Observations	Trace Pumpellyite								
JD2903		0.05	< 5	1.5	0.2	0.5	1.5		
Observations	Quartz glomerocrysts								
JD2913		0.05	< 5	1.5 (ghost)	1		0.5	0.5	
Observations									
JD2947		0.05	20	2	0.5	0.5 (yellow/brown)			0.5
Observations	Plag occurs as ghosts and as altered crystals, biotite present								
JD2968		0.04	10	1	0.8	0.25			0.25
Observations	Some glomerocrysts of cpx, opx and amph. Sphene present								
JD2969		0.04	5	1	0.5		0.25		
Observations	Plag occurs as ghosts and as altered crystals								
JD2958		0.04	< 5	1	1	0.5	0.5	1	
Observations	Biotite occurs as a phenocryst								
JD2959		0.03	< 5	2 (ghost)	0.8		0.5		
Observations	Glomerocrysts of cpx								
JD2957		0.025	< 5	2	0.8		0.3		
Observations	Opaque phenocrysts, cpx glomerocrysts, chlorite pseudomorph opx								
JD2966		0.05	< 5	1 (ghost)	1		1	1	
Observations	Cpx glomerocrysts								
JD2964		0.02	8	2 (ghost)	1	0.5			
Observations	Amphiboles euhedral, cpx glomerocrysts								
JD2965		0.02	< 5	1.5	0.2		0.2		
Observations									
JD2934		0.04	< 1	0.8 (ghost)	0.5			0.3	0.3
Observations									
JD2933		0.04	< 1	0.5 (ghost)	0.2		0.3		0.3
Observations	Opx altering to chlorite								

Group 1		Fine / medium-grained rocks							Alteration Index
		Modal mineralogy (%)							
Sample		Size	Plag	Cpx	Chl	O/Am	Qtz	Tot	
JD2904		0.1	55	15		20	10	100	3
Observations	Amphiboles not fibrous								
JD2905		0.14	45	15	30		10	100	3.5
Observations									
JD2914		0.1	50	10	30		10	100	3.5
Observations	Trace biotite associated with chlorite								
JD2917		0.25	40	10	25		25	100	3.5
Observations	Some large 2mm plag crystals								

Appendix 1a continued

<u>Group 1</u>		<u>Fine / medium-grained rocks</u>						<u>Alteration Index</u>
<u>Sample</u>	<u>Size</u>	<u>Modal mineralogy (%)</u>						
		<u>Plag</u>	<u>Cpx</u>	<u>Chl</u>	<u>O/Am</u>	<u>Qtz</u>	<u>Tot</u>	
JD2960	0.125	50	10	2	25	10	100	5
<i>Observations</i>	Amphiboles brownish green not fibrous, and embayed							
JD2967	0.08	55	8		22	15	100	5
<i>Observations</i>	Amphiboles brownish green not fibrous, and embayed							
JD2916	0.11	55	15	20		10	100	3.5
<i>Observations</i>								

<u>Group 2</u>		<u>Fine / medium-grained rocks</u>						<u>Alteration Index</u>
<u>Sample</u>	<u>Size</u>	<u>Modal mineralogy (%)</u>						
		<u>Plag</u>	<u>Cpx</u>	<u>Chl</u>	<u>O/Am</u>	<u>Qtz</u>	<u>Tot</u>	
JD2940	0.3-0.5	55	10	30		5	100	5
<i>Observations</i>	Quartz granophyric. Some chlorite in rectangular pseudomorphs							
JD2918	0.3-0.5	42	12	35		10	100	4
<i>Observations</i>								
JD2907	0.3-0.5	45	17	30		6	100	5
<i>Observations</i>	Green/brown amph bordering some cpx.							
JD2906	0.5-0.6	46	12	30		10	100	4
<i>Observations</i>	Some large (1mm) chlorite							
JD2908	0.2-0.4	44	12	34		10	100	4
<i>Observations</i>	Some small green/brown amphiboles							
JD2920	0.5-0.6	40	15	35		10	100	4
<i>Observations</i>	Chlorite occurs as rectangular pseudomorphs							
JD2935	0.4-0.5	47	8	35		10	100	4
<i>Observations</i>								
JD2919	0.5-0.6	45	8	37		10	100	4
<i>Observations</i>	Prehnite in feldspar.							

<u>Group 3</u>		<u>Fine / medium-grained rocks</u>						<u>Alteration Index</u>
<u>Sample</u>	<u>Size</u>	<u>Modal mineralogy (%)</u>						
		<u>Plag</u>	<u>Cpx</u>	<u>Chl</u>	<u>O/Am</u>	<u>Qtz</u>	<u>Tot</u>	
JD2923	0.2	33	20	tr	33	5	100	4
<i>Observations</i>	Biotite changing into chlorite/pumpellyite							
JD2925	0.25	33	22		30	5	100	2
<i>Observations</i>	Biotite changing into chlorite/pumpellyite, large elongate amphiboles							
JD2911	0.15	40	20	tr	33	5	100	2
<i>Observations</i>	Small dark green chlorite replacing biotite							
JD2909	0.2	40	23		30	5	100	3
<i>Observations</i>								
JD2921	0.1	40	20	tr	28	5	100	3
<i>Observations</i>								
JD2922	0.15	38	22		35	3	100	1.5
<i>Observations</i>	Some fine grain inclusions 5mm diameter.							
JD2963	0.1	50	10		35	1	100	2
<i>Observations</i>	Mainly opx							
JD2953	0.12	55	16		25	4	100	5
<i>Observations</i>	Amphibole not fibrous, but elongate up 2mm							
JD2961	0.08	55	15		25	5	100	2.5
<i>Observations</i>	Opx dominant							
JD2949	0.16	55	20		20	5	100	2.5
<i>Observations</i>	Biotite changing to chlorite							

Appendix 1a

Group 3

Fine / medium-grained rocks

Sample	Size	<i>Modal mineralogy (%)</i>						Alteration Index
		Plag	Cpx	Chl	O/Am	Qtz	Tot	
JD2952	0.1	55	15	tr	25	5	100	2.5
<i>Observations:</i>	Small cpx euhedral, larger ones anhedral							
JD2941	0.2	60	12		28	tr	100	1
<i>Observations:</i>	Large 2 mm plag crystals, granophyric quartz							
JD2938	0.2	60	12	tr	28		100	1
<i>Observations:</i>								
JD2936	0.18	60	12	tr	28	tr	100	1
<i>Observations:</i>	Some large plag crystals with altered centres							
JD2937	0.15	60	12	tr	28	tr	100	1
<i>Observations:</i>	Large square crystals of plag with altered centres							
JD2951	0.16	60	15		20	5	100	2.5
<i>Observations:</i>								
JD2946	0.1	60	15	tr	20	tr	100	1.5
<i>Observations:</i>	Brown/yellow amphibole altering to chlorite in centre							
JD2945	0.08	60	20		20	1	100	1
<i>Observations:</i>	Yellow/brown amphibole, replacing opx							
JD2948	0.14	60	15	tr	23	1	100	1
<i>Observations:</i>	Biotite changing to amphibole, chlorite in large 2mm plag							
JD2939	0.15	60	15	tr	25	tr	100	1
<i>Observations:</i>	Chlorite in centre of large plag crystals							
JD2955	0.1	60	15	tr	25	1	100	1
<i>Observations:</i>	Some fine grained inclusions 5mm							
JD2954	0.2	60	15		25	2	100	1
<i>Observations:</i>	Some large 3mm amphiboles.							
JD2956	0.08	65	12		18	5	100	2
<i>Observations:</i>	Small cpx euhedral, larger ones anhedral							
JD2942	0.2	65	10	tr	23	tr	100	1
<i>Observations:</i>	Chlorite in centre of large plag crystals							
JD2950	0.1	65	17	tr	17	1	100	1.5
<i>Observations:</i>	Some large crystals of plag and amph. Small opx with square outline							
JD2943	0.15	65	15	tr	20	tr	100	1
<i>Observations:</i>	Chlorite in centre of large plag crystals							
JD2944	0.18	66	12	tr	20	2	100	2
<i>Observations:</i>	Large 1 mm square opaque minerals							
JD2962	0.15	55	20	tr	20	tr	100	3
<i>Observations:</i>	Opx not fibrous							

Group 4

Fine / medium-grained rocks

Sample	Size	<i>Modal mineralogy (%)</i>						Alteration Index
		Plag	Cpx	Chl	O/Am	Qtz	Tot	
JD2932		35	20	33		10	100	3.5
<i>Observations:</i>	Some small brown amphiboles. Prehnite in feldspar							
JD2931		40	15	35		10	100	4
<i>Observations:</i>	Amphibole not fibrous possible changing to chlorite.							
JD2927		35	20	35		10	100	4
<i>Observations:</i>								
JD2930		35	15	5	25	20	100	4.5
<i>Observations:</i>	Some fine grain inclusions 5 mm in diam. Amphibole altered							
JD2928		30	25		30	13	100	2.5
<i>Observations:</i>	Biotite and pumpellyite interlayered.							

Appendix 1b Trace minerals.

(Opq = opaques; Ep = epidote; Ap = apatite; Bio = biotite; Pu = pumpellyite; Pre= prehnite; opx = orthopyroxene; Cal = calcite; Afs = alkali feldspar)

Group 1 Fine / medium grained

Sample	<u>Trace minerals</u>								
	Opq	Ep	Ap	Bio	Pu	Pre	Opx	Cal	Afs
JD2904	tr		tr		tr	tr			
JD2905	tr	tr	tr	tr	tr	tr			
JD2914	tr	tr	tr	tr					tr
JD2917	tr	tr	tr		tr	tr		tr	tr
JD2960	tr		tr	3	tr				
JD2967	tr		tr	tr	tr				
JD2916	tr	tr	tr		tr	tr			tr

Group 2 Fine / medium grained

Sample	<u>Trace minerals</u>								
	Opq	Ep	Ap	Bio	Pu	Pre	Opx	Cal	Afs
JD2940	tr	tr	tr		tr	tr			tr
JD2918	1	tr	tr		tr				1%
JD2907	tr	2	tr						tr
JD2906	tr	2	tr						tr
JD2908	tr	tr	tr						tr
JD2920	tr		tr						tr
JD2935	tr		tr					tr	tr
JD2919	tr	tr	tr			tr		tr	2%

Group 3 Fine / medium grained

Sample	<u>Trace minerals</u>								
	Opq	Ep	Ap	Bio	Pu	Pre	Opx	Cal	Afs
JD2923	tr	1	tr	1%	1%				5%
JD2925	tr		tr	5%	tr		tr		5%
JD2911	tr		tr	tr					2%
JD2909	tr		tr				tr		2%
JD2921	tr		tr	2%	Tr				5%
JD2922	tr		tr	tr	Tr				2%
JD2963	tr		tr	5%		tr			
JD2953	tr	tr	tr			tr			tr
JD2961	tr		tr	2%					
JD2949	tr		tr	tr					
JD2952	tr		tr				tr		tr
JD2941	tr			tr			tr		
JD2938	tr			1%			tr		
JD2936	tr			tr			tr		tr
JD2937	tr			tr			tr		
JD2951	tr		tr	tr					
JD2946	tr			5%			tr		
JD2945	tr		tr	1%			tr		
JD2948	tr		tr	1%			tr		tr
JD2939	tr			tr			tr		
JD2955	tr		tr	tr			tr		
JD2954	tr		tr	tr			tr		
JD2956	tr		tr	tr			tr		tr
JD2942	tr			2%			tr		
JD2950	tr		tr	tr			tr		
JD2943	tr		tr	1%			tr		
JD2944	tr		tr	tr					
JD2962	tr		tr	5%					

Appendix 1b (cont)

Group 4

Sample	Opq	Ep	Ap	<i>Trace minerals</i>		Pre	Opx	Cal	Afs
				Bio	Pu				
JD2932	tr	2%	tr			tr	tr		
JD2931	tr	tr	tr		Tr				
JD2927	tr	tr			Tr				
JD2930	tr	tr	tr		Tr			tr	
JD2928	tr		tr	1%	1%		tr		

Vein

JD2915 Small quartz crystals 0.6mm
 Glomerocrysts of quartz 2mm
 Pumpellyite around quartz glomerocrysts
 Some grains with fine radiating granophyric texture

Appendix 2.

Description and photomicrographs of representative samples from the Penmaenmawr Intrusion.

1. Sample JD2936 from the Western Quarries (Group 3)

These photomicrographs show a central euhedral crystal of clinopyroxene surrounded by plagioclase laths; other clinopyroxene crystals are easily seen because of their bright interference colours in crossed polarised light. The brown, elongate crystals in plane polarised light are orthopyroxene, partially replaced by fibrous amphibole. Small, brown biotite crystals can be seen in plane polarised light towards the upper right hand side and close to the bottom edge of the photomicrographs.

2. Sample JD2951 from the northern Central Quarries (Group 3)

The prominent green rectangular crystals are fibrous amphibole, which have replaced orthopyroxene, and the brown crystals, showing second-order interference colours in crossed polarised light, are clinopyroxene. Plagioclase feldspar crystals are turbid in plane polarised light and, in crossed polarised light, the multiple twinning, is less clear. Small crystals of alkali feldspar can be seen towards the bottom edge of the photomicrograph showing sharp, well-defined crystal faces.

3. Sample JD2918 from the Central Quarries (Group 2)

The pale-green irregular shapes in plane polarised light are chlorite and the dark-brown crystals, showing higher order interference colours in crossed polarised light, are clinopyroxene. Crystals of plagioclase feldspar form brown turbid masses in plane polarised light but some rectangular crystals can be recognised by fragments of multiple twinning in crossed polarised light. Crystals of quartz can be seen in the upper part of the photomicrographs, distinguished by their lack of turbidity.

4. Samples JD2934 and JD2912 from the Graig Lwyd Quarries (Group1)

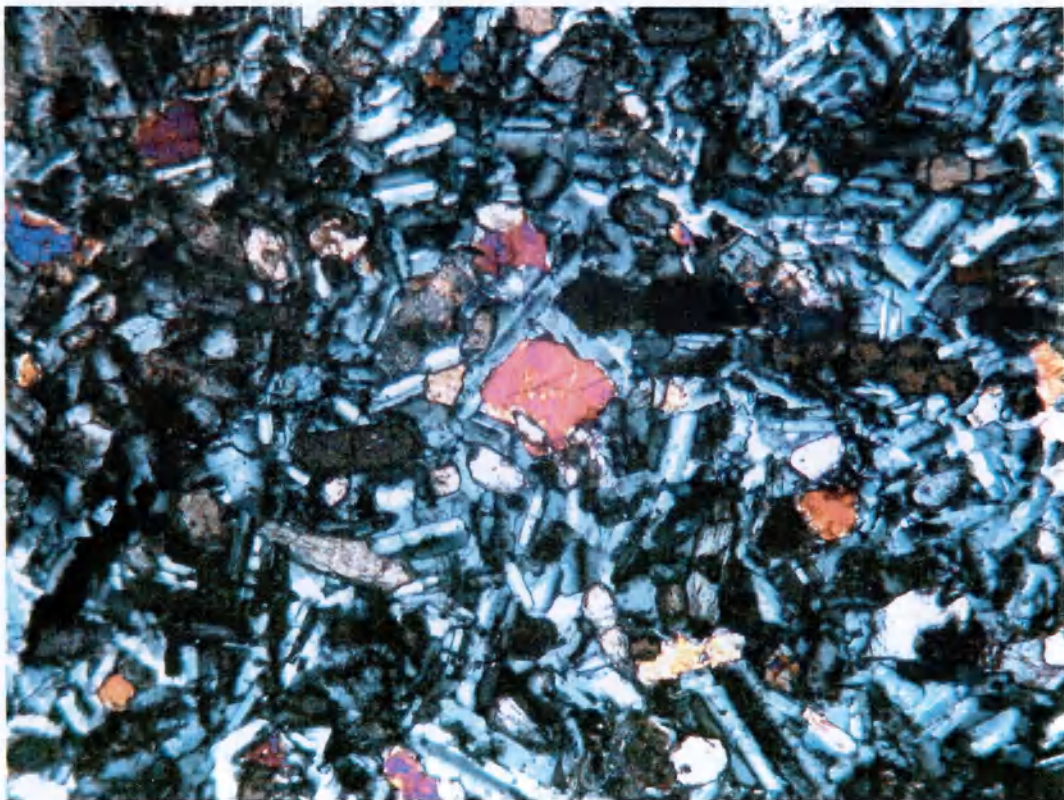
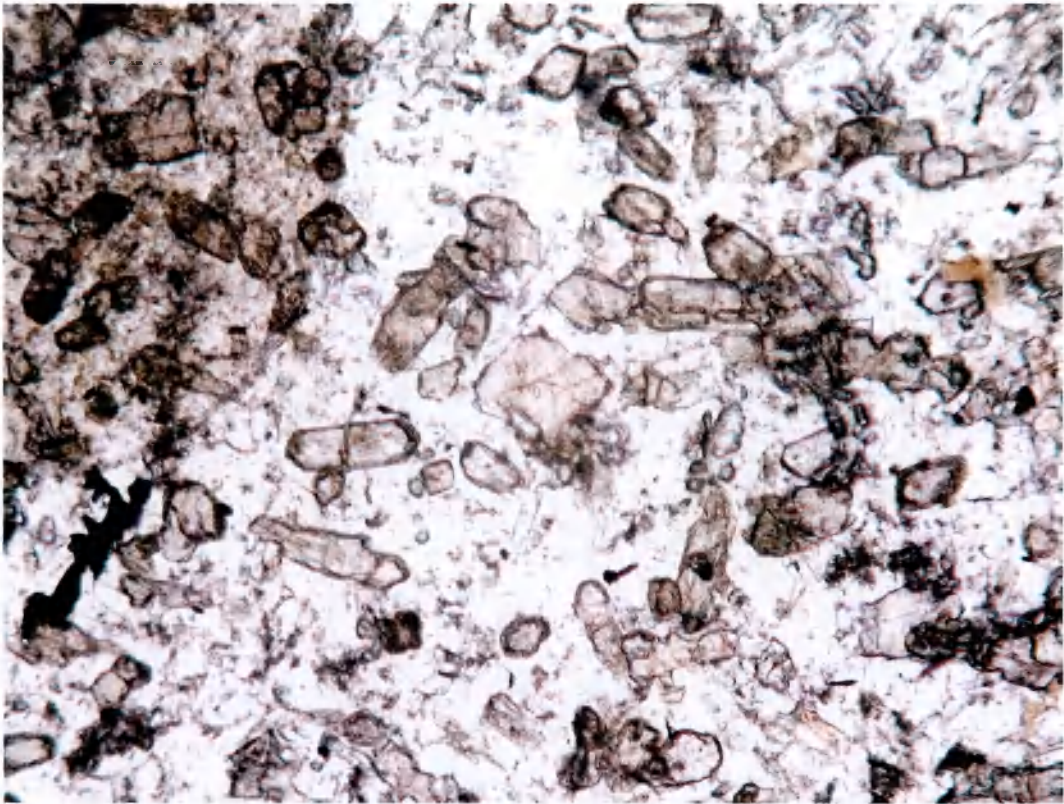
These photomicrographs show rectangular phenocrysts of plagioclase feldspar, filled with dark indeterminate material set in a fine-grained matrix, while in the top photomicrograph the smaller dark crystals are clinopyroxene.

5. Sample JD2932 from the small quarries north-west of the Graig Lwyd Quarries (Group 4)

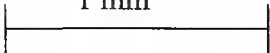
These photomicrographs show a large (2 mm) rectangular crystal of plagioclase feldspar in the centre surrounded by pale green (in plane polarised light) irregular shapes of chlorite and other brown, turbid masses. There is a brown, almost rectangular crystal of clinopyroxene showing bright interference colours in cross polarised light in the top left hand corner and a number of small brown to green crystals of amphibole showing yellow-brown colours and colourless patches in cross polarised light. Crystals of quartz can be seen in the centre of the photomicrographs towards the top and bottom margins.

6. Sample JD2926, a segregation from the Central Quarries

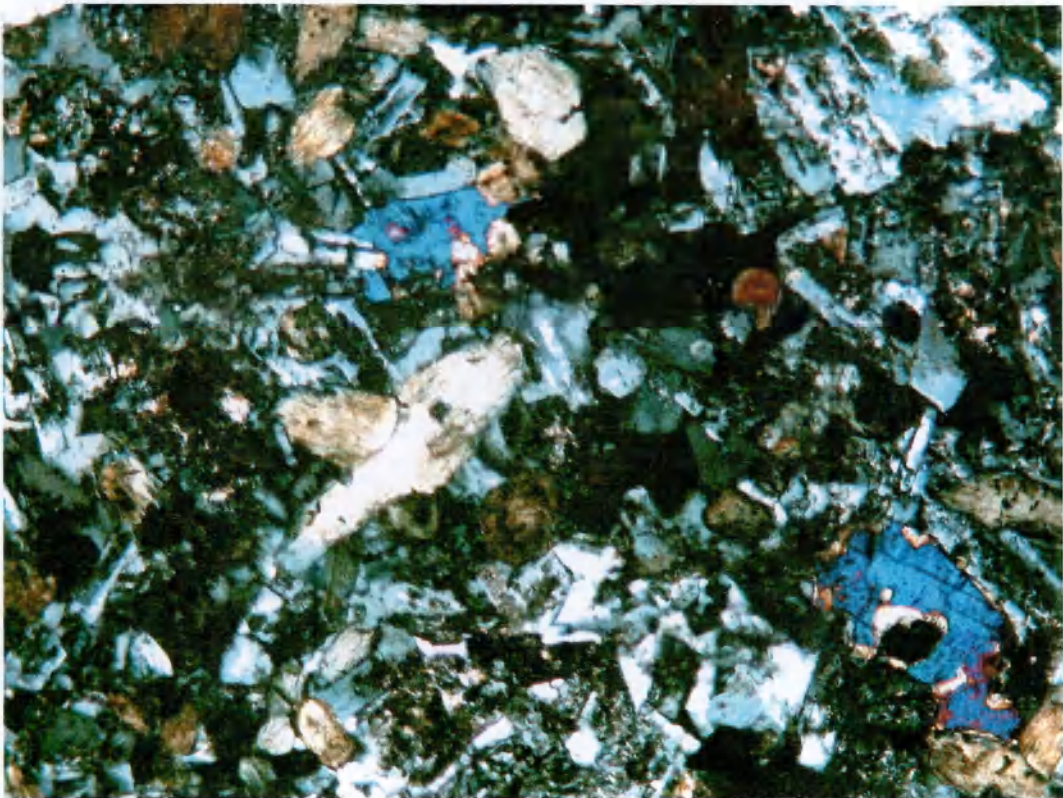
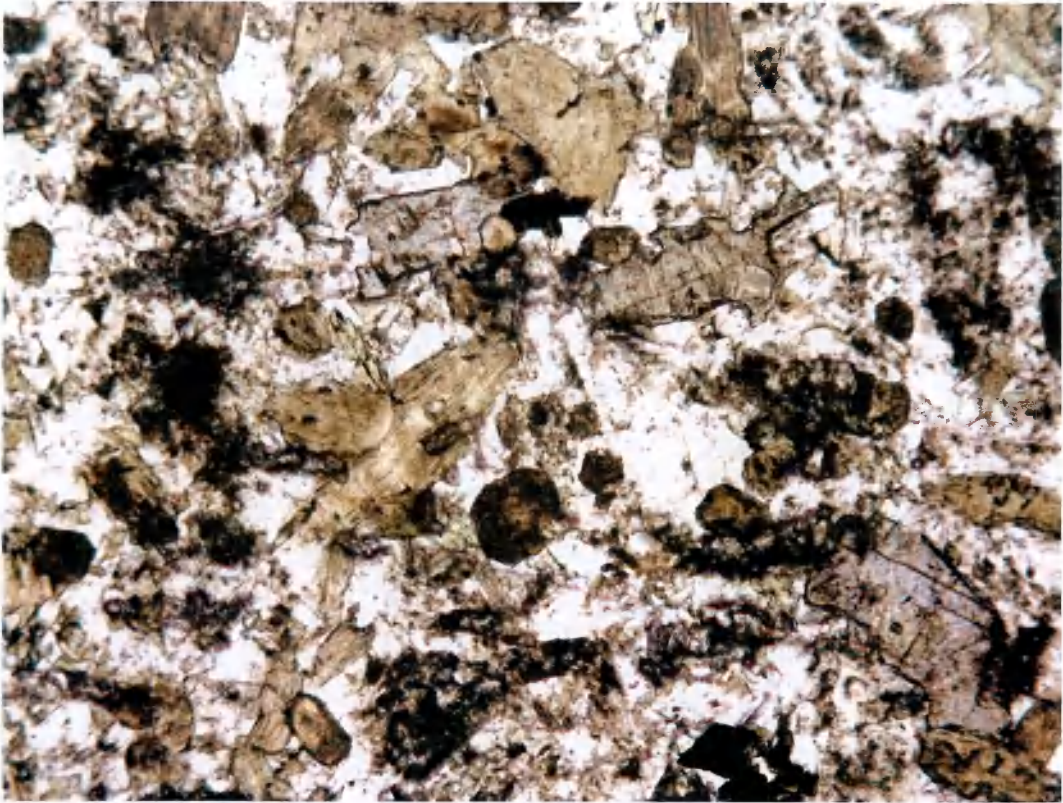
A large crystal of granophyric quartz can be seen in the bottom left hand corner and a large crystal of clinopyroxene being replaced by chlorite accounts for much of the right hand side of the photomicrographs. An almost square crystal of titanite can be seen at the bottom margin.



Scale 1 mm



Appendix 2 (continued) Photomicrographs of sample JD2936 from the Western Quarries (Group 3). Upper in plane polarised light, lower in crossed polarised light.

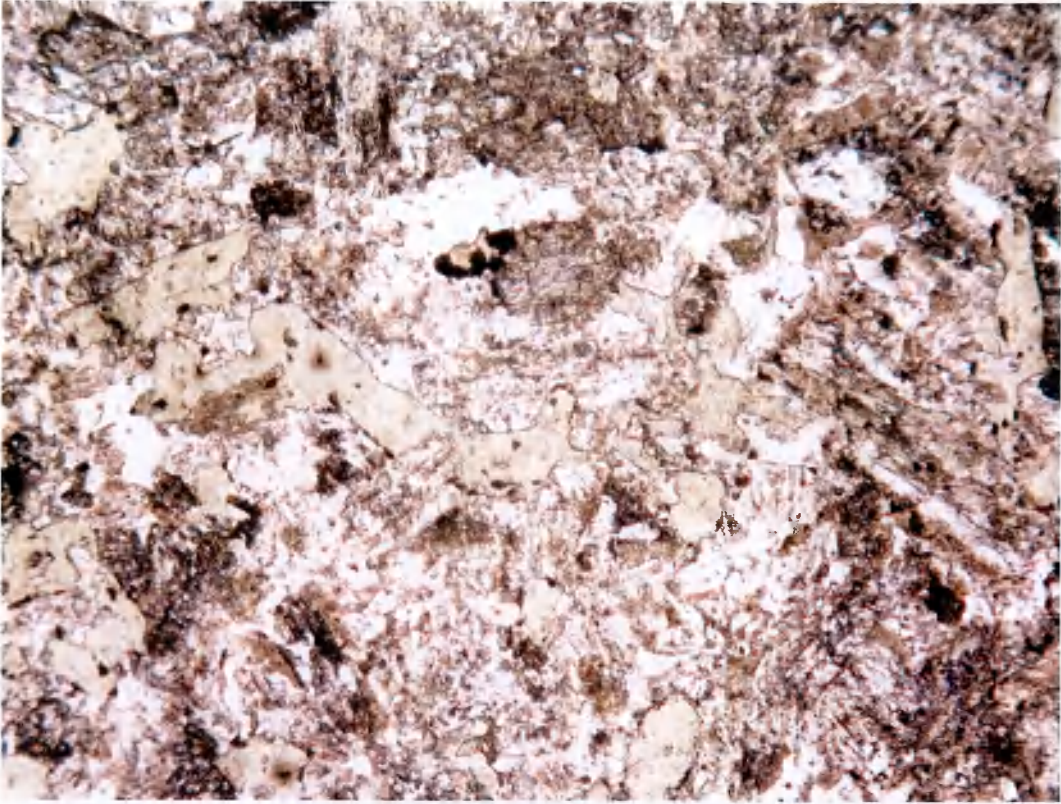


Scale


1mm



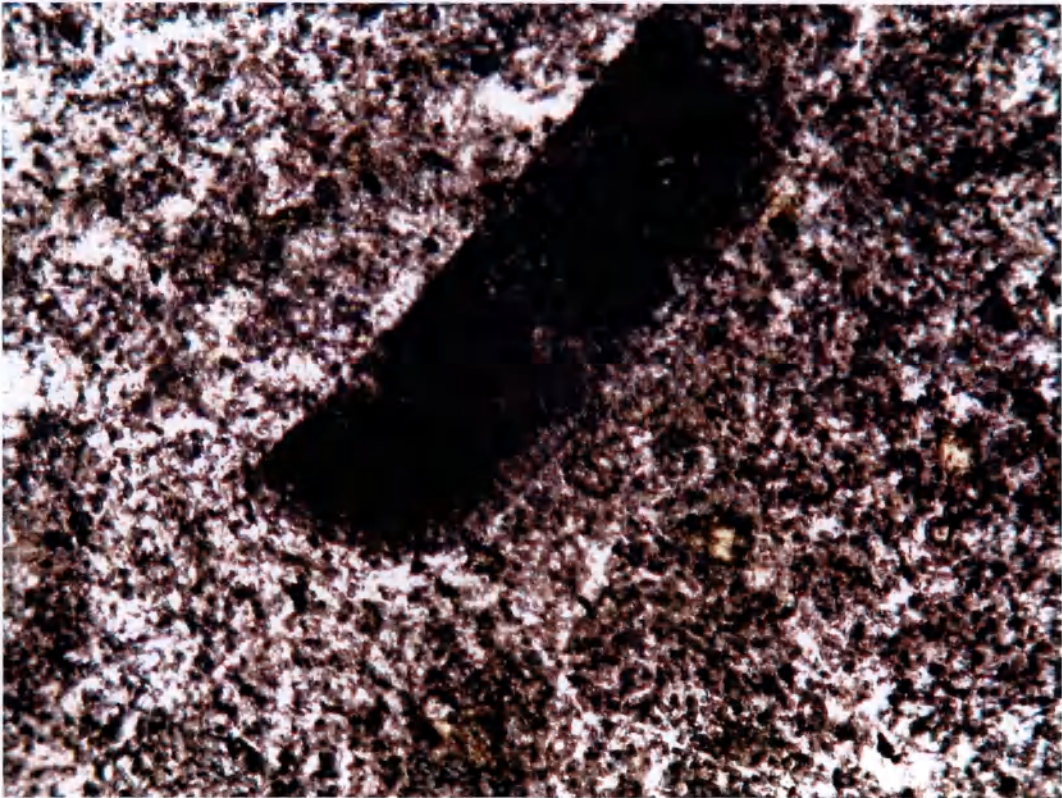
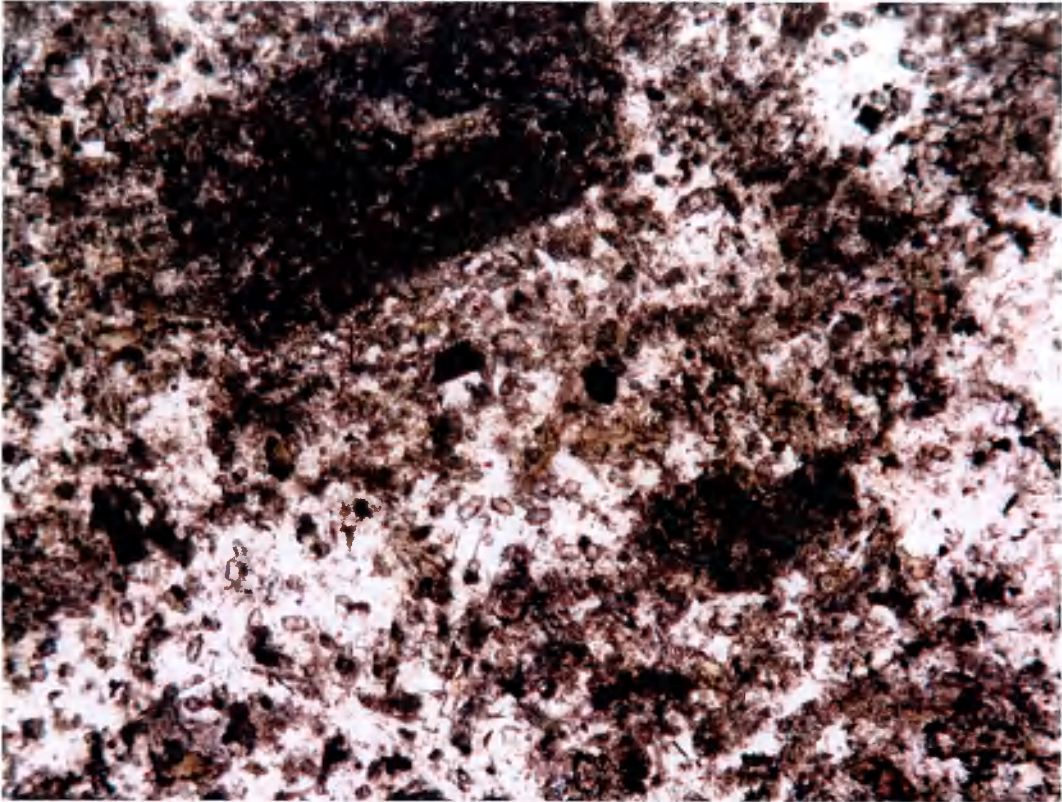
Appendix 2 (continued) Photomicrograph of sample JD2951 from the northern Central Quarries (Group 3). Upper in plane polarised light, lower in crossed polarised light.



Scale 1mm



Appendix 2 (continued) Photomicrograph of sample JD2918 from the main Central Quarries (Group 2). Upper in plane polarised light, lower in crossed polarised light.

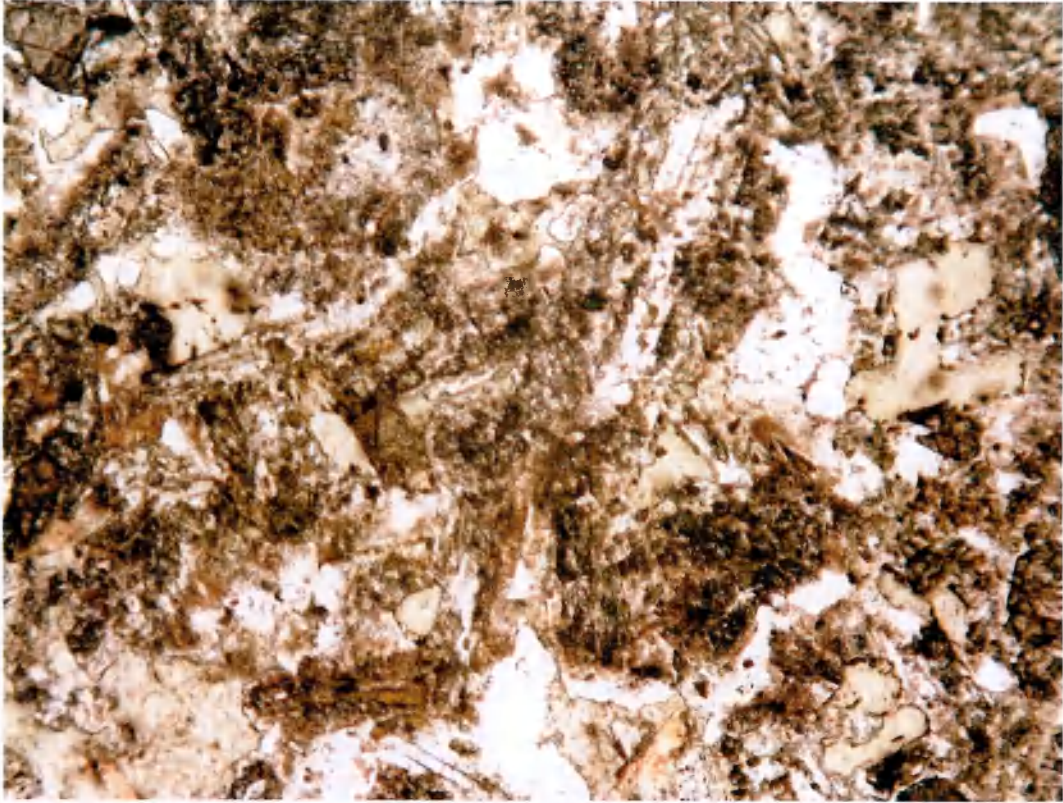


Scale

1mm

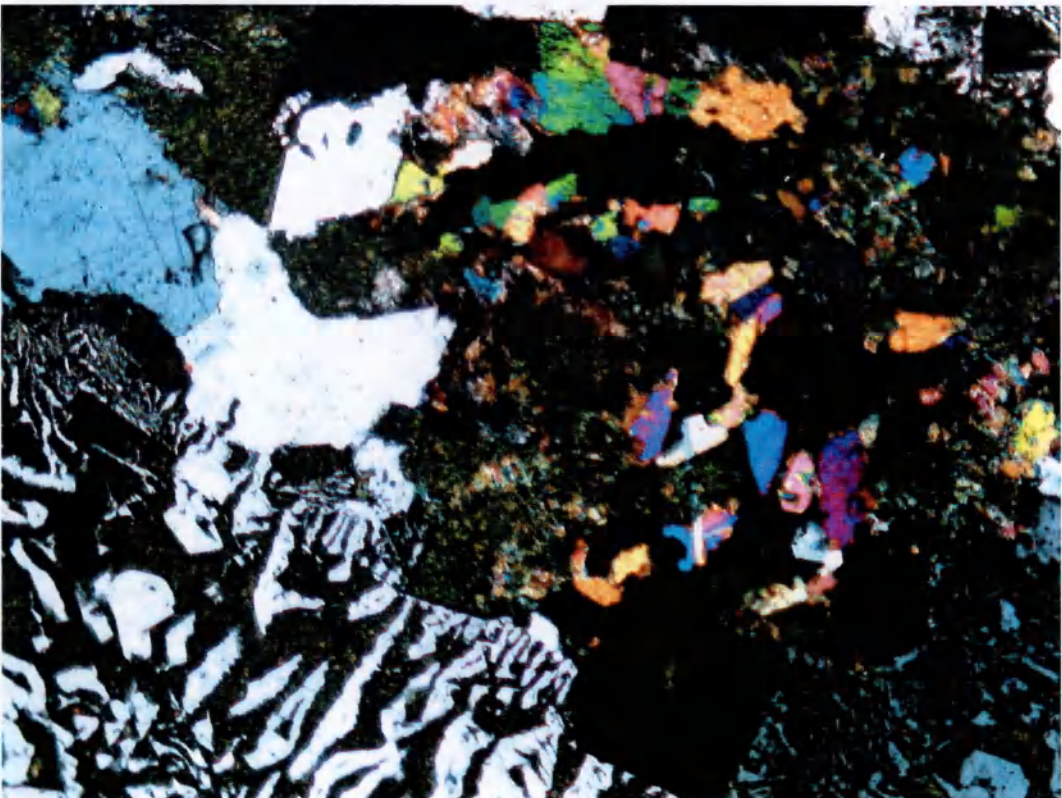


Appendix 2 (continued) Photomicrographs of samples JD2934 (Upper) and JD2912 (Lower) from the Graig Lwyd Quarries (Group 1). Plane polarised light.



Scale 1mm

Appendix 2 (continued). Photomicrograph of sample JD2932 from the Quarries north-west of the Graig Lwyd Quarries (Group 4). Upper in plane polarised light, lower in crossed polarised light.



Scale |-----| 1mm

Appendix 2 (continued). Photomicrograph of sample JD2926, a segregation from the Central Quarries. Upper in plane polarised light, lower in crossed polarised light.

Appendix 3. Electron Microprobe Operating Details and Standards.

Cambridge Instrument Mark 9 and Cameca SX100

20kV, 20 nA probe current, defocused beam of 10 microns
Count times are based on accumulating 40,000 counts at the 10% concentration level. This ensures all elements have equivalent quality Count times vary from 15 to 80 seconds

Calibration Standards

P ₂ O ₅	Apatite
SiO ₂	K feldspar
TiO ₂	Rutile
Al ₂ O ₃	K Feldspar
FeO	Hematite
MnO	Bustamite
MgO	Forsterite
CaO	Bustamite
Na ₂ O	Jadeite
K ₂ O	K Feldspar
SrO	Synthetic SrTiO ₃
BaO	Barite
Y ₂ O ₃	Synthetic Y ₂ O ₃
Cr ₂ O ₃	Crocoite
NiO	Metal
ZnO	Willemite
ThO ₂	Synthetic ThO ₂
UO ₂	Synthetic ThO ₂
Cl	Synthetic KCl
F	Synthetic LiF

Appendix 4. Mineral Chemistry
Plagioclase Feldspar

Wt%	Group 1					
	2914ba	2914aq	2914al	2914as	2947ae	2947ae
SiO ₂	68.28	68.30	68.37	68.98	50.46	57.14
TiO ₂	0.06	0.00	0.00	0.02	0.03	0.00
Al ₂ O ₃	19.39	19.48	19.63	19.57	30.32	25.51
MgO	0.00	0.05	0.00	0.00	0.04	0.02
CaO	0.39	0.26	0.37	0.13	14.79	8.46
MnO	0.01	0.00	0.00	0.00	0.01	0.01
FeO	0.10	0.15	0.04	0.04	0.81	0.22
Na ₂ O	11.76	11.56	11.84	11.81	3.42	6.63
K ₂ O	0.03	0.04	0.07	0.04	0.17	0.58
P ₂ O ₅	0.00	0.00	0.01	0.00	0.02	0.01
TOTAL	100.02	99.84	100.33	100.59	100.07	98.58

Atomic proportions recalculated on the basis of 8 oxygens

Si	2.987	2.989	2.982	2.995	2.309	2.604
Ti	0.002	0.000	0.000	0.001	0.001	0.000
Al	1.000	1.005	1.009	1.002	1.636	1.371
Mg	0.000	0.003	0.000	0.000	0.003	0.001
Ca	0.018	0.012	0.017	0.006	0.725	0.413
Mn	0.000	0.000	0.000	0.000	0.000	0.000
Fe	0.005	0.007	0.002	0.002	0.040	0.011
Na	0.997	0.981	1.001	0.994	0.303	0.586
K	0.002	0.002	0.004	0.002	0.010	0.034
P	0.000	0.000	0.000	0.000	0.001	0.000

% End members

An	1.8	1.2	1.7	0.6	69.8	40.0
Ab	98.0	98.6	97.9	99.2	29.2	56.7
Or	0.2	0.2	0.4	0.2	1.0	3.3

Wt%	Group 1		
	2912EJA	2917NJB	2917CJB
SiO ₂	59.06	67.54	67.84
TiO ₂	0.04	0.02	0.04
Al ₂ O ₃	25.07	19.55	19.37
MgO	0.02	0.02	0.34
CaO	7.47	0.92	0.44
MnO	0.02	0.02	0.03
FeO	0.35	0.13	1.00
Na ₂ O	7.01	11.11	11.02
K ₂ O	0.39	0.08	0.02
P ₂ O ₅			
TOTAL	99.43	99.39	100.10

Atomic proportions recalculated on the basis of 8 oxygens

Si	2.655	2.974	2.969
Ti	0.001	0.001	0.001
Al	1.328	1.015	1.000
Mg	0.001	0.001	0.022
Ca	0.360	0.043	0.021
Mn	0.001	0.001	0.001
Fe	0.017	0.006	0.047
Na	0.611	0.949	0.935
K	0.022	0.004	0.001
P	0.000	0.000	0.000

% End members

An	36.3	4.3	2.2
Ab	61.5	95.3	97.7
Or	2.2	0.4	0.1

Appendix 4.

Plagioclase Feldspar (continued)

Group 2

Wt%	<u>2924ah</u>	<u>2924co</u>	<u>2924cf</u>	<u>2926al</u>
SiO ₂	64.47	67.88	68.30	68.00
TiO ₂	0.01	0.00	0.00	0.00
Al ₂ O ₃	21.43	20.73	20.40	19.41
MgO	0.00	0.06	0.00	0.00
CaO	2.98	0.80	0.86	0.14
MnO	0.00	0.00	0.01	0.00
FeO	0.06	0.34	0.12	0.04
Na ₂ O	10.13	11.47	11.41	11.74
K ₂ O	0.67	0.07	0.08	0.04
P ₂ O ₅	0.00	0.01	0.01	0.01
TOTAL	99.75	101.36	101.18	99.37

Atomic proportions recalculated on the basis of 8 oxygens

Si	2.860	2.937	2.956	2.990
Ti	0.000	0.000	0.000	0.000
Al	1.121	1.057	1.041	1.006
Mg	0.000	0.004	0.000	0.000
Ca	0.142	0.037	0.040	0.007
Mn	0.000	0.000	0.000	0.000
Fe	0.003	0.016	0.006	0.002
Na	0.871	0.962	0.957	1.001
K	0.038	0.004	0.004	0.002
P	0.000	0.000	0.000	0.000

% End members

An	13.5	3.7	4.0	0.7
Ab	82.9	95.9	95.6	99.1
Or	3.6	0.4	0.4	0.2

Group 3

Wt%	<u>2936au</u>	<u>2936ae</u>	<u>2936ar</u>	<u>2936an</u>	<u>2936af</u>	<u>2936am</u>	<u>2936ak</u>
SiO ₂	49.55	51.66	52.20	52.35	52.52	52.55	52.84
TiO ₂	0.05	0.07	0.05	0.06	0.07	0.06	0.07
Al ₂ O ₃	30.42	28.91	29.09	28.07	29.10	28.18	28.59
MgO	0.02	0.02	0.02	0.03	0.02	0.01	0.02
CaO	14.81	13.00	13.06	12.19	12.89	12.01	12.36
MnO	0.00	0.00	0.01	0.02	0.01	0.01	0.02
FeO	0.59	0.54	0.57	0.55	0.47	0.41	0.50
Na ₂ O	3.23	4.21	4.25	4.71	4.34	4.71	4.60
K ₂ O	0.16	0.21	0.24	0.28	0.24	0.20	0.23
P ₂ O ₅	0.01	0.00	0.00	0.01	0.01	0.02	0.00
TOTAL	98.83	98.62	99.47	98.26	99.67	98.16	99.22

Atomic proportions recalculated on the basis of 8 oxygens

Si	2.295	2.385	2.389	2.422	2.396	2.429	2.419
Ti	0.002	0.002	0.002	0.002	0.002	0.002	0.003
Al	1.661	1.573	1.569	1.531	1.565	1.536	1.543
Mg	0.001	0.001	0.001	0.002	0.001	0.001	0.001
Ca	0.735	0.643	0.640	0.605	0.630	0.595	0.606
Mn	0.000	0.000	0.000	0.001	0.000	0.000	0.001
Fe	0.029	0.027	0.028	0.027	0.023	0.021	0.024
Na	0.290	0.377	0.377	0.423	0.384	0.422	0.408
K	0.010	0.012	0.014	0.016	0.014	0.012	0.013
P	0.000	0.000	0.000	0.000	0.000	0.001	0.000

% End members

An	71.0	62.3	62.1	58.0	61.3	57.8	59.0
Ab	28.0	36.5	36.6	40.5	37.4	41.0	39.7
Or	1.0	1.2	1.4	1.5	1.4	1.2	1.3

Appendix 4.

Plagioclase Feldspar (continued)

Group 3

Wt%	2948ag	2948bl	2948ap	2948bm	2948by	2948ai	2948bj
SiO ₂	51.80	52.37	52.57	52.82	52.92	53.25	53.36
TiO ₂	0.06	0.07	0.06	0.06	0.10	0.05	0.08
Al ₂ O ₃	28.37	28.34	27.98	28.29	28.60	28.82	27.69
MgO	0.02	0.01	0.02	0.02	0.03	0.03	0.00
CaO	12.63	12.31	12.15	12.41	12.32	12.50	11.92
MnO	0.00	0.00	0.01	0.00	0.00	0.01	0.00
FeO	0.54	0.47	0.53	0.46	0.45	0.49	0.49
Na ₂ O	4.43	4.57	4.59	4.60	4.60	4.70	4.94
K ₂ O	0.23	0.22	0.26	0.26	0.24	0.23	0.26
P ₂ O ₅	0.03	0.01	0.01	0.02	0.02	0.00	0.01
TOTAL	98.11	98.37	98.17	98.93	99.28	100.07	98.73

Atomic proportions recalculated on the basis of 8 oxygens

Si	2.402	2.418	2.431	2.425	2.420	2.418	2.452
Ti	0.002	0.002	0.002	0.002	0.003	0.002	0.003
Al	1.551	1.542	1.525	1.531	1.542	1.542	1.500
Mg	0.002	0.001	0.002	0.002	0.002	0.002	0.000
Ca	0.627	0.609	0.602	0.611	0.604	0.608	0.587
Mn	0.000	0.000	0.000	0.000	0.000	0.000	0.000
Fe	0.027	0.023	0.026	0.022	0.022	0.024	0.024
Na	0.398	0.409	0.411	0.409	0.407	0.414	0.440
K	0.014	0.013	0.015	0.015	0.014	0.013	0.015
P	0.001	0.000	0.001	0.001	0.001	0.000	0.000

% End members

An	60.3	59.1	58.6	59.0	58.9	58.7	56.3
Ab	38.3	39.7	40.0	39.5	39.7	40.0	42.2
Or	1.3	1.3	1.5	1.4	1.4	1.3	1.4

Group 3

Wt%	2948bo	2948af	2948bw	2948bf	2948bz	2948ar	2948br
SiO ₂	53.47	53.54	53.67	53.92	53.93	54.73	55.50
TiO ₂	0.07	0.07	0.07	0.07	0.06	0.08	0.03
Al ₂ O ₃	27.97	28.48	27.98	27.22	28.24	26.60	26.33
MgO	0.02	0.01	0.03	0.03	0.03	0.01	0.02
CaO	11.81	12.00	11.77	11.01	12.07	10.28	9.88
MnO	0.00	0.00	0.00	0.00	0.01	0.01	0.01
FeO	0.52	0.50	0.47	0.49	0.48	0.41	0.49
Na ₂ O	4.89	4.86	4.93	5.39	4.89	5.81	5.85
K ₂ O	0.30	0.28	0.28	0.30	0.29	0.33	0.39
P ₂ O ₅	0.02	0.02	0.00	0.02	0.02	0.04	0.02
TOTAL	99.07	99.76	99.21	98.44	100.01	98.28	98.52

Atomic proportions recalculated on the basis of 8 oxygens

Si	2.448	2.435	2.453	2.480	2.447	2.516	2.541
Ti	0.003	0.002	0.002	0.002	0.002	0.003	0.001
Al	1.510	1.527	1.507	1.476	1.510	1.442	1.421
Mg	0.001	0.001	0.002	0.002	0.002	0.001	0.002
Ca	0.580	0.585	0.576	0.542	0.587	0.506	0.484
Mn	0.000	0.000	0.000	0.000	0.000	0.000	0.000
Fe	0.025	0.024	0.023	0.024	0.023	0.020	0.024
Na	0.434	0.428	0.437	0.481	0.430	0.517	0.519
K	0.017	0.016	0.017	0.018	0.017	0.019	0.023
P	0.001	0.001	0.000	0.001	0.001	0.002	0.001

% End members

An	56.3	56.9	55.9	52.1	56.8	48.6	47.2
Ab	42.1	41.6	42.4	46.2	41.6	49.6	50.6
Or	1.6	1.6	1.7	1.7	1.6	1.8	2.2

Appendix 4.
Plagioclase Feldspar (continued)

Group 3

Wt%	2956bc	2956aq	2956an	2956bh	2956ao	2956bi	2956ae
SiO ₂	53.02	53.14	53.17	53.43	53.48	53.89	54.56
TiO ₂	0.05	0.04	0.07	0.05	0.06	0.07	0.07
Al ₂ O ₃	28.90	28.91	28.67	28.54	28.93	28.49	27.79
MgO	0.03	0.01	0.02	0.01	0.02	0.02	0.01
CaO	12.84	12.53	12.82	12.44	12.31	12.03	11.15
MnO	0.01	0.00	0.01	0.00	0.00	0.00	0.01
FeO	0.58	0.47	0.64	0.43	0.46	0.43	0.30
Na ₂ O	4.50	4.64	4.56	4.66	4.74	4.91	5.38
K ₂ O	0.23	0.23	0.27	0.21	0.18	0.26	0.17
P ₂ O ₅	0.00	0.00	0.03	0.02	0.01	0.00	0.01
TOTAL	100.15	99.96	100.25	99.79	100.18	100.11	99.43

Atomic proportions recalculated on the basis of 8 oxygens

Si	2.408	2.415	2.413	2.430	2.422	2.441	2.480
Ti	0.002	0.001	0.002	0.002	0.002	0.002	0.002
Al	1.547	1.549	1.534	1.530	1.545	1.522	1.489
Mg	0.002	0.001	0.001	0.001	0.001	0.002	0.000
Ca	0.625	0.610	0.624	0.606	0.597	0.584	0.543
Mn	0.000	0.000	0.000	0.000	0.000	0.000	0.000
Fe	0.028	0.023	0.031	0.021	0.022	0.021	0.014
Na	0.397	0.408	0.402	0.411	0.416	0.431	0.474
K	0.013	0.014	0.015	0.012	0.010	0.015	0.010
P	0.000	0.000	0.001	0.001	0.000	0.000	0.001

% End members

An	60.4	59.1	59.9	58.9	58.4	56.7	52.9
Ab	38.4	39.5	38.6	39.9	40.7	41.8	46.2
Or	1.3	1.4	1.4	1.2	1.0	1.5	1.0

Group 3

Wt%	2956bm	2956bj	2952ac	2952af
SiO ₂	56.39	56.58	55.08	56.87
TiO ₂	0.07	0.09	0.09	0.07
Al ₂ O ₃	27.05	26.76	27.52	26.54
MgO	0.02	0.02	0.03	0.03
CaO	10.32	9.88	10.92	9.82
MnO	0.00	0.00	0.00	0.00
FeO	0.46	0.54	0.51	0.54
Na ₂ O	6.03	6.00	5.38	6.11
K ₂ O	0.24	0.32	0.28	0.34
P ₂ O ₅	0.03	0.03	0.02	0.03
TOTAL	100.61	100.22	99.83	100.35

Atomic proportions recalculated on the basis of 8 oxygens

Si	2.529	2.544	2.494	2.554
Ti	0.002	0.003	0.003	0.002
Al	1.430	1.419	1.469	1.405
Mg	0.001	0.001	0.002	0.002
Ca	0.496	0.476	0.530	0.473
Mn	0.000	0.000	0.000	0.000
Fe	0.022	0.026	0.025	0.026
Na	0.525	0.523	0.473	0.532
K	0.014	0.019	0.016	0.020
P	0.001	0.001	0.001	0.001

% End members

An	47.9	46.8	52.0	46.1
Ab	50.7	51.4	46.4	51.9
Or	1.4	1.9	1.6	2.0

Appendix 4
Plagioclase Feldspar (continued)

Group 3

Wt%	<u>2909am</u>	<u>2909ao</u>	<u>2909ap</u>	<u>2909ca</u>	<u>2909ax</u>
SiO ₂	58.40	58.29	60.29	53.31	61.37
TiO ₂	0.03	0.03	0.05	0.04	0.01
Al ₂ O ₃	24.49	24.37	23.42	28.25	23.34
MgO	0.01	0.01	0.01	0.02	0.08
CaO	7.60	7.30	5.79	11.92	5.51
MnO	0.01	0.01	0.00	0.00	0.00
FeO	0.61	0.43	0.39	0.50	0.18
Na ₂ O	7.29	7.22	7.87	4.88	8.53
K ₂ O	0.51	0.50	0.81	0.29	0.38
P ₂ O ₅	0.02	0.02	0.00	0.01	0.01
TOTAL	98.97	98.18	98.63	99.22	99.41

Atomic proportions recalculated on the basis of 8 oxygens

Si	2.648	2.659	2.727	2.438	2.746
Ti	0.001	0.001	0.002	0.001	0.000
Al	1.309	1.310	1.249	1.523	1.231
Mg	0.001	0.001	0.001	0.001	0.005
Ca	0.369	0.357	0.281	0.584	0.264
Mn	0.000	0.000	0.000	0.000	0.000
Fe	0.030	0.021	0.019	0.025	0.009
Na	0.641	0.639	0.690	0.433	0.740
K	0.030	0.029	0.047	0.017	0.022
P	0.001	0.001	0.000	0.000	0.000

% End members

An	35.5	34.8	27.6	56.5	25.7
Ab	61.6	62.3	67.8	41.9	72.1
Or	2.9	2.8	4.6	1.6	2.1

Group 3

Wt%	<u>2923JRD</u>	<u>2923JND</u>	<u>2923JPD</u>
SiO ₂	54.72	58.42	65.92
TiO ₂	0.08	0.08	0.02
Al ₂ O ₃	28.19	25.97	21.18
MgO	0.00	0.00	0.02
CaO	11.36	8.10	2.50
MnO	0.02	0.00	0.03
FeO	0.39	0.46	0.20
Na ₂ O	4.96	6.57	9.96
K ₂ O	0.28	0.38	0.19
P ₂ O ₅			
TOTAL	100.00	99.98	100.02

Atomic proportions recalculated on the basis of 8 oxygens

Si	2.473	2.616	2.897
Ti	0.003	0.003	0.001
Al	1.502	1.371	1.097
Mg	0.000	0.000	0.001
Ca	0.550	0.389	0.118
Mn	0.001	0.000	0.001
Fe	0.019	0.022	0.009
Na	0.435	0.570	0.849
K	0.016	0.022	0.011
P	0.000	0.000	0.000

% End members

An	54.9	39.7	12.1
Ab	43.5	58.1	86.8
Or	1.6	2.2	1.1

Appendix 4
Plagioclase Feldspar (continued)

Wt%	Group 4				
	<u>2928QJD</u>	<u>2928OJD</u>	<u>2928NJD</u>	<u>2928GBJ</u>	<u>2928PJD</u>
SiO ₂	53.70	53.88	54.45	55.80	62.09
TiO ₂	0.09	0.08	0.09	0.07	0.09
Al ₂ O ₃	28.23	28.47	28.76	27.28	23.28
MgO	0.02	0.00	0.06	0.52	0.02
CaO	10.91	11.20	9.38	8.98	5.21
MnO	0.00	0.02	0.05	0.03	0.02
FeO	0.42	0.44	0.51	1.63	0.32
Na ₂ O	5.02	4.82	4.94	5.81	7.94
K ₂ O	0.19	0.25	0.99	0.24	0.98
P ₂ O ₅					
TOTAL	98.58	99.16	99.23	100.36	99.95

Atomic proportions recalculated on the basis of 8 oxygens

Si	2.460	2.455	2.474	2.509	2.763
Ti	0.003	0.003	0.003	0.002	0.003
Al	1.525	1.530	1.541	1.446	1.221
Mg	0.001	0.000	0.004	0.035	0.001
Ca	0.536	0.547	0.457	0.433	0.248
Mn	0.000	0.001	0.002	0.001	0.001
Fe	0.021	0.021	0.025	0.079	0.015
Na	0.446	0.426	0.435	0.507	0.685
K	0.011	0.015	0.057	0.014	0.056
P	0.000	0.000	0.000	0.000	0.000

% End members

An	54.0	55.4	48.2	45.4	25.1
Ab	44.9	43.1	45.8	53.1	69.3
Or	1.1	1.5	6.0	1.5	5.7

Wt%	Group 4		
	<u>2929aw</u>	<u>2929az</u>	<u>2929at</u>
SiO ₂	54.25	57.29	62.27
TiO ₂	0.06	0.05	0.04
Al ₂ O ₃	26.30	28.28	22.52
MgO	0.92	0.17	0.00
CaO	8.74	1.26	4.84
MnO	0.02	0.02	0.01
FeO	2.55	0.87	0.37
Na ₂ O	5.90	5.72	8.66
K ₂ O	0.26	5.33	0.74
P ₂ O ₅	0.01	0.00	0.01
TOTAL	99.02	99.00	99.45

Atomic proportions recalculated on the basis of 8 oxygens

Si	2.487	2.602	2.785
Ti	0.002	0.002	0.001
Al	1.421	1.514	1.187
Mg	0.063	0.011	0.000
Ca	0.429	0.062	0.232
Mn	0.001	0.001	0.000
Fe	0.125	0.042	0.018
Na	0.525	0.503	0.751
K	0.015	0.309	0.042
P	0.000	0.000	0.000

% End members

An	44.3	7.1	22.6
Ab	54.2	57.6	73.3
Or	1.5	35.4	4.1

Appendix 4.
Alkali feldspar

Wt%	Group 1			
	2914ai	2914av	2912 IJA	2917 RJB
SiO ₂	64.32	64.67	58.76	69.46
TiO ₂	0.03	0.00	0.06	0.04
Al ₂ O ₃	18.09	18.18	26.28	15.54
MgO	0.02	0.00	0.12	0.00
CaO	0.23	0.16	2.44	0.04
MnO	0.01	0.00	0.02	0.02
FeO	0.14	0.28	0.93	0.17
Na ₂ O	0.22	0.16	5.90	0.20
K ₂ O	16.51	16.60	4.37	12.98
P ₂ O ₅	0.00	0.01		
TOTAL	99.57	100.06	98.88	98.45

Atomic proportions recalculated on the basis of 8 oxygens

Si	2.994	2.995	2.665	3.172
Ti	0.001	0.000	0.002	0.001
Al	0.993	0.993	1.405	0.837
Mg	0.001	0.000	0.008	0.000
Ca	0.011	0.008	0.119	0.002
Mn	0.000	0.000	0.001	0.001
Fe	0.007	0.014	0.045	0.008
Na	0.020	0.014	0.519	0.018
K	0.981	0.981	0.253	0.756
P	0.000	0.000	0.000	0.000

% End members

An	1.1	0.8	13.4	0.3
Ab	2.0	1.4	58.2	2.3
Or	96.9	97.8	28.4	97.4

Wt%	Group 1						
	<u>2924ct</u>	<u>2924am</u>	<u>2924bf</u>	<u>2924cq</u>	<u>2924bd</u>	<u>2924az</u>	<u>2924ck</u>
SiO ₂	62.63	62.75	63.77	63.96	64.03	64.13	64.49
TiO ₂	0.01	0.00	0.02	0.21	0.00	0.05	0.04
Al ₂ O ₃	18.09	17.63	18.06	18.19	18.21	18.45	18.49
MgO	0.38	0.00	0.00	0.01	0.00	0.00	0.00
CaO	0.04	0.00	0.09	0.50	0.03	0.07	0.03
MnO	0.04	0.00	0.00	0.00	0.00	0.00	0.00
FeO	1.38	0.03	0.12	0.22	0.03	0.10	0.34
Na ₂ O	0.26	0.21	0.87	0.40	0.34	0.78	0.70
K ₂ O	15.67	16.61	15.65	15.86	16.39	15.59	16.15
P ₂ O ₅	0.00	0.00	0.00	0.01	0.00	0.01	0.01
TOTAL	98.49	97.25	98.58	99.36	99.03	99.20	100.24

Atomic proportions recalculated on the basis of 8 oxygens

Si	2.954	2.997	2.991	2.980	2.994	2.985	2.980
Ti	0.000	0.000	0.001	0.007	0.000	0.002	0.001
Al	1.006	0.993	0.999	0.999	1.004	1.012	1.007
Mg	0.027	0.000	0.000	0.001	0.000	0.000	0.000
Ca	0.002	0.000	0.005	0.025	0.002	0.003	0.001
Mn	0.002	0.000	0.000	0.000	0.000	0.000	0.000
Fe	0.070	0.002	0.006	0.011	0.002	0.005	0.017
Na	0.024	0.019	0.079	0.036	0.031	0.070	0.063
K	0.943	1.012	0.937	0.943	0.978	0.926	0.952
P	0.000	0.000	0.000	0.000	0.000	0.000	0.000

% End members

An	0.2	0.0	0.5	2.5	0.2	0.3	0.1
Ab	2.5	1.8	7.7	3.6	3.1	7.0	6.2
Or	97.3	98.2	91.8	93.9	96.7	92.7	93.7

Appendix 4.

Alkali feldspar (continued)

Group 2

Wt%	<u>2924cd</u>	<u>2924bb</u>	<u>2918HBJ</u>
SiO ₂	64.60	64.73	56.67
TiO ₂	0.01	0.05	0.07
Al ₂ O ₃	18.65	18.27	27.63
MgO	0.00	0.00	0.11
CaO	0.16	0.13	4.96
MnO	0.00	0.00	0.11
FeO	0.25	0.10	0.67
Na ₂ O	0.31	0.30	5.50
K ₂ O	16.40	16.34	3.08
P ₂ O ₅	0.01	0.00	
TOTAL	100.38	99.92	98.80

Atomic proportions recalculated on the basis of 8 oxygens

Si	2.980	2.997	2.577
Ti	0.000	0.002	0.002
Al	1.014	0.997	1.482
Mg	0.000	0.000	0.007
Ca	0.008	0.006	0.242
Mn	0.000	0.000	0.004
Fe	0.012	0.005	0.033
Na	0.028	0.027	0.485
K	0.965	0.965	0.179
P	0.000	0.000	0.000

% End members

An	0.8	0.6	26.7
Ab	2.8	2.7	53.5
Or	96.4	96.7	19.8

Group 3

Wt%	<u>2936ao</u>	<u>2948ak</u>	<u>2956bl</u>	<u>2956br</u>	<u>2952ag</u>
SiO ₂	63.40	63.01	65.23	55.05	65.79
TiO ₂	0.07	0.03	0.02	0.04	0.04
Al ₂ O ₃	17.56	19.82	18.28	31.29	18.41
MgO	0.01	0.00	0.00	0.09	0.00
CaO	0.09	1.95	0.09	0.84	0.15
MnO	0.00	0.00	0.01	0.32	0.00
FeO	0.17	0.16	0.13	0.67	0.14
Na ₂ O	0.97	2.72	1.11	3.76	1.86
K ₂ O	15.49	11.96	15.24	7.30	14.20
P ₂ O ₅	0.01	0.01	0.02	0.01	0.00
TOTAL	97.74	99.66	100.12	99.35	100.58

Atomic proportions recalculated on the basis of 8 oxygens

Si	3.000	2.903	3.001	2.505	3.001
Ti	0.003	0.001	0.001	0.001	0.001
Al	0.979	1.076	0.991	1.678	0.990
Mg	0.000	0.000	0.000	0.006	0.000
Ca	0.004	0.096	0.005	0.041	0.007
Mn	0.000	0.000	0.000	0.012	0.000
Fe	0.009	0.008	0.006	0.033	0.007
Na	0.089	0.243	0.099	0.331	0.164
K	0.935	0.703	0.895	0.424	0.826
P	0.000	0.000	0.001	0.001	0.000

% End members

An	0.4	9.2	0.5	5.2	0.7
Ab	8.7	23.3	9.9	41.6	16.4
Or	91.0	67.5	89.6	53.3	82.8

Appendix 4.

Alkali feldspar (continued)

Group 3

Wt%	<u>2909bv</u>	<u>2909bu</u>	<u>2909bx</u>	<u>2909br</u>	<u>2909bs</u>	<u>2909ae</u>	<u>2909ak</u>
SiO ₂	64.53	64.56	64.59	64.85	65.01	64.16	64.71
TiO ₂	0.02	0.05	0.05	0.00	0.04	0.01	0.02
Al ₂ O ₃	17.99	18.19	18.16	18.07	18.02	17.91	18.18
MgO	0.00	0.00	0.00	0.00	0.00	0.00	0.01
CaO	0.11	0.32	0.29	0.18	0.21	0.19	0.20
MnO	0.00	0.00	0.01	0.00	0.00	0.01	0.00
FeO	0.15	0.19	0.20	0.16	0.15	0.49	0.17
Na ₂ O	1.08	1.90	1.51	1.76	0.88	0.85	1.07
K ₂ O	15.46	13.88	14.50	13.93	15.37	15.48	15.07
P ₂ O ₅	0.00	0.02	0.00	0.00	0.01	0.00	0.00
TOTAL	99.34	99.11	99.31	98.95	99.69	99.10	99.43

Atomic proportions recalculated on the basis of 8 oxygens

Si	3.000	2.992	2.993	3.006	3.006	2.994	2.998
Ti	0.001	0.002	0.002	0.000	0.001	0.000	0.001
Al	0.986	0.994	0.992	0.987	0.982	0.985	0.993
Mg	0.000	0.000	0.000	0.000	0.000	0.000	0.001
Ca	0.005	0.016	0.014	0.009	0.010	0.009	0.010
Mn	0.000	0.000	0.000	0.000	0.000	0.000	0.000
Fe	0.007	0.009	0.010	0.008	0.007	0.024	0.008
Na	0.097	0.171	0.136	0.158	0.079	0.077	0.096
K	0.917	0.821	0.857	0.824	0.907	0.922	0.891
P	0.000	0.001	0.000	0.000	0.000	0.000	0.000

% End members

An	0.5	1.6	1.4	0.9	1.0	0.9	1.0
Ab	9.5	17.0	13.5	15.9	7.9	7.6	9.6
Or	90.0	81.4	85.1	83.1	91.1	91.5	89.4

Group 3

Wt%	<u>2909al</u>	<u>2909an</u>
SiO ₂	64.95	64.64
TiO ₂	0.02	0.03
Al ₂ O ₃	18.14	18.04
MgO	0.00	0.00
CaO	0.23	0.18
MnO	0.00	0.00
FeO	0.21	0.20
Na ₂ O	1.78	2.20
K ₂ O	14.18	13.42
P ₂ O ₅	0.01	0.01
TOTAL	99.52	98.72

Atomic proportions recalculated on the basis of 8 oxygens

Si	2.999	3.000
Ti	0.001	0.001
Al	0.987	0.987
Mg	0.000	0.000
Ca	0.011	0.009
Mn	0.000	0.000
Fe	0.010	0.010
Na	0.159	0.198
K	0.835	0.795
P	0.000	0.000

% End members

An	1.1	0.9
Ab	15.8	19.8
Or	83.1	79.3

Appendix 4.
Alkali feldspar (continued)

Group 4

<u>Wt%</u>	<u>2929ak</u>	<u>2929as</u>	<u>2929ar</u>	<u>2929ax</u>	<u>2929af</u>	<u>2929ap</u>	<u>2929ae</u>
SiO ₂	63.46	63.70	63.73	63.93	64.07	64.99	65.43
TiO ₂	0.01	0.02	0.05	0.02	0.02	0.02	0.04
Al ₂ O ₃	17.92	17.78	17.98	17.74	17.80	17.86	18.59
MgO	0.01	0.00	0.00	0.01	0.00	0.00	0.02
CaO	0.08	0.12	0.10	0.13	0.12	0.20	0.40
MnO	0.00	0.00	0.00	0.00	0.00	0.00	0.00
FeO	0.03	0.08	0.08	0.26	0.18	0.16	0.10
Na ₂ O	0.23	0.33	0.29	0.79	0.62	1.28	3.81
K ₂ O	16.29	16.20	16.41	15.56	15.89	15.10	11.94
P ₂ O ₅	0.02	0.00	0.00	0.00	0.00	0.02	0.02
TOTAL	98.04	98.24	98.63	98.43	98.68	99.62	100.35

Atomic proportions recalculated on the basis of 8 oxygens

Si	2.997	3.002	2.994	3.002	3.003	3.007	2.979
Ti	0.000	0.001	0.002	0.001	0.001	0.001	0.001
Al	0.998	0.988	0.996	0.982	0.983	0.974	0.998
Mg	0.000	0.000	0.000	0.001	0.000	0.000	0.002
Ca	0.004	0.006	0.005	0.006	0.006	0.010	0.020
Mn	0.000	0.000	0.000	0.000	0.000	0.000	0.000
Fe	0.001	0.004	0.004	0.013	0.009	0.008	0.005
Na	0.021	0.030	0.026	0.072	0.056	0.114	0.337
K	0.981	0.974	0.984	0.932	0.950	0.891	0.694
P	0.001	0.000	0.000	0.000	0.000	0.001	0.001

% End members

An	0.4	0.6	0.5	0.6	0.6	1.0	1.9
Ab	2.1	3.0	2.6	7.1	5.5	11.2	32.1
Or	97.5	96.4	96.9	92.3	93.9	87.8	66.0

Appendix 4.
Orthopyroxene

Wt%	Group 1		Group 3			
	2947aa	2936al	2936ai	2936aq	2936aj	2936aq
SiO ₂	52.73	52.90	53.06	53.14	53.30	53.44
TiO ₂	0.33	0.27	0.31	0.36	0.25	0.31
Al ₂ O ₃	1.15	0.67	0.63	0.65	0.73	0.70
MgO	23.06	22.54	22.34	22.53	22.36	22.90
CaO	1.81	2.00	1.91	1.93	2.05	2.05
MnO	0.68	0.52	0.53	0.54	0.50	0.51
FeO	19.89	20.27	20.60	20.55	20.36	20.63
Na ₂ O	0.01	0.04	0.03	0.03	0.02	0.01
K ₂ O	0.01	0.00	0.00	0.02	0.00	0.00
P ₂ O ₅	0.01	0.00	0.00	0.01	0.00	0.00
TOTAL	99.68	99.20	99.41	99.74	99.56	100.53

Atomic proportions recalculated on the basis of 6 oxygens

Si	1.958	1.977	1.981	1.977	1.983	1.972
Ti	0.009	0.007	0.009	0.010	0.007	0.009
Al	0.050	0.029	0.028	0.029	0.032	0.030
Mg	1.276	1.255	1.243	1.249	1.240	1.259
Ca	0.072	0.080	0.077	0.077	0.082	0.081
Mn	0.021	0.016	0.017	0.017	0.016	0.016
Fe	0.618	0.634	0.643	0.639	0.634	0.637
Na	0.001	0.003	0.002	0.002	0.002	0.001
K	0.000	0.000	0.000	0.001	0.000	0.000
P	0.000	0.000	0.000	0.000	0.000	0.000
Mg%	64.9	63.7	63.3	63.6	63.4	63.7
Fe%	31.4	32.2	32.8	32.5	32.4	32.2
Ca%	3.7	4.1	3.9	3.9	4.2	4.1
Total	100	100	100	100	100	100

Group 3

Wt%	Group 3						
	2948aj	2948bq	2948ad	2948bp	2948ao	2948bv	2948bk
SiO ₂	50.97	51.26	51.78	51.91	52.28	52.35	52.48
TiO ₂	0.32	0.34	0.38	0.41	0.36	0.35	0.33
Al ₂ O ₃	2.35	1.40	1.15	0.82	0.74	0.71	0.94
MgO	20.67	21.43	21.36	21.51	21.76	21.43	21.60
CaO	3.75	2.26	2.18	2.07	1.96	2.15	2.43
MnO	0.53	0.53	0.57	0.56	0.54	0.57	0.53
FeO	19.70	20.56	21.79	21.53	21.18	21.38	20.50
Na ₂ O	0.09	0.04	0.04	0.02	0.02	0.04	0.03
K ₂ O	0.12	0.05	0.03	0.00	0.00	0.00	0.02
P ₂ O ₅	0.02	0.01	0.01	0.00	0.01	0.00	0.00
TOTAL	98.52	97.89	99.28	98.82	98.85	98.99	98.86

Atomic proportions recalculated on the basis of 6 oxygens

Si	1.929	1.951	1.953	1.963	1.971	1.974	1.974
Ti	0.009	0.010	0.011	0.012	0.010	0.010	0.009
Al	0.105	0.063	0.051	0.036	0.033	0.031	0.042
Mg	1.166	1.216	1.201	1.212	1.222	1.204	1.211
Ca	0.152	0.092	0.088	0.084	0.079	0.087	0.098
Mn	0.017	0.017	0.018	0.018	0.017	0.018	0.017
Fe	0.623	0.655	0.687	0.681	0.668	0.674	0.645
Na	0.007	0.003	0.003	0.002	0.002	0.003	0.002
K	0.006	0.003	0.002	0.000	0.000	0.000	0.001
P	0.000	0.000	0.000	0.000	0.000	0.000	0.000
Mg%	60.1	61.9	60.8	61.3	62.1	61.3	62.0
Fe%	32.1	33.4	34.8	34.4	33.9	34.3	33.0
Ca%	7.8	4.7	4.5	4.2	4.0	4.4	5.0
Total	100	100	100	100	100	100	100

Appendix 4.

Orthopyroxene (continued)

Wt%	Group 3					
	2948aq	2948bt	2948by	2948al	2956ac	2956bk
SiO ₂	52.69	52.81	52.90	54.25	52.38	52.63
TiO ₂	0.34	0.27	0.35	0.40	0.38	0.33
Al ₂ O ₃	0.81	0.83	0.91	1.46	0.71	0.81
MgO	21.63	22.22	21.63	19.82	20.74	21.19
CaO	2.22	2.27	2.11	2.40	1.95	2.03
MnO	0.56	0.52	0.57	0.51	0.58	0.56
FeO	21.27	20.61	21.29	19.75	22.87	22.34
Na ₂ O	0.04	0.04	0.02	0.04	0.02	0.04
K ₂ O	0.01	0.01	0.01	0.17	0.00	0.01
P ₂ O ₅	0.00	0.00	0.00	0.00	0.00	0.01
TOTAL	99.56	99.57	99.78	98.80	99.64	99.94

Atomic proportions recalculated on the basis of 6 oxygens

Si	1.973	1.971	1.975	2.023	1.974	1.972
Ti	0.010	0.007	0.010	0.011	0.011	0.009
Al	0.036	0.037	0.040	0.064	0.032	0.036
Mg	1.207	1.236	1.203	1.102	1.165	1.183
Ca	0.089	0.091	0.084	0.096	0.079	0.081
Mn	0.018	0.016	0.018	0.016	0.019	0.018
Fe	0.666	0.643	0.665	0.616	0.721	0.700
Na	0.003	0.003	0.002	0.003	0.001	0.003
K	0.000	0.001	0.000	0.008	0.000	0.000
P	0.000	0.000	0.000	0.000	0.000	0.000
Mg%	61.5	62.7	61.6	60.8	59.3	60.2
Fe%	33.9	32.6	34.1	34.0	36.7	35.6
Ca%	4.5	4.6	4.3	5.3	4.0	4.1
Total	100	100	100	100	100	100

Wt%	Group 3				Group 4
	2956bd	2956ag	2956al	2956bn	2928CBJ
SiO ₂	52.64	52.67	52.94	52.96	48.97
TiO ₂	0.32	0.38	0.37	0.39	0.32
Al ₂ O ₃	0.78	0.69	0.63	0.67	3.04
MgO	20.85	20.89	21.64	21.19	17.66
CaO	2.06	2.07	1.91	2.01	4.24
MnO	0.58	0.58	0.54	0.60	0.63
FeO	22.66	22.49	21.74	22.97	22.66
Na ₂ O	0.04	0.02	0.02	0.05	0.09
K ₂ O	0.00	0.01	0.00	0.01	0.12
P ₂ O ₅	0.01	0.00	0.01	0.01	0.00
TOTAL	99.93	99.80	99.79	100.85	97.73

Atomic proportions recalculated on the basis of 6 oxygens

Si	1.975	1.977	1.979	1.971	1.904
Ti	0.009	0.011	0.010	0.011	0.009
Al	0.034	0.031	0.028	0.029	0.139
Mg	1.166	1.169	1.206	1.175	1.023
Ca	0.083	0.083	0.076	0.080	0.177
Mn	0.018	0.018	0.017	0.019	0.021
Fe	0.711	0.706	0.680	0.715	0.737
Na	0.003	0.002	0.001	0.003	0.007
K	0.000	0.000	0.000	0.000	0.006
P	0.000	0.000	0.000	0.000	0.000
Mg%	59.5	59.7	61.5	59.6	52.8
Fe%	36.3	36.1	34.7	36.3	38.0
Ca%	4.2	4.2	3.9	4.1	9.1
Total	100	100	100	100	100

Appendix 4
Clinopyroxene

Wt%	Group 1				2914bc	2914ax
	2912JDD	2912JDE	2912JDF	2912DJA		
SiO ₂	51.40	52.19	51.33	51.93	51.79	52.51
TiO ₂	0.45	0.66	0.50	0.66	0.64	0.44
Al ₂ O ₃	1.92	5.82	2.13	3.13	1.25	3.09
MgO	14.49	7.21	13.98	15.80	13.47	12.17
CaO	19.18	13.68	19.28	19.21	21.00	20.46
MnO	0.41	0.79	0.44	0.27	0.46	0.41
FeO	10.16	15.28	11.31	7.99	11.87	9.29
Na ₂ O	0.22	1.17	0.24	0.24	0.27	0.19
K ₂ O	0.20	0.00	0.17	0.15	0.00	1.35
P ₂ O ₅	0.00	0.34	0.00	0.00	0.01	0.00
TOTAL	98.43	97.14	99.38	99.38	100.76	99.90

Atomic proportions recalculated on the basis of 6 oxygens

Si	1.946	2.009	1.936	1.924	1.943	1.965
Ti	0.013	0.019	0.014	0.018	0.018	0.012
Al	0.086	0.264	0.095	0.137	0.055	0.136
Mg	0.818	0.414	0.786	0.872	0.753	0.678
Ca	0.778	0.564	0.779	0.763	0.844	0.820
Mn	0.013	0.026	0.014	0.008	0.015	0.013
Fe	0.322	0.492	0.357	0.248	0.372	0.291
Na	0.016	0.087	0.018	0.017	0.019	0.014
K	0.010	0.000	0.008	0.007	0.000	0.064
P	0.000	0.017	0.000	0.000	0.000	0.000
Mg%	42.6	28.2	40.9	46.3	38.2	37.9
Fe%	16.8	33.5	18.6	13.2	18.9	16.3
Ca%	40.6	38.4	40.5	40.5	42.9	45.8
Total	100	99.999	100	99.999	100	100

Wt%	Group 1					
	2917CJA	2917AJB	2917IJB	2917OJB	2917PJB	2917TJB
SiO ₂	51.40	51.01	50.83	51.81	45.87	51.59
TiO ₂	0.56	0.52	0.61	0.60	0.40	0.60
Al ₂ O ₃	1.51	1.90	1.37	1.29	3.62	1.37
MgO	12.89	12.49	12.72	12.44	12.29	12.62
CaO	20.58	19.37	20.45	20.53	14.07	20.94
MnO	0.53	0.62	0.55	0.55	0.53	0.55
FeO	10.71	12.41	11.42	11.76	12.03	10.77
Na ₂ O	0.24	0.24	0.26	0.26	0.23	0.29
K ₂ O	0.05	0.03	0.02	0.02	0.03	0.05
P ₂ O ₅	0.01	0.00	0.00	0.00	0.09	0.00
TOTAL	98.48	98.59	98.23	99.26	89.16	98.78

Atomic proportions recalculated on the basis of 6 oxygens

Si	1.960	1.953	1.953	1.968	1.925	1.964
Ti	0.016	0.015	0.018	0.017	0.013	0.017
Al	0.068	0.086	0.062	0.058	0.179	0.061
Mg	0.733	0.713	0.728	0.704	0.769	0.716
Ca	0.841	0.795	0.842	0.836	0.633	0.854
Mn	0.017	0.020	0.018	0.018	0.019	0.018
Fe	0.342	0.397	0.367	0.374	0.422	0.343
Na	0.018	0.018	0.019	0.019	0.019	0.021
K	0.002	0.001	0.001	0.001	0.002	0.002
P	0.000	0.000	0.000	0.000	0.005	0.000
Mg%	38.3	37.4	37.6	36.8	42.2	37.4
Fe%	17.9	20.8	18.9	19.5	23.1	17.9
Ca%	43.9	41.7	43.5	43.7	34.7	44.6
Total	100	100	100	100	100	100

Appendix 4
Clinopyroxene (continued)

Group 1					
Wt%	2947ba	2947ac	2947bd	2947af	2947bc
SiO ₂	50.93	51.58	52.24	52.26	52.46
TiO ₂	0.45	0.46	0.41	0.46	0.16
Al ₂ O ₃	2.41	3.41	1.81	2.12	0.57
MgO	15.08	15.34	17.23	16.56	12.31
CaO	20.45	17.67	19.85	20.41	21.46
MnO	0.32	0.30	0.26	0.27	0.65
FeO	9.04	8.84	7.58	7.64	11.99
Na ₂ O	0.24	0.54	0.22	0.24	0.15
K ₂ O	0.00	0.61	0.01	0.00	0.07
P ₂ O ₅	0.01	0.00	0.02	0.00	0.01
TOTAL	98.91	98.75	99.62	99.96	99.82

Atomic proportions recalculated on the basis of 6 oxygens

Si	1.919	1.931	1.934	1.931	1.989
Ti	0.013	0.013	0.011	0.013	0.004
Al	0.107	0.151	0.079	0.092	0.025
Mg	0.847	0.856	0.951	0.912	0.696
Ca	0.825	0.709	0.787	0.808	0.871
Mn	0.010	0.009	0.008	0.008	0.021
Fe	0.285	0.277	0.235	0.236	0.380
Na	0.017	0.039	0.016	0.017	0.011
K	0.000	0.029	0.000	0.000	0.003
P	0.000	0.000	0.001	0.000	0.000
Mg%	43.3	46.5	48.2	46.6	35.7
Fe%	14.6	15.0	11.9	12.1	19.5
Ca%	42.2	38.5	39.9	41.3	44.7
Total	100	100	100	100	100

Group 2

Wt%	2924al	2924ac	2924ad	2924cl	2924bi	2924ci	2924cs
SiO ₂	46.85	47.39	47.74	48.11	49.06	49.17	52.66
TiO ₂	0.64	0.60	0.73	0.45	0.72	0.51	0.11
Al ₂ O ₃	4.41	4.28	3.74	3.59	2.55	3.31	0.43
MgO	13.16	13.07	12.80	13.10	12.75	12.82	12.61
CaO	18.18	18.04	19.03	17.96	20.49	17.87	21.86
MnO	0.41	0.44	0.40	0.47	0.41	0.46	0.49
FeO	13.67	14.20	13.75	14.85	12.51	15.56	12.71
Na ₂ O	0.26	0.23	0.27	0.24	0.26	0.25	0.26
K ₂ O	0.02	0.01	0.00	0.00	0.00	0.02	0.00
P ₂ O ₅	0.02	0.03	0.01	0.01	0.01	0.02	0.03
TOTAL	97.60	98.27	98.46	98.75	98.77	99.98	101.16

Atomic proportions recalculated on the basis of 6 oxygens

Si	1.830	1.839	1.851	1.862	1.890	1.880	1.977
Ti	0.019	0.017	0.021	0.013	0.021	0.015	0.003
Al	0.203	0.196	0.171	0.164	0.116	0.149	0.019
Mg	0.766	0.756	0.740	0.755	0.732	0.731	0.706
Ca	0.761	0.750	0.790	0.745	0.846	0.732	0.880
Mn	0.014	0.014	0.013	0.015	0.013	0.015	0.016
Fe	0.446	0.461	0.446	0.480	0.403	0.498	0.399
Na	0.019	0.017	0.020	0.018	0.020	0.018	0.019
K	0.001	0.001	0.000	0.000	0.000	0.001	0.000
P	0.001	0.001	0.000	0.000	0.000	0.001	0.001
Mg%	38.8	38.4	37.4	38.1	37.0	37.3	35.6
Fe%	22.6	23.4	22.6	24.2	20.3	25.4	20.1
Ca%	38.6	38.1	40.0	37.6	42.7	37.3	44.3
Total	100	100	100	100	100	100	100

Appendix 4
Clinopyroxene (continued)

<i>Group 1</i>						
<u>Wt%</u>	<u>2947ba</u>	<u>2947ac</u>	<u>2947bd</u>	<u>2947af</u>	<u>2947bc</u>	
SiO ₂	50.93	51.58	52.24	52.26	52.46	
TiO ₂	0.45	0.46	0.41	0.46	0.16	
Al ₂ O ₃	2.41	3.41	1.81	2.12	0.57	
MgO	15.08	15.34	17.23	16.56	12.31	
CaO	20.45	17.67	19.85	20.41	21.46	
MnO	0.32	0.30	0.26	0.27	0.65	
FeO	9.04	8.84	7.58	7.64	11.99	
Na ₂ O	0.24	0.54	0.22	0.24	0.15	
K ₂ O	0.00	0.61	0.01	0.00	0.07	
P ₂ O ₅	0.01	0.00	0.02	0.00	0.01	
TOTAL	98.91	98.75	99.62	99.96	99.82	

Atomic proportions recalculated on the basis of 6 oxygens

Si	1.919	1.931	1.934	1.931	1.989	
Ti	0.013	0.013	0.011	0.013	0.004	
Al	0.107	0.151	0.079	0.092	0.025	
Mg	0.847	0.856	0.951	0.912	0.696	
Ca	0.825	0.709	0.787	0.808	0.871	
Mn	0.010	0.009	0.008	0.008	0.021	
Fe	0.285	0.277	0.235	0.236	0.380	
Na	0.017	0.039	0.016	0.017	0.011	
K	0.000	0.029	0.000	0.000	0.003	
P	0.000	0.000	0.001	0.000	0.000	
Mg%	43.3	46.5	48.2	46.6	35.7	
Fe%	14.6	15.0	11.9	12.1	19.5	
Ca%	42.2	38.5	39.9	41.3	44.7	
Total	100	100	100	100	100	

Group 2

<u>Wt%</u>	<u>2924al</u>	<u>2924ac</u>	<u>2924ad</u>	<u>2924cl</u>	<u>2924bi</u>	<u>2924ci</u>	<u>2924cs</u>
SiO ₂	46.85	47.39	47.74	48.11	49.06	49.17	52.66
TiO ₂	0.64	0.60	0.73	0.45	0.72	0.51	0.11
Al ₂ O ₃	4.41	4.28	3.74	3.59	2.55	3.31	0.43
MgO	13.16	13.07	12.80	13.10	12.75	12.82	12.61
CaO	18.18	18.04	19.03	17.96	20.49	17.87	21.86
MnO	0.41	0.44	0.40	0.47	0.41	0.46	0.49
FeO	13.67	14.20	13.75	14.85	12.51	15.56	12.71
Na ₂ O	0.26	0.23	0.27	0.24	0.26	0.25	0.26
K ₂ O	0.02	0.01	0.00	0.00	0.00	0.02	0.00
P ₂ O ₅	0.02	0.03	0.01	0.01	0.01	0.02	0.03
TOTAL	97.60	98.27	98.46	98.75	98.77	99.98	101.16

Atomic proportions recalculated on the basis of 6 oxygens

Si	1.830	1.839	1.851	1.862	1.890	1.880	1.977
Ti	0.019	0.017	0.021	0.013	0.021	0.015	0.003
Al	0.203	0.196	0.171	0.164	0.116	0.149	0.019
Mg	0.766	0.756	0.740	0.755	0.732	0.731	0.706
Ca	0.761	0.750	0.790	0.745	0.846	0.732	0.880
Mn	0.014	0.014	0.013	0.015	0.013	0.015	0.016
Fe	0.446	0.461	0.446	0.480	0.403	0.498	0.399
Na	0.019	0.017	0.020	0.018	0.020	0.018	0.019
K	0.001	0.001	0.000	0.000	0.000	0.001	0.000
P	0.001	0.001	0.000	0.000	0.000	0.001	0.001
Mg%	38.8	38.4	37.4	38.1	37.0	37.3	35.6
Fe%	22.6	23.4	22.6	24.2	20.3	25.4	20.1
Ca%	38.6	38.1	40.0	37.6	42.7	37.3	44.3
Total	100	100	100	100	100	100	100

Appendix 4

Clinopyroxene (continued)

Group 2

Wt%	2926bg	2926be	2906ADJ	2906CDJ	2906DDJ	2906EDJ
SiO ₂	49.82	50.73	45.08	46.64	48.40	46.80
TiO ₂	0.66	0.82	0.48	0.41	0.46	0.63
Al ₂ O ₃	1.32	1.47	5.91	5.21	4.05	4.47
MgO	12.04	12.48	13.00	14.30	14.09	13.12
CaO	20.62	21.49	15.58	17.00	18.42	17.31
MnO	0.49	0.57	0.51	0.44	0.44	0.50
FeO	11.90	11.35	15.81	13.17	12.43	14.70
Na ₂ O	0.27	0.29	0.00	0.00	0.00	0.00
K ₂ O	0.02	0.00	0.05	0.17	0.13	0.02
P ₂ O ₅	0.01	0.00	0.00	0.00	0.00	0.00
TOTAL	97.13	99.20	96.42	97.34	98.42	97.55

Atomic proportions recalculated on the basis of 6 oxygens

Si	1.946	1.936	1.789	1.813	1.857	1.832
Ti	0.019	0.024	0.014	0.012	0.013	0.019
Al	0.061	0.066	0.277	0.239	0.183	0.206
Mg	0.700	0.710	0.769	0.828	0.806	0.765
Ca	0.863	0.879	0.663	0.708	0.757	0.726
Mn	0.016	0.018	0.017	0.014	0.014	0.017
Fe	0.389	0.362	0.525	0.428	0.399	0.481
Na	0.020	0.022	0.000	0.000	0.000	0.000
K	0.001	0.000	0.003	0.008	0.006	0.001
P	0.000	0.000	0.000	0.000	0.000	0.000
Mg%	35.9	36.4	39.3	42.2	41.1	38.8
Fe%	19.9	18.6	26.8	21.8	20.3	24.4
Ca%	44.2	45.1	33.9	36.0	38.6	36.8
Total	100	100	100	100	100	100

Group 2

Wt%	2918JFD	2918JGD	2918JHD	2918JID	2918JKD	2918JJD	2918JLD
SiO ₂	48.06	43.59	49.40	44.34	49.18	46.50	48.34
TiO ₂	0.70	0.38	0.50	0.49	0.59	0.68	0.35
Al ₂ O ₃	4.97	7.91	4.13	3.41	4.20	6.17	4.76
MgO	13.27	13.26	13.37	12.60	13.47	13.39	13.51
CaO	16.62	12.92	18.17	16.22	17.92	15.39	17.12
MnO	0.45	0.46	0.45	7.41	0.45	0.48	0.44
FeO	14.19	17.35	13.16	11.43	13.38	14.87	14.10
Na ₂ O	0.23	0.21	0.21	0.27	0.24	0.21	0.21
K ₂ O	0.02	0.07	0.12	0.02	0.03	0.07	0.13
P ₂ O ₅	0.01	0.01	0.00	0.03	0.00	0.01	0.00
TOTAL	98.52	96.16	99.51	96.22	99.46	97.77	98.96

Atomic proportions recalculated on the basis of 6 oxygens

Si	1.848	1.737	1.875	1.800	1.870	1.805	1.851
Ti	0.020	0.011	0.014	0.015	0.017	0.020	0.010
Al	0.225	0.372	0.185	0.163	0.188	0.282	0.215
Mg	0.760	0.787	0.756	0.763	0.763	0.775	0.771
Ca	0.685	0.552	0.739	0.706	0.730	0.640	0.702
Mn	0.015	0.016	0.014	0.255	0.014	0.016	0.014
Fe	0.456	0.578	0.418	0.388	0.425	0.483	0.451
Na	0.017	0.016	0.015	0.021	0.018	0.016	0.016
K	0.001	0.004	0.006	0.001	0.001	0.003	0.006
P	0.000	0.001	0.000	0.002	0.000	0.000	0.000
Mg%	40.0	41.1	39.5	41.1	39.8	40.8	40.1
Fe%	24.0	30.2	21.9	20.9	22.2	25.4	23.4
Ca%	36.0	28.8	38.6	38.0	38.1	33.7	36.5
Total	100	100	100	100	100	100	100

Appendix 4
Clinopyroxene (continued)

Group 2

Wt%	2918JMD	2918JND	2918CPD	2918JQD	2918JRD
SiO ₂	51.03	53.01	47.71	43.94	46.42
TiO ₂	0.80	0.32	0.59	0.95	0.42
Al ₂ O ₃	2.85	1.76	4.90	7.47	5.30
MgO	13.24	13.70	13.39	13.70	12.86
CaO	19.65	21.65	16.68	13.57	15.70
MnO	0.44	0.44	0.48	0.46	0.48
FeO	11.91	10.56	13.63	15.22	15.17
Na ₂ O	0.20	0.20	0.21	0.14	0.23
K ₂ O	0.03	0.14	0.10	0.05	0.02
P ₂ O ₅	0.00	0.00	0.02	0.02	0.01
TOTAL	100.15	101.78	97.71	95.52	96.61

Atomic proportions recalculated on the basis of 6 oxygens

Si	1.918	1.953	1.847	1.748	1.830
Ti	0.023	0.009	0.017	0.028	0.012
Al	0.126	0.076	0.224	0.350	0.246
Mg	0.741	0.752	0.772	0.812	0.756
Ca	0.791	0.854	0.692	0.578	0.663
Mn	0.014	0.014	0.016	0.015	0.016
Fe	0.374	0.325	0.441	0.506	0.500
Na	0.015	0.014	0.016	0.011	0.018
K	0.001	0.007	0.005	0.003	0.001
P	0.000	0.000	0.001	0.001	0.001
Mg%	38.9	38.9	40.5	42.8	39.4
Fe%	19.6	16.8	23.2	26.7	26.1
Ca%	41.5	44.2	36.3	30.5	34.5
Total	100	100	100	100	100

Group 3

Wt%	2909ab	2909aj	2909aa	2909bh	2909bm	2909bk	2909bg
SiO ₂	51.11	51.37	51.56	51.17	51.24	51.73	51.76
TiO ₂	0.57	0.61	0.69	0.60	0.36	0.35	0.48
Al ₂ O ₃	1.44	1.29	1.16	1.36	2.10	0.71	0.90
MgO	13.55	13.73	13.85	13.50	15.18	13.51	13.45
CaO	19.10	19.55	19.75	19.18	20.31	20.33	20.47
MnO	0.43	0.44	0.43	0.39	0.28	0.39	0.40
FeO	12.93	12.39	12.70	12.55	9.03	11.88	12.09
Na ₂ O	0.35	0.30	0.27	0.33	0.26	0.29	0.30
K ₂ O	0.00	0.00	0.00	0.05	0.00	0.00	0.00
P ₂ O ₅	0.02	0.01	0.01	0.02	0.00	0.00	0.01
TOTAL	99.49	99.69	100.41	99.15	98.75	99.20	99.84

Atomic proportions recalculated on the basis of 6 oxygens

Si	1.943	1.946	1.942	1.949	1.932	1.968	1.959
Ti	0.016	0.017	0.019	0.017	0.010	0.010	0.014
Al	0.065	0.058	0.052	0.061	0.093	0.032	0.040
Mg	0.767	0.775	0.777	0.766	0.853	0.766	0.759
Ca	0.778	0.794	0.797	0.783	0.821	0.829	0.830
Mn	0.014	0.014	0.014	0.013	0.009	0.013	0.013
Fe	0.411	0.392	0.400	0.400	0.285	0.378	0.383
Na	0.026	0.022	0.020	0.025	0.019	0.022	0.022
K	0.000	0.000	0.000	0.003	0.000	0.000	0.000
P	0.000	0.000	0.000	0.001	0.000	0.000	0.000
Mg%	39.2	39.5	39.4	39.3	43.5	38.8	38.5
Fe%	21.0	20.0	20.3	20.5	14.5	19.2	19.4
Ca%	39.8	40.5	40.4	40.2	41.9	42.0	42.1
Total	100	100	100	100	100	100	100

Appendix 4
Clinopyroxene (continued)

Group 3

Wt%	2909bq	2909bl	2909bt	2936ac	2936ah	2936ab
SiO ₂	51.88	51.96	52.64	51.84	52.08	52.14
TiO ₂	0.37	0.11	0.21	0.43	0.51	0.43
Al ₂ O ₃	1.97	0.49	0.56	2.12	0.96	1.42
MgO	15.10	13.05	13.50	15.14	14.60	15.68
CaO	19.74	21.54	21.35	20.61	20.61	18.68
MnO	0.30	0.43	0.33	0.29	0.29	0.32
FeO	9.81	11.34	11.07	8.90	9.65	10.42
Na ₂ O	0.26	0.28	0.30	0.26	0.30	0.25
K ₂ O	0.00	0.00	0.00	0.00	0.03	0.00
P ₂ O ₅	0.01	0.01	0.02	0.02	0.01	0.03
TOTAL	99.44	99.19	99.99	99.61	99.04	99.36

Atomic proportions recalculated on the basis of 6 oxygens

Si	1.943	1.978	1.981	1.936	1.964	1.954
Ti	0.010	0.003	0.006	0.012	0.014	0.012
Al	0.087	0.022	0.025	0.093	0.043	0.063
Mg	0.843	0.741	0.757	0.842	0.820	0.875
Ca	0.792	0.879	0.861	0.825	0.833	0.750
Mn	0.009	0.014	0.010	0.009	0.009	0.010
Fe	0.307	0.361	0.348	0.278	0.304	0.327
Na	0.019	0.020	0.022	0.019	0.022	0.018
K	0.000	0.000	0.000	0.000	0.002	0.000
P	0.000	0.000	0.001	0.001	0.000	0.001
Mg%	43.4	37.4	38.5	43.3	41.9	44.8
Fe%	15.8	18.2	17.7	14.3	15.5	16.8
Ca%	40.8	44.4	43.8	42.4	42.6	38.4
Total	100	100	100	100	100	100

Group 3

Wt%	2936ad	2936ap	2922FJD	2922GJD	2922HJD	2922IJD
SiO ₂	52.33	52.34	51.71	52.24	51.52	51.72
TiO ₂	0.29	0.66	0.41	0.43	0.35	0.49
Al ₂ O ₃	0.79	1.50	1.52	1.48	1.69	1.97
MgO	14.74	14.81	14.33	14.35	14.07	13.81
CaO	21.93	20.41	20.42	19.66	20.30	20.88
MnO	0.25	0.31	0.39	0.44	0.42	0.48
FeO	8.46	10.37	10.86	11.18	11.03	10.16
Na ₂ O	0.29	0.31	0.00	0.00	0.00	0.00
K ₂ O	0.00	0.00	0.12	0.17	0.10	0.17
P ₂ O ₅	0.01	0.02	0.00	0.00	0.00	0.00
TOTAL	99.07	100.73	99.76	99.95	99.48	99.68

Atomic proportions recalculated on the basis of 6 oxygens

Si	1.968	1.944	1.944	1.956	1.944	1.941
Ti	0.008	0.018	0.012	0.012	0.010	0.014
Al	0.035	0.066	0.067	0.065	0.075	0.087
Mg	0.826	0.820	0.803	0.801	0.791	0.773
Ca	0.884	0.812	0.823	0.789	0.821	0.840
Mn	0.008	0.010	0.012	0.014	0.013	0.015
Fe	0.266	0.322	0.341	0.350	0.348	0.319
Na	0.021	0.022	0.000	0.000	0.000	0.000
K	0.000	0.000	0.006	0.008	0.005	0.008
P	0.000	0.001	0.000	0.000	0.000	0.000
Mg%	41.8	42.0	40.8	41.3	40.4	40.0
Fe%	13.5	16.5	17.3	18.0	17.8	16.5
Ca%	44.7	41.6	41.8	40.7	41.9	43.5
Total	100	100	100	100	100	100

Appendix 4
Clinopyroxene (continued)

Group 3

Wt%	2948bi	2948aq	2948ah	2948an	2948am	2948ac	2948ak
SiO ₂	51.26	51.46	51.53	51.53	51.78	51.87	51.95
TiO ₂	0.35	0.58	0.56	0.67	0.70	0.64	0.67
Al ₂ O ₃	0.70	1.62	1.67	1.50	1.32	1.63	1.51
MgO	14.22	14.26	14.25	14.62	14.39	15.66	15.19
CaO	20.86	20.58	20.33	19.69	20.07	17.91	18.01
MnO	0.27	0.39	0.41	0.37	0.34	0.35	0.38
FeO	9.66	11.00	10.72	11.12	10.95	11.95	12.31
Na ₂ O	0.31	0.31	0.31	0.26	0.32	0.25	0.31
K ₂ O	0.02	0.01	0.01	0.00	0.00	0.01	0.00
P ₂ O ₅	0.02	0.04	0.03	0.01	0.02	0.01	0.01
TOTAL	97.66	100.24	99.83	99.76	99.88	100.27	100.33

Atomic proportions recalculated on the basis of 6 oxygens

Si	1.965	1.931	1.938	1.939	1.946	1.937	1.943
Ti	0.010	0.016	0.016	0.019	0.020	0.018	0.019
Al	0.032	0.072	0.074	0.067	0.059	0.072	0.067
Mg	0.812	0.798	0.799	0.819	0.806	0.872	0.847
Ca	0.857	0.827	0.819	0.794	0.808	0.717	0.722
Mn	0.009	0.012	0.013	0.012	0.011	0.011	0.012
Fe	0.310	0.345	0.337	0.350	0.344	0.373	0.385
Na	0.023	0.023	0.023	0.019	0.023	0.018	0.022
K	0.001	0.000	0.000	0.000	0.000	0.000	0.000
P	0.001	0.001	0.001	0.000	0.000	0.000	0.000
Mg%	41.0	40.5	40.9	41.7	41.2	44.4	43.3
Fe%	15.7	17.5	17.2	17.8	17.6	19.0	19.7
Ca%	43.3	42.0	41.9	40.4	41.3	36.5	37.0
Total	100	100	100	100	100	100	100

Group 3

Wt%	2948bc	2923JHD	2923JID	2923JKD	2923JLD	2923JMD
SiO ₂	51.96	51.48	51.30	50.91	48.56	51.40
TiO ₂	0.77	0.52	0.65	0.63	0.98	0.58
Al ₂ O ₃	1.54	1.87	1.78	1.82	3.26	1.76
MgO	14.93	12.89	12.60	12.30	13.48	12.63
CaO	19.00	20.71	20.87	20.59	15.86	20.44
MnO	0.35	0.52	0.59	0.55	0.34	0.53
FeO	11.56	10.60	11.12	10.72	12.90	11.13
Na ₂ O	0.26	0.29	0.29	0.29	0.83	0.29
K ₂ O	0.00	0.07	0.07	0.10	0.15	0.12
P ₂ O ₅	0.02	0.00	0.00	0.00	0.18	0.00
TOTAL	100.39	98.95	99.27	97.91	96.54	98.88

Atomic proportions recalculated on the basis of 6 oxygens

Si	1.940	1.953	1.947	1.955	1.895	1.955
Ti	0.022	0.015	0.019	0.018	0.029	0.017
Al	0.068	0.084	0.080	0.082	0.150	0.079
Mg	0.831	0.729	0.713	0.704	0.784	0.716
Ca	0.760	0.842	0.849	0.847	0.663	0.833
Mn	0.011	0.017	0.019	0.018	0.011	0.017
Fe	0.361	0.336	0.353	0.344	0.421	0.354
Na	0.019	0.021	0.021	0.022	0.063	0.021
K	0.000	0.003	0.003	0.005	0.007	0.006
P	0.001	0.000	0.000	0.000	0.009	0.000
Mg%	42.6	38.2	37.2	37.2	42.0	37.6
Fe%	18.5	17.6	18.4	18.2	22.5	18.6
Ca%	38.9	44.2	44.3	44.7	35.5	43.8
Total	100	100	100	100	100	100

Appendix 4
Clinopyroxene (continued)

Wt%	Group 3					
	2956af	2956bg	2956bq	2956ah	2956bb	2956be
SiO ₂	51.66	51.74	52.14	52.20	52.38	53.04
TiO ₂	0.71	0.74	0.72	0.48	0.46	0.39
Al ₂ O ₃	1.15	1.51	1.49	1.42	1.82	1.36
MgO	13.68	14.49	14.58	14.98	16.63	14.29
CaO	21.36	19.88	18.83	19.02	18.89	22.07
MnO	0.35	0.35	0.37	0.35	0.30	0.35
FeO	10.50	11.35	12.33	11.70	9.48	9.42
Na ₂ O	0.34	0.30	0.31	0.27	0.22	0.25
K ₂ O	0.01	0.00	0.01	0.00	0.00	0.00
P ₂ O ₅	0.00	0.03	0.02	0.01	0.00	0.01
TOTAL	99.75	100.38	100.79	100.44	100.17	101.18

Atomic proportions recalculated on the basis of 6 oxygens

Si	1.948	1.937	1.945	1.949	1.939	1.959
Ti	0.020	0.021	0.020	0.014	0.013	0.011
Al	0.051	0.067	0.066	0.063	0.079	0.059
Mg	0.769	0.808	0.810	0.833	0.917	0.787
Ca	0.863	0.797	0.752	0.761	0.749	0.873
Mn	0.011	0.011	0.012	0.011	0.009	0.011
Fe	0.331	0.355	0.385	0.365	0.293	0.291
Na	0.025	0.021	0.022	0.019	0.015	0.018
K	0.000	0.000	0.000	0.000	0.000	0.000
P	0.000	0.001	0.001	0.000	0.000	0.000
Mg%	39.2	41.2	41.6	42.5	46.8	40.3
Fe%	16.9	18.1	19.8	18.6	15.0	14.9
Ca%	44.0	40.7	38.6	38.8	38.2	44.7
Total	100	100	100	100	100	100

Group 3

Wt%	2952ae	2952ah
SiO ₂	51.25	52.26
TiO ₂	0.14	0.38
Al ₂ O ₃	3.17	1.96
MgO	13.84	14.51
CaO	14.69	20.79
MnO	0.37	0.35
FeO	14.30	9.57
Na ₂ O	0.33	0.28
K ₂ O	0.07	0.00
P ₂ O ₅	0.01	0.02
TOTAL	98.15	100.12

Atomic proportions recalculated on the basis of 6 oxygens

Si	1.955	1.947
Ti	0.004	0.011
Al	0.143	0.086
Mg	0.786	0.806
Ca	0.600	0.830
Mn	0.012	0.011
Fe	0.456	0.298
Na	0.024	0.020
K	0.003	0.000
P	0.000	0.000
Mg%	42.7	41.7
Fe%	24.8	15.4
Ca%	32.6	42.9
Total	100	100

Appendix 4
Clinopyroxene (continued)

Group 4

Wt%	2929m	2929al	2929ac	2929av	2929ay	2929an	2929ad
SiO ₂	49.33	49.65	49.91	49.99	50.66	50.67	51.36
TiO ₂	0.12	0.11	0.62	0.48	1.06	0.23	0.57
Al ₂ O ₃	1.57	0.99	1.44	2.12	1.20	0.74	1.13
MgO	7.89	7.50	11.82	12.72	12.42	12.45	13.12
CaO	21.54	21.99	19.96	17.60	20.20	20.84	19.23
MnO	1.18	1.17	0.58	0.48	0.52	0.53	0.51
FeO	15.95	16.23	13.27	14.05	12.32	12.72	12.95
Na ₂ O	0.27	0.27	0.32	0.85	0.34	0.30	0.27
K ₂ O	0.01	0.01	0.00	0.20	0.00	0.01	0.00
P ₂ O ₅	0.02	0.00	0.01	0.01	0.02	0.98	0.02
TOTAL	97.87	97.93	97.92	98.49	98.74	99.46	99.14

Atomic proportions recalculated on the basis of 6 oxygens

Si	1.959	1.975	1.942	1.930	1.945	1.933	1.959
Ti	0.004	0.003	0.018	0.014	0.031	0.007	0.016
Al	0.073	0.047	0.066	0.097	0.054	0.033	0.051
Mg	0.467	0.445	0.685	0.732	0.711	0.708	0.746
Ca	0.916	0.938	0.832	0.728	0.831	0.851	0.786
Mn	0.040	0.039	0.019	0.016	0.017	0.017	0.016
Fe	0.530	0.540	0.432	0.454	0.396	0.406	0.413
Na	0.021	0.021	0.024	0.064	0.025	0.022	0.020
K	0.001	0.001	0.000	0.010	0.000	0.001	0.000
P	0.001	0.000	0.000	0.000	0.001	0.031	0.001
Mg%	24.4	23.1	35.1	38.2	36.7	36.0	38.4
Fe%	27.7	28.1	22.2	23.7	20.4	20.7	21.2
Ca%	47.9	48.8	42.7	38.0	42.9	43.3	40.4
Total	100	100	100	100	100	100	100

Wt%	2928DDJ	2928FDJ	2928GJD	2928HJD	2928IJD	2928LJD	2928MJD
SiO ₂	51.67	52.52	51.05	51.70	51.36	51.32	50.75
TiO ₂	0.69	0.57	0.81	0.81	0.78	0.79	1.11
Al ₂ O ₃	2.15	0.80	1.47	1.51	1.62	1.41	1.78
MgO	14.46	12.63	13.82	13.65	13.85	13.75	12.89
CaO	19.06	19.16	18.09	18.26	18.05	17.84	18.53
MnO	0.42	0.50	0.47	0.45	0.44	0.50	0.47
FeO	9.98	13.61	12.70	13.00	12.60	13.12	12.69
Na ₂ O	0.23	0.30	0.26	0.22	0.26	0.24	0.26
K ₂ O	0.14	0.02	0.02	0.02	0.02	0.02	0.00
P ₂ O ₅	0.00	0.01	0.00	0.00	0.00	0.00	0.02
TOTAL	98.80	100.12	98.69	99.62	98.98	98.99	98.50

Atomic proportions recalculated on the basis of 6 oxygens

Si	1.946	1.984	1.948	1.955	1.951	1.954	1.944
Ti	0.020	0.016	0.023	0.023	0.022	0.023	0.032
Al	0.095	0.036	0.066	0.067	0.073	0.063	0.080
Mg	0.811	0.711	0.786	0.769	0.784	0.780	0.736
Ca	0.769	0.776	0.740	0.740	0.735	0.728	0.760
Mn	0.013	0.016	0.015	0.014	0.014	0.016	0.015
Fe	0.314	0.430	0.405	0.411	0.400	0.418	0.406
Na	0.017	0.022	0.019	0.016	0.019	0.018	0.019
K	0.007	0.001	0.001	0.001	0.001	0.001	0.000
P	0.000	0.000	0.000	0.000	0.000	0.000	0.001
Mg%	42.8	37.1	40.7	40.1	40.9	40.5	38.7
Fe%	16.6	22.4	21.0	21.4	20.8	21.7	21.3
Ca%	40.6	40.5	38.3	38.5	38.3	37.8	40.0
Total	100	100	100	100	100	100	100

Appendix 4
Clinopyroxene (continued)

Wt%	Group 4						
	2931JDA	2931JDB	2931JDC	2931JDD	2931JDE	2931JDF	2931JDG
SiO ₂	51.94	50.50	49.57	49.85	51.79	52.27	52.14
TiO ₂	0.61	0.46	0.55	0.57	0.63	0.60	0.61
Al ₂ O ₃	2.03	2.34	3.86	3.69	2.45	2.01	1.81
MgO	12.87	12.47	13.50	12.82	13.30	12.98	12.96
CaO	20.95	19.23	17.98	18.44	20.28	20.47	20.76
MnO	0.47	0.51	0.51	0.51	0.44	0.45	0.45
FeO	11.41	13.62	13.01	13.57	11.17	11.19	11.28
Na ₂ O	0.26	0.26	0.24	0.28	0.20	0.25	0.26
K ₂ O	0.08	0.03	0.03	0.03	0.05	0.05	0.00
P ₂ O ₅	0.00	0.00	0.00	0.01	0.00	0.00	0.00
TOTAL	100.62	99.42	99.25	99.77	100.31	100.27	100.27

Atomic proportions recalculated on the basis of 6 oxygens

Si	1.943	1.929	1.885	1.892	1.937	1.956	1.955
Ti	0.017	0.013	0.016	0.016	0.018	0.017	0.017
Al	0.090	0.105	0.173	0.165	0.108	0.089	0.080
Mg	0.718	0.710	0.765	0.725	0.741	0.724	0.724
Ca	0.840	0.787	0.733	0.750	0.813	0.821	0.834
Mn	0.015	0.016	0.016	0.016	0.014	0.014	0.014
Fe	0.357	0.435	0.414	0.431	0.34	0.350	0.354
Na	0.019	0.019	0.018	0.021	0.015	0.018	0.019
K	0.004	0.000	0.001	0.001	0.002	0.002	0.000
P	0.000	0.000	0.000	0.000	0.000	0.000	0.000
Mg%	37.5	36.7	40.0	38.0	38.9	38.2	37.9
Fe%	18.6	22.5	21.7	22.6	18.3	18.5	18.5
Ca%	43.9	40.7	38.3	39.3	42.7	43.3	43.6
Total	100	100	100	100	100	100	100

Wt%	Group 4	
	2931JDH	2931JDI
SiO ₂	52.34	53.32
TiO ₂	0.28	0.17
Al ₂ O ₃	1.32	0.44
MgO	11.74	11.62
CaO	19.79	20.47
MnO	0.56	0.56
FeO	14.34	14.72
Na ₂ O	0.28	0.28
K ₂ O	0.02	0.02
P ₂ O ₅	0.00	0.00
TOTAL	100.67	101.60

Atomic proportions recalculated on the basis of 6 oxygens

Si	1.976	1.999
Ti	0.008	0.005
Al	0.059	0.019
Mg	0.661	0.649
Ca	0.801	0.822
Mn	0.018	0.018
Fe	0.453	0.462
Na	0.020	0.020
K	0.001	0.001
P	0.000	0.000
Mg%	34.5	33.6
Fe%	23.7	23.9
Ca%	41.8	42.5
Total	100	100

Appendix 4.
Amphiboles

Wt%	Group 1		2914aw	2914ar	2914au	2914ak
	2912JDB	2912JDE				
SiO ₂	45.01	52.19	45.74	46.03	46.88	54.35
TiO ₂	0.04	0.66	1.59	1.18	1.10	0.00
Al ₂ O ₃	11.91	5.82	6.08	5.74	5.71	0.58
MgO	8.80	7.21	11.99	13.39	13.61	12.45
CaO	0.41	13.68	11.25	10.88	11.16	13.03
MnO	0.31	0.79	0.35	0.29	0.30	0.46
FeO	24.50	15.28	17.78	15.77	15.83	17.65
Na ₂ O	0.08	1.17	2.33	2.38	2.40	0.05
K ₂ O	0.02	0.00	1.12	1.07	1.07	0.02
Cr ₂ O ₃	1.61	0.34	0.01	0.02	0.01	0.00
TOTAL	92.69	97.14	98.25	96.75	98.07	98.57

Atomic proportions recalculated on the basis of 23 oxygens

Si	7.021	7.692	6.888	6.962	6.989	7.940
Ti	0.005	0.073	0.180	0.134	0.123	0.000
Al	2.190	1.011	1.079	1.023	1.004	0.099
Mg	2.046	1.584	2.692	3.019	3.024	2.710
Ca	0.069	2.160	1.815	1.763	1.783	2.039
Mn	0.041	0.099	0.045	0.037	0.038	0.056
Fe	3.196	1.883	2.239	1.995	1.974	2.156
Na	0.024	0.334	0.680	0.698	0.692	0.013
K	0.004	0.000	0.215	0.206	0.203	0.003
Cr	0.199	0.040	0.002	0.002	0.001	0.000

Wt%	Group 1	Group 2			
	2917PJB	2926bf	2926bb	2926bh	2926bc
SiO ₂	45.87	46.31	47.07	47.28	48.08
TiO ₂	0.40	1.23	1.19	1.15	0.41
Al ₂ O ₃	3.62	5.83	5.43	5.48	4.90
MgO	12.29	11.60	13.81	13.57	13.64
CaO	14.07	11.08	10.93	11.02	10.82
MnO	0.53	0.43	0.36	0.40	0.48
FeO	12.03	17.63	14.80	15.37	15.79
Na ₂ O	0.23	1.87	1.80	1.80	1.71
K ₂ O	0.03	0.81	0.85	0.76	0.64
Cr ₂ O ₃	0.09	0.01	0.02	0.02	0.02
TOTAL	89.16	96.79	96.26	96.84	96.50

Atomic proportions recalculated on the basis of 23 oxygens

Si	7.378	7.036	7.084	7.086	7.224
Ti	0.048	0.140	0.135	0.130	0.047
Al	0.686	1.045	0.964	0.968	0.867
Mg	2.946	2.626	3.097	3.031	3.053
Ca	2.425	1.803	1.762	1.770	1.742
Mn	0.072	0.056	0.046	0.051	0.061
Fe	1.618	2.240	1.863	1.926	1.984
Na	0.072	0.549	0.524	0.524	0.499
K	0.006	0.157	0.163	0.145	0.123
Cr	0.011	0.001	0.002	0.002	0.002

Appendix 4.
Amphiboles (continued)

Wt%	Group 2				
	2906BDJ	2906FDJ	2906GDJ	2906HDJ	2918JOD
SiO ₂	37.63	46.46	46.53	46.47	48.20
TiO ₂	0.21	1.33	1.19	1.26	1.46
Al ₂ O ₃	11.42	6.02	5.81	5.70	5.76
MgO	13.05	14.24	14.21	14.16	13.55
CaO	8.48	10.87	10.66	10.85	10.66
MnO	0.54	0.26	0.33	0.31	0.31
FeO	21.16	14.88	15.10	14.74	14.86
Na ₂ O	0.00	0.00	0.00	0.00	2.02
K ₂ O	0.00	1.02	0.87	0.90	0.75
Cr ₂ O ₃	0.10	0.00	0.00	0.02	0.00
TOTAL	92.59	95.08	94.70	94.41	97.57

Atomic proportions recalculated on the basis of 23 oxygens

Si	6.070	7.042	7.078	7.086	7.129
Ti	0.026	0.152	0.136	0.144	0.162
Al	2.171	1.075	1.042	1.025	1.004
Mg	3.137	3.216	3.223	3.219	1.838
Ca	1.466	1.765	1.738	1.773	0.039
Mn	0.073	0.034	0.042	0.040	2.987
Fe	2.855	1.886	1.921	1.880	1.689
Na	0.000	0.000	0.000	0.000	0.579
K	0.000	0.197	0.169	0.176	0.141
Cr	0.012	0.000	0.000	0.002	0.000

Wt%	Group 2						
	2924ag	2924ap	2924at	2924cp	2924cc	2924cj	2924cr
SiO ₂	35.73	39.38	45.17	38.04	47.54	47.85	50.97
TiO ₂	0.22	0.35	0.57	0.35	1.16	1.25	0.49
Al ₂ O ₃	12.54	10.40	7.31	11.00	5.70	5.17	3.36
MgO	13.11	13.05	11.77	12.75	13.94	14.75	14.43
CaO	8.05	10.08	9.18	10.51	11.09	11.21	11.87
MnO	0.46	0.49	0.67	0.49	0.28	0.28	0.28
FeO	21.86	20.48	21.68	20.96	15.59	14.34	15.39
Na ₂ O	0.11	0.14	0.42	0.15	2.14	2.10	1.21
K ₂ O	0.00	0.01	0.15	0.00	0.95	0.81	0.45
Cr ₂ O ₃	0.00	0.00	0.00	0.02	0.00	0.00	0.00
TOTAL	92.07	94.38	96.91	94.28	98.39	97.75	98.45

Atomic proportions recalculated on the basis of 23 oxygens

Si	5.833	6.220	6.894	6.056	7.031	7.078	7.447
Ti	0.027	0.042	0.065	0.042	0.129	0.139	0.054
Al	2.413	1.937	1.316	2.065	0.993	0.901	0.578
Mg	3.188	3.073	2.678	3.026	3.073	3.251	3.143
Ca	1.407	1.705	1.501	1.792	1.757	1.776	1.859
Mn	0.064	0.066	0.087	0.066	0.035	0.034	0.034
Fe	2.984	2.705	2.767	2.791	1.928	1.774	1.880
Na	0.035	0.042	0.124	0.046	0.613	0.602	0.344
K	0.001	0.001	0.028	0.001	0.179	0.153	0.083
Cr	0.000	0.000	0.000	0.003	0.000	0.000	0.000

Appendix 4.
Amphiboles (continued)

Wt%	Group 3					
	2936aj	2956ai	2956ap	2956aj	2956ak	2956ad
SiO ₂	47.24	38.10	41.92	42.29	42.39	46.62
TiO ₂	0.03	0.00	0.09	0.03	0.01	0.06
Al ₂ O ₃	4.67	10.60	7.51	8.15	7.89	5.50
MgO	16.30	17.98	17.18	16.80	16.85	16.48
CaO	10.35	3.84	6.60	7.11	7.93	9.70
MnO	0.32	0.25	0.32	0.27	0.29	0.30
FeO	14.60	19.83	18.31	18.02	17.55	15.98
Na ₂ O	0.12	0.06	0.09	0.11	0.13	0.16
K ₂ O	0.05	0.03	0.02	0.04	0.04	0.05
Cr ₂ O ₃	0.01	0.00	0.00	0.00	0.01	0.01
TOTAL	93.69	90.70	92.03	92.81	93.09	94.85

Atomic proportions recalculated on the basis of 23 oxygens

Si	7.205	6.140	6.622	6.612	6.612	7.062
Ti	0.003	0.000	0.010	0.003	0.001	0.006
Al	0.840	2.014	1.398	1.502	1.452	0.982
Mg	3.704	4.317	4.044	3.914	3.916	3.720
Ca	1.691	0.664	1.117	1.191	1.325	1.574
Mn	0.041	0.035	0.043	0.035	0.038	0.038
Fe	1.862	2.672	2.418	2.356	2.289	2.025
Na	0.037	0.019	0.028	0.034	0.040	0.046
K	0.010	0.005	0.004	0.007	0.008	0.009
Cr	0.001	0.000	0.000	0.001	0.002	0.002

Wt%	Group 3						
	2923JAD	2923JBD	2923JED	2923JFD	2923JGD	2923JSD	2923JUD
SiO ₂	37.53	41.80	39.28	38.59	42.39	40.11	39.47
TiO ₂	0.04	0.04	0.04	0.05	0.05	0.05	0.07
Al ₂ O ₃	10.40	8.37	9.63	9.84	8.34	9.54	9.35
MgO	14.24	14.28	14.49	14.57	14.12	14.54	14.71
CaO	6.54	8.09	7.83	7.29	9.06	8.66	8.12
MnO	0.38	0.39	0.32	0.35	0.42	0.37	0.35
FeO	20.06	19.18	18.76	19.25	18.59	18.76	18.93
Na ₂ O	0.24	0.13	0.20	0.16	0.18	0.23	0.20
K ₂ O	0.02	0.02	0.02	0.03	0.02	0.02	0.02
Cr ₂ O ₃	0.01	0.01	0.01	0.02	0.01	0.01	0.01
TOTAL	89.46	92.31	90.58	90.15	93.18	92.29	91.23

Atomic proportions recalculated on the basis of 23 oxygens

Si	6.205	6.634	6.371	6.304	6.657	6.389	6.368
Ti	0.004	0.004	0.004	0.007	0.006	0.006	0.009
Al	2.028	1.565	1.842	1.894	1.544	1.791	1.778
Mg	3.511	3.378	3.503	3.548	3.306	3.453	3.537
Ca	1.159	1.375	1.361	1.276	1.524	1.478	1.404
Mn	0.054	0.052	0.044	0.049	0.055	0.050	0.048
Fe	2.773	2.546	2.544	2.630	2.441	2.499	2.555
Na	0.076	0.039	0.062	0.052	0.055	0.072	0.062
K	0.002	0.002	0.002	0.004	0.002	0.002	0.002
Cr	0.002	0.002	0.002	0.005	0.002	0.002	0.002

Appendix 4.

Amphiboles (continued)

Wt%	Group 3					
	<u>2948bg</u>	<u>2948be</u>	<u>2948bs</u>	<u>2948ae</u>	<u>2948aj</u>	<u>2948bq</u>
SiO ₂	43.20	46.12	46.91	48.81	50.97	51.26
TiO ₂	0.09	0.06	0.17	0.94	0.32	0.34
Al ₂ O ₃	7.17	5.52	4.72	5.59	2.35	1.40
MgO	19.27	18.72	19.21	16.75	20.67	21.43
CaO	5.02	6.38	5.59	11.57	3.75	2.26
MnO	0.31	0.35	0.38	0.17	0.53	0.53
FeO	17.14	16.58	17.17	10.97	19.70	20.56
Na ₂ O	0.13	0.14	0.15	1.42	0.09	0.04
K ₂ O	0.30	0.21	0.22	0.88	0.12	0.05
Cr ₂ O ₃	0.01	0.02	0.02	0.00	0.02	0.01
TOTAL	92.63	94.08	94.52	97.10	98.52	97.89

Atomic proportions recalculated on the basis of 23 oxygens

Si	6.703	7.012	7.097	7.126	7.395	7.480
Ti	0.010	0.007	0.019	0.103	0.035	0.038
Al	1.311	0.989	0.841	0.963	0.402	0.241
Mg	4.456	4.241	4.331	3.645	4.469	4.660
Ca	0.834	1.040	0.906	1.810	0.584	0.354
Mn	0.041	0.045	0.048	0.021	0.065	0.065
Fe	2.225	2.107	2.173	1.339	2.390	2.509
Na	0.038	0.041	0.043	0.401	0.026	0.012
K	0.059	0.040	0.042	0.164	0.023	0.010
Cr	0.002	0.003	0.003	0.000	0.002	0.002

Wt%	Group 3					
	<u>2922CJD</u>	<u>2922DJD</u>	<u>2922EJD</u>	<u>2952ab</u>	<u>2952ai</u>	
SiO ₂	48.04	56.87	42.10	45.99	50.55	
TiO ₂	0.05	0.05	0.05	0.03	0.22	
Al ₂ O ₃	6.56	6.47	7.85	6.03	2.97	
MgO	13.68	11.15	15.52	15.99	18.62	
CaO	8.61	6.20	8.51	9.40	6.34	
MnO	0.34	0.25	0.32	0.45	0.65	
FeO	16.60	14.19	18.67	16.44	18.48	
Na ₂ O	0.00	0.00	0.00	0.21	0.15	
K ₂ O	0.03	0.03	0.05	0.02	0.07	
Cr ₂ O ₃	0.02	0.02	0.02	0.00	0.01	
TOTAL	93.93	95.23	93.09	94.55	98.06	

Atomic proportions recalculated on the basis of 23 oxygens

Si	7.289	8.141	6.616	7.008	7.384
Ti	0.006	0.006	0.006	0.003	0.025
Al	1.173	1.092	1.455	1.082	0.511
Mg	3.094	2.380	3.636	3.631	4.054
Ca	1.400	0.952	1.434	1.534	0.992
Mn	0.044	0.030	0.043	0.058	0.081
Fe	2.106	1.699	2.454	2.096	2.258
Na	0.000	0.000	0.000	0.061	0.042
K	0.007	0.006	0.009	0.004	0.013
Cr	0.002	0.002	0.002	0.001	0.001

Appendix 4.
Amphiboles (continued)

Wt%	Group 3						
	<u>2909ac</u>	<u>2909ad</u>	<u>2909ah</u>	<u>2909af</u>	<u>2909ag</u>	<u>2909ai</u>	<u>2909av</u>
SiO ₂	43.35	40.04	46.85	34.43	36.93	38.16	34.08
TiO ₂	0.06	0.04	1.54	0.03	0.04	0.03	0.02
Al ₂ O ₃	6.98	8.65	6.20	12.27	10.81	10.46	13.26
MgO	15.06	15.01	12.97	16.33	15.69	15.97	16.68
CaO	10.06	8.22	13.24	4.33	5.78	6.16	2.93
MnO	0.34	0.34	0.24	0.30	0.30	0.31	0.27
FeO	17.57	18.63	14.24	21.64	20.46	20.31	22.84
Na ₂ O	0.19	0.16	1.53	0.09	0.12	0.13	0.08
K ₂ O	0.04	0.07	0.76	0.12	0.11	0.09	0.16
Cr ₂ O ₃	0.02	0.02	0.02	0.03	0.01	0.02	0.01
TOTAL	93.66	91.18	97.58	89.58	90.24	91.64	90.32

Atomic proportions recalculated on the basis of 23 oxygens

Si	6.756	6.453	6.970	5.731	6.059	6.149	5.632
Ti	0.007	0.005	0.172	0.003	0.005	0.004	0.002
Al	1.282	1.644	1.087	2.409	2.092	1.987	2.584
Mg	3.497	3.604	2.875	4.051	3.836	3.834	4.109
Ca	1.679	1.420	2.111	0.773	1.016	1.063	0.518
Mn	0.044	0.046	0.030	0.042	0.042	0.042	0.038
Fe	2.289	2.511	1.772	3.012	2.807	2.737	3.156
Na	0.059	0.050	0.441	0.029	0.038	0.042	0.025
K	0.008	0.014	0.145	0.025	0.022	0.019	0.033
Cr	0.003	0.003	0.002	0.005	0.002	0.003	0.002

Wt%	Group 3						
	<u>2909bi</u>	<u>2909au</u>	<u>2909be</u>	<u>2909bo</u>	<u>2909bn</u>	<u>2909cf</u>	<u>2909bc</u>
SiO ₂	34.78	36.92	38.19	39.57	39.69	40.09	40.46
TiO ₂	0.04	0.05	0.03	0.03	0.05	0.05	0.03
Al ₂ O ₃	12.46	11.52	10.40	9.06	9.17	8.93	8.82
MgO	16.45	16.04	15.72	15.58	15.28	15.19	15.48
CaO	3.75	5.42	6.06	7.29	8.01	7.76	7.67
MnO	0.29	0.30	0.30	0.31	0.33	0.29	0.34
FeO	21.78	20.65	20.05	19.28	18.63	19.15	19.13
Na ₂ O	0.11	0.13	0.16	0.15	0.18	0.17	0.16
K ₂ O	0.14	0.14	0.11	0.06	0.10	0.08	0.07
Cr ₂ O ₃	0.00	0.01	0.00	0.03	0.02	0.02	0.01
TOTAL	89.80	91.17	91.01	91.36	91.44	91.73	92.18

Atomic proportions recalculated on the basis of 23 oxygens

Si	5.761	5.990	6.186	6.371	6.376	6.425	6.445
Ti	0.005	0.006	0.003	0.003	0.006	0.006	0.004
Al	2.434	2.204	1.987	1.719	1.738	1.687	1.657
Mg	4.062	3.879	3.795	3.739	3.658	3.628	3.676
Ca	0.665	0.943	1.051	1.257	1.379	1.332	1.310
Mn	0.041	0.042	0.041	0.043	0.044	0.040	0.045
Fe	3.017	2.802	2.717	2.596	2.503	2.566	2.549
Na	0.035	0.041	0.049	0.047	0.055	0.054	0.051
K	0.030	0.029	0.023	0.013	0.020	0.016	0.015
Cr	0.000	0.001	0.001	0.003	0.003	0.003	0.001

Appendix 4.
Amphiboles (continued)

<i>Group 3</i>							
Wt%	<u>2909bj</u>	<u>2909bz</u>	<u>2909bb</u>	<u>2909bf</u>	<u>2909ba</u>	<u>2909at</u>	<u>2909bd</u>
SiO ₂	40.87	41.50	41.52	42.02	42.18	43.21	50.69
TiO ₂	0.03	0.06	0.05	0.06	0.07	0.05	0.04
Al ₂ O ₃	8.61	8.23	8.26	8.28	7.69	7.80	7.38
MgO	15.43	15.12	15.18	14.89	14.93	15.48	11.93
CaO	7.99	8.97	8.86	8.94	9.25	8.94	5.99
MnO	0.32	0.34	0.35	0.37	0.33	0.33	0.26
FeO	18.76	18.65	18.20	18.45	17.91	18.61	15.84
Na ₂ O	0.18	0.20	0.20	0.17	0.22	0.13	0.13
K ₂ O	0.07	0.08	0.06	0.08	0.08	0.05	0.07
Cr ₂ O ₃	0.02	0.02	0.01	0.02	0.02	0.00	0.03
TOTAL	92.28	93.17	92.69	93.28	92.68	94.59	92.35

Atomic proportions recalculated on the basis of 23 oxygens

Si	6.493	6.539	6.558	6.596	6.654	6.673	7.651
Ti	0.003	0.007	0.006	0.007	0.009	0.005	0.004
Al	1.613	1.529	1.538	1.532	1.431	1.420	1.313
Mg	3.653	3.551	3.573	3.483	3.510	3.563	2.683
Ca	1.360	1.514	1.500	1.504	1.564	1.479	0.969
Mn	0.043	0.046	0.047	0.049	0.044	0.043	0.033
Fe	2.493	2.458	2.404	2.422	2.363	2.404	2.000
Na	0.055	0.061	0.060	0.053	0.067	0.040	0.039
K	0.015	0.016	0.013	0.016	0.016	0.009	0.013
Cr	0.002	0.003	0.002	0.002	0.002	0.000	0.004

<i>Group 4</i>					
Wt%	<u>2928CBJ</u>	<u>2928DBJ</u>	<u>2928AJD</u>	<u>2928CJD</u>	<u>2928EDJ</u>
SiO ₂	48.97	42.54	45.12	43.33	42.15
TiO ₂	0.32	0.13	0.18	0.13	0.18
Al ₂ O ₃	3.04	7.40	5.51	7.06	7.61
MgO	17.66	15.53	16.88	16.15	15.70
CaO	4.24	6.91	5.02	6.52	5.08
MnO	0.63	0.48	0.55	0.51	0.54
FeO	22.66	19.91	21.14	19.91	21.87
Na ₂ O	0.09	0.15	0.09	0.13	0.13
K ₂ O	0.08	0.02	0.06	0.06	0.02
Cr ₂ O ₃	0.12	0.13	0.21	0.18	0.15
TOTAL	97.81	93.20	94.76	93.98	93.43

Atomic proportions recalculated on the basis of 23 oxygens

Si	7.294	6.692	6.953	6.743	6.647
Ti	0.036	0.015	0.021	0.015	0.021
Al	0.534	1.371	1.000	1.295	1.414
Mg	3.922	3.643	3.878	3.746	3.690
Ca	0.676	1.165	0.829	1.088	0.858
Mn	0.079	0.064	0.072	0.067	0.072
Fe	2.823	2.619	2.725	2.591	2.884
Na	0.027	0.044	0.027	0.038	0.039
K	0.009	0.002	0.008	0.008	0.002
Cr	0.022	0.025	0.041	0.037	0.030

Appendix 4.
Amphiboles (continued)

Wt%	Group 4			
	2931JDJ	2931JDK	2931JDL	2931JDM
SiO ₂	48.40	43.74	48.63	48.61
TiO ₂	1.39	0.70	1.31	1.22
Al ₂ O ₃	5.71	7.91	5.65	5.55
MgO	13.37	12.27	13.16	13.97
CaO	10.73	7.54	10.75	10.74
MnO	0.31	0.45	0.43	0.34
FeO	15.84	21.54	16.72	15.75
Na ₂ O	2.07	1.10	2.03	1.99
K ₂ O	0.83	0.45	0.87	0.84
Cr ₂ O ₃	0.02	0.00	0.00	0.00
TOTAL	98.67	95.70	99.55	99.01

Atomic proportions recalculated on the basis of 23 oxygens

Si	7.115	6.768	7.113	7.115
Ti	0.153	0.081	0.144	0.135
Al	0.989	1.443	0.975	0.957
Mg	2.929	2.831	2.869	3.048
Ca	1.691	1.250	1.686	1.685
Mn	0.039	0.058	0.054	0.042
Fe	1.947	2.788	2.045	1.928
Na	0.590	0.331	0.577	0.566
K	0.155	0.088	0.163	0.156
Cr	0.002	0.000	0.000	0.000

Wt%	Group 4		
	2929au	2929ag	2929ab
SiO ₂	36.65	39.68	39.81
TiO ₂	0.02	0.04	0.03
Al ₂ O ₃	11.44	9.72	10.86
MgO	13.58	12.45	12.89
CaO	6.22	9.47	8.38
MnO	0.57	0.53	0.46
FeO	21.34	20.21	21.14
Na ₂ O	0.15	0.19	0.19
K ₂ O	0.03	0.03	0.03
Cr ₂ O ₃	0.03	0.00	0.04
TOTAL	90.03	92.32	93.83

Atomic proportions recalculated on the basis of 23 oxygens

Si	6.064	6.388	6.297
Ti	0.003	0.005	0.003
Al	2.231	1.845	2.024
Mg	3.349	2.988	3.038
Ca	1.102	1.634	1.421
Mn	0.080	0.072	0.061
Fe	2.953	2.721	2.796
Na	0.047	0.060	0.059
K	0.005	0.005	0.007
Cr	0.004	0.000	0.006

Appendix 4.
Chlorite

Wt%	Group 1						
	2914an	2914af	2914bb	2914ay	2914ag	2914ao	2914ap
SiO ₂	26.88	27.15	27.21	27.24	27.42	28.00	28.01
TiO ₂	0.00	0.01	0.01	0.02	0.02	0.00	0.01
Al ₂ O ₃	18.37	18.43	18.45	18.31	17.68	18.19	18.23
MgO	13.09	13.32	13.23	13.09	13.54	13.72	13.93
CaO	0.12	0.20	0.19	0.18	0.15	0.19	0.16
MnO	0.49	0.62	0.47	0.59	0.56	0.62	0.65
FeO	29.36	27.64	28.12	28.31	27.72	27.54	27.52
Na ₂ O	0.00	0.02	0.03	0.00	0.00	0.02	0.02
K ₂ O	0.01	0.02	0.03	0.02	0.01	0.02	0.02
P ₂ O ₅	0.03	0.02	0.04	0.04	0.02	0.03	0.02
TOTAL	88.35	87.43	87.78	87.80	87.12	88.33	88.57

Atomic proportions recalculated on the basis of 28 oxygens

Si	5.749	5.817	5.815	5.828	5.898	5.918	5.904
Ti	0.000	0.002	0.002	0.003	0.003	0.000	0.002
Al	4.632	4.655	4.648	4.619	4.483	4.533	4.530
Mg	4.172	4.253	4.213	4.174	4.340	4.322	4.376
Ca	0.027	0.046	0.044	0.041	0.035	0.043	0.036
Mn	0.089	0.113	0.085	0.107	0.102	0.111	0.116
Fe	5.251	4.953	5.025	5.066	4.986	4.868	4.851
Na	0.000	0.008	0.012	0.000	0.000	0.008	0.008
K	0.003	0.005	0.008	0.005	0.003	0.005	0.005
P	0.005	0.004	0.007	0.007	0.004	0.005	0.004
MgO/(MgO+Fe)	0.3	0.3	0.3	0.3	0.3	0.3	0.3
Non I C	19.9	19.8	19.8	19.8	19.8	19.8	19.8
I C	0.0	0.1	0.1	0.0	0.0	0.1	0.0

Wt%	Group 1				
	2914az	2912JDH	2912JDC	2912JDL	2912JDA
SiO ₂	28.54	25.10	27.93	29.31	29.39
TiO ₂	0.00	0.05	0.02	0.05	0.07
Al ₂ O ₃	18.29	14.92	16.88	15.35	15.75
MgO	14.10	10.67	12.79	13.08	12.11
CaO	0.18	0.21	0.22	0.69	1.23
MnO	0.61	0.40	0.39	0.36	0.42
FeO	27.59	27.03	29.81	28.72	29.27
Na ₂ O	0.01	0.02	0.02	0.10	0.08
K ₂ O	0.00	0.00	0.03	0.12	0.12
P ₂ O ₅	0.03	0.00	0.00	0.00	0.00
TOTAL	89.35	78.41	88.10	87.81	88.46

Atomic proportions recalculated on the basis of 28 oxygens

Si	5.951	6.072	6.000	6.285	6.277
Ti	0.000	0.009	0.003	0.008	0.011
Al	4.496	4.255	4.275	3.881	3.966
Mg	4.381	3.847	4.095	4.180	3.855
Ca	0.040	0.054	0.051	0.159	0.282
Mn	0.108	0.082	0.071	0.065	0.076
Fe	4.811	5.468	5.356	5.151	5.229
Na	0.004	0.009	0.008	0.042	0.033
K	0.000	0.000	0.008	0.033	0.033
P	0.005	0.000	0.000	0.000	0.000
MgO/(MgO+Fe)	0.3	0.3	0.3	0.3	0.3
Non I C	19.7	19.7	19.8	19.6	19.4
I C	0.0	0.1	0.1	0.2	0.3

Appendix 4.
Chlorite (continued)

Wt%	Group 1						
	<u>2917EJB</u>	<u>2917BJB</u>	<u>2917VJB</u>	<u>2917MJB</u>	<u>2917GJB</u>	<u>2917DJB</u>	<u>2917AJA</u>
SiO ₂	26.71	27.06	27.07	27.20	27.35	29.13	29.17
TiO ₂	0.02	0.02	0.02	1.46	0.05	0.05	0.05
Al ₂ O ₃	18.52	17.85	16.84	17.36	17.84	16.40	16.27
MgO	12.79	13.18	13.53	12.32	13.64	14.40	14.83
CaO	0.15	0.14	0.18	1.96	0.25	1.58	0.49
MnO	0.64	0.61	0.71	0.61	0.65	0.72	0.69
FeO	28.80	28.59	27.34	26.83	27.49	24.93	26.17
Na ₂ O	0.00	0.04	0.04	0.02	0.02	0.04	0.08
K ₂ O	0.01	0.01	0.01	0.01	0.02	0.02	0.03
P ₂ O ₅	0.00	0.00	0.00	0.00	0.00	0.00	0.00
TOTAL	87.78	87.52	85.79	87.85	87.31	87.35	87.80

Atomic proportions recalculated on the basis of 28 oxygens

Si	5.750	5.829	5.930	5.825	5.869	6.179	6.170
Ti	0.003	0.003	0.003	0.235	0.008	0.008	0.008
Al	4.701	4.533	4.349	4.383	4.513	4.101	4.057
Mg	4.104	4.231	4.417	3.932	4.362	4.552	4.675
Ca	0.035	0.032	0.042	0.450	0.057	0.359	0.111
Mn	0.117	0.111	0.132	0.111	0.118	0.129	0.124
Fe	5.186	5.151	5.009	4.806	4.933	4.423	4.629
Na	0.000	0.017	0.017	0.008	0.008	0.016	0.033
K	0.003	0.003	0.003	0.003	0.005	0.005	0.008
P	0.000	0.000	0.000	0.000	0.000	0.000	0.000
MgO/(MgO+Fe)	0.3	0.3	0.3	0.3	0.3	0.4	0.4
Non I C	19.9	19.9	19.8	19.1	19.8	19.4	19.7
I C	0.0	0.1	0.1	0.5	0.1	0.4	0.2

Group 2

Wt%	<u>2926ae</u>	<u>2926ab</u>	<u>2926bi</u>	<u>2926bi</u>	<u>2926ah</u>
SiO ₂	25.78	27.94	28.29	28.92	29.54
TiO ₂	0.00	0.90	0.00	1.32	0.00
Al ₂ O ₃	16.04	16.76	17.67	16.34	19.04
MgO	12.40	13.11	13.99	14.69	14.83
CaO	0.08	0.78	0.10	1.42	0.02
MnO	0.33	0.34	0.33	0.29	0.33
FeO	29.12	28.80	29.20	26.46	29.47
Na ₂ O	0.00	0.00	0.00	0.00	0.01
K ₂ O	0.00	0.00	0.02	0.00	0.01
P ₂ O ₅	0.00	0.01	0.00	0.01	0.00
TOTAL	83.75	88.62	89.60	89.45	93.24

Atomic proportions recalculated on the basis of 28 oxygens

Si	5.863	5.943	5.934	6.020	5.916
Ti	0.000	0.143	0.000	0.206	0.000
Al	4.301	4.205	4.369	4.008	4.495
Mg	4.202	4.155	4.372	4.556	4.427
Ca	0.019	0.177	0.022	0.316	0.005
Mn	0.063	0.062	0.058	0.051	0.055
Fe	5.538	5.124	5.123	4.607	4.936
Na	0.001	0.000	0.000	0.001	0.004
K	0.000	0.000	0.006	0.001	0.002
P	0.000	0.001	0.000	0.001	0.000
MgO/(MgO+Fe)	0.3	0.3	0.3	0.4	0.3
Non I C	20.0	19.5	19.9	19.2	19.8
I C	0.0	0.2	0.0	0.3	0.0

Appendix 4.
Chlorite (continued)

Wt%	Group 2						
	<u>2924cg</u>	<u>2924bc</u>	<u>2924ca</u>	<u>2924af</u>	<u>2924ai</u>	<u>2924ax</u>	<u>2924cn</u>
SiO ₂	26.89	27.08	27.14	27.26	27.43	27.53	27.63
TiO ₂	0.01	0.00	0.64	0.00	0.03	0.00	0.01
Al ₂ O ₃	17.45	18.83	17.89	17.98	17.23	18.51	18.27
MgO	12.92	13.18	12.59	12.96	13.50	13.48	13.49
CaO	0.16	0.24	0.53	0.15	0.19	0.11	0.19
MnO	0.45	0.48	0.47	0.43	0.43	0.48	0.46
FeO	27.40	28.64	28.93	28.16	27.41	28.69	28.48
Na ₂ O	0.00	0.02	0.01	0.03	0.04	0.01	0.01
K ₂ O	0.00	0.01	0.00	0.01	0.04	0.01	0.00
P ₂ O ₅	0.00	0.01	0.00	0.00	0.01	0.00	0.00
TOTAL	85.29	88.48	88.19	86.97	86.31	88.82	88.53

Atomic proportions recalculated on the basis of 28 oxygens

Si	5.911	5.755	5.809	5.883	5.951	5.821	5.856
Ti	0.002	0.000	0.103	0.000	0.005	0.000	0.002
Al	4.522	4.717	4.514	4.575	4.407	4.614	4.565
Mg	4.233	4.174	4.016	4.168	4.365	4.248	4.261
Ca	0.038	0.055	0.122	0.035	0.044	0.025	0.043
Mn	0.084	0.086	0.085	0.079	0.079	0.086	0.083
Fe	5.037	5.090	5.179	5.083	4.973	5.074	5.048
Na	0.000	0.008	0.004	0.013	0.017	0.004	0.004
K	0.000	0.003	0.000	0.003	0.011	0.003	0.000
P	0.000	0.002	0.000	0.000	0.002	0.000	0.000
MgO/(MgO+Fe)	0.3	0.3	0.3	0.3	0.3	0.3	0.3
Non I C	19.8	19.8	19.6	19.8	19.8	19.8	19.8
I C	0.0	0.1	0.1	0.1	0.1	0.0	0.0

Wt%	Group 2						
	<u>2924ak</u>	<u>2924ae</u>	<u>2924bh</u>	<u>2924ay</u>	<u>2924au</u>	<u>2924ab</u>	<u>2924as</u>
SiO ₂	27.75	27.75	28.33	28.35	28.41	28.43	28.69
TiO ₂	0.00	0.00	0.00	0.00	0.05	0.03	0.03
Al ₂ O ₃	17.59	18.06	17.55	18.51	18.28	17.50	18.18
MgO	13.58	13.46	14.16	13.93	13.71	13.51	13.83
CaO	0.25	0.16	0.28	0.18	0.19	0.30	0.16
MnO	0.45	0.46	0.43	0.49	0.44	0.47	0.47
FeO	27.89	28.22	27.48	28.15	27.77	28.23	28.70
Na ₂ O	0.03	0.00	0.00	0.02	0.01	0.04	0.01
K ₂ O	0.01	0.02	0.02	0.01	0.01	0.02	0.00
P ₂ O ₅	0.01	0.01	0.00	0.00	0.00	0.00	0.01
TOTAL	87.54	88.12	88.25	89.63	88.87	88.52	90.08

Atomic proportions recalculated on the basis of 28 oxygens

Si	5.937	5.900	5.989	5.908	5.960	6.014	5.960
Ti	0.000	0.000	0.000	0.000	0.008	0.005	0.005
Al	4.437	4.527	4.374	4.547	4.521	4.364	4.452
Mg	4.330	4.265	4.461	4.326	4.286	4.259	4.282
Ca	0.057	0.036	0.063	0.040	0.043	0.068	0.036
Mn	0.082	0.083	0.077	0.086	0.078	0.084	0.083
Fe	4.990	5.018	4.858	4.906	4.872	4.994	4.986
Na	0.012	0.000	0.000	0.008	0.004	0.016	0.004
K	0.003	0.005	0.005	0.003	0.003	0.005	0.000
P	0.002	0.002	0.000	0.000	0.000	0.000	0.002
MgO/(MgO+Fe)	0.3	0.3	0.3	0.3	0.3	0.3	0.3
Non I C	19.8	19.8	19.8	19.8	19.7	19.7	19.8
I C	0.1	0.0	0.1	0.1	0.1	0.1	0.0

Appendix 4.

Chlorite (continued)

Wt%	Group 2					
	<u>2924ar</u>	<u>2924ce</u>	<u>2918JBD</u>	<u>2918JAD</u>	<u>2918JDP</u>	<u>2918JCD</u>
SiO ₂	28.71	29.39	28.77	28.91	29.39	29.53
TiO ₂	0.02	0.07	0.02	0.02	1.50	0.03
Al ₂ O ₃	17.57	17.18	17.24	17.82	17.10	17.22
MgO	14.22	12.09	15.02	14.51	13.69	15.06
CaO	0.25	2.21	0.18	0.24	1.81	0.29
MnO	0.44	0.54	0.55	0.62	0.66	0.67
FeO	27.77	28.94	27.25	26.60	25.43	26.59
Na ₂ O	0.02	0.05	0.06	0.04	0.02	0.06
K ₂ O	0.02	0.02	0.02	0.03	0.03	0.03
P ₂ O ₅	0.00	0.01	0.00	0.00	0.00	0.00
TOTAL	89.02	90.49	89.13	88.81	89.65	89.51

Atomic proportions recalculated on the basis of 28 oxygens

Si	6.017	6.123	6.013	6.038	6.074	6.116
Ti	0.003	0.011	0.003	0.003	0.233	0.005
Al	4.341	4.220	4.248	4.387	4.166	4.205
Mg	4.441	3.754	4.679	4.516	4.217	4.648
Ca	0.056	0.493	0.040	0.054	0.401	0.064
Mn	0.078	0.095	0.097	0.110	0.116	0.118
Fe	4.867	5.043	4.763	4.646	4.395	4.606
Na	0.008	0.020	0.024	0.016	0.008	0.024
K	0.005	0.005	0.005	0.008	0.008	0.008
P	0.000	0.002	0.000	0.000	0.000	0.000
MgO/(MgO+Fe)	0.3	0.3	0.4	0.4	0.4	0.4
Non I C	19.7	19.2	19.8	19.7	19.0	19.7
I C	0.1	0.5	0.1	0.1	0.4	0.1

Group 2

Wt%	<u>2906IDJ</u>	<u>2906MDJ</u>	<u>2906LDJ</u>	<u>2906KDJ</u>
SiO ₂	26.98	27.34	27.53	28.74
TiO ₂	0.03	0.02	0.03	0.03
Al ₂ O ₃	18.10	18.08	17.46	18.56
MgO	13.96	14.17	14.69	13.48
CaO	0.19	0.25	0.22	0.21
MnO	0.64	0.67	0.62	0.67
FeO	27.26	27.64	27.56	27.19
Na ₂ O	0.00	0.00	0.00	0.00
K ₂ O	0.00	0.01	0.01	0.01
P ₂ O ₅	0.00	0.00	0.00	0.00
TOTAL	87.18	88.21	88.14	88.92

Atomic proportions recalculated on the basis of 28 oxygens

Si	5.795	5.810	5.853	6.007
Ti	0.005	0.003	0.005	0.005
Al	4.583	4.530	4.377	4.573
Mg	4.469	4.488	4.655	4.199
Ca	0.044	0.057	0.050	0.047
Mn	0.116	0.121	0.112	0.119
Fe	4.897	4.912	4.901	4.752
Na	0.000	0.000	0.000	0.000
K	0.000	0.003	0.003	0.003
P	0.000	0.000	0.000	0.000
MgO/(MgO+Fe)	0.3	0.3	0.4	0.3
Non I C	19.9	19.9	19.9	19.7
I C	0.0	0.1	0.1	0.1

Appendix 4.
Chlorite (continued)

Wt%	Group 3				
	<u>2909aw</u>	<u>2923BBJ</u>	<u>2923JTD</u>	<u>2923ABJ</u>	<u>2923JVD</u>
SiO ₂	28.81	26.68	27.15	28.04	28.69
TiO ₂	0.00	0.02	0.03	0.02	0.03
Al ₂ O ₃	16.82	17.38	17.01	18.20	15.82
MgO	16.33	13.95	15.11	13.79	16.48
CaO	0.16	0.08	0.24	0.17	0.11
MnO	0.30	0.36	0.35	0.35	0.34
FeO	25.32	27.27	26.26	25.76	25.34
Na ₂ O	0.01	0.04	0.02	2.76	0.02
K ₂ O	0.03	0.00	0.23	0.02	0.02
P ₂ O ₅	0.02	0.00	0.00	0.00	0.00
TOTAL	87.80	85.80	86.40	89.12	86.86

Atomic proportions recalculated on the basis of 28 oxygens

Si	6.048	5.829	5.865	5.879	6.105
Ti	0.000	0.003	0.005	0.003	0.005
Al	4.163	4.477	4.332	4.498	3.968
Mg	5.109	4.542	4.864	4.309	5.226
Ca	0.036	0.019	0.056	0.038	0.025
Mn	0.053	0.067	0.064	0.062	0.061
Fe	4.446	4.983	4.744	4.517	4.509
Na	0.004	0.017	0.008	1.122	0.008
K	0.008	0.000	0.063	0.005	0.005
P	0.004	0.000	0.000	0.000	0.000
MgO/(MgO+Fe)	0.4	0.3	0.4	0.4	0.4
Non I C	19.8	19.9	19.9	19.3	19.9
I C	0.0	0.0	0.1	1.2	0.0

Wt%	Group 4			
	<u>2928FBJ</u>	<u>2931JDO</u>	<u>2931JDR</u>	<u>2931JDN</u>
SiO ₂	28.8	27.5	28.4	30.6
TiO ₂	0.0	0.0	0.0	0.0
Al ₂ O ₃	15.8	18.1	17.9	18.3
MgO	16.8	13.9	14.0	12.9
CaO	0.1	0.1	0.3	0.3
MnO	0.3	0.6	0.5	0.5
FeO	25.7	28.1	27.3	26.1
Na ₂ O	0.0	0.0	0.0	0.7
K ₂ O	0.0	0.0	0.0	0.0
P ₂ O ₅	0.0	0.0	0.0	0.0
TOTAL	87.5	88.3	88.5	89.4

Atomic proportions recalculated on the basis of 28 oxygens

Si	6.084	5.833	5.982	6.294
Ti	0.003	0.005	0.003	0.005
Al	3.945	4.539	4.436	4.451
Mg	5.287	4.392	4.387	3.947
Ca	0.023	0.023	0.074	0.055
Mn	0.057	0.101	0.095	0.092
Fe	4.537	4.995	4.813	4.494
Na	0.008	0.008	0.008	0.268
K	0.000	0.003	0.005	0.005
P	0.000	0.000	0.000	0.000
MgO/(MgO+Fe)	0.4	0.3	0.3	0.3
Non I C	19.9	19.9	19.7	19.3
I C	0.0	0.0	0.1	0.3

Appendix 4.

Fe-Ti oxides (opaques)

Group 1

Wt%	<u>2914ab</u>	<u>2914ad</u>	<u>2914aa</u>	<u>2914ae</u>
SiO ₂	0.09	20.80	22.35	30.17
TiO ₂	50.94	51.66	57.70	36.14
Al ₂ O ₃	0.03	0.17	0.18	1.98
MgO	0.03	0.00	0.00	0.01
CaO	0.00	18.17	20.08	29.16
MnO	4.76	2.11	0.01	0.00
FeO	41.56	7.53	0.65	0.59
Na ₂ O	0.00	0.00	0.00	0.00
K ₂ O	0.00	0.00	0.00	0.00
P ₂ O ₅	0.00	0.00	0.01	0.00
TOTAL	97.41	100.44	100.97	98.05

Atomic proportions recalculated on the basis of 6 oxygens

Si	0.005	0.848	0.871	1.207
Ti	1.987	1.584	1.692	1.088
Al	0.002	0.008	0.008	0.093
Mg	0.002	0.000	0.000	0.001
Ca	0.000	0.794	0.839	1.250
Mn	0.209	0.073	0.000	0.000
Fe	1.803	0.257	0.021	0.020
Na	0.000	0.000	0.000	0.000
K	0.000	0.000	0.000	0.000
P	0.000	0.000	0.000	0.000

Group 1

Wt%	<u>2947ab</u>	<u>2947be</u>	<u>2947ad</u>
SiO ₂	0.09	0.16	1.60
TiO ₂	50.52	13.85	12.64
Al ₂ O ₃	0.05	0.51	1.16
MgO	0.03	0.00	0.07
CaO	0.01	0.26	1.17
MnO	6.39	2.39	1.50
FeO	41.82	73.79	73.43
Na ₂ O	0.01	0.00	0.03
K ₂ O	0.00	0.01	0.00
P ₂ O ₅	0.00	0.00	0.00
TOTAL	98.92	90.97	91.60

Atomic proportions recalculated on the basis of 6 oxygens

Si	0.005	0.011	0.109
Ti	1.953	0.726	0.646
Al	0.003	0.042	0.093
Mg	0.002	0.000	0.007
Ca	0.001	0.019	0.085
Mn	0.278	0.141	0.086
Fe	1.798	4.302	4.171
Na	0.001	0.000	0.004
K	0.000	0.001	0.000
P	0.000	0.000	0.000

Appendix 4.

Fe-Ti oxides (opaques) (continued)

Group 2

<u>Wt%</u>	<u>2924cb</u>	<u>2924aa</u>	<u>2924ao</u>	<u>2924an</u>
SiO ₂	6.05	13.56	21.12	28.01
TiO ₂	50.38	66.69	59.82	9.92
Al ₂ O ₃	0.20	0.42	0.28	14.13
MgO	0.00	0.01	0.00	9.27
CaO	5.46	12.63	18.71	8.47
MnO	4.75	0.91	0.23	0.37
FeO	33.18	9.36	1.90	20.93
Na ₂ O	0.02	0.01	0.01	0.01
K ₂ O	0.00	0.01	0.01	0.01
P ₂ O ₅	0.00	0.00	0.00	0.03
TOTAL	100.04	103.59	102.07	91.14

Atomic proportions recalculated on the basis of 6 oxygens

Si	0.288	0.541	0.820	1.229
Ti	1.806	2.002	1.746	0.327
Al	0.011	0.020	0.013	0.731
Mg	0.000	0.001	0.000	0.606
Ca	0.279	0.540	0.778	0.398
Mn	0.192	0.031	0.008	0.014
Fe	1.323	0.312	0.062	0.768
Na	0.002	0.001	0.001	0.001
K	0.000	0.001	0.000	0.001
P	0.000	0.000	0.000	0.001

Group 2

<u>Wt%</u>	<u>2926aa</u>	<u>2926aw</u>	<u>2926ap</u>	<u>2926ay</u>
SiO ₂	30.49	30.73	30.75	30.81
TiO ₂	34.71	33.05	34.12	34.40
Al ₂ O ₃	2.75	3.28	2.44	2.78
MgO	0.05	0.89	0.19	0.01
CaO	28.72	27.35	28.47	28.74
MnO	0.00	0.02	0.00	0.01
FeO	1.38	1.40	1.48	1.54
Na ₂ O	0.00	0.02	0.00	0.00
K ₂ O	0.01	0.01	0.00	0.01
P ₂ O ₅	0.01	0.00	0.01	0.02
TOTAL	98.12	96.72	97.47	98.29

Atomic proportions recalculated on the basis of 6 oxygens

Si	1.219	1.239	1.237	1.229
Ti	1.044	1.002	1.032	1.032
Al	0.130	0.156	0.116	0.131
Mg	0.003	0.053	0.011	0.000
Ca	1.230	1.182	1.227	1.228
Mn	0.000	0.001	0.000	0.000
Fe	0.046	0.047	0.050	0.051
Na	0.000	0.001	0.000	0.000
K	0.001	0.000	0.000	0.000
P	0.000	0.000	0.000	0.001

Appendix 4.

Fe-Ti oxides (opaques) (continued)

Group 3

Wt%	<u>2948ba</u>	<u>2948ab</u>	<u>2948bb</u>	<u>2948aa</u>
SiO ₂	0.08	0.11	0.12	0.13
TiO ₂	46.14	45.70	3.88	3.80
Al ₂ O ₃	0.01	0.01	1.16	1.39
MgO	0.05	0.04	0.00	0.00
CaO	0.02	0.03	0.03	0.00
MnO	4.06	4.03	0.11	0.06
FeO	46.90	47.37	81.94	83.99
Na ₂ O	0.00	0.02	0.01	0.00
K ₂ O	0.00	0.00	0.00	0.00
P ₂ O ₅	0.00	0.00	0.00	0.00
TOTAL	97.27	97.30	87.24	89.37

Atomic proportions recalculated on the basis of 6 oxygens

Si	0.004	0.006	0.009	0.010
Ti	1.853	1.839	0.228	0.218
Al	0.001	0.001	0.107	0.125
Mg	0.004	0.003	0.000	0.000
Ca	0.001	0.002	0.002	0.000
Mn	0.183	0.183	0.007	0.004
Fe	2.095	2.120	5.356	5.353
Na	0.000	0.002	0.002	0.000
K	0.000	0.000	0.000	0.000
P	0.000	0.000	0.000	0.000

Group 3

Group 4

Wt%	<u>2956bo</u>	<u>2956ab</u>	<u>2956ba</u>	<u>2929aa</u>
SiO ₂	0.08	0.08	0.10	0.09
TiO ₂	44.95	48.26	46.92	48.29
Al ₂ O ₃	0.02	0.02	0.00	0.02
MgO	0.06	0.00	0.02	0.04
CaO	0.03	0.04	0.01	0.01
MnO	2.99	4.03	3.51	3.79
FeO	48.75	46.01	47.41	46.62
Na ₂ O	0.02	0.00	0.00	0.00
K ₂ O	0.00	0.00	0.00	0.00
P ₂ O ₅	0.00	0.00	0.00	0.00
TOTAL	96.89	98.43	97.96	98.86

Atomic proportions recalculated on the basis of 6 oxygens

Si	0.004	0.004	0.005	0.005
Ti	1.823	1.898	1.867	1.893
Al	0.001	0.001	0.000	0.001
Mg	0.005	0.000	0.001	0.003
Ca	0.002	0.002	0.001	0.000
Mn	0.137	0.179	0.157	0.167
Fe	2.199	2.013	2.097	2.032
Na	0.002	0.000	0.000	0.000
K	0.000	0.000	0.000	0.000
P	0.000	0.000	0.000	0.000

Appendix 4.

Fe-Ti oxides (opaques) (continued)

Group 3

Wt%	2909ar	2909cb	2909cc	2909cd	2909ce	2956aa
SiO ₂	0.09	0.14	0.17	0.18	0.18	0.16
TiO ₂	47.26	47.74	7.70	9.11	8.01	2.79
Al ₂ O ₃	0.01	0.00	1.48	1.37	1.22	1.29
MgO	0.02	0.04	0.00	0.00	0.00	0.00
CaO	0.02	0.08	0.08	0.07	0.10	0.00
MnO	4.71	4.09	0.18	0.02	0.03	0.11
FeO	45.30	45.37	80.13	79.14	78.96	85.72
Na ₂ O	0.00	0.03	0.02	0.00	0.02	0.00
K ₂ O	0.00	0.02	0.00	0.00	0.00	0.00
P ₂ O ₅	0.00	0.00	0.00	0.01	0.00	0.00
TOTAL	97.41	97.51	89.76	89.89	88.52	90.08

Atomic proportions recalculated on the basis of 6 oxygens

Si	0.005	0.007	0.012	0.013	0.013	0.012
Ti	1.884	1.895	0.425	0.497	0.448	0.160
Al	0.000	0.000	0.128	0.117	0.107	0.116
Mg	0.002	0.003	0.000	0.000	0.000	0.000
Ca	0.001	0.005	0.006	0.005	0.008	0.000
Mn	0.212	0.183	0.011	0.001	0.002	0.007
Fe	2.008	2.003	4.915	4.797	4.906	5.473
Na	0.000	0.003	0.003	0.000	0.003	0.000
K	0.000	0.001	0.000	0.000	0.000	0.000
P	0.000	0.000	0.000	0.001	0.000	0.000

Group 3

Wt%	2936at	2936aw	2936aa	2936as	2952aa
SiO ₂	0.10	0.11	0.11	0.14	0.14
TiO ₂	47.20	43.66	43.72	2.72	3.25
Al ₂ O ₃	0.01	0.04	0.04	0.90	2.04
MgO	0.02	0.03	0.05	0.00	0.00
CaO	0.05	0.01	0.02	0.05	0.02
MnO	4.31	3.30	3.44	0.11	0.13
FeO	45.40	49.30	48.96	84.42	84.46
Na ₂ O	0.00	0.00	0.00	0.01	0.02
K ₂ O	0.00	0.01	0.00	0.00	0.00
P ₂ O ₅	0.00	0.00	0.00	0.02	0.02
TOTAL	97.09	96.46	96.35	88.35	90.07

Atomic proportions recalculated on the basis of 6 oxygens

Si	0.005	0.006	0.006	0.011	0.011
Ti	1.886	1.790	1.793	0.160	0.184
Al	0.001	0.003	0.003	0.083	0.181
Mg	0.002	0.003	0.004	0.000	0.000
Ca	0.003	0.000	0.001	0.004	0.001
Mn	0.194	0.153	0.159	0.007	0.008
Fe	2.017	2.248	2.233	5.520	5.325
Na	0.000	0.000	0.000	0.001	0.003
K	0.000	0.001	0.000	0.000	0.000
P	0.000	0.000	0.000	0.001	0.001

Appendix 4
Apatite

Wt%	Group 1		Group 2		Group 3	
	<u>2914ah</u>		<u>2926af</u>		<u>2909as</u>	<u>2948bd</u>
SiO ₂	0.24		0.37		0.33	0.30
TiO ₂	0.01		0.00		0.02	0.00
Al ₂ O ₃	0.00		0.00		0.00	0.00
MgO	0.05		0.03		0.03	0.07
CaO	55.30		53.99		53.67	54.84
MnO	0.04		0.05		0.03	0.05
FeO	0.18		0.14		0.12	0.14
Na ₂ O	0.12		0.16		0.15	0.10
K ₂ O	0.00		0.00		0.05	0.00
P ₂ O ₅	40.66		39.35		39.91	40.79
TOTAL	96.60		94.09		94.30	96.29

Atomic proportions recalculated on the basis of 26 oxygens

Si	0.043	0.068	0.047	0.060	0.054
Ti	0.001	0.000	0.000	0.003	0.000
Al	0.000	0.000	0.000	0.000	0.000
Mg	0.013	0.009	0.008	0.009	0.018
Ca	10.539	10.573	10.686	10.456	10.459
Mn	0.006	0.008	0.008	0.004	0.007
Fe	0.027	0.021	0.034	0.018	0.021
Na	0.041	0.055	0.059	0.051	0.034
K	0.000	0.000	0.002	0.010	0.000
P	6.123	6.090	6.056	6.143	6.148

Biotite

Wt%	Group 3			<u>2948bu</u>	<u>2948bh</u>	<u>2948bn</u>
	<u>2922BJD</u>	<u>2922KJD</u>	<u>2922LJD</u>			
SiO ₂	33.58	35.09	36.75	36.84	38.17	39.62
TiO ₂	2.63	2.27	4.02	2.75	4.29	3.26
Al ₂ O ₃	14.04	13.55	13.10	12.72	12.52	11.81
MgO	15.39	15.38	14.29	15.49	15.45	17.52
CaO	0.45	0.11	0.40	0.11	0.01	0.03
MnO	0.25	0.18	0.17	0.14	0.11	0.08
FeO	21.47	19.92	18.39	16.54	14.04	12.48
Na ₂ O	0.00	0.00	0.00	0.13	0.20	0.17
K ₂ O	4.14	6.09	7.64	8.19	9.23	9.34
Cr ₂ O ₃	0.03	0.00	0.02	0.00	0.00	0.00
P ₂ O ₅	0.00	0.00	0.00	0.00	0.01	0.00
TOTAL	91.98	92.59	94.78	92.89	94.00	94.31

Atomic proportions recalculated on the basis of 24 oxygens

Si	5.750	5.960	6.090	6.191	6.280	6.434
Ti	0.339	0.290	0.501	0.347	0.530	0.398
Al	2.834	2.713	2.559	2.520	2.428	2.261
Mg	3.927	3.893	3.529	3.879	3.787	4.240
Ca	0.083	0.020	0.071	0.019	0.001	0.005
Mn	0.036	0.026	0.024	0.019	0.015	0.011
Fe	3.074	2.830	2.549	2.325	1.932	1.694
Na	0.000	0.000	0.000	0.041	0.062	0.052
K	0.904	1.320	1.615	1.757	1.938	1.935
P	0.000	0.000	0.000	0.000	0.001	0.000

Appendix 5

The Open University standard procedures, technical and instrumental specification and precision for X-ray fluorescence (XRF) analysis for whole rock major and trace element compositions.

1. Samples collected from the Penmaenmawr Intrusion were split, removing weathered edges and veins, jaw-crushed and milled.

2. For major elements

Rock powders were dried in an oven at 110°C overnight and made into glass discs (36mm in diameter) by a 20 minute fusion of 1 part dried rock powder with 5 parts of dried lithium metaborate/tetraborate flux (Johnson Matthey Spectroflux 100B) in Pt-5%Au crucibles at 1100°C. The melt was swirled repeatedly to ensure complete dissolution and homogenisation, then poured into a mould and pressed on a hot plate to form a thin (1.5mm thickness) disc.

3. For LOI (loss on ignition)

Between 1 and 2 grams of the dried rock powders were accurately weighed and then ignited in silica crucibles at 1000°C for between 30 and 45 minutes. After ignition they were accurately weighed again and the percentage weight loss calculated.

4. For trace elements

Rock powders (between 9 and 10 gm for each sample) were thoroughly mixed with a few drops (0.6-0.7ml) of polyvinylpyrrolidone (PVP)-methyl cellulose binder. The moist powders were pressed at 10-15 ton in⁻² to a minimum thickness of 3.5 mm and dried overnight.

5. Instrumentation

The XRF analysis was carried out in an ARL 8420+ dual goniometer wavelength dispersive XRF spectrometer, equipped with:-

3 kW Rh anode end-window X-ray tube

Flow proportional and scintillation counters – full collimated

Diffraction crystals: AX06 (multiplayer), PET (penta-erythrytol), Ge111, LiF200, LiF220.

6. Analytical packages

Analytical conditions and detection limits are specified for major and trace elements.

Appendix 5 (continued)

7. Quality of results

Elemental intensities are corrected for background and known peak overlap interferences. Instrumental intensity drift is taken into account using a drift monitor. Calibration lines are produced from large number of reference materials (ca 60 for major elements, ca 35 for trace elements) encompassing a wide range of silicate compositions.

Major element matrix corrections employ the empirical Traill-Lachance procedure and trace element matrix corrections involve ratioing with the Compton scattered tube liners, or for elements $Z < 27$ (+Ba) a Lucas-Tooth correction involving iron and Compton scatter peak intensities.

Major element data quality is assessed by running two monitor samples (containing high and low concentrations of each element, which may be checked against acceptable ranges (max and min) of concentrations. A range of natural rock compositions (4 samples) are run to monitor trace element data.

8. Precision of XRF analyses.

The precision of the XRF analyses depends on the concentration of the elements concerned and the values below are based on the Open University's quality control procedures. The precision for major element compositions are derived from the 2 sigma error (95% probability) quoted for monitor samples analysed at the same time as the Penmaenmawr samples. The precision for trace elements are taken from the best approximation curves that reflect varying precision with concentration determined by repeat measurements (precision) on a range of samples.

Major Elements	Range of compositions From the Penmaenmawr Intrusion	Precision
SiO ₂	55.59% – 65.90%	±0.18%
TiO ₂	0.53% – 1.37%	±0.01%
Al ₂ O ₃	13.39% – 16.98%	±0.04%
Fe ₂ O ₃	4.96% - 9.51%	±0.03%
MnO	0.11% – 0.23%	±0.003%
MgO	1.77% – 6.42%	±0.03%
CaO	2.67% - 8.37%	±0.02%
Na ₂ O	2.09% – 5.41%	±0.03%
K ₂ O	0.60% - 3.75%	±0.02%
P ₂ O ₅	0.07% - 0.27%	±0.006%

Trace elements	Range of compositions From the Penmaenmawr Intrusion	Precision
Rb	17ppm – 158ppm	±1.5ppm
Sr	74ppm – 189ppm	±2ppm
Y	28ppm – 61ppm	±1.5pp
Zr	86ppm – 257ppm	±2.5ppm
Nb	5ppm – 16ppm	±1.2ppm
Ba	125ppm – 522ppm	±15ppm
Ni	14ppm – 78ppm	±2.5ppm
Cr	26ppm – 227ppm	±5ppm
V	74ppm – 145ppm	±7ppm
Co	13ppm – 32ppm	not available
Zn	53ppm – 107ppm	±2.8ppm
Pb	4ppm – 30ppm	±3ppm
Th	3ppm – 11ppm	±2.6ppm
Cu	17ppm – 133ppm	±2.2ppm

Appendix 6. Whole rock geochemistry

Group 1

	JD2901	JD2902	JD2903	JD2904	JD2905	JD2912	JD2913	JD2914	JD2916	JD2917	JD2933
Major Elements (Wt%)											
SiO ₂	61.06	62.62	62.58	62.88	61.31	63.65	63.55	60.39	63.60	63.11	62.58
TiO ₂	0.84	0.84	0.84	0.84	1.00	0.81	0.79	1.08	0.79	0.82	0.83
Al ₂ O ₃	14.93	15.10	15.10	15.12	14.64	15.00	14.90	15.13	14.93	15.09	15.04
Fe ₂ O ₃	5.94	6.10	6.08	6.10	6.70	5.75	5.63	6.99	5.64	6.11	6.01
MnO	0.11	0.15	0.15	0.15	0.31	0.14	0.14	0.21	0.15	0.24	0.17
MgO	2.53	2.61	2.61	2.61	3.43	2.36	2.31	2.98	2.33	2.85	2.67
CaO	4.10	4.87	4.72	4.86	3.41	4.62	4.44	4.56	4.36	2.67	4.87
Na ₂ O	2.09	3.41	3.53	3.45	3.31	3.55	3.51	3.28	3.86	4.40	3.71
K ₂ O	2.51	2.59	2.66	2.59	2.99	2.75	2.79	3.02	2.62	2.99	2.17
P ₂ O ₅	0.19	0.19	0.19	0.19	0.19	0.18	0.18	0.21	0.18	0.17	0.19
LOI	5.65	1.56	1.83	1.37	2.35	1.15	1.71	2.28	1.95	1.98	1.81
TOTAL	99.95	100.04	100.29	100.16	99.65	99.96	99.95	100.12	100.41	100.44	100.04
MgO/(MgO+Fe ₂ O ₃)	0.30	0.30	0.30	0.30	0.34	0.29	0.29	0.30	0.29	0.32	0.31
Na ₂ O+K ₂ O	4.60	6.00	6.19	6.04	6.30	6.30	6.30	6.30	6.48	7.39	5.88
Trace elements (ppm)											
Rb	129	94	87	96	98	105	104	106	97	112	65
Sr	73	122	118	116	67	111	107	104	105	116	126
Y	47	49	49	47	50	51	50	53	50	46	50
Zr	197	195	195	194	185	206	201	192	198	183	200
Nb	13	12	12	12	13	14	14	12	13	13	14
Ba	322	357	377	351	380	354	374	356	332	445	422
Pb	6	10	12	11	6	14	13	16	13	4	7
Th	9	8	8	8	8	7	6	9	8	7	7
U	2	3	3	1	2	3	2	2	3	2	2
Sc	22	19	20	19	19	18	15	19	15	17	19
V	91	87	93	88	118	86	80	136	83	91	101
Cr	62	67	62	70	66	60	57	100	63	65	71
Co	21	20	20	20	26	18	19	25	19	20	21
Ni	26	28	29	27	30	23	24	29	24	24	27
Cu	26	28	28	28	37	27	23	40	22	23	26
Zn	68	72	72	72	89	71	67	107	68	76	53
Ga	16	16	17	17	17	18	17	18	16	16	17

Appendix 6. Whole rock geochemistry (continued)

	Group 1										
	JD2934	JD2947	JD2957	JD2958	JD2959	JD2960	JD2964	JD2965	JD2966	JD2968	JD2969
Major Elements (Wt%)											
SiO ₂	62.58	65.35	63.76	64.50	64.78	62.85	63.65	64.07	63.80	65.19	63.91
TiO ₂	0.82	0.72	0.72	0.70	0.71	0.89	0.74	0.70	0.74	0.72	0.78
Al ₂ O ₃	15.06	14.74	14.76	14.80	14.96	14.96	14.75	14.75	14.66	14.57	14.64
Fe ₂ O ₃	5.99	5.45	5.45	5.27	5.39	6.40	5.51	5.42	5.45	5.42	5.97
MnO	0.16	0.14	0.15	0.14	0.14	0.19	0.14	0.15	0.18	0.13	0.15
MgO	2.66	2.09	2.46	2.36	2.38	2.61	2.50	2.45	2.33	2.07	2.52
CaO	4.79	3.86	4.40	4.31	4.34	4.23	4.10	4.17	4.07	4.19	3.38
Na ₂ O	3.57	3.62	3.54	3.61	3.58	3.53	4.04	3.84	3.55	3.80	5.41
K ₂ O	2.64	3.15	2.84	2.91	2.91	2.77	2.75	2.85	2.91	2.99	0.60
P ₂ O ₅	0.19	0.14	0.16	0.15	0.16	0.18	0.17	0.16	0.16	0.13	0.14
LOI	1.47	0.87	1.52	1.59	0.98	1.73	1.52	1.60	1.69	0.91	2.10
TOTAL	99.93	100.12	99.76	100.34	100.33	100.34	99.86	100.16	99.54	100.12	99.59
MgO/(MgO+Fe ₂ O ₃)	0.31	0.28	0.31	0.31	0.31	0.29	0.31	0.31	0.30	0.28	0.30
Na ₂ O+K ₂ O	6.21	6.77	6.38	6.52	6.49	6.30	6.79	6.69	6.46	6.79	6.01
Trace elements (ppm)											
Rb	96	121	108	106	109	104	94	108	111	114	17
Sr	123	116	112	118	109	147	126	111	114	96	149
Y	51	53	50	51	51	50	49	49	50	52	50
Zr	193	210	202	201	200	190	197	196	198	206	195
Nb	12	12	12	13	12	12	11	11	11	12	11
Ba	348	429	384	379	385	382	401	355	363	369	288
Pb	11	12	12	13	15	12	13	13	17	15	9
Th	8	10	8	10	9	7	9	9	9	11	8
U	1	2	2	4	2	3	3	3	2	2	2
Sc	18	17	18	15	19	19	18	16	16	15	18
V	92	85	78	76	74	115	82	75	76	85	104
Cr	79	39	57	59	55	46	60	60	53	43	49
Co	20	16	15	13	16	17	16	15	16	13	18
Ni	29	20	25	22	25	22	25	25	22	18	24
Cu	30	28	26	27	28	33	24	25	28	25	25
Zn	70	69	71	69	71	78	66	67	74	67	67
Ga	17	17	16	17	17	17	16	16	15	16	16

Appendix 6. Whole rock geochemistry (continued)

Group 2

	JD2906	JD2907	JD2908	JD2918	JD2919	JD2920	JD2935	JD2940	JD2967
Major Elements (Wt%)									
SiO ₂	60.52	60.87	60.14	61.00	63.40	59.74	61.61	61.76	61.77
TiO ₂	1.01	0.95	0.91	0.97	1.22	0.79	1.04	1.01	0.92
Al ₂ O ₃	14.79	14.74	14.90	14.73	14.04	15.31	14.42	14.60	14.91
Fe ₂ O ₃	7.02	6.78	6.82	6.66	6.82	7.27	6.68	6.83	6.38
MnO	0.18	0.15	0.15	0.18	0.19	0.19	0.17	0.23	0.20
MgO	3.25	3.09	2.99	3.13	2.13	4.43	3.01	3.26	2.41
CaO	4.94	5.31	6.00	4.79	3.77	4.15	4.82	3.68	3.75
Na ₂ O	3.49	3.25	3.12	3.37	3.50	3.96	3.47	3.47	3.61
K ₂ O	2.53	2.58	2.19	2.73	2.83	2.19	2.70	3.15	2.84
P ₂ O ₅	0.16	0.16	0.16	0.17	0.25	0.14	0.17	0.17	0.18
LOI	2.19	2.22	2.51	2.39	2.14	2.29	2.18	2.25	1.85
TOTAL	100.08	100.10	99.89	100.13	100.29	100.46	100.27	100.41	98.83
MgO/(MgO+Fe ₂ O ₃)	0.32	0.31	0.30	0.32	0.24	0.38	0.31	0.32	0.27
Na ₂ O+K ₂ O	6.02	5.83	5.31	6.10	6.33	6.15	6.17	6.62	6.45
Trace elements (ppm)									
Rb	96	98	81	99	99	77	100	120	109
Sr	100	109	97	74	86	120	87	105	146
Y	45	45	45	46	62	41	51	52	51
Zr	168	175	161	170	227	147	182	199	185
Nb	12	12	11	12	15	10	12	10	11
Ba	346	340	324	338	286	314	333	471	385
Pb	9	11	11	10	30	14	11	8	23
Th	8	7	6	6	10	5	7	8	8
U	2	2	1	3	2	1	3	3	3
Sc	21	24	22	20	19	21	24	24	21
V	134	125	122	132	120	117	140	131	116
Cr	79	81	86	78	36	127	99	65	47
Co	28	26	26	24	22	30	26	19	16
Ni	34	36	37	33	18	48	32	30	23
Cu	40	44	42	39	133	33	53	52	32
Zn	76	70	73	80	72	95	71	88	97
Ga	16	16	17	15	15	18	15	17	17

Appendix 6. Whole rock geochemistry (continued)

Group 3

	JD2909	JD2911	JD2921	JD2922	JD2923	JD2925	JD2936	JD2937	JD2938	JD2939	JD2941
Major Elements (Wt%)											
SiO ₂	58.93	59.44	58.60	58.65	59.72	58.81	57.18	57.58	56.37	57.58	57.89
TiO ₂	0.81	0.75	0.68	0.75	0.79	0.73	0.54	0.60	0.53	0.58	0.61
Al ₂ O ₃	15.38	15.87	15.85	15.67	15.37	15.86	16.09	15.99	16.30	16.06	15.88
Fe ₂ O ₃	7.01	6.87	6.76	6.89	6.74	6.90	6.72	6.93	7.05	6.77	6.83
MnO	0.16	0.15	0.17	0.15	0.15	0.16	0.15	0.15	0.16	0.15	0.15
MgO	4.25	4.04	4.66	4.47	3.81	4.20	6.20	5.76	6.42	5.91	5.49
CaO	6.06	6.43	6.28	6.78	5.95	6.36	8.12	7.77	8.37	7.76	7.71
Na ₂ O	3.16	3.18	3.13	3.10	3.31	3.28	2.84	2.92	2.80	2.91	2.84
K ₂ O	2.21	1.84	2.07	1.78	2.12	1.95	1.38	1.44	1.17	1.47	1.51
P ₂ O ₅	0.12	0.12	0.12	0.12	0.14	0.12	0.07	0.09	0.08	0.08	0.08
LOI	1.93	1.20	1.82	1.65	1.79	1.59	0.88	0.84	0.83	0.93	1.21
TOTAL	100.02	99.89	100.13	100.01	99.89	99.95	100.16	100.07	100.08	100.20	100.20
MgO/(MgO+Fe ₂ O ₃)	0.38	0.37	0.41	0.39	0.36	0.38	0.48	0.45	0.48	0.47	0.45
Na ₂ O+K ₂ O	5.37	5.02	5.20	4.88	5.43	5.23	4.22	4.36	3.97	4.38	4.35
Trace elements (ppm)											
Rb	81	65	78	58	73	76	51	52	43	54	57
Sr	164	122	165	138	129	137	111	109	117	109	103
Y	39	38	36	38	42	37	29	32	28	31	33
Zr	140	139	126	132	150	132	96	105	86	104	109
Nb	8	9	8	9	9	9	6	6	6	6	7
Ba	328	276	282	252	288	276	202	216	185	221	231
Pb	8	9	8	9	11	10	4	7	6	7	7
Th	7	7	4	5	4	5	6	3	4	5	6
U	1	0	3	0	1	2	1	1	0	1	2
Sc	22	21	21	22	23	21	25	24	27	21	25
V	117	102	105	123	125	115	110	116	106	112	115
Cr	111	105	159	123	99	129	227	195	226	200	184
Co	27	25	27	26	26	25	29	29	28	28	29
Ni	46	45	54	48	40	45	75	69	78	72	68
Cu	39	41	39	39	37	31	38	39	31	37	41
Zn	69	70	69	68	70	67	62	64	65	65	68
Ga	16	18	15	18	17	17	18	18	17	16	17

Appendix 6. Whole rock geochemistry (continued)

Group 3

	JD2942	JD2943	JD2944	JD2945	JD2946	JD2948	JD2949	JD2950	JD2951	JD2952	JD2953
Major Elements (Wt%)											
SiO ₂	57.36	57.84	59.21	59.62	60.20	57.68	59.10	56.78	58.30	58.30	57.21
TiO ₂	0.56	0.60	0.84	0.89	1.09	0.59	0.77	0.54	0.68	0.64	0.67
Al ₂ O ₃	16.09	15.83	15.46	15.51	15.36	16.98	15.64	16.06	15.98	15.64	15.58
Fe ₂ O ₃	6.84	6.73	7.12	7.29	7.70	6.63	7.01	6.93	6.44	6.80	6.92
MnO	0.15	0.15	0.17	0.16	0.17	0.15	0.16	0.16	0.17	0.20	0.19
MgO	5.98	5.53	4.38	4.28	3.35	5.19	4.40	6.24	4.88	5.17	5.41
CaO	7.81	7.48	6.36	6.47	5.65	6.95	6.45	8.17	6.52	6.56	6.13
Na ₂ O	2.80	2.94	3.19	3.21	3.43	3.18	3.18	2.76	3.06	3.11	3.46
K ₂ O	1.32	1.51	2.04	2.05	2.25	1.58	1.93	1.40	2.12	1.99	1.80
P ₂ O ₅	0.08	0.09	0.14	0.16	0.21	0.09	0.12	0.07	0.10	0.09	0.10
LOI	1.06	1.16	1.23	0.55	0.76	1.20	1.48	1.02	1.75	1.75	2.76
TOTAL	100.04	99.86	100.14	100.18	100.17	100.22	100.25	100.13	100.00	100.25	100.24
MgO/(MgO+Fe ₂ O ₃)	0.47	0.45	0.38	0.37	0.30	0.44	0.39	0.47	0.43	0.43	0.44
Na ₂ O+K ₂ O	4.12	4.45	5.23	5.26	5.68	4.76	5.11	4.16	5.18	5.10	5.26
Trace elements (ppm)											
Rb	48	58	75	78	84	58	69	50	76	74	69
Sr	110	106	117	112	133	137	135	119	149	167	149
Y	30	32	41	41	47	28	38	30	35	35	34
Zr	99	114	149	156	173	101	138	92	125	120	122
Nb	6	6	9	9	11	6	8	5	7	7	6
Ba	201	223	293	290	330	235	271	205	359	125	238
Pb	5	7	9	9	10	9	8	5	8	9	10
Th	4	7	6	8	8	6	6	5	6	6	7
U	2	1	2	1	2	2	2	2	1	2	1
Sc	26	23	25	21	25	19	25	23	23	25	23
V	109	109	130	125	133	96	122	109	111	120	116
Cr	197	195	121	114	62	136	121	226	153	177	182
Co	30	29	24	26	21	25	27	29	28	26	29
Ni	74	69	47	45	30	57	49	78	60	65	62
Cu	42	38	51	49	47	34	44	33	43	47	44
Zn	63	62	74	75	79	64	67	64	61	69	80
Ga	18	18	18	17	17	17	18	17	18	16	17

Appendix 6. Whole rock geochemistry (continued)

Group 3

	JD2954	JD2955	JD2956	JD2961	JD2962	JD2963
Major Elements (Wt%)						
SiO ₂	59.39	58.64	59.07	59.93	59.43	59.53
TiO ₂	0.73	0.64	0.69	0.75	0.80	0.74
Al ₂ O ₃	15.35	15.90	15.65	15.46	15.42	15.29
Fe ₂ O ₃	6.74	6.81	6.78	6.82	6.99	6.71
MnO	0.14	0.15	0.15	0.19	0.15	0.14
MgO	4.63	5.25	5.01	4.62	4.67	4.55
CaO	6.71	7.16	6.78	5.97	6.63	6.57
Na ₂ O	3.08	3.04	3.10	3.17	3.24	3.15
K ₂ O	2.02	1.78	1.94	2.46	2.00	2.04
P ₂ O ₅	0.10	0.09	0.10	0.11	0.12	0.11
LOI	1.01	1.13	1.24	1.12	0.68	1.07
TOTAL	99.90	100.58	100.51	100.61	100.12	99.90
MgO/(MgO+Fe ₂ O ₃)	0.41	0.44	0.42	0.40	0.40	0.40
Na ₂ O+K ₂ O	5.10	4.82	5.04	5.63	5.24	5.19
Trace elements (ppm)						
Rb	75	64	74	93	71	81
Sr	111	126	130	189	134	103
Y	38	34	36	41	42	40
Zr	139	117	128	140	144	140
Nb	8	7	6	8	8	8
Ba	281	252	258	336	279	267
Pb	9	8	7	11	8	8
Th	7	5	5	8	6	6
U	2	2	2	2	1	2
Sc	21	24	24	24	26	23
V	126	125	119	136	135	128
Cr	148	176	158	151	145	150
Co	26	27	29	26	26	27
Ni	57	64	57	55	56	52
Cu	52	44	44	51	57	48
Zn	65	64	65	67	71	65
Ga	16	16	17	17	17	18

Appendix 6. Whole rock geochemistry (continued)

Major Elements (Wt%)	Group 4										Others	
	JD2927	JD2928	JD2929	JD2930	JD2931	JD2932	JD2924A	JD2924B	JD2926	JD2926	JD2924A	JD2924B
SiO ₂	59.53	58.86	61.87	60.51	61.25	60.88	62.33	55.59	65.90	62.33	55.59	65.90
TiO ₂	0.75	0.92	0.86	0.85	0.96	0.94	1.06	0.69	1.37	1.06	0.69	1.37
Al ₂ O ₃	15.40	15.69	15.26	15.33	14.99	15.02	14.48	15.66	13.39	14.48	15.66	13.39
Fe ₂ O ₃	6.88	7.47	6.34	6.65	6.92	6.81	6.61	9.51	4.96	6.61	9.51	4.96
MnO	0.22	0.19	0.21	0.21	0.21	0.23	0.15	0.19	0.12	0.15	0.19	0.12
MgO	4.21	3.99	2.90	3.53	3.17	3.39	2.87	4.81	1.77	2.87	4.81	1.77
CaO	4.81	5.91	4.42	5.04	4.32	4.77	3.75	4.13	4.09	3.75	4.13	4.09
Na ₂ O	3.61	3.18	3.54	3.35	3.62	3.44	3.50	4.44	3.05	3.50	4.44	3.05
K ₂ O	2.28	2.19	2.78	2.42	2.62	2.60	3.16	2.34	3.75	3.16	2.34	3.75
P ₂ O ₅	0.13	0.17	0.19	0.16	0.19	0.17	0.19	0.11	0.27	0.19	0.11	0.27
LOI	2.41	1.35	1.75	2.07	2.05	2.22	1.91	2.40	1.33	1.91	2.40	1.33
TOTAL	100.23	99.92	100.12	100.12	100.30	100.46	100.00	99.86	100.00	100.00	99.86	100.00
MgO/(MgO+Fe ₂ O ₃)	0.38	0.35	0.31	0.35	0.31	0.33	0.30	0.34	0.26	0.30	0.34	0.26
Na ₂ O+K ₂ O	5.89	5.37	6.32	5.77	6.24	6.04	6.66	6.78	6.80	6.66	6.78	6.80
Trace elements (ppm)												
Rb	80	80	111	90	95	95	122	93	158	122	93	158
Sr	116	167	183	143	104	111	125	125	85	125	125	85
Y	41	40	48	44	50	47	49	48	61	49	48	61
Zr	150	147	181	163	180	175	200	114	257	200	114	257
Nb	10	9	12	10	11	11	11	7	16	11	7	16
Ba	336	321	407	319	359	353	483	522	407	483	522	407
Pb	6	9	15	10	10	9	8	4	13	8	4	13
Th	5	4	7	5	8	5	10	6	11	10	6	11
U	2	1	3	2	2	2	3	1	3	3	1	3
Sc	18	23	19	22	23	20	18	28	13	18	28	13
V	108	127	99	115	132	125	147	145	101	147	145	101
Cr	110	94	68	106	74	87	60	158	26	60	158	26
Co	27	27	22	24	25	26	18	32	14	18	32	14
Ni	44	43	28	36	31	34	30	44	14	30	44	14
Cu	33	36	35	38	37	41	38	17	85	38	17	85
Zn	81	74	75	78	83	78	73	114	41	73	114	41
Ga	16	17	18	18	17	15	16	16	14	16	16	14

Appendix 7.

The results of major element fractional crystallisation modelling based on sample JD2938 as the assumed parental magma (Assumed parent), and more evolved samples as the daughter magmas.

GROUP 2

DAUGHTER SAMPLE = JD2918

	Composition					Proportions of minerals required by the model	
	Daughter	Calculated Parent	Assumed Parent	Difference	(Difference) ²		
SiO ₂	62.41	56.68	56.80	-0.12469	0.01555		
TiO ₂	0.99	0.47	0.53	-0.05599	0.00313	Plag	0.3989
Al ₂ O ₃	15.07	16.26	16.42	-0.15779	0.02490	OPX	0.1671
Fe ₂ O ₃	6.81	7.22	7.10	0.12082	0.01460	CPX	0.1052
MnO	0.19	0.20	0.16	0.03810	0.00145	Biotite	0.0059
MgO	3.20	6.26	6.47	-0.20963	0.04394	Ilmenite	0.0000
CaO	4.90	8.41	8.43	-0.02480	0.00062	Apatite	0.0000
Na ₂ O	3.45	3.32	2.82	0.50178	0.25178	Total (T)	0.6772
K ₂ O	2.79	1.07	1.18	-0.10722	0.01150	Liquid (L)	0.3228
P ₂ O ₅	0.19	0.07	0.09	-0.02362	0.00056	T + L	1.0000
Total	100.00			-0.04304	R ² =0.36802		

GROUP 2

DAUGHTER SAMPLE = JD2919

	Composition					Proportions of minerals required by the model	
	Daughter	Calculated Parent	Assumed Parent	Difference	(Difference) ²		
SiO ₂	64.60	56.65	56.80	-0.15034	0.02260		
TiO ₂	1.24	0.51	0.53	-0.01515	0.00023	Plag	0.4336
Al ₂ O ₃	14.31	16.25	16.42	-0.16721	0.02796	OPX	0.1750
Fe ₂ O ₃	6.95	7.26	7.10	0.16449	0.02706	CPX	0.1138
MnO	0.19	0.20	0.16	0.03603	0.00130	Biotite	0.0132
MgO	2.17	6.21	6.47	-0.26105	0.06815	Ilmenite	0.0000
CaO	3.84	8.41	8.43	-0.02288	0.00052	Apatite	0.0000
Na ₂ O	3.57	3.34	2.82	0.52405	0.27463	Total (T)	0.7356
K ₂ O	2.88	1.00	1.18	-0.18110	0.03280	Liquid (L)	0.2644
P ₂ O ₅	0.25	0.07	0.09	-0.01844	0.00034	T + L	1.0000
Total	100.00			-0.09159	R ² =0.45559		

GROUP 2

DAUGHTER SAMPLE = JD2924A

	Composition					Proportions of minerals required by the model	
	Daughter	Calculated Parent	Assumed Parent	Difference	(Difference) ²		
SiO ₂	63.54	56.68	56.80	-0.12247	0.01500		
TiO ₂	1.08	0.47	0.53	-0.05972	0.00357	Plag	0.4219
Al ₂ O ₃	14.76	16.25	16.42	-0.16700	0.02789	OPX	0.1712
Fe ₂ O ₃	6.74	7.16	7.10	0.06211	0.00386	CPX	0.1163
MnO	0.15	0.19	0.16	0.02618	0.00069	Biotite	0.0059
MgO	2.93	6.31	6.47	-0.16136	0.02604	Ilmenite	0.0000
CaO	3.82	8.39	8.43	-0.03862	0.00149	Apatite	0.0000
Na ₂ O	3.57	3.35	2.82	0.53275	0.28382	Total (T)	0.7152
K ₂ O	3.22	1.10	1.18	-0.08415	0.00708	Liquid (L)	0.2848
P ₂ O ₅	0.19	0.06	0.09	-0.03051	0.00093	T + L	1.0000
Total	100.00			-0.04280	R ² =0.37036		

Appendix 7. (Continued)

The results of major element fractional crystallisation modelling based on sample JD2938 as the assumed parental magma (Assumed parent), and more evolved samples as the daughter magmas.

GROUP 2

DAUGHTER SAMPLE = JD2935

	Composition					Proportions of minerals required by the model	
	Daughter	Calculated Parent	Assumed Parent	Difference	(Difference) ²		
SiO ₂	62.81	56.66	56.80	-0.13750	0.01891		
TiO ₂	1.06	0.49	0.53	-0.03849	0.00148	Plag	0.4085
Al ₂ O ₃	14.70	16.25	16.42	-0.16749	0.02805	OPX	0.1705
Fe ₂ O ₃	6.81	7.22	7.10	0.12330	0.01520	CPX	0.1024
MnO	0.17	0.19	0.16	0.03076	0.00095	Biotite	0.0084
MgO	3.07	6.25	6.47	-0.21793	0.04749	Ilmenite	0.0000
CaO	4.91	8.40	8.43	-0.02794	0.00078	Apatite	0.0000
Na ₂ O	3.54	3.36	2.82	0.53779	0.28922	Total (T)	0.6898
K ₂ O	2.75	1.05	1.18	-0.13318	0.01774	Liquid (L)	0.3102
P ₂ O ₅	0.18	0.06	0.09	-0.02906	0.00084	T + L	1.0000
Total	100.00			-0.05974	R ² =0.42067		

GROUP 2

DAUGHTER SAMPLE = JD2940

	Composition					Proportions of minerals required by the model	
	Daughter	Calculated Parent	Assumed Parent	Difference	(Difference) ²		
SiO ₂	62.92	56.68	56.80	-0.12118	0.01469		
TiO ₂	1.03	0.46	0.53	-0.07294	0.00532	Plag	0.4153
Al ₂ O ₃	14.87	16.25	16.42	-0.16606	0.02758	OPX	0.1653
Fe ₂ O ₃	6.96	7.16	7.10	0.05555	0.00309	CPX	0.1190
MnO	0.23	0.21	0.16	0.04922	0.00242	Biotite	0.0021
MgO	3.32	6.32	6.47	-0.15311	0.02344	Ilmenite	0.0000
CaO	3.75	8.39	8.43	-0.03862	0.00149	Apatite	0.0000
Na ₂ O	3.54	3.36	2.82	0.53634	0.28766	Total (T)	0.7018
K ₂ O	3.21	1.11	1.18	-0.07348	0.00540	Liquid (L)	0.2982
P ₂ O ₅	0.17	0.06	0.09	-0.03395	0.00115	T + L	1.0000
Total	100.00			-0.01824	R ² =0.37224		

GROUP 3

DAUGHTER SAMPLE = JD2911

	Composition					Proportions of minerals required by the model	
	Daughter	Calculated Parent	Assumed Parent	Difference	(Difference) ²		
SiO ₂	60.23	56.69	56.80	-0.11100	0.01232		
TiO ₂	0.76	0.50	0.53	-0.03489	0.00122	Plag	0.3089
Al ₂ O ₃	16.08	16.31	16.42	-0.11455	0.01312	OPX	0.1314
Fe ₂ O ₃	6.96	7.33	7.10	0.23140	0.05354	CPX	0.0895
MnO	0.15	0.18	0.16	0.01989	0.00040	Biotite	0.0115
MgO	4.09	6.19	6.47	-0.28083	0.07887	Ilmenite	0.0000
CaO	6.52	8.44	8.43	0.00998	0.00010	Apatite	0.0000
Na ₂ O	3.22	3.19	2.82	0.36970	0.13668	Total (T)	0.5413
K ₂ O	1.86	1.04	1.18	-0.14208	0.02019	Liquid (L)	0.4587
P ₂ O ₅	0.13	0.06	0.09	-0.02638	0.00070	T + L	1.0000
Total	100.00			-0.07877	R ² =0.31712		

Appendix 7. (Continued).

The results of major element fractional crystallisation modelling based on sample JD2938 as the assumed parental magma (Assumed parent), and more evolved samples as the daughter magmas.

GROUP 3

DAUGHTER SAMPLE = JD2923

	Composition					Proportions of minerals required by the model	
	Daughter	Calculated Parent	Assumed Parent	Difference	(Difference) ²		
SiO ₂	60.88	56.68	56.80	-0.12034	0.01448		
TiO ₂	0.80	0.48	0.53	-0.05456	0.00298	Plag	0.3442
Al ₂ O ₃	15.67	16.28	16.42	-0.14350	0.02059	OPX	0.1454
Fe ₂ O ₃	6.87	7.27	7.10	0.16667	0.02778	CPX	0.0937
MnO	0.15	0.18	0.16	0.02152	0.00046	Biotite	0.0097
MgO	3.88	6.23	6.47	-0.24103	0.05810	Ilmenite	0.0000
CaO	6.07	8.42	8.43	-0.01127	0.00013	Apatite	0.0000
Na ₂ O	3.37	3.28	2.82	0.45795	0.20972	Total (T)	0.5930
K ₂ O	2.16	1.06	1.18	-0.11818	0.01397	Liquid (L)	0.4070
P ₂ O ₅	0.15	0.07	0.09	-0.02457	0.00060	T + L	1.0000
Total	100.00			-0.06730	R ² =0.34880		

GROUP 3

DAUGHTER SAMPLE = JD2925

	Composition					Proportions of minerals required by the model	
	Daughter	Calculated Parent	Assumed Parent	Difference	(Difference) ²		
SiO ₂	59.79	56.68	56.80	-0.11533	0.01330		
TiO ₂	0.74	0.47	0.53	-0.05922	0.00351	Plag	0.3041
Al ₂ O ₃	16.12	16.29	16.42	-0.12644	0.01599	OPX	0.1316
Fe ₂ O ₃	7.01	7.31	7.10	0.21212	0.04499	CPX	0.0891
MnO	0.16	0.19	0.16	0.02529	0.00064	Biotite	0.0040
MgO	4.27	6.21	6.47	-0.26213	0.06871	Ilmenite	0.0000
CaO	6.47	8.44	8.43	0.00625	0.00004	Apatite	0.0000
Na ₂ O	3.33	3.25	2.82	0.43459	0.18887	Total (T)	0.5288
K ₂ O	1.98	1.06	1.18	-0.11959	0.01430	Liquid (L)	0.4712
P ₂ O ₅	0.13	0.07	0.09	-0.02481	0.00062	T + L	1.0000
Total	100.00			-0.02927	R ² =0.35097		

GROUP 3

DAUGHTER SAMPLE = JD2939

	Composition					Proportions of minerals required by the model	
	Daughter	Calculated Parent	Assumed Parent	Difference	(Difference) ²		
SiO ₂	58.00	56.77	56.8	-0.03186	0.00101		
TiO ₂	0.59	0.53	0.53	-0.00423	0.00002	Plag	0.1582
Al ₂ O ₃	16.18	16.34	16.42	-0.07529	0.00567	OPX	0.0650
Fe ₂ O ₃	6.82	7.05	7.1	-0.04585	0.00210	CPX	0.0419
MnO	0.15	0.16	0.16	0.00496	0.00002	Biotite	0.0073
MgO	5.95	6.45	6.47	-0.02000	0.00040	Ilmenite	0.0000
CaO	7.82	8.39	8.43	-0.03628	0.00132	Apatite	0.0000
Na ₂ O	2.93	3.01	2.82	0.18587	0.03455	Total (T)	0.2724
K ₂ O	1.48	1.18	1.18	0.00087	0.00000	Liquid (L)	0.7269
P ₂ O ₅	0.08	0.06	0.09	-0.02790	0.00078	T + L	0.9993
Total	100.00			-0.04970	R ² =0.04587		

Appendix 7. (Continued).

The results of major element fractional crystallisation modelling based on sample JD2938 as the assumed parental magma (Assumed parent), and more evolved samples as the daughter magmas.

GROUP 3

DAUGHTER SAMPLE = JD2941

Composition

	Calculated		Assumed	Difference	(Difference) ²	Proportions of minerals required by the model	
	Daughter	Parent	Parent				
SiO ₂	58.48	56.76	56.80	-0.03978	0.00158		
TiO ₂	0.62	0.51	0.53	-0.02129	0.00045	Plag	0.2022
Al ₂ O ₃	16.04	16.35	16.42	-0.06865	0.00471	OPX	0.0864
Fe ₂ O ₃	6.90	7.17	7.10	0.06641	0.00441	CPX	0.0469
MnO	0.15	0.17	0.16	0.00703	0.00005	Biotite	0.0119
MgO	5.55	6.36	6.47	-0.11461	0.01314	Ilmenite	0.0000
CaO	7.79	8.42	8.43	-0.01120	0.00013	Apatite	0.0000
Na ₂ O	2.87	2.99	2.82	0.17104	0.02926	Total (T)	0.3474
K ₂ O	1.53	1.15	1.18	-0.02782	0.00077	Liquid (L)	0.6526
P ₂ O ₅	0.07	0.05	0.09	-0.04183	0.00175	T + L	1.0000
Total	100.00			-0.08070	R ² =0.05625		

GROUP 3

DAUGHTER SAMPLE = JD2943

Composition

	Calculated		Assumed	Difference	(Difference) ²	Proportions of minerals required by the model	
	Daughter	Parent	Parent				
SiO ₂	58.60	56.75	56.80	-0.04972	0.00247		
TiO ₂	0.61	0.51	0.53	-0.02166	0.00047	Plag	0.2041
Al ₂ O ₃	16.04	16.32	16.42	-0.09709	0.00943	OPX	0.0816
Fe ₂ O ₃	6.82	7.09	7.10	-0.00691	0.00005	CPX	0.0548
MnO	0.15	0.17	0.16	0.00668	0.00004	Biotite	0.0145
MgO	5.60	6.39	6.47	-0.07502	0.00563	Ilmenite	0.0000
CaO	7.58	8.39	8.43	-0.03742	0.00140	Apatite	0.0000
Na ₂ O	2.98	3.05	2.82	0.23273	0.05417	Total (T)	0.3550
K ₂ O	1.53	1.16	1.18	-0.01982	0.00039	Liquid (L)	0.6450
P ₂ O ₅	0.09	0.06	0.09	-0.02936	0.00086	T + L	1.0000
Total	100.00			-0.09758	R ² =0.07491		

GROUP 3

DAUGHTER SAMPLE = JD2945

Composition

	Calculated		Assumed	Difference	(Difference) ²	Proportions of minerals required by the model	
	Daughter	Parent	Parent				
SiO ₂	59.84	56.67	56.80	-0.13118	0.01721		
TiO ₂	0.89	0.51	0.53	-0.02146	0.00046	Plag	0.3292
Al ₂ O ₃	15.57	16.30	16.42	-0.12113	0.01467	OPX	0.1415
Fe ₂ O ₃	7.32	7.36	7.10	0.25929	0.06723	CPX	0.0822
MnO	0.16	0.18	0.16	0.02389	0.00057	Biotite	0.0000
MgO	4.30	6.17	6.47	-0.29782	0.08869	Ilmenite	0.0000
CaO	6.49	8.45	8.43	0.01706	0.00029	Apatite	0.0000
Na ₂ O	3.22	3.26	2.82	0.44015	0.19373	Total (T)	0.5529
K ₂ O	2.06	1.03	1.18	-0.15328	0.02349	Liquid (L)	0.4471
P ₂ O ₅	0.15	0.07	0.09	-0.01882	0.00035	T + L	1.0000
Total	100.00			-0.00329	R ² =0.40671		

Appendix 7. (Continued).

The results of major element fractional crystallisation modelling based on sample JD2938 as the assumed parental magma (Assumed parent), and more evolved samples as the daughter magmas.

GROUP 3

DAUGHTER SAMPLE = JD2946

	Composition					Proportions of minerals required by the model	
	Daughter	Calculated Parent	Assumed Parent	Difference	(Difference) ²		
SiO ₂	60.56	56.54	56.80	-0.25637	0.06573		
TiO ₂	1.10	0.54	0.53	0.01311	0.00017	Plag	0.3676
Al ₂ O ₃	15.45	16.30	16.42	-0.12365	0.01529	OPX	0.1547
Fe ₂ O ₃	7.75	7.50	7.10	0.40480	0.16386	CPX	0.0983
MnO	0.17	0.19	0.16	0.03060	0.00094	Biotite	0.0000
MgO	3.37	6.04	6.47	-0.42525	0.18084	Ilmenite	0.0000
CaO	5.68	8.47	8.43	0.03965	0.00157	Apatite	0.0000
Na ₂ O	3.45	3.34	2.82	0.52361	0.27417	Total (T)	0.6206
K ₂ O	2.26	0.98	1.18	-0.20451	0.04183	Liquid (L)	0.3794
P ₂ O ₅	0.21	0.08	0.09	-0.00567	0.00003	T + L	1.0000
Total	100.00			-0.00368	R ² =0.74442		

GROUP 3

DAUGHTER SAMPLE = JD2949

	Composition					Proportions of minerals required by the model	
	Daughter	Calculated Parent	Assumed Parent	Difference	(Difference) ²		
SiO ₂	59.84	56.69	56.80	-0.10758	0.01157		
TiO ₂	0.78	0.49	0.53	-0.03650	0.00133	Plag	0.3081
Al ₂ O ₃	15.84	16.30	16.42	-0.12392	0.01536	OPX	0.1290
Fe ₂ O ₃	7.10	7.29	7.10	0.19476	0.03793	CPX	0.0854
MnO	0.16	0.18	0.16	0.02282	0.00052	Biotite	0.0059
MgO	4.46	6.22	6.47	-0.25106	0.06303	Ilmenite	0.0000
CaO	6.53	8.43	8.43	0.00133	0.00000	Apatite	0.0000
Na ₂ O	3.22	3.23	2.82	0.40511	0.16412	Total (T)	0.5284
K ₂ O	1.95	1.06	1.18	-0.11747	0.01380	Liquid (L)	0.4716
P ₂ O ₅	0.12	0.06	0.09	-0.02947	0.00087	T + L	1.0000
Total	100.00			-0.04197	R ² =0.30853		

GROUP 3

DAUGHTER SAMPLE = JD2951

	Composition					Proportions of minerals required by the model	
	Daughter	Calculated Parent	Assumed Parent	Difference	(Difference) ²		
SiO ₂	59.34	56.75	56.80	-0.05401	0.00292		
TiO ₂	0.69	0.46	0.53	-0.07164	0.00513	Plag	0.2797
Al ₂ O ₃	16.27	16.31	16.42	-0.10908	0.01190	OPX	0.1236
Fe ₂ O ₃	6.55	7.06	7.10	-0.03761	0.00141	CPX	0.0831
MnO	0.17	0.19	0.16	0.02968	0.00088	Biotite	0.0006
MgO	4.97	6.43	6.47	-0.03773	0.00142	Ilmenite	0.0000
CaO	6.64	8.39	8.43	-0.03993	0.00159	Apatite	0.0000
Na ₂ O	3.11	3.15	2.82	0.32579	0.10614	Total (T)	0.4870
K ₂ O	2.16	1.20	1.18	0.02269	0.00051	Liquid (L)	0.5130
P ₂ O ₅	0.10	0.05	0.09	-0.03507	0.00123	T + L	1.0000
Total	100.00			-0.00690	R ² =0.13314		

Appendix 7. (Continued).

The results of major element fractional crystallisation modelling based on sample JD2938 as the assumed parental magma (Assumed parent), and more evolved samples as the daughter magmas.

GROUP 3

DAUGHTER SAMPLE = JD2955

	Composition					Proportions of minerals required by the model	
	Daughter	Calculated Parent	Assumed Parent	Difference	(Difference) ²		
SiO ₂	58.96	56.74	56.80	-0.06018	0.00362		
TiO ₂	0.64	0.48	0.53	-0.05246	0.00275	Plag	0.2481
Al ₂ O ₃	15.99	16.31	16.42	-0.10752	0.01156	OPX	0.1036
Fe ₂ O ₃	6.85	7.14	7.10	0.03584	0.00128	CPX	0.0670
MnO	0.15	0.17	0.16	0.01213	0.00015	Biotite	0.0080
MgO	5.28	6.36	6.47	-0.10836	0.01174	Ilmenite	0.0000
CaO	7.20	8.40	8.43	-0.02741	0.00075	Apatite	0.0000
Na ₂ O	3.05	3.12	2.82	0.30229	0.09138	Total (T)	0.4268
K ₂ O	1.79	1.17	1.18	-0.01456	0.00021	Liquid (L)	0.5732
P ₂ O ₅	0.09	0.05	0.09	-0.03526	0.00124	T + L	1.0000
Total	100.00			-0.05548	R ² =0.12470		

GROUP 3

DAUGHTER SAMPLE = JD2962

	Composition					Proportions of minerals required by the model	
	Daughter	Calculated Parent	Assumed Parent	Difference	(Difference) ²		
SiO ₂	59.76	56.69	56.80	-0.10726	0.01151		
TiO ₂	0.80	0.50	0.53	-0.03251	0.00106	Plag	0.3136
Al ₂ O ₃	15.51	16.28	16.42	-0.14234	0.02026	OPX	0.1318
Fe ₂ O ₃	7.03	7.22	7.10	0.12418	0.01542	CPX	0.0776
MnO	0.15	0.18	0.16	0.01665	0.00028	Biotite	0.0050
MgO	4.70	6.27	6.47	-0.20134	0.04054	Ilmenite	0.0000
CaO	6.67	8.41	8.43	-0.01877	0.00035	Apatite	0.0000
Na ₂ O	3.26	3.27	2.82	0.45334	0.20552	Total (T)	0.5280
K ₂ O	2.01	1.09	1.18	-0.09364	0.00877	Liquid (L)	0.4720
P ₂ O ₅	0.11	0.06	0.09	-0.03416	0.00117	T + L	1.0000
Total	100.00			-0.03584	R ² =0.30487		

Appendix 8

The results of major element fractional crystallisation modelling based on sample JD2925 as the assumed parental magma (assumed parent), and progressively more evolved samples as the daughter magmas.

GROUP 3

DAUGHTER SAMPLE = JD2911

	Composition					Proportions of minerals required by the model	
	Daughter	Calculated Parent	Assumed Parent	Difference	(Difference) ²		
SiO ₂	60.23	59.79488037	59.79	0.004880369	2.3818E-05		
TiO ₂	0.76	0.787785225	0.74	0.047785225	0.002283428	Plag	0.0124
Al ₂ O ₃	16.08	16.15144794	16.12	0.031447939	0.000988973	OPX	0.0011
FeO	6.96	7.051821992	7.01	0.041821992	0.001749079	CPX	0.0005
MnO	0.15	0.148811648	0.16	-0.011188352	0.000125179	Biotite	0.0152
MgO	4.09	4.238649046	4.27	-0.031350954	0.000982882	Ilmenite	0
CaO	6.52	6.481444103	6.47	0.011444103	0.000130967	Apatite	2E-05
Na ₂ O	3.22	3.194945769	3.33	-0.135054231	0.018239645	Total (T)	0.0293
K ₂ O	1.86	1.922552005	1.98	-0.057447995	0.003300272	Liquid (L)	0.9707
P ₂ O ₅	0.13	0.127332334	0.13	-0.002667666	7.11644E-06	T + L	1.0000
Total	100.00			-0.100329569	R ² =0.0278		

GROUP 3

DAUGHTER SAMPLE = JD2923

	Composition					Proportions of minerals required by the model	
	Daughter	Calculated Parent	Assumed Parent	Difference	(Difference) ²		
SiO ₂	60.88	59.77210251	59.79	-0.017897492	0.00032032		
TiO ₂	0.80	0.77954833	0.74	0.03954833	0.00156407	Plag	0.0876
Al ₂ O ₃	15.67	16.0861241	16.12	-0.033875904	0.001147577	OPX	0.031
FeO	6.87	6.964534402	7.01	-0.045465598	0.002067121	CPX	0.009
MnO	0.15	0.155383385	0.16	-0.004616615	2.13131E-05	Biotite	0.0079
MgO	3.88	4.274157351	4.27	0.004157351	1.72836E-05	Ilmenite	0.0015
CaO	6.07	6.444418561	6.47	-0.025581439	0.00065441	Apatite	0
Na ₂ O	3.37	3.389960792	3.33	0.059960792	0.003595297	Total (T)	0.1369
K ₂ O	2.16	1.950623383	1.98	-0.029376617	0.000862986	Liquid (L)	0.8631
P ₂ O ₅	0.15	0.130426236	0.13	0.000426236	1.81677E-07	T + L	1.0000
Total	100.00			-0.052720955	R ² =0.0103		

GROUP 3

DAUGHTER SAMPLE = JD2946

	Composition					Proportions of minerals required by the model	
	Daughter	Calculated Parent	Assumed Parent	Difference	(Difference) ²		
SiO ₂	60.56	59.4780369	59.79	-0.311963102	0.097320977		
TiO ₂	1.10	0.940050839	0.74	0.200050839	0.040020338	Plag	0.1169
Al ₂ O ₃	15.45	16.07075242	16.12	-0.049247584	0.002425324	OPX	0.0329
FeO	7.75	7.423071581	7.01	0.413071581	0.170628131	CPX	0.023
MnO	0.17	0.168631849	0.16	0.008631849	7.45088E-05	Biotite	0
MgO	3.37	3.832300118	4.27	-0.437699882	0.191581186	Ilmenite	0
CaO	5.68	6.506256253	6.47	0.036256253	0.001314516	Apatite	0
Na ₂ O	3.45	3.498102751	3.33	0.168102751	0.028258535	Total (T)	0.1728
K ₂ O	2.26	1.906524	1.98	-0.073476	0.005398723	Liquid (L)	0.8272
P ₂ O ₅	0.21	0.175103826	0.13	0.045103826	0.002034355	T + L	1.0000
Total	100.00			-0.001169469	R ² =0.5391		

Appendix 8 (Continued)

The results of major element fractional crystallisation modelling based on sample JD2925 as the assumed parental magma (assumed parent), and progressively more evolved samples as the daughter magmas.

GROUP 3

DAUGHTER SAMPLE = JD2949

Composition

	Calculated		Assumed	Difference	(Difference) ²	Proportions of minerals required by the model	
	Daughter	Parent	Parent				
SiO ₂	59.84	59.74805076	59.79	-0.041949237	0.001759738		
TiO ₂	0.78	0.765884122	0.74	0.025884122	0.000669988	Plag	0.0196
Al ₂ O ₃	15.84	16.07036329	16.12	-0.049636708	0.002463803	OPX	0.0000
FeO	7.10	6.970016293	7.01	-0.039983707	0.001598697	CPX	0.0000
MnO	0.16	0.157059192	0.16	-0.002940808	8.64835E-06	Biotite	0.0000
MgO	4.46	4.372952088	4.27	0.102952088	0.010599132	Ilmenite	0.0000
CaO	6.53	6.616067647	6.47	0.146067647	0.021335758	Apatite	0.0000
Na ₂ O	3.22	3.263720012	3.33	-0.066279988	0.004393037	Total (T)	0.0196
K ₂ O	1.95	1.917847168	1.98	-0.062152832	0.003862975	Liquid (L)	0.9804
P ₂ O ₅	0.12	0.117843408	0.13	-0.012156592	0.000147783	T + L	1.0000
Total	100.00			-0.000196014	R ² =0.0468		

Appendix 9

Estimates of the composition of a cumulate, based on the sum of the compositions and proportions of the minerals being removed during the proposed fractional crystallisation of sample JD2925.

Figures in the table below are calculated by multiplying the mineral compositions, from Table 11.1, with the proportions of that mineral required to be removed from the melt to produce the daughter sample JD2923, from Table 11.3.

Element	Plag 63.9%	Opx 22.6%	Cpx 6.6%	Bio 5.7%	Ilm 1.1%	Total (Est'd Cum) Wt%	JD2938 Wt%	Diff	R ²
SiO ₂	35.24	11.96	3.43	2.09	0.00	52.72	56.80	-4.07	16.59
TiO ₂	0.38	0.08	0.03	0.18	0.33	0.66	0.53	0.13	0.02
Al ₂ O ₃	17.63	0.21	0.10	0.74	0.01	18.68	16.42	2.26	5.11
Fe ₂ O ₃	0.30	4.82	0.73	0.98	0.74	7.57	7.10	0.47	0.22
MnO	0.01	0.12	0.03	0.01	0.03	0.19	0.16	0.03	0.01
MgO	0.01	4.90	0.94	0.89	0.00	6.75	6.47	0.28	0.08
CaO	6.98	0.49	1.32	0.01	0.00	8.80	8.43	0.37	1.13
Na ₂ O	3.48	0.01	0.02	0.00	0.00	3.51	2.82	0.69	0.48
K ₂ O	0.20	0.00	0.00	0.42	0.00	0.63	1.18	-0.55	0.31
P ₂ O ₅	0.01	0.00	0.00	0.00	0.00	0.01	0.08	-0.07	0.01
Total							100		22.93

Using Plagioclase feldspar and orthopyroxene as the only fractionating minerals.

Element	Plag. 64%	Opx 34%	Total (Est'd Cum) Wt%	JD2938 Wt%	Diff.	R ²
SiO ₂	35.30	18.00	53.29	56.80	-3.50	12.28
TiO ₂	0.04	0.12	0.16	0.53	-0.38	0.14
Al ₂ O ₃	17.66	0.31	17.97	16.42	1.54	2.38
Fe ₂ O ₃	0.30	7.26	7.56	7.10	0.46	0.21
MnO	0.01	0.19	0.20	0.16	0.03	0
MgO	0.01	7.37	7.39	6.47	0.92	0.84
CaO	6.99	0.74	7.73	8.43	-0.70	0.49
Na ₂ O	3.49	0.01	3.50	2.82	0.68	0.46
K ₂ O	0.20	0.01	0.21	1.18	-0.97	0.95
P ₂ O ₅	0.01	0.00	0.01	0.08	-0.07	0.01
Total				100		17.76

Appendix 10

The results of major element fractional crystallisation modelling based on sample JD2906 as the assumed parental magma (assumed parent) and progressively more evolved samples from Group 2 as the daughter magmas.

GROUP 2

DAUGHTER SAMPLE = JD2918

	Composition					Proportions of minerals required by the model	
	Daughter	Calculated Parent	Assumed Parent	Difference	(Difference) ²		
SiO ₂	62.41	61.79	61.82	-0.02734	0.00075		
TiO ₂	0.99	1.09	1.03	0.06103	0.00372	Plag	0.0261
Al ₂ O ₃	15.07	15.13	15.11	0.01782	0.00032	OPX	0.0124
Fe ₂ O ₃	6.81	7.11	7.17	-0.05669	0.00321	CPX	0.0019
MnO	0.19	0.20	0.19	0.01010	0.00010	Biotite	0.0047
MgO	3.20	3.35	3.32	0.03283	0.00108	Ilmenite	0.0000
CaO	4.90	5.03	5.05	-0.01990	0.00040	Apatite	0.0000
Na ₂ O	3.45	3.44	3.57	-0.13239	0.01753	Total (T)	0.0451
K ₂ O	2.79	2.67	2.58	0.09256	0.00857	Liquid (L)	0.9549
P ₂ O ₅	0.19	0.18	0.16	0.02171	0.00047	T + L	1.0000
Total	100.00			-0.00026	R ² =0.03614		

GROUP 2

DAUGHTER SAMPLE = JD2935

	Composition					Proportions of minerals required by the model	
	Daughter	Calculated Parent	Assumed Parent	Difference	(Difference) ²		
SiO ₂	62.81	61.80	61.82	-0.02472	0.00061		
TiO ₂	1.06	1.13	1.03	0.10231	0.01047	Plag	0.0521
Al ₂ O ₃	14.70	15.03	15.11	-0.07536	0.00568	OPX	0.0193
Fe ₂ O ₃	6.81	7.08	7.17	-0.08724	0.00761	CPX	0.0000
MnO	0.17	0.18	0.19	-0.01168	0.00014	Biotite	0.0044
MgO	3.07	3.33	3.32	0.00848	0.00007	Ilmenite	0.0000
CaO	4.91	5.12	5.05	0.07204	0.00519	Apatite	0.0058
Na ₂ O	3.54	3.54	3.57	-0.03347	0.00112	Total (T)	0.0815
K ₂ O	2.75	2.59	2.58	0.00526	0.00003	Liquid (L)	0.9185
P ₂ O ₅	0.18	0.17	0.16	0.00585	0.00003	T + L	1.0000
Total	100.00			-0.03852	R ² =0.03095		

GROUP 2

DAUGHTER SAMPLE = JD2940

	Composition					Proportions of minerals required by the model	
	Daughter	Calculated Parent	Assumed Parent	Difference	(Difference) ²		
SiO ₂	62.92	61.64	61.82	-0.18085	0.03271		
TiO ₂	1.03	1.08	1.03	0.04941	0.00244	Plag	0.0682
Al ₂ O ₃	14.87	15.12	15.11	0.01035	0.00011	OPX	0.0000
Fe ₂ O ₃	6.96	6.97	7.17	-0.19786	0.03915	CPX	0.0412
MnO	0.23	0.23	0.19	0.04115	0.00169	Biotite	0.0047
MgO	3.32	3.53	3.32	0.21132	0.04465	Ilmenite	0.0000
CaO	3.75	4.89	5.05	-0.15949	0.02544	Apatite	0.0000
Na ₂ O	3.54	3.52	3.57	-0.05134	0.00264	Total (T)	0.1142
K ₂ O	3.21	2.86	2.58	0.28496	0.08120	Liquid (L)	0.8858
P ₂ O ₅	0.17	0.15	0.16	-0.00832	0.00007	T + L	1.0000
Total	100.00			-0.00068	R ² =0.23010		

Appendix 10 (continued)

The results of major element fractional crystallisation modelling based on sample JD2906 as the assumed parental magma (assumed parent) and progressively more evolved samples from Group 2 as the daughter magmas.

GROUP 2

DAUGHTER SAMPLE = JD2924A

	Composition				Proportions of minerals required by the model	
	Daughter	Calculated Parent	Assumed Parent	Difference		
SiO ₂	63.54	61.73	61.82	-0.08878	0.00788	
TiO ₂	1.08	1.16	1.03	0.12707	0.01615	Plag 0.0897
Al ₂ O ₃	14.76	15.09	15.11	-0.02419	0.00059	OPX 0.0178
Fe ₂ O ₃	6.74	7.02	7.17	-0.15174	0.02302	CPX 0.0363
MnO	0.15	0.17	0.19	-0.02177	0.00047	Biotite 0.0070
MgO	2.93	3.39	3.32	0.07400	0.00548	Ilmenite 0.0000
CaO	3.82	4.99	5.05	-0.06172	0.00381	Apatite 0.0000
Na ₂ O	3.57	3.53	3.57	-0.03910	0.00153	Total (T) 0.1509
K ₂ O	3.22	2.76	2.58	0.18273	0.03339	Liquid (L) 0.8491
P ₂ O ₅	0.19	0.16	0.16	0.00260	0.00001	T + L 1.0000
Total	100.00			-0.00090	R ² =0.09233	

GROUP 2

DAUGHTER SAMPLE = JD2918

	Composition				Proportions of minerals required by the model	
	Daughter	Calculated Parent	Assumed Parent	Difference		
SiO ₂	64.60	61.81	61.82	-0.01460	0.00021	
TiO ₂	1.24	1.11	1.03	0.08241	0.00679	Plag 0.1257
Al ₂ O ₃	14.31	15.09	15.11	-0.01877	0.00035	OPX 0.0364
Fe ₂ O ₃	6.95	7.10	7.17	-0.07004	0.00491	CPX 0.0277
MnO	0.19	0.19	0.19	-0.00404	0.00002	Biotite 0.0006
MgO	2.17	3.32	3.32	0.00402	0.00002	Ilmenite 0.0000
CaO	3.84	5.01	5.05	-0.03870	0.00150	Apatite 0.0283
Na ₂ O	3.57	3.49	3.57	-0.08488	0.00720	Total (T) 0.2188
K ₂ O	2.88	2.50	2.58	-0.07979	0.00637	Liquid (L) 0.7812
P ₂ O ₅	0.25	0.20	0.16	0.03684	0.00136	T + L 1.0000
Total	100.00			-0.18755	R ² =0.02872	

Appendix 11.

The results of major element fractional crystallisation modelling based on sample JD2903 as the assumed parental magma (assumed parent), and progressively more evolved samples from Group 1 as the daughter magmas.

GROUP 1

DAUGHTER SAMPLE = JD2933

	Composition					Proportions of minerals required by the model	
	Daughter	Calculated Parent	Assumed Parent	Difference	(Difference) ²		
SiO ₂	63.71	63.52	63.56	-0.04469	0.00200		
TiO ₂	0.84	0.86	0.86	-0.00301	0.00001	Plag	0.0000
Al ₂ O ₃	15.31	15.29	15.34	-0.04692	0.00220	OPX	0.0000
Fe ₂ O ₃	6.12	6.20	6.18	0.01935	0.00037	CPX	0.0000
MnO	0.17	0.17	0.15	0.01986	0.00039	Biotite	0.0000
MgO	2.72	2.81	2.65	0.16267	0.02646	Ilmenite	0.0000
CaO	4.96	4.93	4.79	0.13558	0.01838	Apatite	0.0072
Na ₂ O	3.78	3.75	3.59	0.16336	0.02669	Total (T)	0.0072
K ₂ O	2.21	2.25	2.70	-0.45234	0.20461	Liquid (L)	0.9928
P ₂ O ₅	0.18	0.18	0.18	-0.00130	0.00000	T + L	1.0000
Total	100.00			-0.04745	R ² =0.28112		

GROUP 1

DAUGHTER SAMPLE = JD2912

	Composition					Proportions of minerals required by the model	
	Daughter	Calculated Parent	Assumed Parent	Difference	(Difference) ²		
SiO ₂	64.41	63.55	63.56	-0.00749	0.00006		
TiO ₂	0.82	0.91	0.86	0.04511	0.00203	Plag	0.0319
Al ₂ O ₃	15.18	15.32	15.34	-0.02086	0.00044	OPX	0.0134
Fe ₂ O ₃	5.82	6.14	6.18	-0.03538	0.00125	CPX	0.0000
MnO	0.14	0.15	0.15	-0.00105	0.00000	Biotite	0.0034
MgO	2.39	2.65	2.65	0.00440	0.00002	Ilmenite	0.0000
CaO	4.68	4.80	4.79	0.00900	0.00008	Apatite	0.0068
Na ₂ O	3.59	3.57	3.59	-0.02449	0.00060	Total (T)	0.0555
K ₂ O	2.78	2.69	2.70	-0.01384	0.00019	Liquid (L)	0.9445
P ₂ O ₅	0.19	0.18	0.18	-0.00022	0.00000	T + L	1.0000
Total	100.00			-0.04482	R ² =0.00467		

GROUP 1

DAUGHTER SAMPLE = JD2957

	Composition					Proportions of minerals required by the model	
	Daughter	Calculated Parent	Assumed Parent	Difference	(Difference) ²		
SiO ₂	64.90	63.55	63.56	-0.01383	0.00019		
TiO ₂	0.73	0.96	0.86	0.09678	0.00937	Plag	0.0538
Al ₂ O ₃	15.02	15.32	15.34	-0.02272	0.00052	OPX	0.0170
Fe ₂ O ₃	5.55	6.11	6.18	-0.06730	0.00453	CPX	0.0000
MnO	0.15	0.17	0.15	0.01943	0.00038	Biotite	0.0093
MgO	2.51	2.68	2.65	0.02770	0.00077	Ilmenite	0.0004
CaO	4.48	4.77	4.79	-0.02292	0.00053	Apatite	0.0000
Na ₂ O	3.60	3.60	3.59	0.01423	0.00020	Total (T)	0.0804
K ₂ O	2.89	2.67	2.70	-0.02544	0.00065	Liquid (L)	0.9196
P ₂ O ₅	0.17	0.17	0.18	-0.00647	0.00004	T + L	1.0000
Total	100.00			-0.00054	R ² =0.01716		

Appendix 11. (continued)

The results of major element fractional crystallisation modelling based on sample JD2903 as the assumed parental magma (assumed parent), and progressively more evolved samples from Group 1 as the daughter magmas.

GROUP 1

DAUGHTER SAMPLE = JD2958

	Composition			Difference	(Difference) ²	Proportions of minerals required by the model	
	Daughter	Calculated Parent	Assumed Parent				
SiO ₂	65.32	63.54	63.56	-0.02180	0.00048		
TiO ₂	0.70	0.97	0.86	0.11283	0.01273	Plag	0.0669
Al ₂ O ₃	14.99	15.31	15.34	-0.03436	0.00118	OPX	0.0247
Fe ₂ O ₃	5.34	6.10	6.18	-0.08465	0.00716	CPX	0.0004
MnO	0.14	0.17	0.15	0.01588	0.00025	Biotite	0.0112
MgO	2.39	2.68	2.65	0.03361	0.00113	Ilmenite	0.0010
CaO	4.36	4.75	4.79	-0.03661	0.00134	Apatite	0.0000
Na ₂ O	3.66	3.64	3.59	0.05472	0.00299	Total (T)	0.1041
K ₂ O	2.95	2.66	2.70	-0.03579	0.00128	Liquid (L)	0.8959
P ₂ O ₅	0.15	0.18	0.18	-0.00450	0.00002	T + L	1.0000
Total	100.00			-0.00068	R ² =0.02857		

GROUP 1

DAUGHTER SAMPLE = JD2947

	Composition			Difference	(Difference) ²	Proportions of minerals required by the model	
	Daughter	Calculated Parent	Assumed Parent				
SiO ₂	65.85	63.54	63.56	-0.02285	0.00052		
TiO ₂	0.72	0.90	0.86	0.04494	0.00202	Plag	0.0969
Al ₂ O ₃	14.85	15.32	15.34	-0.02219	0.00049	OPX	0.0315
Fe ₂ O ₃	5.49	6.13	6.18	-0.04900	0.00240	CPX	0.0135
MnO	0.14	0.16	0.15	0.01334	0.00018	Biotite	0.0091
MgO	2.11	2.67	2.65	0.01712	0.00029	Ilmenite	0.0013
CaO	3.89	4.77	4.79	-0.02245	0.00050	Apatite	0.0000
Na ₂ O	3.65	3.63	3.59	0.03721	0.00138	Total (T)	0.1523
K ₂ O	3.17	2.72	2.70	0.01804	0.00033	Liquid (L)	0.8477
P ₂ O ₅	0.13	0.16	0.18	-0.01514	0.00023	T + L	1.0000
Total	100.00			-0.00098	R ² =0.00835		

Appendix 12 Location of Samples

The map references (to the nearest metre) were scaled from a 1:3000 plan of the quarry. All grid references are within the British national grid SH 100,000 metre grid square.

The heights above sea level (metres) were estimated from the contours on a 1:3000 plan of the quarry.

Sample	Easting	Northing	Height above sea level (m)
JD2901	71793	75305	310
JD2902	71795	75285	308
JD2903	71795	75317	309
JD2904	71627	75405	307
JD2905	71535	75315	320
JD2906	70280	75370	353
JD2907	70170	75335	351
JD2908	70168	75325	352
JD2909	69960	75560	353
JD2911	70140	75677	351
JD2912	71775	75195	345
JD2913	71625	75160	343
JD2914	71498	75180	344
JD2916	71558	75170	343
JD2917	71463	75220	344
JD2918	69968	75282	354
JD2919	70075	75137	352
JD2920	69923	75387	353
JD2921	69925	75477	354
JD2922	69920	75632	351
JD2923	70160	75740	354
JD2925	70120	75625	356
JD2927	71158	75482	252
JD2928	71155	75567	221
JD2929	71323	75422	285
JD2930	71150	75395	276
JD2931	71153	75317	310
JD2932	71265	75297	313
JD2933	71753	75440	275
JD2934	71675	75400	275
JD2935	70035	75132	371
JD2936	69440	75562	252
JD2937	69355	75475	252
JD2938	69468	75575	287
JD2939	69393	75420	288
JD2940	69885	75210	370
JD2941	69530	75567	323
JD2942	69623	75682	325

Appendix 12 Location of Samples (continued)

Sample	Easting	Northing	Height above sea level (m)
JD2943	69550	75457	324
JD2944	69478	75335	324
JD2945	69338	75242	324
JD2946	69420	75182	326
JD2947	69838	74995	340
JD2948	70008	75750	300
JD2949	70083	75750	300
JD2950	70040	75805	260
JD2951	70113	75857	260
JD2952	70538	75892	145
JD2953	70608	75825	146
JD2954	69465	75767	145
JD2955	69650	75892	145
JD2956	69950	76072	145
JD2957	71250	74712	370
JD2958	71150	74755	370
JD2959	70815	74825	380
JD2960	70510	74900	360
JD2961	70050	76190	50
JD2962	69683	76050	50
JD2963	70350	76170	50
JD2964	71675	74965	380
JD2965	71510	74780	380
JD2966	70843	74845	380
JD2967	70180	75002	360
JD2968	69605	75017	340
JD2969	69480	75090	320

REFERENCES

- Allen, P M. 1982. Lower Palaeozoic volcanism in Wales, the Welsh Borderland, Avon and Somerset. 65-91 in *Igneous rocks of the British Isles*. Sutherland, D S (editor). Wiley, London.
- Anderson, T B, and Cameron, T D. 1979. A structural profile of Caledonian deformation in Down. 263-267 in *The Caledonides of the British Isles – reviewed*. Harris, A L, Holland, C H, and Leake, B E (editors). *Special Publication of the Geological Society of London*, No. 8.
- Anderton, R, Bridges, P H, Leeder, M R, and Sellwood, B W. 1979. *A Dynamic Stratigraphy of the British Isles*. George Allen and Unwin, London.
- Ball, T K, and Merriman, R J. 1989. The petrology and geochemistry of the Ordovician Llewelyn Volcanic Group, Snowdonia, North Wales. *British Geological Survey Research Report*, No. SG/89/1.
- Bevins, R E, and Rowbotham, G. 1983. Low-grade metamorphism within the Welsh sector of the paratectonic Caledonides. *Geological Journal*, Vol. 18, 141-167.
- Bevins, R E, and Merriman, R J. 1988. Compositional controls on coexisting prehnite-actinolite and prehnite-pumpellyite facies assemblages in the Tal y Fan metabasite intrusion, North Wales: implications for Caledonian metamorphic field gradients. *Journal of Metamorphic Geology*, Vol. 6, 17-39.
- Bevins, R E, and Robinson, D. 1993. Parageneses of Ordovician sub-greenschist facies metabasites from Wales, U.K. *European Journal of Mineralogy*, Vol. 5, 1-11.
- Bevins, R E, Kokelaar, B P, and Dunkley, P N. 1984. Petrology and geochemistry of lower to middle Ordovician igneous rocks: a volcanic arc to marginal basin transition. *Proceedings of the Geologists' Association*, Vol. 95, 337-347.
- Bevins, R E, Lees, G J, Roach, R A, Rowbotham, G, and Floyd, P A. 1994. Petrogenesis of the St David's Head Layered Intrusion, Wales: a complex history of multiple magma injection and in situ crystallisation. *Transactions of the Royal Society of Edinburgh: Earth Sciences*, Vol. 85, 91-121.
- Blake, S, and Campbell, I H. 1986. The dynamics of magma-mixing during flow in volcanic conduits. *Contributions to Mineralogy and Petrology*, Vol. 94, 72-81.
- Bourne, J H. 1993. Use of magnetic susceptibility, density and modal mineral data as a guide to the composition of granitic plutons. *Mathematical Geology*, Vol. 25, 357-375.
- British Geological Survey. 1985. Bangor. Sheet 106. Solid. 1:50,000. (Southampton: Ordnance Survey for British Geological Survey.)
- Cameron, E M, and Carrigan, W J. 1987. Oxygen fugacity of Archean felsic magmas: relationship to gold mineralisation. *Geol. Survey Can*, paper 87-1A, 281-298.

Castro, A., Moreno-Ventas, I, and De La Rosa, J D. 1990. Microgranular enclaves as indicators of hybridisation processes in granitoid rocks, Hercynian Belt, Spain. *Geological Journal*, Vol. 25, 391-404.

Clough, T H McK, and Cummins, W A. 1988. Stone Axe Studies, Volume 2, The petrology of prehistoric stone implements from the British Isles. *Council for British Archeology Research Report*, No. 67.

Cocks, L R M, and Fortey, R A. 1982. Faunal evidence for oceanic separations in the Paleozoic of Britain. *Journal of the Geological Society of London*, Vol. 139, 467-480.

Coward, M P, and Siddans, A W B. 1979. The tectonic evolution of the Welsh Caledonides. 187-198 in *The Caledonides of the British Isles – reviewed*. Harris, A L, Holland, C H, and Leake, B E (editors). *Special Publication of the Geological Society of London*, No. 8.

Croudace, I W. 1982. The geochemistry and petrogenesis of the Lower Paleozoic granitoids of the Lleyn Peninsula, North Wales. *Geochimica et Cosmochimica Acta*, Vol. 46, 609-622.

Deer, W A, Howie, R A, and Zussman, J. 1992. *An Introduction to the Rock-Forming Minerals*. Second Edition. Longman Group UK Limited, Harlow.

Evans, J A. 1989. Resetting of the Rb-Sr whole rock system of an Ordovician microgranite during low grade metamorphism. *Geological Magazine*, Vol. 126, 675-679.

Evans, J A. 1991. Resetting of Rb-Sr whole rock ages during Acadian low grade metamorphism in North Wales. *Journal of the Geological Society, London*, Vol. 148, 703-710.

Evans, J A, Millar, I L, and Noble, S R. 1995. Hydration during uplift is recorded by reset Rb-Sr whole-rock ages. *Journal of the Geological Society, London*, Vol. 152, 209-212.

Fitton, J G, Thirlwell, M F, and Hughes, D J. 1982. Volcanism in the Caledonian orogenic belt of Britain. 611-636 in *Andesites*. Thorpe, R S (editor). John Wiley & Sons, London.

Fortey, R A, and Cocks, L R M. 1988. Arenig to Llandovery faunal distribution in the Caledonides. 233-246 in *The Caledonian-Appalachian Orogen*. Harris, A L, and Fettes, D J. (editors). *Special Publication of the Geological Society of London*, No.38.

Fortey, R A, Harper, D A T, Ingham, J K, Owen, A W, Parkes, M A, Rushton, A W A, and Woodcock, N H. 2000. A revised correlation of Ordovician rocks in the British Isles. *Geological Society of London, Special Report*, No. 24.

Gibbons, W, and Harris, A L. (Eds).1994. A revised correlation of Precambrian rocks in the British Isles. *Geological Society of London Special Report*, No. 22.

Gibbons, W, and Young, T P. 1999. Mid-Caradoc magmatism in central Llŷn, rhyolite petrogenesis, and the evolution of Snowdonia volcanic corridor in NW Wales. *Journal of the Geological Society, London*, Vol. 156, 301-316.

Hall, A. 1987. *Igneous Petrology*. Longman Group UK Limited, Harlow.

- Hey, M H. 1954. A new review of the chlorites. *Mineralogical Magazine*, Vol. 30, 277.
- Howells, M F, and Leveridge, B E. 1980. The Capel Curig Volcanic Formation. *Report of the Institute of Geological Sciences*, No. 80/6.
- Howells, M F, Reedman, A J, and Leveridge, B E. 1985. *Geology of the country around Bangor. Explanation for 1:50,000 geological sheet 106 (England and Wales)*. HMSO, London: for the British Geological Survey.
- Howells, M F, Reedman, A J, and Campbell, S D G. 1991. *Ordovician (Caradoc) marginal basin volcanism in Snowdonia (north-west Wales)*. HMSO, London: for the British Geological Survey.
- Howells, M F, Leveridge, B E, Addison, R, and Reedman, A J. 1983. The lithostratigraphical subdivision of the Ordovician underlying the Snowdon and Crafnant volcanic groups, North Wales. *Report of the Institute of Geological Science*, No. 83/1.
- Huppert, H E, Sparks, R S J, and Turner, J S. 1983. Laboratory Investigations of viscous effects in replenished magma chambers. *Earth and Planetary Science Letters*, Vol. 65, 377-381.
- Janousek, V, Rogers, G, Bowes, D R, and Vankova, V. 1997. Cryptic trace-element variation as an indicator of reverse zoning in a granitic pluton: the Ricany granite, Czech Republic. *Journal of the Geological Society, London*, Vol. 154, 807-815.
- Kokelaar, B P. 1979. Tremadoc to Llanvirn volcanism on the southeast side of the Harlech Dome (Rhobell Fawr), N. Wales. 591-596 in *The Caledonides of the British Isles – reviewed*. Harris, A L, Holland, C H, and Leake, B E (editors). *Special Publication of the Geological Society of London*, No. 8.
- Kokelaar, B P. 1988. Tectonic controls of Ordovician arc and marginal basin volcanism in Wales. *Journal of the Geological Society of London*, Vol. 145, 759-775.
- Kokelaar, B P, Howells, M F, Bevins, R E, Roach, R A, and Dunkley, P N. 1984. The Ordovician marginal basin of Wales. 245-269 in *Marginal basin geology; volcanic and associated sedimentary and tectonic processes in modern and ancient marginal basins*. Kokelaar, B P and Howells, M F (editors). *Special publication of the Geological Society of London*, No. 16.
- Le Maitre, R W, Bateman, P, Dudek, A, Keller, J, Lameyre Le Bas, M J, Sabine, P A, Schmid, R, Sorensen, H, Streckeisen, A, Woolley, A R, and Zenettin, B. 1989. *A classification of igneous rocks and glossary of terms*. Blackwell, Oxford.
- Marsh, B.D. 1996. The 1995 Hallimond lecture. Solidification fronts and magmatic evolution. *Mineralogical Magazine*, Vol. 60, 5-40.
- Marshall, L A, and Sparks, R S J. 1984. Origin of some mixed-magma and net-veined ring intrusions. *Journal of the Geological Society, London*, Vol. 141, 171-182.
- McBirney, A R, 1984. *Igneous Petrology*. Oxford University Press, Oxford.

- McBirney, A R, and Noyes, R M. 1979. Crystallisation and layering in the Skaergaard intrusion. *Journal of Petrology*, Vol 20, 487-554.
- McBirney, A R, Baker, B H, and Nilson, R H. 1985. Liquid Fractionation. Part one: Basic principles and experimental simulations. *Journal of Volcanology and Geothermal Research*, Vol. 24, 1-24.
- McKerrow, W S. 1988. The development of the Iapetus Ocean from the Arenig to the Wenlock. 405-414 in *The Caledonian-Appalachian Orogen*. Harris, A L, and Fettes, D J (editors). *Special Publication of the Geological Society of London*, No. 38.
- Merriman, R J, and Roberts, B. 1985. A survey of white mica crystallinity and polytypes in pelitic rocks of Snowdonia and Llyn, North Wales. *Mineralogical magazine*, Vol. 49, 305-319.
- Merriman, R J, Bevins, R E, and Ball, T K. 1986. Petrological and Geological Variations within the Tal y Fan Intrusion; a Study of Element Mobility During Low-Grade Metamorphism with Implications for Petrotectonic Modelling. *Journal of Petrology*, Vol. 27, 1409-1436.
- Morimoto, N. 1988. Nomenclature of Pyroxenes. *Am Mineral*. Vol. 73, 1123-33.
- The Open University. 1990. *Understanding the Continents: Tectonic and Thermal Processes of the Lithosphere*, Block 3 Volcanic Arcs.
- Parada, M A, Larrondo, P, Palacios, C. 2000. Compositional zoning of the cretaceous Caleu pluton, coast range of central Chile; evidence for magma chamber evolution. *ACTAS, Simposio Internacional*, No. 3, Vol. 2, 679-682.
- Pearce, J A, and Cann, J R. 1973. Tectonic setting of basic volcanic rocks determined using trace element analyses. *Earth and Planetary Science Letters*, Vol. 19, 290-300.
- Pickering, K T, Basset, M G, and Siveter, D J. 1988. Late Ordovician-early Silurian destruction of the Iapetus Ocean: Newfoundland, British Isles and Scandinavia – a discussion. *Transactions of the Royal Society of Edinburgh: Earth Sciences*, Vol. 79, 361-382.
- Pitcher, W S. 1993. *The nature and origin of granite*. Chapman & Hall, London.
- Poli, G E, and Tommasini, S. 1991. Model for the origin and significance of microgranular enclaves in calc-alkaline granitoids. *Journal of petrology*, Vol. 32, 657-666.
- Preston, R J. 2001. Composite minor intrusions as windows into subvolcanic magma reservoir processes: mineralogical and geochemical evidence for complex magmatic plumbing systems in the British Tertiary Igneous Province. *Journal of the Geological Society, London*, Vol. 158, 47-58.
- Rast, N, Sturt, B A, and Harris, A L. 1988. Early deformation in the Caledonian-Appalachian orogen. 111-122 in *The Caledonian-Appalachian Orogen*. Harris, A L, and Fettes, D J (editors). *Special Publication of the Geological Society of London*, No. 38.

- Roberts, B. 1979. *The Geology of Snowdonia and Llŷn: an Outline and Fieldguide*. Adam Hilger Ltd, Bristol.
- Roberts, B. 1981. Low grade and very low grade regional metabasic Ordovician rocks of Llŷn and Snowdonia, Gwynedd. *Geological Magazine*, Vol. 118, 189-200
- Roberts, B and Merriman, R J. 1985. The distinction between Caledonian burial and regional metamorphism in metapelites from north Wales: an analysis of isocryst patterns. *Journal of the Geological Society of London*, Vol. 142, 615-624.
- Rollinson, H R. 1993. *Using Geochemical Data; Evaluation, Presentation, Interpretation*. Longman Group UK Limited, Harlow.
- Sargent, H C. 1915. The Penmaenmawr Intrusions. *Geological Magazine*, Vol. II, 15-27.
- Sargent, H C. 1924. Notes on the Petrology of Penmaenmawr Mountain (Part 1). *Proceedings of Liverpool and Manchester Geological Society*, Vol. 14, 82-98
- Sargent, H C. 1925. Notes on the Petrology of Penmaenmawr Mountain (Part 11) – The Acid Segregations and Veins. *Proceedings of Liverpool and Manchester Geological Society*, Vol.14, 123-142.
- Saunders, A D, and Tarney, J. 1984. Geochemical characteristics of basaltic volcanism within back arc basins. 59-76 in *Marginal basin geology; volcanic and associated sedimentary and tectonic processes in modern and ancient marginal basins*. Kokelaar, B P, and Howells, M F (editors). *Special Publication of the Geological Society of London*, No. 16.
- Schwab, F L, Nystuen, J P, and Gunderson, L. 1988. Pre Arenig evolution of the Appalachian-Caledonide orogen: sedimentation and stratigraphy. 75-92 in *The Caledonian-Appalachian Orogen*. Harris, A L, and Fettes, D J (editors). *Special Publication of the Geological Society of London*, No. 38.
- Scotese, C R, and McKerrow, W S. 1990. Revised World Maps and Introduction. 1-24 in *Palaeozoic Palaeogeography and Biogeography*. McKerrow, W L, and Scotese, C R. (editors). *Geological Society, London, Memoir*, 12.
- Shackleton, R M. 1954. The structural evolution of North Wales. *Liverpool and Manchester Geological Journal*, Vol. 1, 261-296.
- Soper, N J, and Hutton, D H W. 1984. Late Caledonian sinistral displacements in Britain: implications for a three-plate collision model. *Tectonics*, Vol. 3, 781-794.
- Soper, N J, and Woodcock, N H. 1990. Silurian collision and sediment dispersal patterns in southern Britain. *Geological Magazine*, Vol. 127, 527-542.
- Soper, N J, Webb, B C, and Woodcock, N H. 1987. Late Caledonian (Acadian) transpression in north-west England: timing, geometry and geotectonic significance. *Proceedings of the Yorkshire Geological Society*, Vol. 46, 175-192.

- Soper, N J, England, R W, Snyder, D B, and Ryan, P D. 1992. The Iapetus suture zone in England, Scotland and eastern Ireland: a reconciliation of geological and deep seismic data. *Journal of the Geological Society, London*, Vol. 149, 697-700.
- Sparks, R S J, Sigurdsson, H, and Wilson, L. 1977. Magma Mixing: a mechanism for triggering acid explosive eruptions. *Nature*, Vol. 267, 315-318.
- Sparks, R S J, Huppert, H E, and Turner, J S. 1984. The fluid dynamics of evolving magma chambers. *Philosophical Transactions of the Royal Society of London*, Vol. 310, 511-534.
- S Penn Associates. 1991. Penmaenmawr Quarry, Shear Zone Investigation, Geophysical Report. Unpublished report for ARC Northern.
- Stillman, C J. 2001. Caledonian Igneous Activity. 145-178 in *The Geology of Ireland*. Holland, C H (editor). Dunedin Academic Press.
- Stormer, J C, and Nicholls, J. 1978. XLFRAC – a program for the interactive testing of magmatic differentiation models. *Computers and Geosciences*, Vol. 4, No. 2, 143-159.
- Thorpe, R S. 1979. Late Precambrian igneous activity in Southern Britain. 579-584 in *The Caledonides of the British Isles - reviewed*. Harris, A L, Holland, C H and Leake, B E (editors). *Special Publication of the Geological Society of London*, No. 8.
- Thorpe, R S, Beckinsale, R D, Patchett, P J, Piper, J D A, Davies, G R, and Evans, J A. 1984. Crustal growth and late Precambrian-early Palaeozoic plate tectonic evolution of England and Wales. *Journal of the Geological Society of London*, Vol. 141, 521-536.
- Thorpe, R S, Leat, P T, Bevins, R E, and Hughes, D J. 1989. Late orogenic alkaline/subalkaline Silurian volcanism of the Skomer Volcanic Group in the Caledonides of south Wales. *Journal of the Geological Society of London*, Vol. 146, 125-132.
- Tindle, A G, and Webb, P C. 1994. A spreadsheet program to classify microprobe-derived amphibole analyses. *Computers and Geosciences*, Vol. 20, 1201-1228.
- Tindle, A G, McGarvie, D W, and Webb, P C. 1988. The role of hybridization and crystal fractionation in the evolution of the Cairnsmore of Carsphairn Intrusion, Southern Uplands of Scotland. *Journal of the Geological Society of London*, Vol. 145, 11-21.
- Tremlett, W E. 1997. Geochemical variation in the Penmaenmawr intrusion (North Wales). *Geological Journal*, Vol. 32, 173-187.
- Wager, L R, and Deer, W A. 1939. Geological investigations in East Greenland, Part III. The petrology of the Skaergaard Intrusion, Kangerdlugssuaq, East Greenland. *Meddelelser om Gronland*, 105, 1-352.
- Wager, L R, and Brown, G M. 1968. *Layered Igneous Rocks*. Oliver and Boyd, Edinburgh.
- Williams-Thorpe, O, and Thorpe, R S. 1993. Magnetic susceptibility used in non-destructive provenancing of Roman granite columns. *Archeometry*, 35, 2, 185-195.

Williams-Thorpe, O, Jones, M C, Tindle, A G, and Thorpe, R S. 1996. Magnetic susceptibility variations at Mons Claudianus and in Roman columns: a method of provenancing to within a single quarry. *Archeometry*, 38, 1, 1-27.

Wilson, M. 1989. *Igneous Petrogenesis*. Unwin Hyman, London.

Winchester, J A, and Floyd, P A. 1977. Geochemical discrimination of different magma series and their differentiation products using immobile elements. *Chemical Geology*, Vol. 20, 325-343.

Woodward, N, and Strachan R. 2000. *Geological History of Britain and Ireland*. Blackwell Science Ltd, Oxford.